JUL 24 1950

THE JOURNAL OF CHEMICAL PHYSICS

Volume 18

1950

LIBRARY
UNIVERSITY OF ILLINOIS

Term ending December 31, 1951

FORREST CLEMENTS
BRYCE CRAWFORD, JR.
RALPH H. HALFORD
GEORGE KIMBALL
K. J. LAIDLER
WILLARD F. LIBBY
J. REID NIELSEN

...be typewritten on sheets separate from the ... Each table must have a caption which will ... the table intelligible without reference ... Avoid complicated column headings.

... possible figures should be planned for the ... of a column (3 in.). A convenient reduction ratio is ... Lettering should be large enough so that ... when reduced it shall not be less than about ... mm). Line drawings must be in *india ink* on ... or tracing cloth. Coordinate paper is not ... If used must be blue-lined and the coordinate ... which are to show must be inked over. Photographs ... have maximum black and white contrast. Identify ... drawing or photograph on the back with the ... and the figure number. Figures should be ... consecutively. Captions should be typed on a ... sheet of paper.

... number of alterations in proof are unavoidable, ... the cost of making extensive alterations after the ... has been set in type will be charged to the author.

... and all correspondence concerning papers in the ... publication should be addressed to the Publica... Manager, American Institute of Physics, 57 East ... Street, New York 22, New York.

Subscription Price

	U. S. and Canada	Elsewhere
To members and associate members of the American Institute of Physics	$12.00	$13.00
To all others	15.00	16.00

Back Number Prices

...arly rate when complete year is available: $13.00.

...gle copies: $1.25 each.

...scriptions, renewals, and orders for single copies ... should be addressed to the American Institute of Physics, ... 57 East 55 Street, New York 22, New York.

... change of address should be sent to the American ... Institute of Physics.

... Lancaster, Pennsylvania.

... Entered as second class matter ... 1912.

... Act of ... and February 3, 1925.

Physics
Faxon

THE JOURNAL
OF
CHEMICAL PHYSICS

VOLUME 18, NUMBER 7 JULY, 1950

Effects of Dielectric Saturation upon the Diffuse Double Layer and the Free Energy of Hydration of Ions*

DAVID C. GRAHAME
Department of Chemistry, Amherst College, Amherst, Massachusetts
(Received March 13, 1950)

The theory of the diffuse double layer is developed for the case of a dielectric of variable dielectric constant. Using experimental data by Malsch, calculations have been made of the properties of the diffuse double layer. It is found that those properties which are experimentally significant are almost unaffected by the onset of dielectric saturation. The Born equation for the free energy of hydration of ions is elaborated to include the effects of dielectric saturation, and it is found that these effects are negligible in the case of the alkali halide ions.

IN connection with our studies of the properties of the electrical double layer it has become necessary to ascertain what effects, if any, are to be attributed to the onset of dielectric saturation in the *diffuse* double layer. At a most conservative estimate the electric intensity or field strength within the diffuse double layer reaches values of 3×10^6 volts/cm, and although data are lacking as to the magnitude of the dielectric constant at such field strengths, the results of measurements made at much lower field strengths[1] leave little room for doubt that the dielectric constant falls to low values within the diffuse double layer. It will be shown below that although this conclusion is almost undoubtedly correct, the effects of dielectric saturation on the properties of the double layer are not such as to alter materially the results of calculations made on the assumption of a constant dielectric constant. In particular, the qualitative significance of results which depend upon those calculations[2] is not altered.

Previous treatments of the kinetic theory of the diffuse double layer have been carried through on the assumption that the dielectric constant of the solvent medium was a constant, independent of field strength. This was done chiefly because the dielectric constant was not known as a function of field strength, but also, perhaps, because the mathematical difficulties were sufficiently troublesome even without this added complication. As it turns out, however, the added complication is purely arithmetical, which is to say that whereas the numerical computations are rendered more difficult, the mathematical problem is unaltered except for changes in the functions to be integrated. Since any function can be integrated by numerical means if not otherwise, it will be assumed in the next section that all necessary integrations are possible. In the same way it will be assumed that the elimination of a given constant between two not inconsistent equations is always possible, at least in the types of equations with which we shall have to deal.

I. THE MATHEMATICAL PROBLEM

This section deals with the general problem of solving the basic differential equation of the diffuse double layer where the dielectric constant is regarded as an unspecified function of the field strength. A discussion of the analogous problem where the dielectric constant is a true constant has already been presented by the author,[2] and in order to save space, only brief explanations will be given of points treated in detail there. As much as possible, the nomenclature will also be the same.

The fundamental differential equation to be solved is the Poisson equation in one dimension,

$$d^2\psi/dx^2 = -4\pi\rho/DD_0, \qquad (1)$$

where ψ is the electrical potential at a point of charge

* The present work has been carried out in connection with a project supported by the Research Corporation and by the ONR.
[1] Malsch, Physik. Zeits. **29**, 770 (1928); *ibid.* **30**, 837 (1929).
[2] Grahame, Chem. Rev. **41**, 441 (1947). See especially pp. 470–487.

density ρ and x is a distance measured normal to the interface, increasing as one moves from the interface into the electrolytic solution. D is the *differential* dielectric constant, to be called the dielectric *coefficient*, and represents the rate of change of the electric displacement with the electric intensity.[3] D_0 is a quantity termed by the author the diabattivity, equal to $10^9/c^2 = 1.1128\times10^{-12}$ coulomb-volt^{-1}-cm^{-1}, and introduced[2] in order to avoid the difficulties which otherwise attend efforts to express the dielectric constant in units suitable for calculation.

If D were a constant, Eq. (1) could be integrated from a definite value of x to infinity (the interior of the solution) to give

$$d\psi/dx = 4\pi\eta/DD_0, \tag{a}$$

where η is defined by the relation,

$$\eta = \int_x^\infty \rho dx, \tag{2}$$

and is called the *surface* charge density at the plane to which $d\psi/dx$ refers. It will be seen that η is the total charge contained in a column of solution of unit cross section and extending from the plane in question into the interior of the solution, where the charge density ρ is zero.

Equation (a) obviously may not be employed over a region of variable dielectric coefficient. In that case the counterpart of Eq. (a), obtained by integrating Eq. (1), becomes

$$\int_0^{s^0} Dds = 4\pi\eta^d/D_0, \tag{3}$$

where s has been written for the field strength, $d\psi/dx$. s^0 is the value of s at the limit of integration, now taken to be the outer Helmholtz plane.[2] This latter is defined as the plane of closest approach of the centers of the cations to the surface. The anions can in general come closer, it is believed, but the equations to be developed below are valid only in those regions to which all ionic types have access without energy barriers other than Coulombic.

The superscript d in η^d refers to the diffuse double layer and indicates that η^d is the charge per unit area in the entire diffuse double layer, starting from the outer Helmholtz plane.

One interesting conclusion can be drawn from Eq. (3). For a given value of η^d the limiting value of the field strength, s^0, is independent of the concentration of the solution. Since it is found in experiments on the double layer that η^d reaches nearly the same upper limit (of about 26 μcoulomb/cm^2) at all concentrations, this means that there is also a fairly definite upper limit to the field strengths which may be encountered within the diffuse double layer. According to the tables to be presented, this upper limit probably amounts to about 6×10^6 volts/cm, at which field strength the dielectric coefficient of water is presumed to have dropped to about 27. Both of these values are quite uncertain, but it will turn out that they are also comparatively unimportant.

Further integration of Eq. (3) requires a knowledge of η^d as a function of x, and this cannot be had without introducing a new basic assumption. For this purpose one uses the Boltzmann equation and proceeds exactly as in the classical case (i.e., where D is a constant) to find the relation[2]

$$\rho = \sum n_{0i} z_i \epsilon \exp(-z_i\epsilon\psi/kT), \tag{4}$$

where n_{0i} is the number of ions of type i per unit of volume in the interior of the solution, z_i is their "valence," including sign, ϵ is the unit electronic charge, and k is Boltzmann's constant. The summation extends over all ionic species in the solution.

Introducing into Eq. (1) the identity

$$\frac{1}{2}\frac{d}{d\psi}\left(\frac{d\psi}{dx}\right)^2 = \frac{d^2\psi}{dx^2}, \tag{5}$$

one has

$$Dds^2 = -\frac{8\pi\rho}{D_0}d\psi \tag{6}$$

or through Eq. (4) after integration

$$\int_0^{s^0} Dds^2 = \frac{8\pi kT}{D_0}\sum n_{0i}[\exp(-z_i\epsilon\psi^0/kT) - 1]. \tag{7}$$

Here the quantity ψ^0 is the potential of the outer Helmholtz plane measured relative to the interior of the solution.

Elimination of s^0 between Eqs. (3) and (7) gives η^d as a function of ψ^0. As explained above, this elimination can always be done numerically if not otherwise. Supposing this problem solved, let η^d be the *abc* function of ψ^0,

$$\eta^d = abc(\psi^0). \tag{8}$$

The differential capacity of the diffuse double layer, C^d, is defined by the relation

$$C^d = d\eta^d/d\psi^0 \tag{9}$$

and can in principle be evaluated by differentiation of Eq. (8). Unless this latter is a known function, however, it will usually be easier to find the differential capacity as the product of $d\eta^d/ds$ and $ds/d\psi^0$, using Eqs. (3) and (7) as follows:

$$d\eta^d/ds = DD_0/4\pi$$

$$ds/d\psi^0 = -\frac{4\pi\epsilon}{DD_0 s^0}\sum n_{0i} z_i \exp(-z_i\epsilon\psi^0/kT)$$

$$C^d = d\eta^d/d\psi^0 = -(\epsilon/s^0)\sum n_{0i} z_i \exp(-z_i\epsilon\psi^0/kT). \tag{10}$$

[3] P. Debye, *Polar Molecules* (Chemical Catalog Company, Inc., New York, 1929). See especially p. 110 *et seq.*

Because of the appearance in this equation of the quantity s^0, the evaluation of C^d must be preceded by the solution of Eq. (7).

For symmetrical valence types Eqs. (4), (7), and (10) take on the simpler forms:

$$\rho = -2n_0 z\epsilon \sinh z\epsilon\psi^0/kT \tag{4'}$$

$$\int_0^{s^0} Dds^2 = \frac{32\pi kTn_0}{D_0} \sinh^2 \frac{z\epsilon\psi^0}{2kT} \tag{7'}$$

$$C^d = d\eta^d/d\psi^0 = \frac{2z\epsilon n_0}{s^0} \sinh \frac{z\epsilon\psi^0}{kT}. \tag{10'}$$

In order to find ψ as a function of x it is convenient to write Eq. (3) in the form

$$s = bcd(\eta) \tag{11}$$

where the *bcd* function is defined by the equation itself in conjunction with Eq. (3). Strictly speaking, the s in this equation is neither s as originally defined nor s^0, the value of s at the outer Helmholtz plane. It is the limit of integration of the left-hand member of Eq. (3) when the integration extends from the interior of the solution to some arbitrarily selected plane, not closer to the interface than the outer Helmholtz plane. Then η in Eq. (11) is the corresponding value of the surface charge density.

Without the superscripts Eq. (8) could have been written

$$\eta = abc(\psi) \tag{8'}$$

in which form it can be combined with Eq. (11) to yield

$$\frac{d\psi}{s} = \frac{d\psi}{bcd(abc(\psi))} = dx. \tag{12}$$

Equation (12) can obviously be integrated to give ψ as a function of x. The constant of integration is essentially arbitrary, but is conveniently chosen to give the same values of x as the classical theory at sufficiently small values of ψ.

Finally it is desired to find $\eta_+{}^d$ and $\eta_-{}^d$, the contributions of cations and of anions separately to the charge of the diffuse double layer. These are defined by the equations

$$\eta_i{}^d = \int (\rho_i - n_{0i} z_i \epsilon) dx, \tag{13}$$

where ρ_i, standing for either ρ_+ or ρ_-, is the charge density of the corresponding ion. It is given by the Boltzmann equation as

$$\rho_i = n_{0i} z_i \epsilon \exp(-z_i \epsilon\psi/kT). \tag{14}$$

Substituting this into Eq. (13) gives

$$\eta_i{}^d = n_{0i} z_i \epsilon \int [\exp(-z_i \epsilon\psi/kT) - 1] dx \tag{15}$$

or from Eq. (12)

$$\eta_i{}^d = n_{0i} z_i \epsilon \int [\exp(-z_i \epsilon\psi/kT) - 1] \frac{d\psi}{bcd[abc(\psi)]}. \tag{16}$$

This completes the formal solution of the mathematical problem stated at the beginning of this section. Some of these equations are particularized and solved more explicitly in Section III.

II. THE DIELECTRIC COEFFICIENT OF WATER AS A FUNCTION OF FIELD STRENGTH

Experimental data are not yet available for the evaluation of the dielectric coefficient of water at the very high field strengths believed to be present in the diffuse double layer. The only theory so far proposed is that of Debye[3,4] and is based upon the Mosotti hypothesis, which is admittedly not applicable to so polar a liquid as water. Malsch has measured the dielectric coefficient of a number of liquids at field strengths up to a mean value of 250,000 volts/cm and has verified that the coefficient falls off as the square of the field strength, as required by the theory.[5]

At much higher field strengths than those investigated by Malsch the dielectric coefficient must approach a limiting value similar to that of non-polar liquids at zero field strength. Debye[3] and Webb[6] have used the value 3 for this purpose in a similar application, and the same will be done here. Fortunately any small value could be used with no significant change in the results to be obtained.

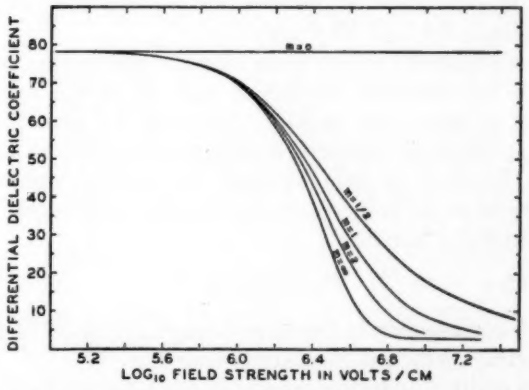

FIG. 1. Differential dielectric coefficient of water as a function of field strength where $b = 1.2 \times 10^{-13}$ cm²/volt² and m is the parameter in Eq. (17).

[4] P. Debye, Handb. d. Radiologie **VI**, p. 754.

[5] To be sure, the observable effects for water were so small that it was impossible to assert unequivocally that the field strength entered as the second power. But since it did so in every other case studied, and since the theoretical basis for expecting this behavior is fairly direct, it seems fair to conclude that at low field strengths, water behaves qualitatively like the other dielectrics studied. It may be mentioned in passing that the method of treating his data used by Malsch yields *differential* dielectric coefficients, or approximately so. The evaluation of the constant b depends critically upon this fact.

[6] J. Webb, J. Am. Chem. Soc. **48**, 2589 (1926).

TABLE I. Potential, ψ^0, of the outer Helmholtz plane as a function of η^d, the charge of the diffuse double layer at 25°C, where $b=1.2\times10^{-13}$ cm²/volt², and $m=0$, $\frac{1}{2}$, 1, 2, or ∞.

η^d μcoulomb/cm²	Tenth-normal aqueous solution of 1:1 electrolyte ψ^0 in millivolts				
	$m=0$	$m=\frac{1}{2}$	$m=1$	$m=2$	$m=\infty$
1	13.67	13.67	13.67	13.67	13.67
2	26.48	26.50	26.51	26.51	26.54
4	48.03	48.14	48.16	48.16	48.16
6	64.60	64.90	64.91	64.93	64.94
8	77.61	78.19	78.19	78.19	78.26
10	88.20	89.16	89.16	89.22	89.27
12	97.06	98.47	98.60	98.64	98.71
14	104.7	106.6	106.8	106.9	106.9
16	111.3	113.8	114.2	114.4	114.9
18	117.2	120.4	120.9	121.6	122.9
20	122.6	126.4	127.4	128.4	133.2
22	127.4	132.1	133.5	135.6	146.2
24	131.8	137.3	139.4	143.6	158.4
26	135.9	142.3	145.4	153.0	168.8

A family of functions having the desired characteristics is given by

$$D=\frac{a}{[1+(b/m)s^2]^m}+c, \tag{17}$$

where b is a parameter determined by experiment, $c=3$ as discussed above, and $a=\mathbf{D}-c$, where $\mathbf{D}$ is the ordinary dielectric constant at zero field strength. The coefficient of s^2 has been written as b/m because this makes it possible to evaluate b from experiment in advance of any decision concerning the best value of m. (In the series expansion of Eq. (17), m does not enter until the term in s^4, which means that it can be neglected at field strengths where the effect of the constant b can be ascertained experimentally.) From the results of Malsch, $b=1.2\times10^{-13}$ cm²/volt².

The parameter m has to do with the abruptness with which the dielectric coefficient falls off in the region where it falls most rapidly. This may be seen from Fig. 1, where the dielectric coefficient of water is plotted as a function of field strength for several assumed values of m. As m increases, the function approaches in the limit the function

$$D=ae^{-bs^2}+c, \tag{18}$$

which corresponds to the most abrupt falling off of the dielectric coefficient compatible with Eq. (17).

No really convincing argument can be given for preferring one value of m to another except that very large values ($m>2$) can be excluded on the basis of experimental evidence to be presented below. Very small values would correspond to a very early breakdown of the square-of-the-field-strength law, which seems physically improbable. In any case, it will turn out that the particular value of m is of minor consequence as far as the main purpose of the calculation is concerned. Calculations have been made for m-values of $\frac{1}{2}$, 1, 2, and ∞. The classical calculation (constant dielectric coefficient) corresponds to $m=0$ and will be so designated in the tables.

As a sort of mean of the values of m which may be considered likely, the equations will be derived for the case where $m=\frac{1}{2}$. This may be regarded as the most probable value of m in the present state of knowledge, but fortunately the choice is not at all critical, as the results of the tables to be presented will show.

III. THEORY OF THE DIFFUSE DOUBLE LAYER

Setting $m=\frac{1}{2}$ gives for the variation of dielectric coefficient with field strength

$$D=\frac{a}{(1+2bs^2)^{\frac{1}{2}}}+c. \tag{19}$$

Introducing this into Eq. (7) and integrating gives

$$\frac{a}{b}(2bs^2+1)^{\frac{1}{2}}-\frac{a}{b}+cs^2 = \frac{8\pi kT}{D_0}\sum n_{0i}[\exp(-z_i\epsilon\psi^0/kT)-1], \tag{20}$$

For electrolytes of symmetrical valence type this reduces to the form

$$\frac{a}{b}(2bs^2+1)^{\frac{1}{2}}-\frac{a}{b}+cs^2=\frac{32\pi kTn_0}{D_0}\sinh^2\frac{z\epsilon\psi^0}{2kT}. \tag{21}$$

In these equations and in those which follow, the superscript is omitted from s^0, it being sufficiently clear what is meant without it.

Introducing Eq. (19) into Eq. (3) gives, after integration,

$$\frac{a}{(2b)^{\frac{1}{2}}}\ln(s(2b)^{\frac{1}{2}}+(2bs^2+1)^{\frac{1}{2}})+cs=4\pi\eta^d/D_0. \tag{22}$$

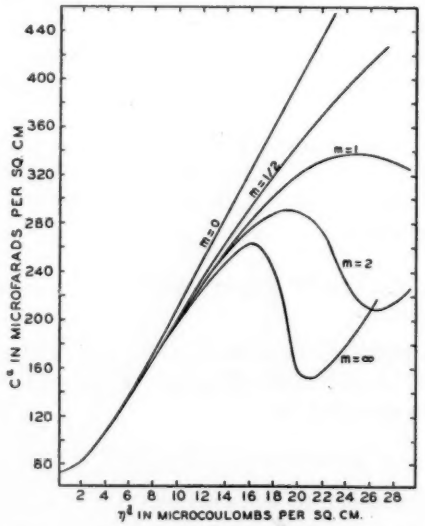

FIG. 2. Differential capacity of the diffuse double layer *vs.* charge on the diffuse double layer for 1:1 tenth-normal electrolytes in water at 25°C.

TABLE II. Field strength, s^0, at the outer Helmholtz plane of the diffuse double layer as a function of η^d, the charge of the diffuse double layer at 25°C, where $b=1.2\times10^{-13}$ cm²/volt² and $m=0, \frac{1}{2}, 1, 2,$ or ∞.

η^d μcoulomb/cm²	Tenth-normal aqueous solution of 1:1 electrolyte s^0 in megavolts/cm $m=0$	$m=\frac{1}{2}$	$m=1$	$m=2$	$m=\infty$
1	0.1438	0.1440	0.1440	0.1440	0.1440
2	0.2878	0.2889	0.2889	0.2889	0.2890
4	0.575	0.583	0.583	0.583	0.583
6	0.863	0.888	0.889	0.889	0.890
8	1.151	1.210	1.212	1.213	1.217
10	1.439	1.555	1.561	1.570	1.578
12	1.726	1.929	1.955	1.970	1.992
14	2.01	2.34	2.40	2.44	2.50
16	2.30	2.79	2.91	3.02	3.23
18	2.59	3.29	3.51	3.78	4.71
20	2.88	3.85	4.28	4.93	10.92
22	3.16	4.47	5.24	6.96	18.44
24	3.45	5.16	6.49	11.11	26.0
26	3.74	5.94	8.23	17.58	33.5

TABLE III. Dielectric coefficient at the outer Helmholtz plane of the diffuse double layer as a function of η^d, the charge of the diffuse double layer at 25°C, where $b=1.2\times10^{-13}$ cm²/volt² and $m=0, \frac{1}{2}, 1, 2,$ or ∞.

η^d μcoulomb/cm²	Tenth-normal aqueous solution of 1:1 electrolyte dielectric coefficient $m=0$	$m=\frac{1}{2}$	$m=1$	$m=2$	$m=\infty$
1	78.49	78.30	78.30	78.30	78.30
2	78.49	77.75	77.75	77.74	77.74
4	78.49	75.59	75.53	75.50	75.47
6	78.49	72.22	71.94	71.80	71.66
8	78.49	67.94	67.18	66.72	66.21
10	78.49	63.05	61.41	60.28	58.98
12	78.49	57.87	54.76	52.66	49.86
14	78.49	52.64	47.71	44.02	38.95
16	78.49	47.58	40.44	34.62	24.75
18	78.49	42.80	33.41	24.78	8.08
20	78.49	38.39	26.61	15.86	3.00
22	78.49	34.36	20.58	7.96	3.00
24	78.49	30.75	15.47	4.09	3.00
26	78.49	27.53	11.27	3.20	3.00

In conjunction with Eq. (20) or (21), this equation makes it possible to compute ψ^0 and η^d as functions, one of the other, or of s. The differential capacity may now be found from Eqs. (10) or (10′).

When $m=\infty$, that is, using Eq. (18) instead of Eq. (19) the corresponding equations become

$$\frac{a}{b}(1-e^{-bs^2})+cs^2=\frac{8\pi kT}{D_0}\sum n_{0i}[\exp(-z_i\epsilon\psi^0/kT)-1], \quad (23)$$

$$\frac{a}{b}(1-e^{-bs^2})+cs^2=\frac{32\pi kTn_0}{D_0}\sinh^2\frac{z\epsilon\psi^0}{2kT}, \quad (24)$$

$$\frac{4\pi\eta^d}{D_0}=\frac{a}{2}-(\pi/b)^{\frac{1}{2}}H(b^{\frac{1}{2}}s)+cs, \quad (25)$$

where $H(w)$ is the error integral defined by

$$H(w)=\frac{2}{\pi}\int_0^w e^{-v^2}dv.$$

Equation (24), like Eq. (21), is restricted to electrolytes of symmetrical valence type.

The most significant comparison which can be made of the effect of one's choice of m upon the predicted properties of the diffuse double layer is that obtained by comparing values of ψ^0 at a given value of η^d. Since η^d never goes beyond about 26 μcoulomb/cm², it is not necessary to consider values larger than this. For a tenth-normal solution of a 1:1 electrolyte, Table I presents the results of calculations of ψ^0 obtained by assuming values of m ranging from $m=0$ (the classical case) to $m=\infty$ (Eq. (18)). Except for the values at $m=\infty$, the extreme differences in ψ^0 amount to no more than 13 percent. Over the range of values of η^d which are of greatest interest, the differences are so small that it would not usually be worth while taking them into consideration at all, and this conclusion holds even when $m=\infty$. Experimental considerations will be adduced to show that the value of m probably does not exceed 2, however.

A few calculations have been made at other concentrations and for other electrolyte types than those shown in Table I. The results of these calculations show no new features in these cases, and lead to the conclusion that the results deduced above are generally valid.

The values of the maximum field strength, s or s^0, are much more sensitive than is ψ^0 to one's choice of m, and the same is true of the values of the dielectric coefficient in the outer Helmholtz plane. These facts are shown in Tables II and III. The significance of these results is that the uncertainty in the value of m affects very greatly the somewhat hypothetical properties of the solvent in the outer Helmholtz plane, but is of almost negligible effect upon observable properties such as the surface charge density.

The variation of potential with distance has been calculated from Eq. (12) taking $m=\infty$. Even for this extreme case, the results are so much like the classical case that it has not seemed worth while reporting them in detail. For lesser values of m, one may presumably use the classical method of calculation without sensible error from the neglect of the variation of dielectric coefficient with field strength.

This result makes possible a simple method of calculating $\eta_+{}^d$ and $\eta_-{}^d$. At elevated field strengths, where the classical calculation might be expected to differ from that obtained with another value of m, one or the other of the above-mentioned quantities will be small. Because the variation of ψ with x is almost the same as in the classical case, the calculation of this one by the classical theory will be entirely adequate for almost any purpose. Then the other can be obtained by difference from η^d, which is already known from Table I, for instance.

The differerential capacity C^d of the diffuse double layer is a sensitive function of m, and its behavior may

TABLE IV. Free energy of hydration of charged spheres of radius r_e.

r_e A	$-\Delta F^0$ Eq. (32) $m=2$ kcal.	$-\Delta F^0$ Eq. (32) $m=\frac{1}{2}$ kcal.	$-\Delta F^0$ Born Eq. ($m=0$) kcal.	Ion of eff. rad. $=r_e$ L-P-S[8]	$-\Delta F^0$ obs. L-P-S[8] kcal.
1.45	110.2	112.5	113.0	Li^+	114.6
1.46	109.6	111.8	112.3	F^-	113.9
1.60	100.8	102.1	102.4	none	
1.80	90.4	90.9	91.1	Na^+	89.7
1.91	85.4	85.7	85.8	Cl^-	84.2
2.05	79.7	79.9	80.0	Br^-	78.0
2.18	75.1	75.1	75.2	K^+	73.5
2.26	72.4	72.5	72.5	I^-	70.0
2.33	70.3	70.3	70.3	Rb^+	67.5
2.54	64.5	64.5	64.5	Cs^+	60.8

be used to infer something about the value of m as follows. Values of C^d calculated as a function of η^d for various values of m are shown in Fig. 2. The important feature of this figure is the sudden falling off of C^d at values of η^d which depend upon the value of m. For $m=\infty$, the effect occurs at about 19 μcoulomb/cm^2, which is well within the range of experimentally accessible values of η^d and should produce an observable effect if m is large. Since the diffuse double layer is in series with the much smaller capacity of the non-diffuse part of the double layer,[2] the expected effect is somewhat obscured, particularly since one does not know the capacity of the non-diffuse part with any certainty. However, the true capacity of the non-diffuse part can be calculated from the over-all capacity if a correct theory of the *diffuse* double layer is available. Since dielectric saturation in the diffuse double layer is not expected to produce discontinuities or irregularities in the capacity of the non-diffuse part, any theory of the diffuse double layer which leads to such irregularities at potentials where dielectric saturation sets in is ruled out. The observed fact is that the calculated capacity of the non-diffuse part of the double layer is a smooth function of potential for any value of m up to about $m=2$. This rules out larger values of m and makes smaller values somewhat more probable. If the value of b should be somewhat larger than that indicated by Malsch's results, m would have to be correspondingly lower. In any case the qualitative conclusions reached in the foregoing paragraphs will be correct if the value of b is not too greatly different from that adopted.

IV. THE FREE ENERGY OF HYDRATION OF GASEOUS IONS

It is possible to use any member of the family of Eqs. (17) to calculate the free energy of hydration of a gaseous ion, using essentially the method of Born.[7] One supposes an ion to have an effective radius r_e, within which the gradients of the field are identical whether the ion is in a dielectric medium or in vacuum. Beyond this critical radius the field strength is given by

$$s=(\lambda\epsilon)/(r^2D_0I), \tag{26}$$

where I is the *integral* dielectric coefficient of the medium, defined as the ratio of the electric displacement to the electric intensity or field strength. It is related to the differential coefficient through the equation

$$I=(1/s)\int Dds. \tag{27}$$

When $m=\frac{1}{2}$ the integral dielectric coefficient accordingly becomes

$$I=\frac{a}{u}[\ln(u+(1+u^2)^{\frac{1}{2}})+c], \tag{28}$$

where $u^2=2bs^2$.

λ in Eq. (26) is the charge on the ion (units of electronic charge) but differs from z, the valence, in that it is regarded as a variable parameter during the (hypothetical) charging or discharging of an ion. The free energy of hydration of a gaseous ion is then computed as the work required to discharge the ion in vacuum minus the work required to charge it in the dielectric medium. The former is given by

$$w_1=-\epsilon^2/rD_0. \tag{29}$$

Here r is not the effective radius of the ion but the crystal radius. To introduce the effective radius, let w_e be the work required to move the ionic charge reversibly from an ion of radius r to a sphere of radius r_e. It is unnecessary to evaluate this quantity since it cancels out of the final expression. The assumption is made, however, that its value is the same in the presence or in the absence of the dielectric medium. Recalling that w_1 is the work required to discharge the ion in vacuum, one has that

$$w_1=w_e-\epsilon^2/r_eD_0. \tag{30}$$

The work required to *charge* the ion in the dielectric medium is similarly given by

$$w_2=-w_e+\int\psi d(\lambda\epsilon) \tag{31}$$

where ψ is the potential of the sphere of radius r_e at any instant during the charging process. For univalent ions, λ varies from 0 to 1 during this process. The free energy of hydration of an ion of radius r is the sum of w_1 and w_2 and equals the free energy of hydration of a sphere of radius r_e. Per mole, this amounts to

$$\Delta F^0=-N\epsilon^2/r_eD_0+N\int\psi d(\lambda\epsilon), \tag{32}$$

ψ is a function of λ and is evaluated by the integration of sdr.

$$\psi=\int_\infty^{r_e}sdr \tag{33}$$

[7] Born, Zeits. f. Physik 1, 4 (1920). See also Webb (*loc. cit.*) and Latimer, Pitzer, and Slansky, reference 8.

s is found as a function of r through Eqs. (26) and (28) (or a corresponding equation in case m is given some value other than $\frac{1}{2}$).

This program has been carried through for $m=\frac{1}{2}$ and $m=2$, each for several values of r_e. The results are shown in Table IV along with values obtained from the Born equation ($m=0$). It is seen at once that this elaboration of the calculation to include the effect of the variation of dielectric coefficient with field strength has had almost no effect upon the results, which are practically identical with those of the simple Born equation, except possibly for Li^+ and F^- when $m=2$. Even in this case the deviation is too small to be considered significant.

Latimer, Pitzer, and Slansky[8] showed that the Born equation gave reasonably good agreement with experimental values of the free energy of hydration of the gaseous ions of the alkali halides when the effective radii of cations and anions were taken 0.85 and 0.1A, respectively, greater than their crystal radii. The results of the present calculation show that these authors were correct in assuming that the neglect of dielectric saturation effects would make no appreciable difference in their results. This was just the reverse of the assumption made by Webb,[6] who regarded dielectric saturation as a matter of such importance that it could not be neglected.

In this connection it is interesting to note that any calculation of the effect of dielectric saturation upon the free energy of hydration of the gaseous ions of the alkali halides will have the effect of reducing the absolute values of ΔF^0 for all ions, but especially of the smaller ions. This will always have the effect of worsening the fit with the experimental values, since the calculated values for the smaller ions are already too small when the adjustable parameters are chosen in such a way as to achieve a fit for the larger ions. One can therefore say with virtual certainty that the neglect of dielectric saturation effects is not the principal remaining defect of the Born equation.[9] Further improvement must probably be sought in a more refined treatment of the effective radius.

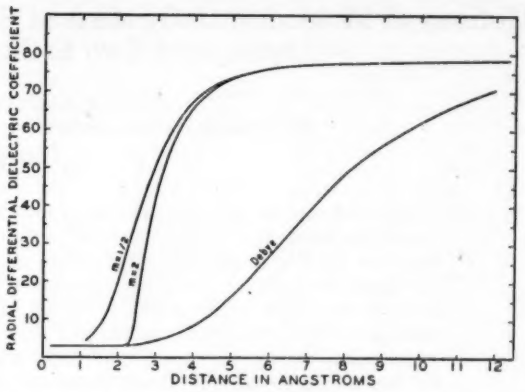

FIG. 3. Dielectric constant of water as a function of the distance from the center of a univalent ion.

In the past considerable attention has been given to the problem of calculating the dielectric constant of water in the field of an ion. Since this quantity is evaluated in the calculation discussed above, it has seemed worth while presenting the results. This is done in Fig. 3 where the radial differential dielectric coefficient of water is plotted as a function of the distance from a singly charged ion. For comparison, Debye's values (read from his curve[3] as well as possible) have been shown also. The large differences reflect the difference in the fundamental postulates upon which the calculations are based. The new curves may be said to represent an extrapolation of the experimental values of Malsch, different values of m corresponding to different methods of extrapolation.

ACKNOWLEDGMENTS

The author wishes to express his gratitude to Miss Esther Coffin and to Miss Jean Cummings for carrying out the rather laborious calculations involved in the preparation of the tables. He is also grateful to the Research Corporation and to the Office of Naval Research for financial support of the project of which this work has been a part.

[8] Latimer, Pitzer, and Slansky, J. Chem. Phys. **7**, 108 (1939).

[9] *Note added in proof.*—This conclusion also increases one's confidence in the conclusions of Section III since it indicates that dielectric saturation does not set in at field strengths as low as had previously been supposed.

Motions of Molecules in Condensed Systems. VI. The Infra-Red Spectra for Vapor, Liquid, and Two Solid Phases of Methyl Chloroform

ROBERT KARPLUS* AND RALPH S. HALFORD†
Mallinckrodt Chemical Laboratory, Harvard University, Cambridge, Massachusetts
(Received July 14, 1949)

Infra-red spectra are compared for equivalent absorbing paths of methyl chloroform (1,1,1-trichloroethane) as vapor at 25°, liquid at −28°, solid I at −40° and solid II at −55°C. The spectra differ in the respects: (1) *P-Q-R* branches observed on some bands in the vapor disappear in the condensed phases, (2) bands generally are sharpened and ones attributable to combinations are intensified by condensation, and (3) three weak bands at 830, 1288, and 1313 cm^{-1} are present in the condensed states only. Although selection rules for the vapor exclude only the torsional mode and its combinations with other, totally symmetric ones, these weak bands would yield what appears to be the unreasonably high value of 300 cm^{-1} for the torsional frequency. The fundamental frequencies are discussed briefly and it is pointed out that the spectra are almost entirely explicable upon the basis of only ten of the twelve expected ones for this molecule.

INTRODUCTION

METHYL chloroform (1,1,1-trichloroethane) is a substance whose vapor, liquid, and two solid phases are fairly easily accessible, whose infra-red spectrum had not been reported at the time we initiated this work. For these reasons it seemed to be an appropriate choice to be included in an exploratory program[1,2] of comparing spectra for equivalent absorbing paths of the same substance when it exists separately in the several different phases.

With this substance, in contrast to some of the other ones studied, we should expect few, if any, changes in the number of active frequencies to accompany the successive stages of condensation and it is gratifying that few were indeed observed. In this respect the spectra are almost identical. There was the possibility, however, that differences might be observed between spectra for the two solid phases which could be traced, in the absence of any other complications, to the onset of more or less free rotation of the molecules upon passing from the low to the high temperature form. This possibility was not realized; the two spectra in question were found to be virtually indistinguishable under the resolving power available to us. The spectra for both solid phases differ significantly, on the other hand, from the one for the vapor phase where the usual branches, attributable to unresolved rotational fine structure, are clearly displayed in several of the bands. These bands become much narrower in the condensed phases. Evidently, the ability of a fundamental molecular vibration to couple with whatever lattice modes are derived from the molecular rotations is profoundly, and perhaps similarly, affected in all condensed phases. Moreover, the effect is clearly something more than the simple pressure broadening that can be observed with a gas.

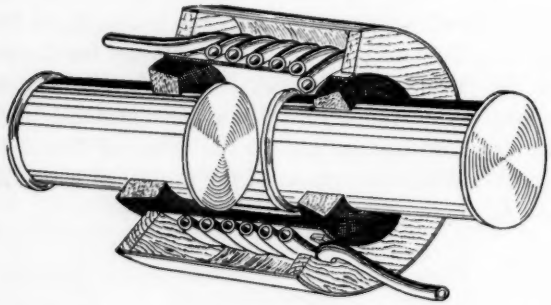

FIG. 1. Perspective of cell assembly. Constant temperature, refrigerated housing for cells containing liquid or solid.

EXPERIMENTAL METHODS

The methyl chloroform was an Eastman product, further purified by careful fractional distillation followed by four successive, partial crystallizations. In the course of these operations more than one-half of the original material was discarded. The purified liquid was stored in a dark place without desiccant. Small amounts, as needed, were distilled into the cells from a flask containing phosphorous pentoxide, whereupon their residues were discarded.

A thermostat was devised, suitable for maintaining the cell and its contents at selected temperatures above and below the melting and transition points,[3] near −32° and −50°C, respectively. The design of the spectrometer made it inconvenient to employ a refrigerated cell like the one described by Avery and Ellis[4] so, instead, a transmission cell was used. This cell, a sandwich of methyl chloroform between disks of rocksalt, was constructed, filled, and sealed as described elsewhere.[1b] It was then fixed in place at the center of a length of copper pipe. This pipe and a surrounding coil of copper

* Now at Institute for Advanced Study, Princeton, New Jersey.
† Now at Department of Chemistry, Columbia University, New York, New York.

[1] (a) R. S. Halford, J. Chem. Phys. **14**, 8 (1946); (b) R. S. Halford and O. A. Schaeffer, J. Chem. Phys. **14**, 141 (1946); (c) G. B. Carpenter and R. S. Halford, J. Chem. Phys. **15**, 96 (1947); (d) W. Keller and R. S. Halford, J. Chem. Phys. **17**, 26 (1949); (e) H. Winston and R. S. Halford, J. Chem. Phys. **17**, 607 (1949).

[2] See also (a) D. F. Hornig, J. Chem. Phys. **16**, 1063 (1948); (b) R. D. Mair and D. F. Hornig, J. Chem. Phys. **17**, 1236 (1949).

[3] Rubin, Levedahl, and Yost, J. Am. Chem. Soc. **66**, 279 (1944).

[4] W. H. Avery and C. F. Ellis J. Chem. Phys. **10**, 10 (1942).

tubing, soldered to it, are shown cutaway in Fig. 1. The ends of the pipe were closed, as shown there, with rubber stoppers holding lengths of wide glass tubing whose ends both were closed with salt windows. The central, cold region was protected further by a radiation shield shown surrounding the cooling coils. The whole assembly rested upon a stand, not shown, having extra supports for the glass tubes to insure good alignment throughout.

The desired temperature was produced, and maintained satisfactorily constant, by a double reservoir system. Supernatant fluid from a dry ice-acetone bath was circulated intermittently through a coil immersed in a second reservoir of acetone. The fluid from this second reservoir was circulated continuously through the coils surrounding the cell. The intermittent flow in the first cooling circuit was controlled automatically[1b] by a thermocouple inside the cold region, calibrated to indicate the temperature of the cell. This temperature could be maintained at any desired level above $-58°$ for some hours with the arrangement just described. The temperature distribution upon an outer face of the cell was explored and found to be uniform within one degree, the precision of our measurement.

The spectra for the liquid and both solid phases were recorded in their entirety for a cell having a well 70μ deep. Thicker and thinner layers were then examined and used to edit the first spectra. Comparisons of all three condensed phases were made always with exactly the same contents in each cell. The liquid spectrum was observed at $-28°$, the high temperature solid at $-40°$, and the low temperature solid at $-55°$C. The high temperature solid was transparent to visible radiation and could be distinguished by its appearance from the liquid for a brief time only, after the latter was freshly frozen. A few striations healed quickly to produce again a uniform specimen. The low temperature solid was, on the other hand, coarse and granular, strongly reflecting. Correction for this reflection was made by consulting the regions wherein the raw data indicated that no appreciable absorption was occurring.

The vapor spectrum was studied at room temperature in a cell of the usual design, 30 cm long. The vapor pressure was adjusted to a value calculated to given an absorbing path equivalent to the one for 70μ thickness of liquid. Higher and lower pressures were also studied.

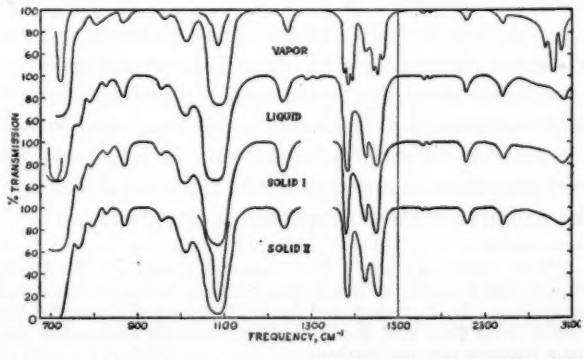

FIG. 2. Infra-red spectra for methyl chloroform (absorbing paths equivalent to 70μ thickness of liquid). Vapor at 25°, liquid at $-28°$, solid I at $-40°$ and solid II at $-55°$C.

TABLE I. The infra-red bands of methyl chloroform (intensities are in percent peak absorption).

cm^{-1}	Vapor intensity	cm^{-1}	Liquid intensity	cm^{-1}	Solid I[c] intensity	cm^{-1}	Solid II[d] intensity
720	100	713	100	713	100	710	100
766[a]	?	766[a]	?	766	?	766	?
820	13	792	?	790	?	793	?
802		830	5	826	8	825	5
866	10	868	19	869	20	868	16
960	8	955	12	955	12	954	12
1010	28	1007	35	1010	36	1010	40
1068[a]	?	1068[a]	?	?		1068[a]	?
1088	100	1084	100	1084	100	1084	100
1246	19	1238	24	1236	25	1234	18
		1289	3				
		1313	2				
1386	68	1382	86	1382	84	1382	83
1426	37	1423	60	1425	60	1425	58
1554	58	1448	83	1450	82	1450	79
1730[b]		1740[b]	?	1730[b]	?	?[b]	
1790[b]	?	1800[b]	?	1790[b]	?	?[b]	
2130	9	2130	15	2130	18	2135	14
2460	10	2460	15	2460	15	2460	14
2845	30						
2935	50	Absorption near 3000 cm^{-1}					
3010	35						

[a] Shoulder.
[b] Those bands are very weak. They showed only for the thickest samples.
[c] High temperature solid.
[d] Low temperature solid.

Spectra were recorded with the instrument described by Gershinowitz and Wilson.[5] The blank for the condensed phases was the same as for the vapor, a 30-cm length of tubing, closed with rocksalt windows and evacuated. This was appropriate because water vapor was removed from the interior of the refrigeration assembly, also 30 cm long. The blank was not refrigerated. Some additional spectra, to which we shall refer in our discussion, were observed with another instrument.

RESULTS

The spectra for the several phases are shown in Fig. 2 and summarized in Table I. These spectra are comparable below, but not above 2500 cm^{-1}.

During the period of time spanned by the original observations, the spectrometer was undergoing renovations designed to increase its effectiveness and was not always in the best of adjustment. An opportunity was found later to remeasure the vapor spectrum after the improvements in the spectrometer had been completed. The new spectrum was found to be much better resolved at the highest frequencies shown but not significantly better below 2500. Because the newly resolved frequencies are of interest in connection with the assignment of frequencies to normal modes in this molecule, and because the poor resolution in the original records would detract anyway from any comparison of the high

[5] H. Gershinowitz and E. B. Wilson, Jr., J. Chem. Phys. 6, 197 (1938).

frequency region, we have included the more recent spectrum for the vapor rather than the original one.

Two years after the original experiments had been completed, a Baird Associates[6] instrument became available in the Harvard Laboratories. The spectra for vapor and liquid were remeasured with this instrument. Earlier results for these phases were verified except for locations of two weak bands near 1300 cm^{-1}, which had been found originally in the spectra of all condensed phases; these were still absent from the vapor spectrum as before. Their new locations in the liquid phase, as well as their absence from the vapor phase, were verified by a repetition of the observations in this vicinity using again the original spectrometer. Because there was no opportunity to repeat the entire investigation, this region has been deleted from the spectra for the two solid phases.

Except as noted explicitly above, the spectra are believed to be otherwise comparable.

DISCUSSION

The molecule of methyl chloroform exemplifies the symmetry group C_{3v}. Of the twelve fundamental frequencies for the isolated molecule, five are totally symmetric (||) and allowed in both Raman and infra-red spectra, six are doubly degenerate ($\perp$) and allowed in both Raman and infra-red spectra, one other is forbidden in both of these spectra. The forbidden mode is the torsional motion; its combinations with the totally symmetric modes will also be forbidden.

In the liquid phase there will be effectively no symmetry[1a] and in the two solid phases the effective[1a] symmetry, if any, is likely to be less than that of C_{3v}. In these phases the torsional mode, and its combinations with totally symmetric modes, will no longer be forbidden. With these exceptions only, the same frequencies should be observed in all four phases. This expectation is indeed borne out in the observed spectra which show the same frequencies throughout except for three weak bands at 830, 1288, and 1313, which are observed in the condensed phases only. The latter two are probably present in the solid phases as well as the liquid, their locations only are thought to be uncertain as explained above. These three frequencies presumably involve the frequency for the torsional mode.

With the help of polarization measurements[7] for the Raman lines,[7–9] and by subsequent deduction, the strong bands at 1010, at 1386, and at 2935 cm^{-1} may be assigned to parallel-type vibrations, while those at 720, 1088, 1454, and 3010 cm^{-1} may be assigned to perpendicular vibrations. The remaining, weaker bands, with three exceptions mentioned above and another appearing at 802 in the vapor spectrum as well, can then be interpreted as overtones and combinations of these frequencies along with the low lying ones at 240($\perp$), 343(||), and 522(||), which have all been observed[7–9] in the Raman effect. It will be noted that the infra-red and Raman spectra both appear to be largely explicable upon the basis of only ten of the allowed frequencies for the isolated molecule, that the frequency for one perpendicular mode has not been definitely detected, unless it be the twice reported,[7,8] very weak Raman line at 308. This would be an appropriate frequency for the missing mode, whose motion will involve the rocking of the two end groups toward each other, and it seems rather high for the torsional mode.‡ If the frequency at 308 is accepted as one or the other of these fundamental modes, its combinations with 522 and 1010 will fall at 830 and 1318, respectively, corresponding very well with two of the four unidentified bands, leaving only two others to be explained and one low frequency fundamental to be found. A more detailed discussion leading to specific assignment of frequencies has been attempted elsewhere.[10]

Condensation is accompanied by considerable intensification of the combination bands and by the disappearance of *P-Q-R* branch structure on the bands at 1086, 1384, and 1454 cm^{-1}. These observations are consistent with those of other investigations.[1] They are attributed to the stronger interactions among the molecules in the condensed phases, accompanied perhaps by consequently greater deviations[2a] of the potential energy from simple quadratic form. In particular, the rotational coordinates are no longer ignorable ones and the rotational fine structure is therefore strongly affected. It is disappointing, if not surprising, that the band envelopes in the spectra for the two solids are so similar if free rotation of the molecules occurs, as alleged, in the high temperature solid but not in the low temperature one.

It has been brought to our attention that our spectra show, near 3000 cm^{-1}, in spite of their poor quality in this region, a consequence of condensation which may be significant in another connection. The center of absorption appears to shift from 2935 in the vapor phase to about 3010 cm^{-1} in the condensed phases. A similar phenomenon has been interpreted elsewhere to indicate the disappearance of rotational isomers upon condensation. Inasmuch as no rotational isomers are possible in methyl chloroform, it was suggested that our observations appear to cast some doubt upon the validity of the aforementioned interpretation.

[6] Baird, O'Brian, Ogden, and Lee, J. Opt. Soc. Am. **37**, 754 (1947).
[7] F. Wagner, Zeits. f. physik. Chemie **B45**, 341 (1939).
[8] K. W. F. Kohlrausch and F. Koeppl, Monats. f. Chem. **65**, 185 (1937).
[9] G. F. Hull, J. Chem. Phys. **3**, 534 (1935).

‡ *Note added in proof:* The torsional frequency in Methyl Fluoroform, a similar molecule, has just been evaluated as 230±40 by Professor B. P. Dailey and Mr. H. Minden of Columbia University from their new study of the microwave absorption spectrum (private communication).
[10] R. Karplus, dissertation, Harvard University (1948).

Low Frequency Dispersion in Ionic Crystals Containing Foreign Ions*

R. G. BRECKENRIDGE**
Laboratory for Insulation Research, Massachusetts Institute of Technology, Cambridge, Massachusetts
(Received November 28, 1949)

The anomalous electrical response at low frequencies previously observed in pure ionic crystals has been studied in ionic crystals containing foreign ions. Measurements of the dielectric loss at one kc as a function of temperature have been made on four salts with a variety of foreign ions at several concentrations. A number of loss maxima were observed which depended in height on the concentration of the foreign ion and the heat treatment of the crystal; and, in their position on the temperature scale on the nature of the salt and foreign ion. An interpretation of the results in terms of defect pairs of various types is presented.

INTRODUCTION

THE anomalous electrical response previously reported[1] in pure ionic crystals has now been studied in ionic crystals containing foreign ions. The frequency and temperature dependence of the dielectric constant and loss[1] indicated the existence of a relaxation process resembling a typical Debye dipole rotation phenomenon in crystals that had been recently grown from the melt or heated to a temperature close to the melting point and cooled rapidly. The source of the polarization in this process has been a matter of considerable interest. It was suggested[1] that in the crystals containing Schottky defects the dipoles probably consisted of an associated pair of anion and cation vacancies on adjacent sites; and, since transfer studies had indicated that only cations were mobile at low temperatures, it was assumed that the reorientation of the pair involved the motion of the positive ions. There were, however, a number of other possibilities that could not be excluded with the information at hand. Dienes[2] has recently calculated the activation energy required for the migration of a pair of vacancies through the motion of the negative ion and found it to be of the order of a few tenths of an electron volt. This energy is in the range measured and thus must be considered. As is well known, pairs are expected to be formed between divalent impurity cations and vacant cation sites. Grimley[3] has attributed the observed effect to pairs of this type. In addition, there was a possibility that the effect might be due in some unexplained way to single vacancies.

In addition to such effects in the alkali halides the nature of the lattice defects in AgCl has been a matter of interest. The presence of two loss maxima in this crystal was taken to indicate Frenkel defects since both the interstitial ion and the vacant site should be mobile. Instead of this interpretation, Grimley[3] suggests the presence of two foreign ions.

Measurements on crystals containing known concentrations of foreign ions may be expected to shed considerable light on these questions; consequently, studies have been made on crystals from a number of sources, containing a variety of foreign ions and at several concentrations. The results, besides supplying information about points that have been raised previously, provide new information about the mobilities of foreign ions in ionic crystals.

PROCEDURE

One group of samples for this investigation was prepared by coating pure crystals of *ca.* $0.020\times\frac{1}{2}\times\frac{1}{2}$ in. with a thin layer of the desired impurity and heating until the foreign salt had been distributed evenly through the volume by diffusion. This treatment, which left a clear crystal, normally required several hours at a temperature slightly (*ca.* 25°C) below the melting point. The crystal was then cooled rapidly in air. The source materials for samples prepared in this way were NaCl, AgCl, and KBr from the Harshaw Chemical Company, Cleveland, Ohio, and KCl, grown by A. von Hippel in this Laboratory. The salts added were c.p. grades of Cd, Ni, Cu, and Pb chlorides. The concentration of impurity ion was determined after the electrical measurements were completed by dissolving the crystal in a suitable electrolyte and analyzing the solution polarographically[4] using the method of standard additions. In the case of AgCl, the crystal was dissolved in KCN solution and the silver plated out. Then the Cd^{++} was determined in the residue. All concentrations are given in mole percent.

Several other crystals, including $NaCl+PbCl_2$ and a series of $NaCl+MnCl_2$, were grown at the Naval Research Laboratory, Washington, D. C., and obtained through the courtesy of the Crystal Section of that Laboratory. The composition of these crystals had also been determined polarographically at the N.R.L. The crystals containing the larger amounts of $PbCl_2$ were somewhat clouded, indicating that the lead chloride was not completely in solid solution.

The remaining crystals, including NaCl+TlCl and AgCl, had been grown previously by Professor A. von Hippel. The compositions of these were also determined using the polarograph.

* Sponsored by the ONR, the Army Signal Corps, and the Air Force under ONR Contract N5ori-07801.
** Present address: National Bureau of Standards, Washington 25, D. C.
[1] R. G. Breckenridge, J. Chem. Phys. **16**, 959 (1948).
[2] G. J. Dienes, J. Chem. Phys. **16**, 620 (1948).
[3] T. B. Grimley, J. Chem. Phys. **17**, 496 (1949).
[4] Schulman, Battey, and Jelatis, Rev. Sci. Inst. **18**, 226 (1947).

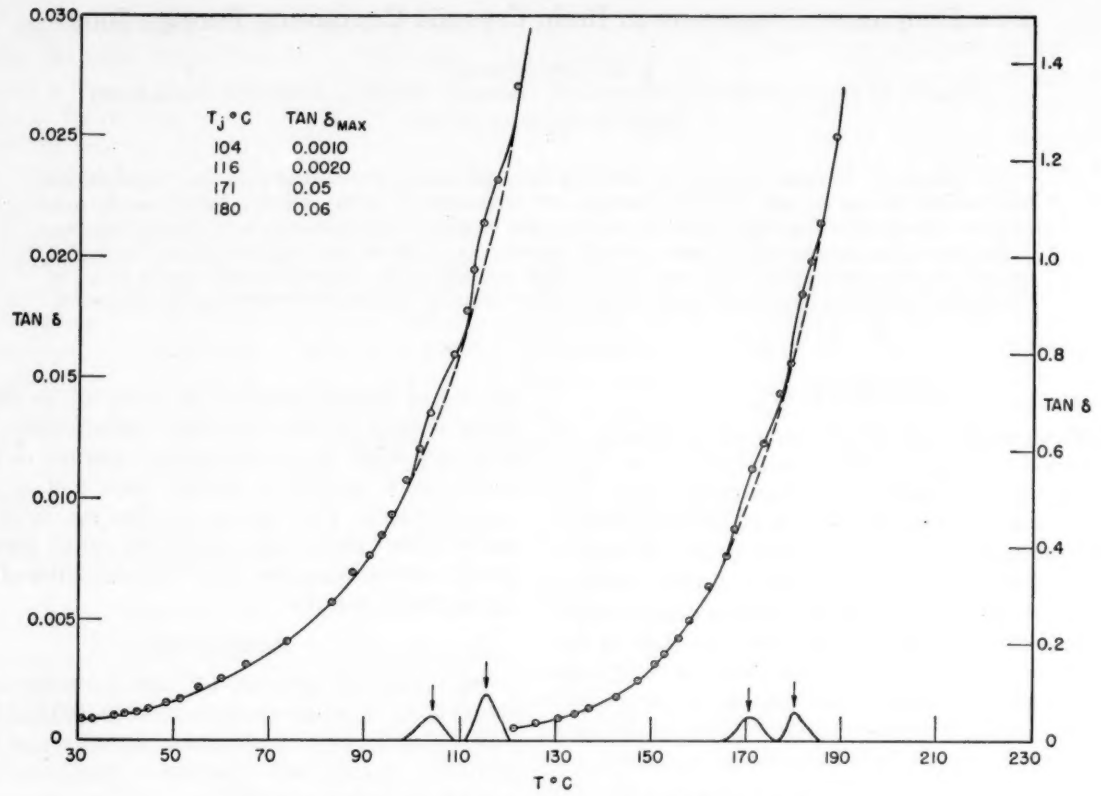

FIG. 1. Loss tangent of NaCl crystal+0.18 percent $CdCl_2$.

As mentioned previously,[1] heating to within 25°C of the melting point and quenching the crystal rapidly was needed to make the effect visible in the untreated crystals. This procedure was followed for the crystals grown some time ago, while the samples in which the impurity was introduced by heating were measured immediately afterwards. Several samples of NaCl $+PbCl_2$ from the Naval Research Laboratory were, however, measured without heat treatment, for comparison.

The electrodes and measuring equipment were those described previously.[1] All measurements were made at a fixed frequency (10^3 c.p.s.) as a function of temperature.

RESULTS

Typical results of measurements on an alkali halide containing a divalent impurity ion are given in Fig. 1 for NaCl+0.18 percent $CdCl_2$. It will be observed that four peaks are found, one at 116°C corresponding to that in the pure NaCl, another of comparable height but somewhat broader and displaced in temperature, and two considerably larger peaks (cf. change in scale) at higher temperatures. The same data are given in Fig. 2 plotted as the logarithm of the loss tangent as a function of the reciprocal of the absolute temperature. The increases in loss due to the relaxation processes are visible as deviations from straight lines; however, a single straight line cannot be used indicating a change in the type of conductivity over the range of measurement.

Similar results on NaCl with various other addition agents are shown in Fig. 3 (X percent $MnCl_2$); Fig. 4 (0.042 percent $NiCl_2$); Fig. 5 (0.01 percent $PbCl_2$, preheated); and Fig. 6 (0.035 percent $PbCl_2$, unheated). The height of the peak is obtained by subtracting the dashed portion of the smooth curve in the linear plots or, alternatively, the straight line on the semilog plots from the observed curve. The data are summarized in Table I.

The characteristics of KBr and KCl containing divalent foreign ions parallel those found for NaCl. This is illustrated in Fig. 7 (KCl+0.057 percent $CdCl_2$); Fig. 8 (KBr+0.059 percent $CdCl_2$); and Fig. 9 (KBr $+0.027$ percent $PbCl_2$). In these cases, the KCl seems to act like NaCl; while for KBr, the first additional peak appears above that of the pure crystal rather than below it (cf. Table I).

Somewhat similar results are obtained with univalent foreign ions as shown in Fig. 10 (NaCl+0.029 percent CuCl), Fig. 11 (NaCl+0.056 percent TlCl), and Fig. 12 (NaCl+0.5 percent AgCl). In these cases the Cu^+ behaves as did the other crystals but for Tl^+ and Ag^+ five peaks are found, one of which is that of the pure crystal, two at high temperatures resemble those found for the divalent impurity ions, and two additional peaks, one above and the other below that for the pure crystal appear, the lower peak being the broader one.

A still more complex situation is revealed for AgCl +0.14 percent $CdCl_2$ (Figs. 13 and 14). Here two of the maxima, those at −126°C and −155°C, are the ones previously reported for the pure material while four new loss peaks have now appeared. All these data are also summarized in Table I.

ACTIVATION ENERGIES AND POLARIZATION PROCESSES

The loss maxima may be used to determine the activation energies for the various mechanisms of polarization. A simple analysis given previously[1] showed that

$$2\pi\nu_m\tau_0=\exp(-U/kT_j) \qquad (1)$$

where ν_m is the measuring frequency, τ_0 is the time constant for the natural frequency of lattice vibrations,[1] T_j is the observed temperature for maximum loss, k is Boltzmann's constant, and U is the activation energy for the jumping process.

The values of U calculated from Eq. (1) are given in Table I in electron volts. A plot of the activation energies for various salts in NaCl as a function of the cation size, using Goldschmidt's values for the ionic radii, is shown in Fig. 15. U_1, the energy found for the polarization process in the pure crystal, is constant (average *ca.* 0.69 ev); U_4, the energy corresponding to the large peak at high temperatures increases practically linearly with the foreign ion size. In the Cu case, the added salt was $CuCl_2$, but the energy found suggests that the ion is present as Cu^+. The energy U_3 for the moderate peak, increases as the foreign ion size increases up to the value for Na^+, then it remains roughly constant at a value of 0.80 ev. The small peak U_2 at low temperatures seems to approach the value of U_1 for ion sizes close to Na^+ and to become lower as the size changes from Na^+, reaching roughly 0.60 ev for ions both much larger or smaller than Na^+.

Our primary objective is an identification of the various loss maxima observed with the appropriate process in the crystal. Let us consider briefly the situation believed to exist in the crystal. The addition of a divalent foreign ion is observed to increase the electrical conductivity in the alkali halides and AgCl markedly.[5] The interpretation given is that for each divalent cation introduced into the lattice a vacant cation site is produced to preserve electrical neutrality. This is somewhat oversimplified, since it would require a completely random distribution of the foreign ions on the cation sites. Actually there may be considerable aggregation of the foreign ions (note the cloudy NaCl +$PbCl_2$), and the heat treatments may affect the distribution appreciably. In any case, however, we may assume that, irrespective of heat treatment, a great many cation vacancies are present of which a

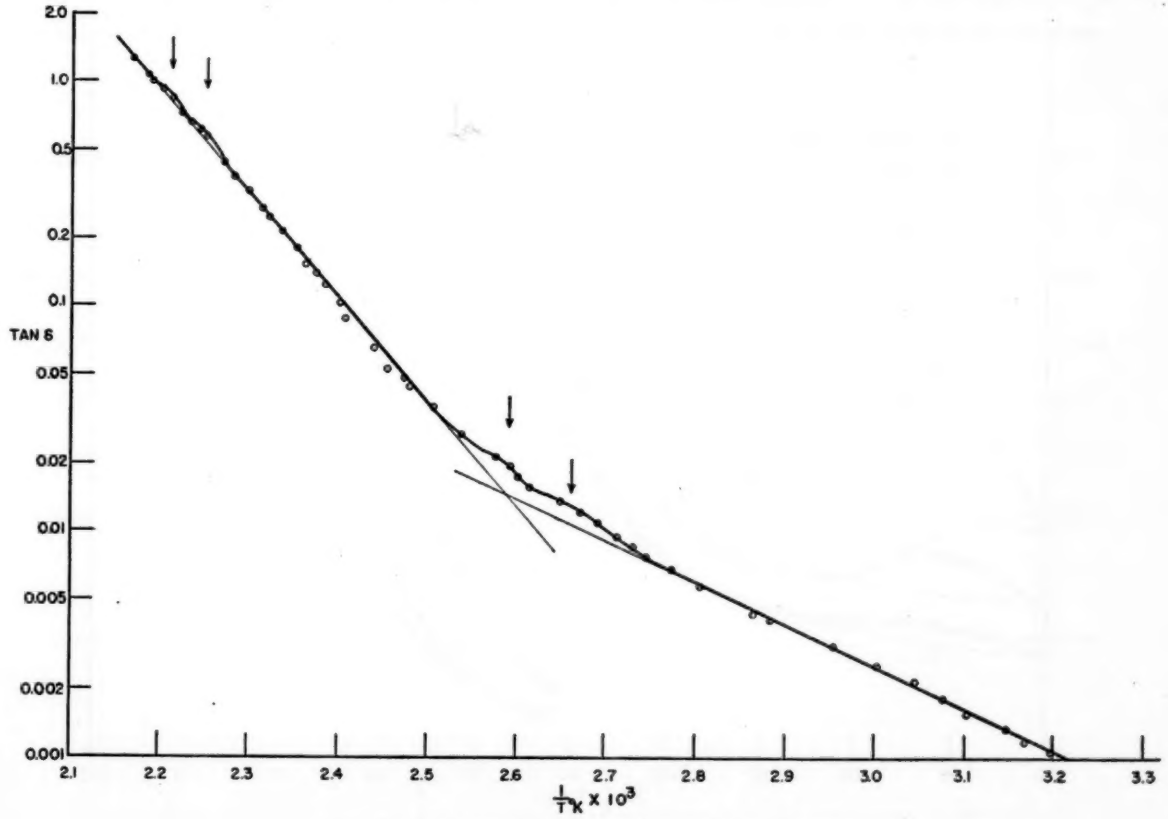

FIG. 2. Loss tangent of NaCl crystal+0.18 percent $CdCl_2$.

[5] E. Koch and C. Wagner, Zeits. phys. Chem. (B) **38**, 295 (1937).

fraction is paired with the foreign ions because of the Coulomb forces between them. On heating the crystal to a temperature close to the melting point and quenching it rapidly, a considerable number of anion vacancies are introduced as well. A fraction of these will also be paired with cation vacancies because of Coulomb attraction.[6] The number of anion vacancies will, in general, be much smaller than the number of foreign ions or cation vacancies at low temperatures. It should be noted that, in addition to the formation of pairs by electrostatic forces, elastic stresses in the lattice near a foreign ion may be partially relieved if the foreign ion is adjacent to a vacant site; thus there might be a tendency to form foreign ion-vacancy pairs even in the absence of Coulomb forces.

Of the peaks in the alkali halides containing foreign ions, a reasonable interpretation is given most readily for the peak of highest energy, U_4. We have observed that this peak is present in both the heated and unheated crystals containing divalent ions (Figs. 5 and 6); hence it is present irrespective of the anion vacancies in the crystal. The height of the peak depends on the concentration of the foreign ion (Fig. 3), and the energy depends on the nature of the foreign ion (Fig. 15), indicating a value of 0.80 ev for a cation size corresponding to Na^+. It should be noted that this is in good agreement with the value (0.77 ev) found by Mapother and Maurer[7] for the self-diffusion of radioactive sodium in NaCl in the same temperature range. Finally the peak is a large one (Figs. 1–12) indicating a large dipole moment, large numbers of pairs, or both. These facts are all readily explained if it is assumed that this peak corresponds to a place interchange of the foreign ion and an adjacent cation vacancy.

A somewhat more tentative assignment may be made for the peak next highest in energy. We may summarize the pertinent observations. The peak is large, indicating large numbers, large moment, or both (Figs. 1–12); its height depends on the foreign ion concentration (Fig. 3); and, as shown in Fig. 15, for foreign ions larger than Na^+ the energy has an almost constant value at *ca.* 0.80 ev while for ions smaller than Na^+ it decreases. This peak is also observed in the unheated $NaCl+PbCl_2$ (Fig. 6).

A reasonable explanation of all these facts may be obtained from a consideration of the configuration of ions surrounding a foreign ion-vacancy pair (Fig. 16). It will be observed that the vacancy associated with the M^{++} ion may occupy any of the 12 sites in the nearest neighbor positions without dissociation of the pair. Under the influence of the applied field a reorientation of the pair may be achieved either by a place interchange of the foreign ion and the vacant site, or by a place interchange of the vacancy and one of the normal ions on the adjoining sites. The first process we have identified with the peak of highest energy, the

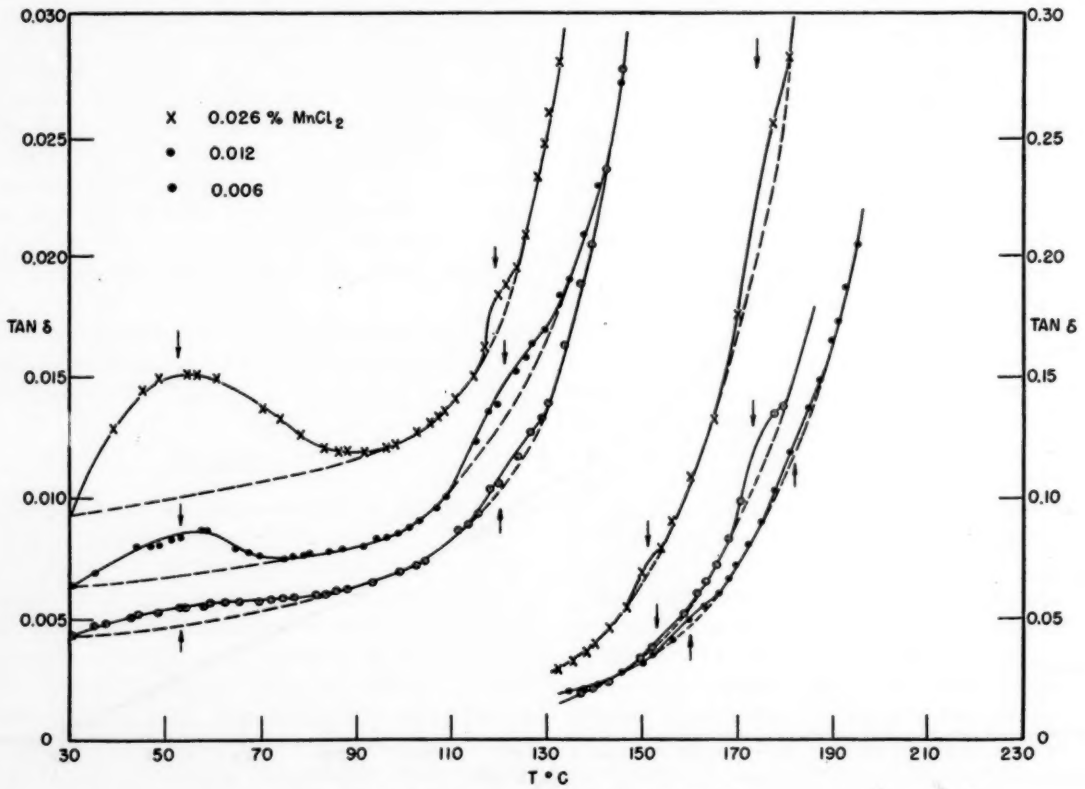

FIG. 3. Loss tangent of NaCl crystal+$MnCl_2$.

[6] F. Seitz, Rev. Mod. Phys. **18**, 384 (1946).
[7] D. Mapother and R. Maurer, Phys. Rev. **73**, 1260 (1948).

second process is suggested as the mechanism giving rise to the second peak. It will be noted that the behavior expected for such a mechanism would explain the experimental observations. The process will closely resemble self-diffusion, and, as pointed out, the value found for foreign ions whose radius is equal to or larger than Na^+ is almost constant and equal to the value observed for self-diffusion in NaCl. The number of such configurations would depend on the foreign ion concentration, and it would be expected to be large. The process should take place in unheated crystals containing divalent ions, but for univalent ions heating should be necessary to give sufficient cation vacancies to make the effect observable. Unfortunately no measurements were made on unheated samples of NaCl with monovalent impurity ions.

If this interpretation is accepted, the results would indicate a value of 0.7 ev as a reasonable estimate for the activation energy of self-diffusion in KBr since Pb^{++} has an ionic radius close to K^+. Similarly, 0.8 ev is indicated for KCl, although this may be low since Cd^{++} is appreciably smaller than K^+.

The nature of the peak found in the pure crystal may be considered next. Since there has been controversy on this point, we shall discuss the pertinent features in some detail. The results reported in this paper have apparently eliminated the possibility of the effect being due to single cation vacancies. In Fig. 3 especially, it is clear that the height of this peak is only slightly influenced by the presence of the foreign ion; yet increasing the concentration of divalent ions should increase the number of cation vacancies considerably.

Grimley's[3] assignment of this peak to pairs formed with a divalent impurity ion and a vacant cation site is also untenable for a number of reasons. The most direct evidence is the behavior with heat treatment. As stated in reference 1, the effect was observable in the Harshaw crystals which are grown from the melt in large blocks without further heat treatment, but crystals from other sources required heating to within 25°C of the melting point and rapid cooling before measurement. On the other hand, heating the small crystals to *ca.* 500°C for some time, followed by slow cooling, makes the effect unmeasurable. This behavior is anticipated from vacancies produced by the heat treatment, but is inconsistent with that observed for crystals with known impurities. In Fig. 6 we see that the unheated NaCl $+PbCl_2$ from the Naval Research Laboratories shows only a faint indication of a peak at *ca.* 120°C but on heating (Fig. 5) the peak appears.

Quantitative observation of $\tan\delta_{max}$ for known impurity content also indicates that a residual impurity is unlikely. In Fig. 6 we see that $\tan\delta_{max}=0.012$ is found for NaCl+0.035 percent $PbCl_2$ in an unheated crystal. In reference 1 a Harshaw crystal of NaCl measured without heating gave $\tan\delta_{max}=0.024$ which would correspond to at least 0.05 percent impurity. This is considerably larger than the maximum impurity present in the A.C.S. reagent grade NaCl which is the reported starting material for the crystal growth.

There is further evidence bearing on this point. If the loss maximum at 120°C is due to the reorientation of pairs of the type suggested by Grimley,[3] the value

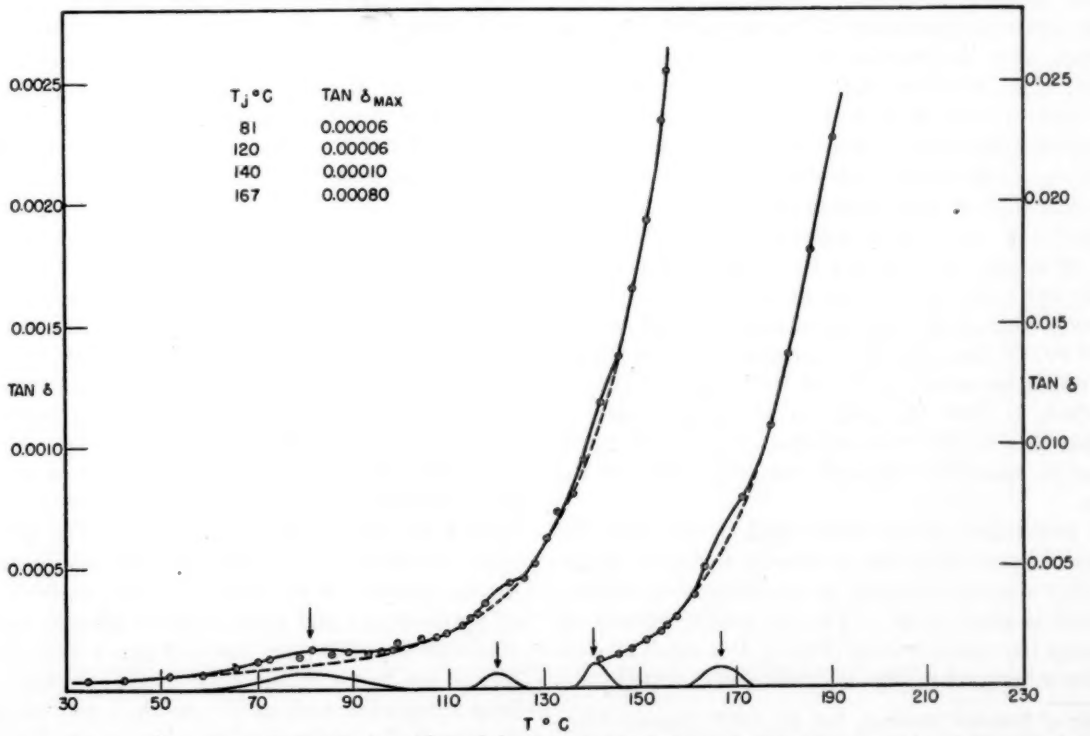

FIG. 4. Loss tangent of NaCl crystal+0.042 percent $NiCl_2$.

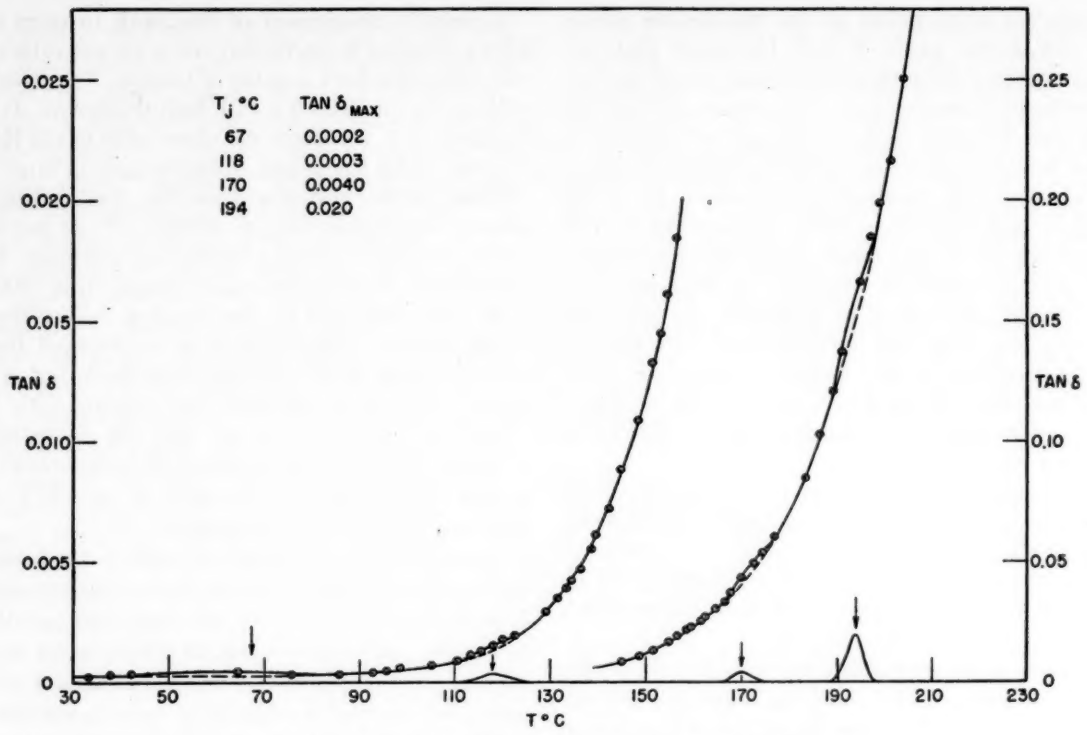

FIG. 5. Loss tangent of NaCl crystal+0.01 percent $PbCl_2$ (heated).

of $U=0.68$ ev would indicate an impossibly small ionic radius (*ca.* 0.1A) for the impurity ion (Fig. 15).

The remaining alternative is that the reorientation takes place through the motion of the negative ions. While this possibility cannot be excluded, the evidence available suggests that it is unlikely. The various energies reported previously[1] follow sequences that are consistent with the motion of the cations, e.g., KCl, 0.78 ev; KBr, 0.53 ev; KI, 0.1 ev; RbCl, 0.75 ev; RbBr, 0.58 ev; and RbI, 0.21 ev. In addition, if it is assumed that the peak is actually due to anion migration, it should be possible to observe a peak from the cation migration as well. Measurements made on NaCl, KBr, and LiF over a wide frequency range[1,8] covered values of energy from *ca.* 0.1 to 0.8 ev with evidence for only one peak. This would require that the energy for cation migrations has unreasonably small values, *ca.* 0.05 ev. On the other hand, a value $\geqslant 0.8$ ev for the anion migration would seem not unlikely. Our conclusion, then, is that the peak in the pure crystal is probably due to the reorientation of pairs of cation and anion vacancies through the migration of the cations.

The remaining rather broad peak found near the pure crystal peak may also be given a tentative assignment. Our observations may be summarized as follows: The peak is small (Figs. 1–12); its height depends on the foreign ion concentration (Fig. 3); it is much broader than the other peaks (Fig. 3), indicating a distribution of activation energies; and it appears only on heat-treating the crystal (Fig. 6).

If, again, it is assumed that because of the elastic forces a foreign ion may be more readily accommodated in the lattice at a site adjacent to a vacancy, we would expect to find foreign ions near pairs of vacancies as well, giving the configuration shown schematically in Fig. 17. It will be noted that the reorientation of the pair without dissociation may be achieved in several ways. The jumps indicated by U_2 and U_2^1 in the absence of the foreign ion would be the U_1 of the pure crystal. The presence of the foreign ion, however, may be expected to modify the energy U_1 somewhat; and U_2^1 would differ from U_2 since it would produce a slightly different configuration. Similarly, U_2^{11} involving the motion of the foreign ion should also be different since it would depend on the nature of the foreign ion.

This model accounts for the experimental observations reasonably well. Since the configuration requires pairs of vacancies formed by heat treatment, it does not occur in the unheated crystals. The number of such complexes would obviously depend on the foreign ion concentration, but the peak is small since the number of pairs is usually very small. The presence of three processes with slightly different energies accounts for the breadth of the peak. U_2, U_2^1, and U_2^{11} should all approach U_1 and tend to give a sharper peak, as is observed for Cd^{++} in NaCl (Figs. 1 and 2), if the foreign ion has a radius close to that of Na^+. A very large foreign ion such as Tl^+ in NaCl may be expected to stretch the lattice locally, allowing the Na^+ ions to

[8] *Tables of Dielectric Materials*, Vol. III, ONR Contract N5ori-78, T. O. 1, NR-074-041, Lab. Ins. Res., M. I. T., June, 1948.

TABLE I. Low frequency dispersion in ionic crystals containing foreign ions.

Salt impurity mole %		NaCl $CdCl_2$ 0.18	NaCl $MnCl_2$ 0.006	NaCl $MnCl_2$ 0.012	NaCl $MnCl_2$ 0.026	NaCl $NiCl_2$ 0.042	NaCl $PbCl_2$ 0.01	NaCl $PbCl_2$(un) 0.035	KCl $CdCl_2$ 0.057	KBr $CdCl_2$ 0.059	KBr $PbCl_2$ 0.027	KBr CuCl 0.029	NaCl TlCl 0.056	NaCl AgCl 0.5	AgCl $CdCl_2$ 0.14
T_j°C		116[a]	121[a]	121[a]	119[a]	120[a]	118[a]		165[a]	37[a]	38[a]	108[a]	111[a]	117[a]	−155[a]
		104	53	53	53	81	67		108	79	63	66	63	60	−126[a]
		171	160	153	151	140	170	179	174	134	133	136	173	165	− 92
		180	182	173	174	160	194	195	181	180	157	153	197	189	− 69
													141	125	−136
															−110
$\tan\delta_{max}\times10^4$		20	6	14	16	0.6	3		20	1	3	6	8	8	2
		10	8	16	50	0.6	2		2	2	8	6	17	5	1
		500	16	20	30	1.	40	40	24	3	36	50	400	150	550
		600	50	110	190	8.	200	80	45	24	40	180	1200	600	500
													40	16	2
															70
U ev	U_1	0.69[a]	0.70[a]	0.70[a]	0.70[a]	0.70[a]	0.70[a]		0.77[a]	0.54[a]	0.54[a]	0.68[a]	0.68[a]	0.69[a]	0.21[a]
	U_2	0.67	0.58	0.58	0.58	0.63	0.60		0.67	0.62	0.59	0.60	0.60	0.59	0.26[a]
	U_3	0.79	0.77	0.76	0.75	0.73	0.79	0.80	0.79	0.71	0.71	0.73	0.79	0.78	0.32
	U_4	0.80	0.81	0.79	0.79	0.77	0.83	0.83	0.80	0.79	0.75	0.76	0.83	0.82	0.36
	U_5												0.73	0.71	0.24
	U_6														0.28
n(No./ m^3)$\times10^{22}$	n_1	1.0	0.3	0.71	0.81	0.03	0.15		1.0	0.03	0.1	0.3	0.4	0.4	0.2
	n_2	0.49	0.3	0.75	2.1	0.03	0.09		0.09	0.07	0.3	0.2	0.74	0.2	0.1
	n_3	30.	0.9	1.1	1.6	0.05	2.3	0.5	1.2	0.1	1.5	2.6	23.	8.5	94.
	n_4	8.	0.7	1.6	2.7	0.1	3.0	0.6	0.58	0.27	0.44	9.9	72.	36.	24.
	n_5												2.	0.82	0.2
	n_6														1.
$X\times10^8$	X_1	0.44	0.1	0.31	0.35	0.01	0.07		0.62	0.02	0.07	0.1	0.2	0.2	0.1
	X_2	0.21	0.1	0.33	0.93	0.01	0.04		0.06	0.05	0.2	0.1	0.33	0.1	0.05
	X_3	15.	0.4	0.49	0.71	0.02	1.0	0.2	0.76	0.07	1.1	1.2	10.	3.8	40.
	X_4	4.	0.3	0.70	1.2	0.05	1.3	0.3	0.35	0.19	0.31	4.4	33.	16.	10.
	X_5												1.	0.36	0.1
	X_6														0.5

[a] Peak found previously (see reference 1) in the pure crystal.

move readily; while a very small ion such as Mn^{++} in NaCl would be very mobile in preference to the Na^+, thus giving a decrease in U_2 in both cases. It does not explain the fact, however, that the broad peak in KBr occurs at a slightly higher energy than that found in the pure crystal, and it is actually higher for Cd^{++} than for Pb^{++}. The explanation of this must await further investigation.

This model gives a suggestion for the existence of extra peaks in NaCl+TlCl and AgCl, since for these large ions U_2^{II} may be appreciably larger than U_2 or U_2^{I} and appear as a separate peak. In both cases, the

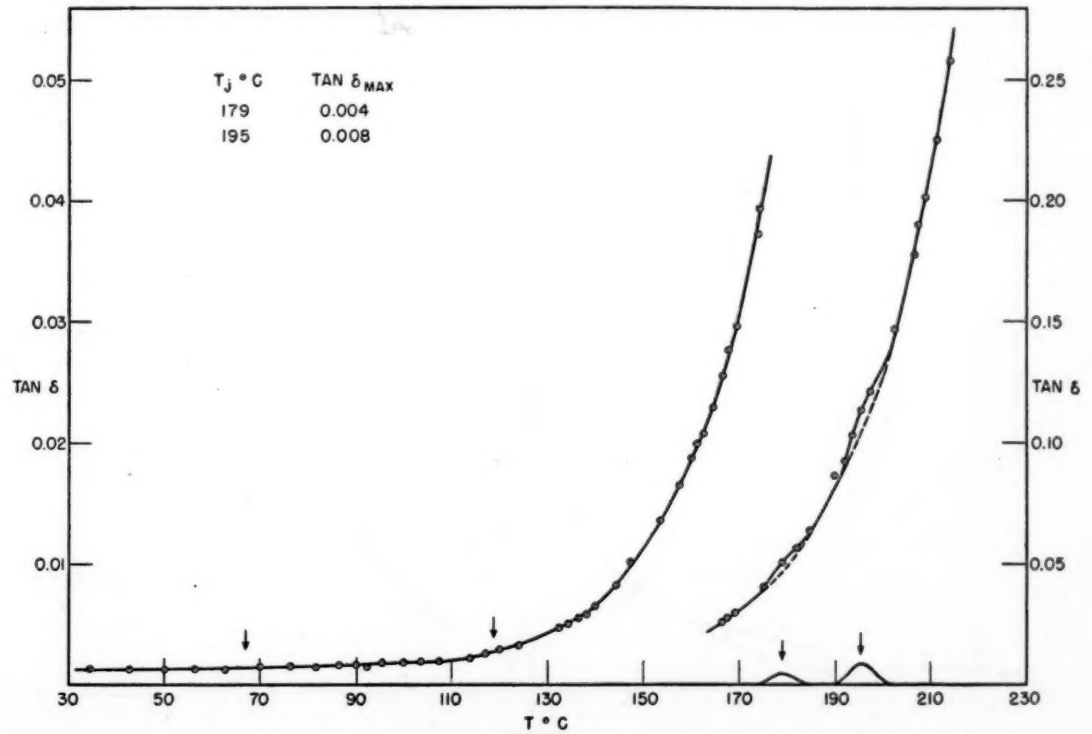

FIG. 6. Loss tangent of NaCl crystal+0.035 percent $PbCl_2$ (unheated).

fifth peak is slightly above the value of U_1 as would be expected. The rather extreme breadth of the low energy peak also suggests that in these cases U_2 and U_2^1 are appreciably different.

NUMBER OF LATTICE DEFECTS

The assignment of the various loss maxima to definite processes in the crystal allows a more detailed study to be made of the numbers of the different types of defects

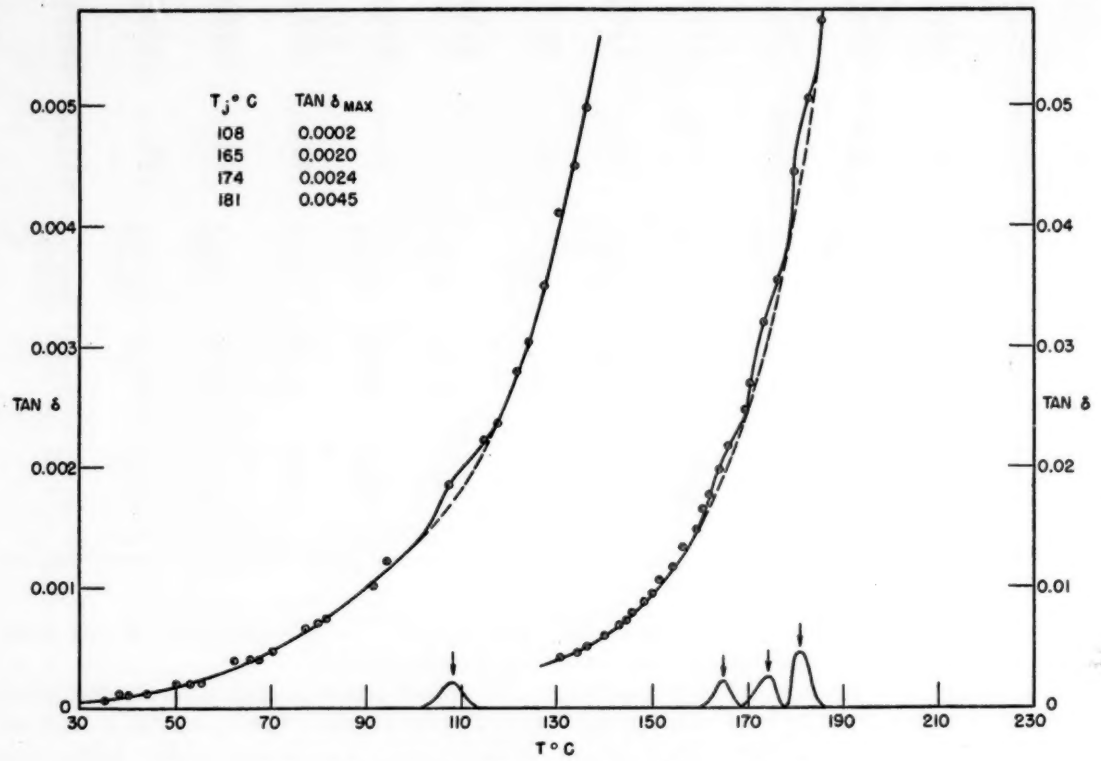

FIG. 7. Loss tangent of KCl crystal−0.057 percent $CdCl_2$.

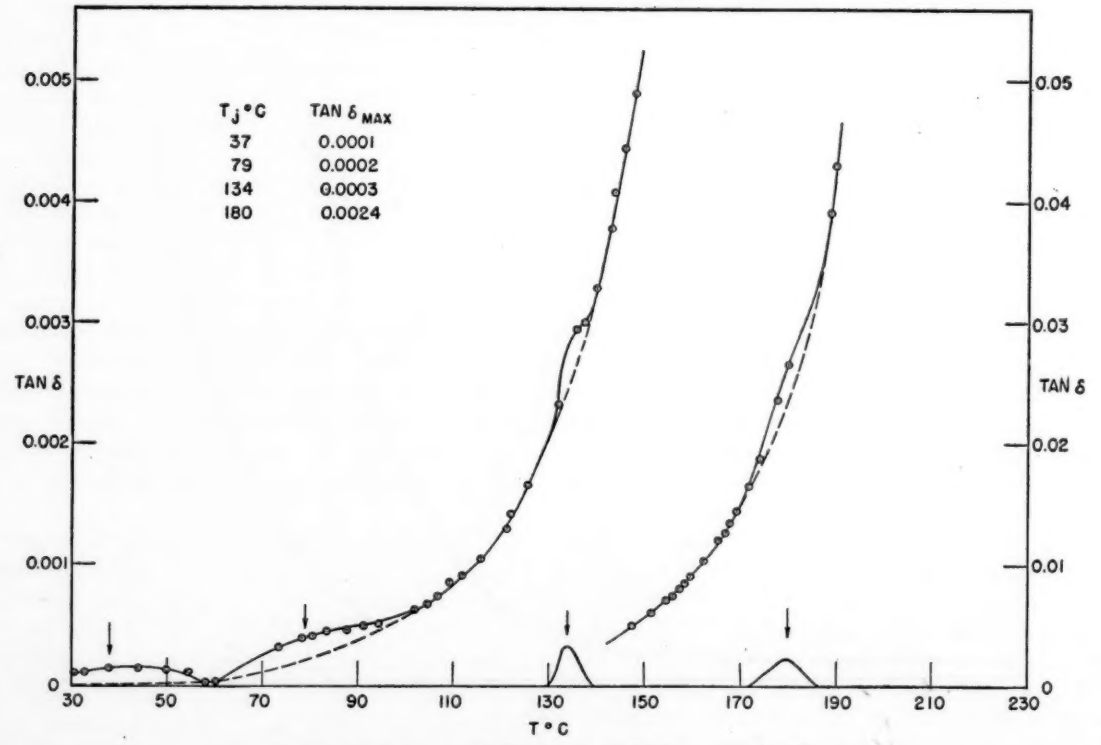

FIG. 8. Loss tangent of KBr crystal+0.059 percent $CdCl_2$.

present since the models give information about the charges involved and the distances they move. In reference 1 it was shown that if the reorientation of the pairs was described as a redistribution of the ionic charges between two potential wells under the influence of the applied field, the height of the loss peak could be related to the effective moment of the moving charges and the number present as follows:

$$\tan\delta_{max} \simeq \frac{n(Zed)^2(K'_\infty+2)^2}{18\epsilon_0 kT_j K'_\infty}, \quad (2)$$

where n is the number of polarizing units per unit

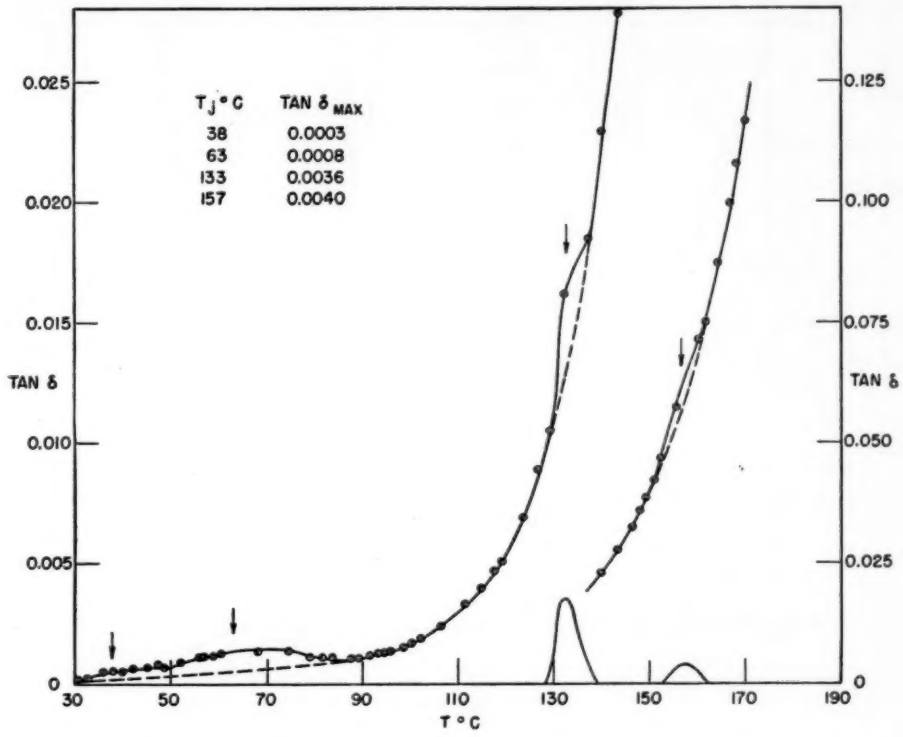

FIG. 9. Loss tangent of KBr crystal+0.027 percent $PbCl_2$.

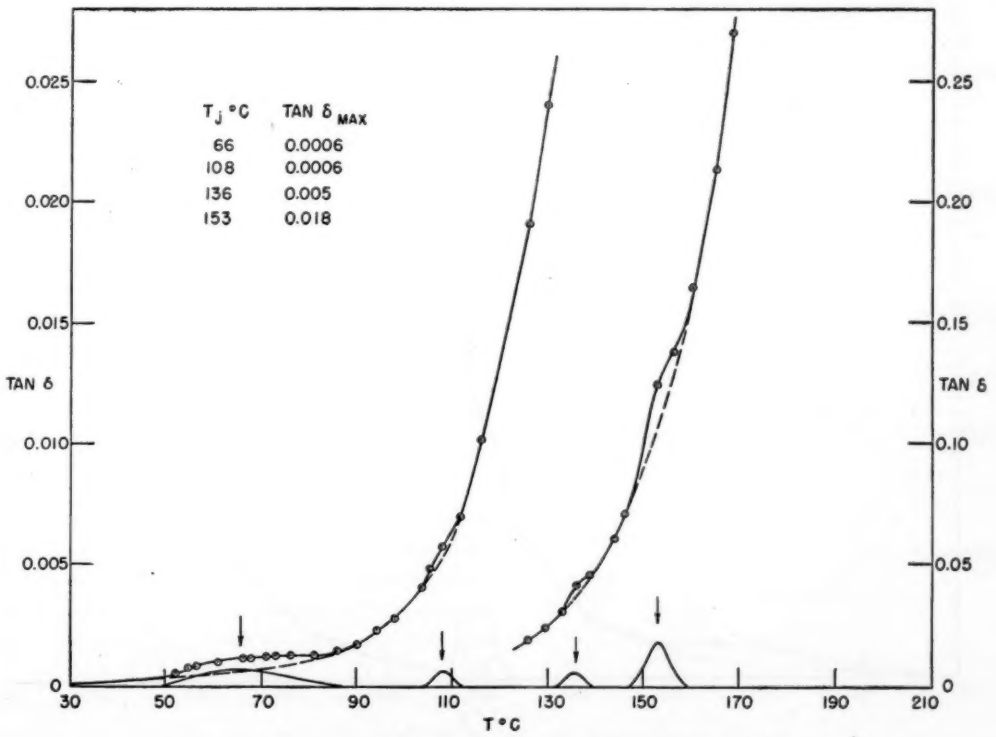

FIG. 10. Loss tangent of NaCl crystal with 0.029 percent CuCl.

volume, Z the ion valence, e the absolute value of the electronic charge, and d twice the separation of the potential wells (in reference 1, d was taken as the lattice constant a). K'_∞ is the dielectric constant at frequencies above the dispersion region, ϵ_0 is the dielectric constant of free space, and kT_j are as in Eq. (1). Rationalized m.k.s. units are used so that $\epsilon_0 = 8.865 \times 10^{-12}$ farad/m; $e = 1.59 \times 10^{-19}$ coulomb;

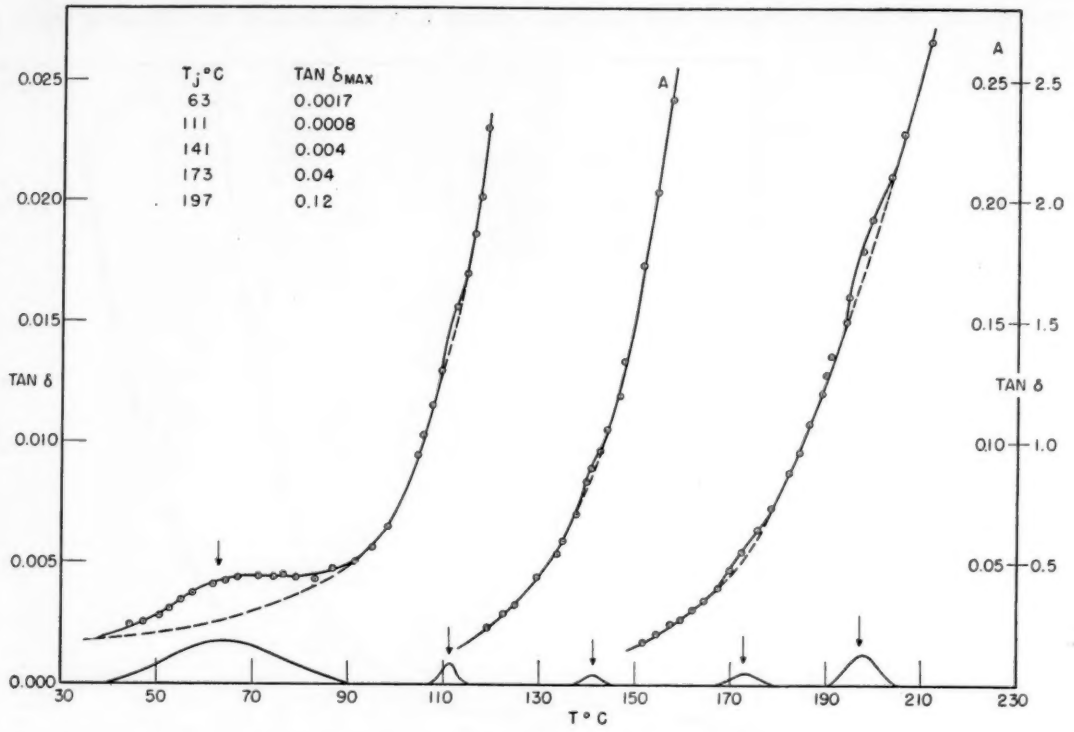

FIG. 11. Loss tangent of NaCl crystal+0.056 percent TlCl.

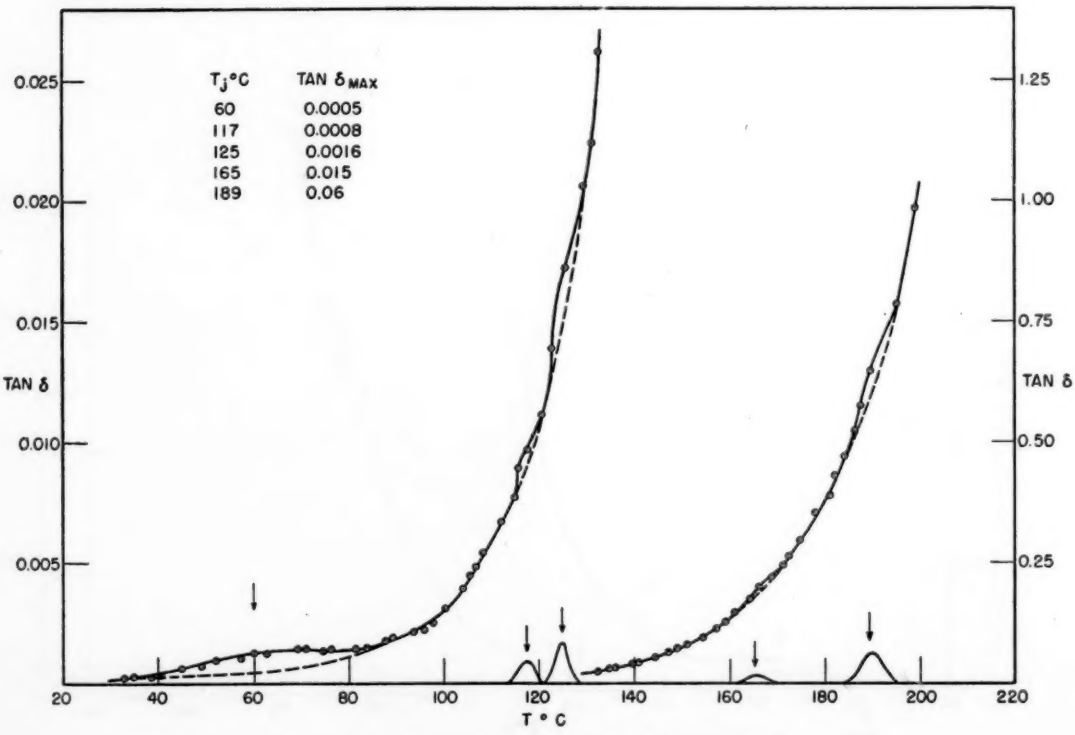

FIG. 12. Loss tangent of NaCl crystal+0.5 percent AgCl.

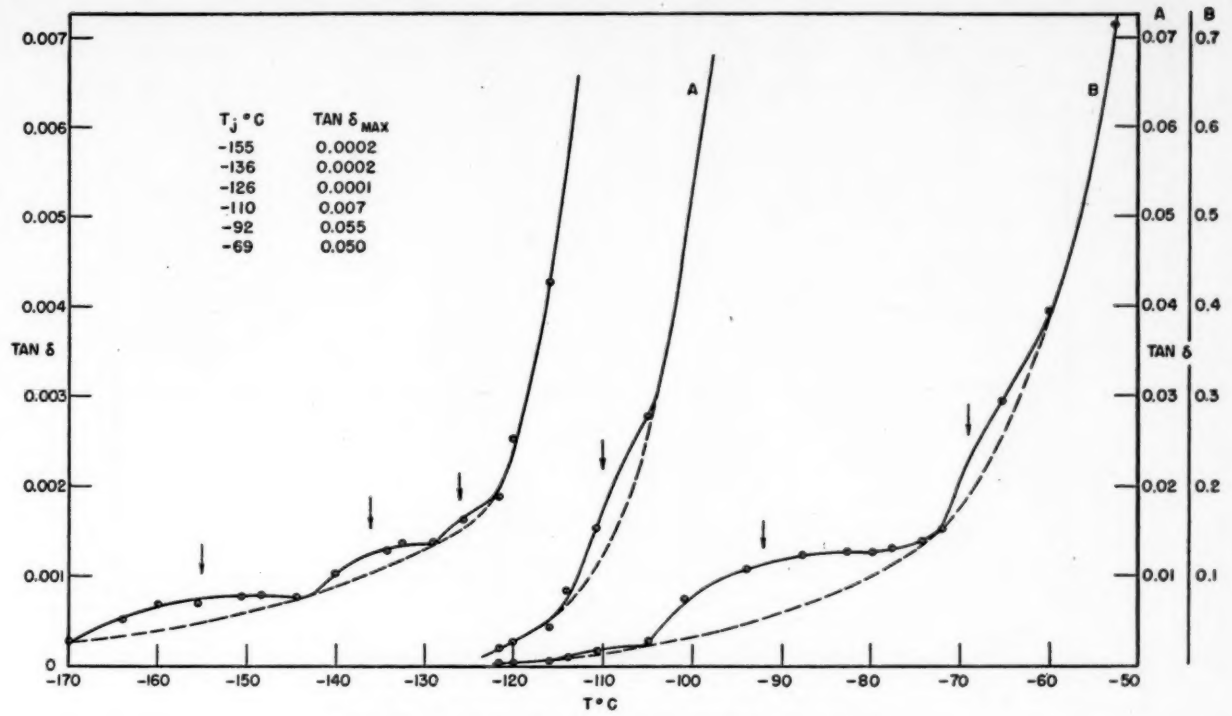

FIG. 13. Loss tangent of AgCl crystal+0.14 percent $CdCl_2$.

$k=1.38\times10^{-23}$ joule/deg.; d is in meters, and n is in number/m^3. Because an approximate expression for the internal field in a dielectric is used in deriving Eq. (2), the results are probably good only to an order of magnitude although the relative values may be more reliable.

The process we have assigned to U_4 for divalent foreign ions moves a charge $2e$ a distance $a/2$ in the field direction (Fig. 16), while U_3 moves a unit charge the same distance. For univalent foreign ion-cation vacancy pairs, both processes move unit charges a distance $a/2$ in the field direction. The number of pairs, n, computed from Eq. (2) and the mole fraction of each, x, are given in Table I.

The models suggested also give some information about the relative numbers of pairs of each type. It will be observed in Fig. 16 that there are four normal ions that may jump without dissociating the pair for each foreign ion. It is anticipated then that $n_3=4n_4$. This ratio is not observed experimentally, in general. Usually $n_4>n_3$, the larger values being observed for ions whose size differs considerably from the size of the ions in the normal lattice (e.g., Mn^{++} in NaCl, Cd^{++} in KBr). It will be noted also that the ratio n_4/n_3 increases with increasing concentration (e.g., Mn^{++} in NaCl). This suggests that there may be a considerable aggregation of foreign ion-cation vacancy pairs in larger complexes to accommodate the foreign ions in the lattice.

We have computed the number of pairs of vacancies, n_1, and the number of clusters of type n_2 on the assumption that a unit charge moves a distance $a/2$. This is

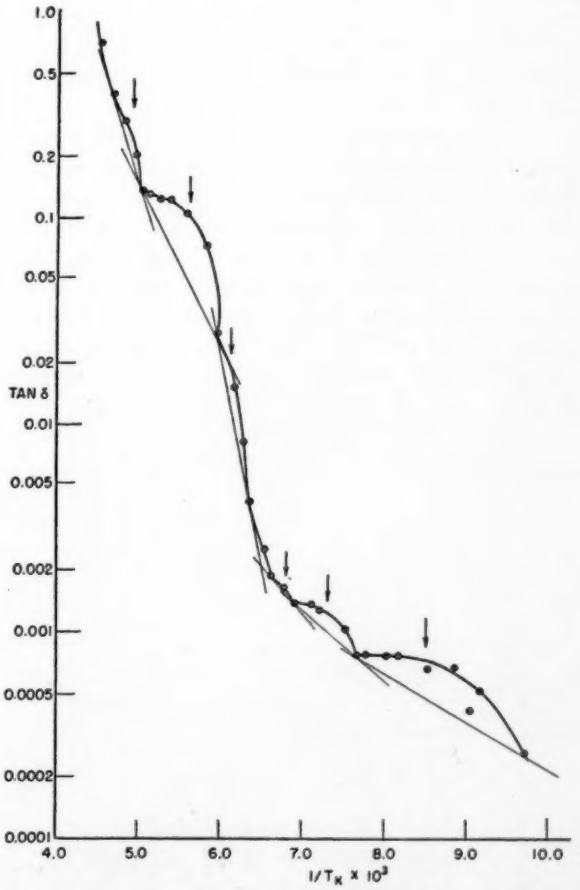

FIG. 14. Loss tangent of AgCl crystal+0.14 percent $CdCl_2$.

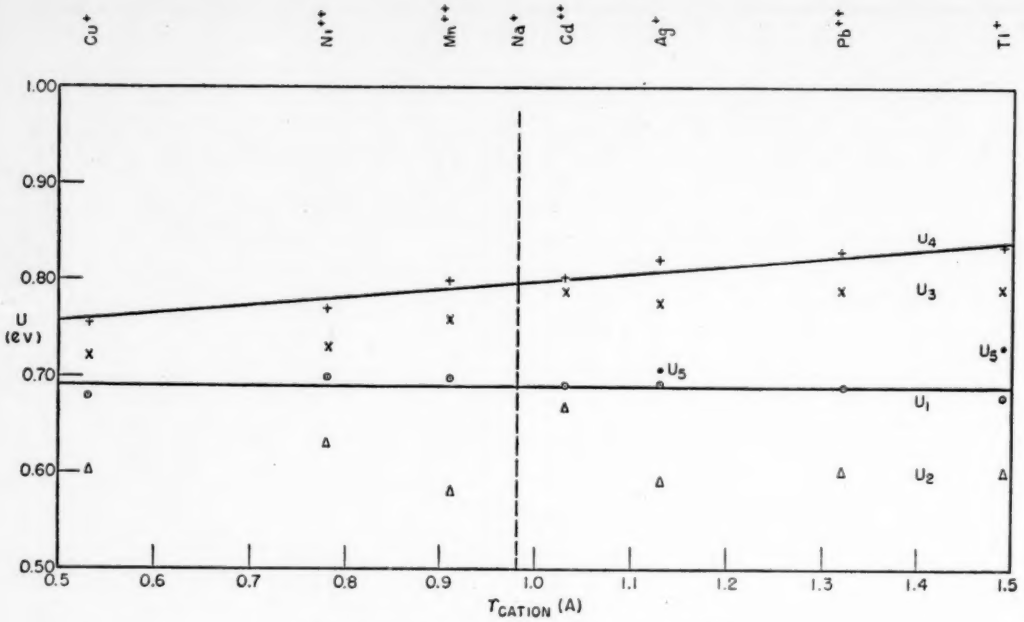

FIG. 15. Activation energies for foreign ions in NaCl.

satisfactory for n_1, but can be only an approximation for n_2 since, on the basis of our model, a portion of this peak arises from the motion of the divalent ion. In general, it will be observed that n_1 and n_2 are of comparable magnitudes, but that the ratio n_2/n_1 increases with increasing concentration. This also suggests further aggregation of pairs.

The dependence of the number of pairs of various types on the foreign ion concentration may be used to obtain further information about the situation in the crystal. A simple thermodynamic calculation of the degree of association is possible if some restrictions are considered. Schottky defects must migrate to a free surface of the crystal to disappear, hence at low temperatures ($\lesssim ca.$ 500°C) where the mobility is low a nonequilibrium but constant number of defects is normally present. The various types of pairs may be formed internally so thermal equilibrium in this respect may persist to much lower temperatures.

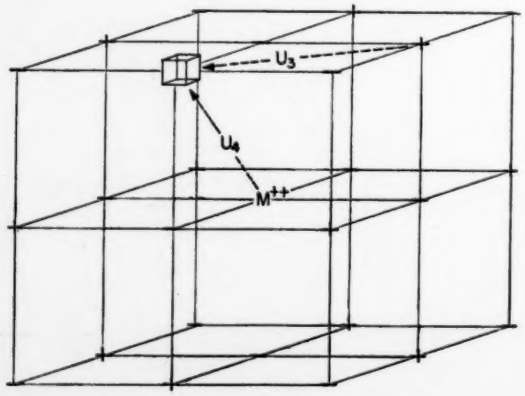

FIG. 16. Mechanisms for pair reorientation.

The three equilibria that are being simultaneously satisfied may be represented schematically as

$$M+\square \overset{K_2}{\rightleftharpoons} M\cdot\square$$

$$M\cdot\square\cdot\bigcirc \overset{K_3}{\rightleftharpoons} \square\cdot\bigcirc + M$$

$$\downarrow\uparrow K_1$$

$$\bigcirc+\square,$$

where M represents a foreign ion, $\square$ a cation, and $\bigcirc$ an anion vacancy, the total number of both being constant. If Y = mole fraction of foreign ion, X_1 = mole fraction of vacancy pairs, X_2 = mole fraction of groups $M\cdot\square\cdot\bigcirc$, X_4 = mole fraction of $M\cdot\square$ pairs, X_n = mole fraction of anion vacancies = mole fraction of cation vacancies produced thermally, we may write the mass action expressions as

$$K_1=\frac{X_1}{(X_n-X_1)(Y+X_n-X_4-X_1-X_2)}, \tag{3}$$

$$K_2=\frac{X_4}{(Y-X_4-X_2)(Y+X_n-X_4-X_1-X_2)}, \tag{4}$$

$$K_3=\frac{X_2}{(Y-X_4-X_2)X_1}. \tag{5}$$

Experimentally we have found $X_4 \ll Y$. Because of the contribution of elastic forces to pair formation with foreign ions, we anticipate $K_2 > K_1$ so that $X_1 \lesssim X_4$, and, as we have seen, $X_2 \simeq X_1$. With these simplifications the equations become

$$X_1=K_1(X_n-X_1)(Y+X_n) \tag{3a}$$

$$X_4=K_2Y(Y+X_n) \tag{4a}$$

$$X_2=K_3YX_1. \tag{5a}$$

Since the heat treatment of our samples has been the same, we may assume X_n is approximately constant for the series of Mn^{++} in NaCl. The curve for X_4 as a function of Y shown in Fig. 18 is obtained for values of $X_n=5\times10^{-4}$ and $K_2=7$. We see for this value of X_n, $X_1\ll X_n$, and Eqs. (3a) and (5a) simplify further to

$$X_1=K_1X_n(Y+X_n) \tag{3b}$$

$$X_2=K_1K_3YX_n(Y+X_n). \tag{5b}$$

The curves for X_1 and X_2 as functions of Y are obtained for $K_1=0.8$ and $K_3=1.2\times10^4$. While the values for the constants are only very rough, they are nevertheless instructive. We have found X_4/Y experimentally to be *ca.* 5×10^{-3} and from the value found for X_n we see that in the pure crystal $X_1/X_n\simeq4\times10^{-4}$. These values are in agreement with the observations of Maurer[9] on the conductivity of $NaCl+CdCl_2$ crystals which indicated negligible association of the foreign ions, and with the investigations of Alger[10] on the number of color centers in alkali halide crystals bombarded with high energy x-rays. This work indicated a fraction $\leqslant0.025$ of the vacancies present as pairs.

Since K_1 presumably does not depend on the impurity ion, we can calculate values of K_2, X_n, and K_3 for the other foreign ions in NaCl assuming $X_1\ll X_n$ in all cases. The results are given in Table II.

The values found are consistent with the idea of large association of ions whose size differs markedly from Na^+, the numerical values suggesting that the elastic forces are of equal importance to electrostatic forces in producing association. The strong tendency to accommodate the foreign ions near existing vacancies is well illustrated by the large values of K_3.

FOREIGN ION MOBILITIES

If the assignment of the high energy loss peak to the suggested mechanism is correct, a method has been provided for the study of foreign ion mobilities in a crystal lattice since the process is that usually assumed for the migration of an ion in an ionic crystal. There are very few data available for comparison, but the

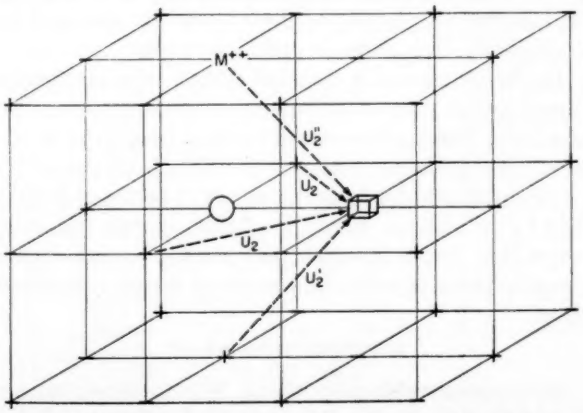

FIG. 17. Reorientation of foreign ion-vacancy pair complexes.

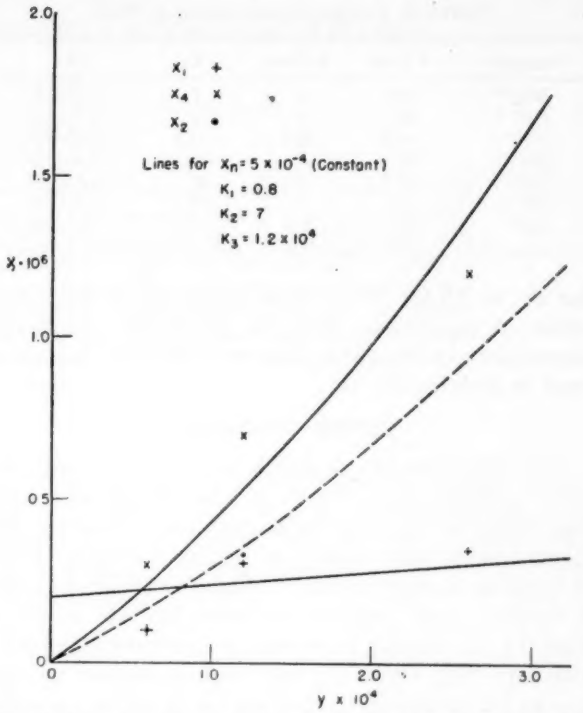

FIG. 18. Ion-vacancy pairs as function of foreign ion concentration.

results quoted by Arzybyschew[11] on $NaCl+Cu^+$ and $NaCl+Ni^{++}$ may be mentioned. This author gives $E=1.09$ and 1.10 ev respectively from measurements at temperatures above 675°C, i.e., in the characteristic conductivity region, as compared with 0.75 and 0.78 ev in the low temperature structure-sensitive range investigated in this paper. The results are not directly comparable because of the difference in temperature. Our indicated value for the activation energy for diffusion of an ion the size of Na^+ in NaCl should, however, be expected to agree with the self-diffusion measurements of Mapother and Maurer[7] for the same temperature range. The linear increase in U_4 with ion size irrespective of charge indicates that the mobilities are predominantly determined by the mechanical rather than the electrical properties of the ion.

A determination of the constant term in the mobility equation is of interest, but accurate values cannot be obtained with the information available. It was shown previously[12] that the constant term could be given as

$$U_{0k}=0.490\times10^{-12}\frac{Zed^2(K'_\infty+2)^2}{\epsilon_0\tau_0kT_j}\left[\frac{m^2}{\text{volt sec.}}\right], \tag{6}$$

where the terms are as previously defined. For NaCl this becomes

$$U_{0k}=\frac{616Z}{T_j}\left[\frac{\text{cm}^2}{\text{volt sec.}}\right]. \tag{7}$$

Using the values of T_j given in Table I and the appropriate valence, we find U_0 ranging from 1.3 cm^2/volt sec.

[9] R. J. Maurer, Tech. Rept. 6, ONR Contract N6ori-47, Carnegie Inst. Tech., September, 1948.
[10] R. S. Alger, Tech. Rept. XV, ONR Contract N5ori-07801, Lab. Ins. Res., M.I.T., January, 1949.
[11] S. A. Arzybyschew, Physik. Zeits. Sowjetunion **11**, 636 (1937).
[12] R. G. Breckenridge, Tech. Rept. XI, ONR Contract N5ori-78, T. O. 1, Lab. Ins. Res., M.I.T., April, 1948.

TABLE II. Foreign ion association in NaCl.

Impurity	$Y\times10^4$	$X_n\times10^4$	K_2	K_3
Mn^{++}	0.6	5.	7.	1.2×10^4
Cd^{++}	18.	3.	1.	2.7×10^2
Ni^{++}	4.2	0.3	0.3	2.1×10^3
Pb^{++}	1.	2.	40.	5.8×10^3
Cu^{+}	2.9	3.	30.	3.1×10^3
Tl^{+}	5.6	2.	80.	3.2×10^3
Ag^{+}	50.	0.4	0.6	1.1×10^2

for Tl^+ to 2.8 for Ni^{++}. These values are of the proper order of magnitude, but the previously mentioned uncertainty in Eq. (2) is reflected here since Eq. (2) is used in deriving Eq. (6).

SILVER CHLORIDE

The measurements on AgCl, both pure and with the Cd^{++} addition, have shown a behavior differing from the alkali halides. Our basic question is whether the silver halides have Frenkel or Schottky defects. There is insufficient experimental evidence available to make a detailed study possible, but some features shown in Figs. 13 and 14 may be given a preliminary interpretation. We may assign the loss peak of highest energy, U_6, to the motion of the foreign ion in cation vacancy-foreign ion pairs; and the peak of comparable size at slightly lower temperature, U_5, to the motion of normal cations on adjacent sites to the pair since this configuration should be present with either Frenkel or Schottky defects. The numbers and mole fractions of such pairs have been calculated using the assumptions as to charge and distance given previously for the alkali halides. The results are included in Table I.

It will be noted that in this case the ratio n_5/n_6 is almost exactly 4 as would be predicted on the proposed model. This indicates that the highly polarizable AgCl lattice can accommodate a considerable number of foreign ions without aggregation of the foreign ions. The value of $U_6=0.36$ ev found for Cd^{++} and $U_5=0.31$ ev suggest that the energy for self-diffusion in AgCl should be about 0.3 ev since Cd^{++} and Ag^+ are not too dissimilar in size.

There is greater difficulty in explaining the loss maxima at lower temperatures involving the peaks found in the original crystal. The interpretation of the two peaks in reference 1 as indicating Frenkel defects was questioned by Grimley[3] on the ground that a pair formed between a vacant cation site and an interstitial cation would be unstable. This is, of course, true; however, if Frenkel defects are present in dynamic equilibrium, the configuration must exist in finite amounts since it is the initial stage in the formation and the final stage in the disappearance of a Frenkel defect. The possibility should not be excluded on this basis alone.

Recently, an investigation of the structure and growth mechanism of photolytic silver in silver bromide[13] strongly suggested the presence of interstitial cations in the interior of the crystal. Since no differences in the type of defect would be anticipated between silver bromide and chloride, Frenkel defects seem possible for silver chloride.

It must be admitted that the information at this time is by no means conclusively in favor of the presence of Frenkel defects, since a number of reasonable alternatives may be suggested.

The thermal treatment of the samples was such that a nonequilibrium state is undoubtedly present. This state might easily include Frenkel defects, even if Schottky defects are the normal type since it would seem that the energies of formation should not differ greatly in AgCl.

A possibility requiring only Schottky defects is that the two peaks arise from the reorientation of pairs of vacancies via the motion of both anion and cation vacancies. While this was not observed in the alkali halides, the high polarizability of the silver halides should make the energies more nearly equal for both types of jumps. The observed energy difference, 0.05 ev, seems rather small however.

Grimley's[3] suggestion that the peaks are due to two impurity ions is untenable since, as we have seen, a single foreign ion produces three peaks in addition to the one in the pure crystal. It would seem that there is a possibility that the original crystal contained Schottky defects and a single impurity ion, giving four peaks of which only the larger two corresponding to U_3 and U_4 were observed. If this is so, we must assume that the peaks at 0.24 and 0.28 ev in the Cd^{++} case correspond to U_2 and U_1. Consequently, the $U_3=0.21$ ev and $U_4=0.26$ ev for the unknown impurity are of lower energy than the energy for moving the pair alone, which seems unreasonable.

While the purity of the crystal with respect to foreign ions is stated to be high, it is possible that on exposure to light appreciable amounts of atomic silver are produced. This suggests an attractive alternative since it is expected that because of the elastic forces near the large silver atom, there would be considerable association with vacancy pairs. This would immediately explain the two peaks in the original crystal and the multiplicity of maxima in the Cd^{++} case.

In the absence of a detailed picture, the numbers of these various pairs have been computed assuming $Z=1$ and $d=a/2$ since these values would be typical in any case. The results are included in Table I. Of the several possibilities, the explanation, either in terms of Frenkel defects or atomic silver impurity, seems the more reasonable, but a complete picture must await further investigations of crystals known to contain no excess silver.

ACKNOWLEDGMENT

The author wishes to thank W. B. Westphal and E. McCarty of the Measurements Group of this Laboratory for the dielectric measurements and E. Hungerman for the polarographic analyses reported in this paper.

[13] C. R. Berry and R. L. Griffith, Phy. Rev. 78, 317 (1950).

Periodicity of Some Molecular Properties of Diatomic Hydrides

RAYMOND K. SHELINE
Institute for Nuclear Studies, University of Chicago, Chicago, Illinois
(Received January 30, 1950)

The log of the force constants of the ground electronic states of all available diatomic hydrides is plotted *versus* the log of the atomic number of the element to which the hydrogens are bonded. A definite periodicity associated with the periods in the periodic table results. This periodicity is used to predict the force constants of ten diatomic hydrides which have as yet not been investigated. A plot of hydride interatomic distance *versus* the atomic number of the "united atom" shows a similar periodicity and strong shell structure and allows the prediction of 13 new interatomic distances for hydrides. These data are interpreted as evidence for the "united atom" model for hydrides. Finally plots of the low lying atomic energy states for atoms suggest that the seemingly inconsistent *d* shell periodicity may be the result of the mixing of energy states and hence a different type of hybridization trend in the *d* shell.

INTRODUCTION

A NUMBER of investigators have attempted to find functional relationships between various atomic parameters and the force constants of molecules. Most of these methods relate some negative power of the interatomic distance and/or the position in the periodic table (either empirically or by the use of electronegativities) to the force constant.[1–9]

Gordy,[9] who most recently has suggested a method of calculating force constants from atomic parameters and the interatomic distance, has two adjustable constants, a and b, in his equation which follows:

$$k=aN\left(\frac{\chi_A\chi_B}{d^2}\right)^{\frac{3}{4}}+b,$$

where N = bond order, χ = electronegativities, d = interatomic distance.

With two sets of adjustable constants he is able to reproduce the force constants of the diatomic hydrides of the first four groups in the periodic table within a reasonable degree of accuracy. However individual diatomic hydrides are very badly reproduced and the hydrides of groups V and VI and the *d* shell hydrides are not even attempted. Thus, Gordy's system, which is probably the best yet suggested for obtaining constants and bond distances, and those of the other investigators[1–8] suffer because of the very analyticity of the methods proposed. Each of the investigators has equations which fit one or more particular types of molecules particularly well and have a general overall validity. That so many different relations have been proposed and apply in a degree to warrant publication indicates that these approaches lack specificity.

Accordingly, it is the express purpose of this research to single out a group of simple molecules, the diatomic hydrides, and plot their force constants and interatomic distances against their positions in the periodic table. It is felt that the graphical method will be more useful than an analytical one because it will show the peculiarities as well as the general character of the periodicities. J. R. Platt, in new calculations in the article which follows this one, has calculated on a theoretical basis the force constants of the hydrides. His success in reproducing the *d* shell hydride force constants is particularly striking.

FORCE CONSTANTS

A complete quantum mechanical treatment even for the hydrides LiH to HF is probably beyond the realm of present possibility. However, Stehn[10] and King[11] have derived equations for the energies of the first row hydrides in terms of exchange and Coulomb integrals empirically determined but self-consistent. King has also plotted the log of the force constant *versus* the log of the atomic number for the first row hydrides.

Since all the empirical relationships between force constants and atomic parameters indicate that the force constants are a fairly smooth but rapidly varying function of interatomic distance, it is to be expected that a log-log plot of atomic number *versus* force constant would be meaningful.

The atomic radius within a period is inversely related to the atomic number and the force constant is linearly related to the interatomic distance to a power. Since for diatomic hydrides the interatomic distance is approximately linearly proportional to the atomic radius of the element to which the H is bonded, the force constant must be linearly related to the atomic number to a power. Therefore it is seen that the log of the force constant should be linearly related to the log of the atomic number. This argument is expressed algebraically as follows:

$$cr'^b=Z=c'r.$$

[1] R. M. Badger, J. Chem. Phys. **2**, 128 (1934); **3**, 710 (1935).
[2] P. M. Moore, Phys. Rev. **34**, 57 (1929).
[3] D. Clark, Phil. Mag. **18**, 459 (1934).
[4] H. S. Allen and A. K. Longair, Phil. Mag. **19**, 1032 (1935).
[5] M. L. Huggins, J. Chem. Phys. **3**, 473 (1933); **4**, 308 (1936).
[6] G. B. B. M. Sutherland, J. Chem. Phys. **8**, 161 (1940).
[7] J. W. Linnett, Trans. Faraday Soc. **36**, 1123 (1940).
[8] C. K. Wu and C-T. Yang, J. Phys. Chem. **48**, 295 (1944).
[9] W. Gordy, J. Chem. Phys. **14**, 305 (1946).
[10] J. R. Stehn, J. Chem. Phys. **5**, 186 (1937).
[11] G. W. King, J. Chem. Phys. **6**, 378 (1938).

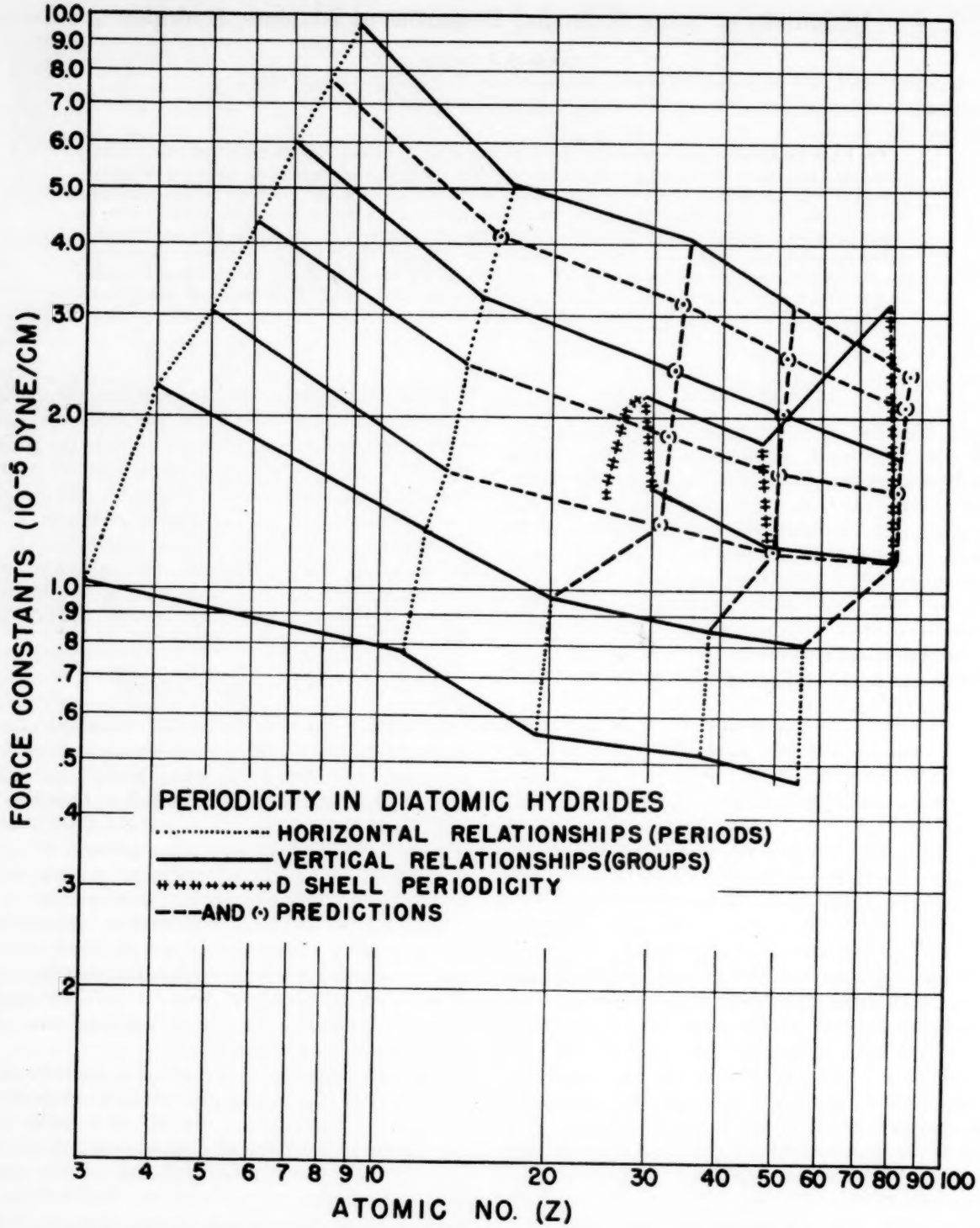

FIG. 1. Log of the force constant of diatomic hydrides plotted against the atomic number of the atom to which the hydrogen is bonded.

Since $k=c''r^a$

$$k=\frac{c''}{(c')^a}\cdot Z^a.$$

Therefore, $\log k=a\log Z+C$ where r' = atomic radius of the element bonded to the hydrogen, r = interatomic distance of the diatomic hydride, k = force constant of the diatomic hydride, Z = atomic number of the element bonded to the hydrogen c, c', c'' = proportionality constants.

In order to test this linearity the force constants of the diatomic hydrides were computed with the simple

harmonic formula:

$$\omega_e = (1/2\pi)(k/\mu)^{\frac{1}{2}},$$

from the ω_e values selected by Herzberg.[12] These force constants are listed in Table I together with the other molecular parameters. Figure 1 shows the plot of the log of the force constant *versus* the log of the atomic number. The periodicity is quite remarkable. Specifically the following characteristics should be noted:

1. The periodicity observed is extremely similar to atomic periodicity as for example the ionization potential of the atoms plotted against their atomic number. The force constant trend strongly indicates that there is a bond stability connected with creating a "united atom" with enough electrons to complete a shell. Thus the force constant for HF which is isoelectronic with neon reaches a maximum and then drops to a minimum at NaH, isoelectronic with Ca (NeH breaks the complete continuity of the sequence.) This maximum minimum trend repeats each time a shell is completed in the "united atom."

2. Between group II and group III elements a discontinuity in the numerical value of the force constants of the diatomic hydrides might have been expected to accompany the change from $s-s$ to $s-p$ bonding. King has suggested that the equilibrium distance and force constants are predominantly determined by $2s$ electrons in the entire series from Be to F, whereas the exchanges associated with $p\sigma$-electrons in the elements from B to F, although large, have a flat minimum thus not affecting the force constants or equilibrium distances. The fact that a discontinuity does not occur with the special stability of half-filled p orbitals lends weight to King's argument.

3. The lack of linear periodicity in the hydrides bonded to an element completing its d shell, yet a definite trend connected with half-filling the d shell is an interesting feature of Fig. 1. These facts seem to indicate that $s-d$ bonding has a considerable effect on the potential function in such a way as to affect force constants contrary to the effect observed in $s-p$ bonding. Apparently those elements which have half-filled or entirely filled the d orbitals show a smaller force constant than the other d orbitals. Between the half-filled d orbitals and the entirely filled d orbitals a trend may be observed which reaches a maximum at Cu, one element before dropping to a very low force constant at Zn with the completion of the d shell.

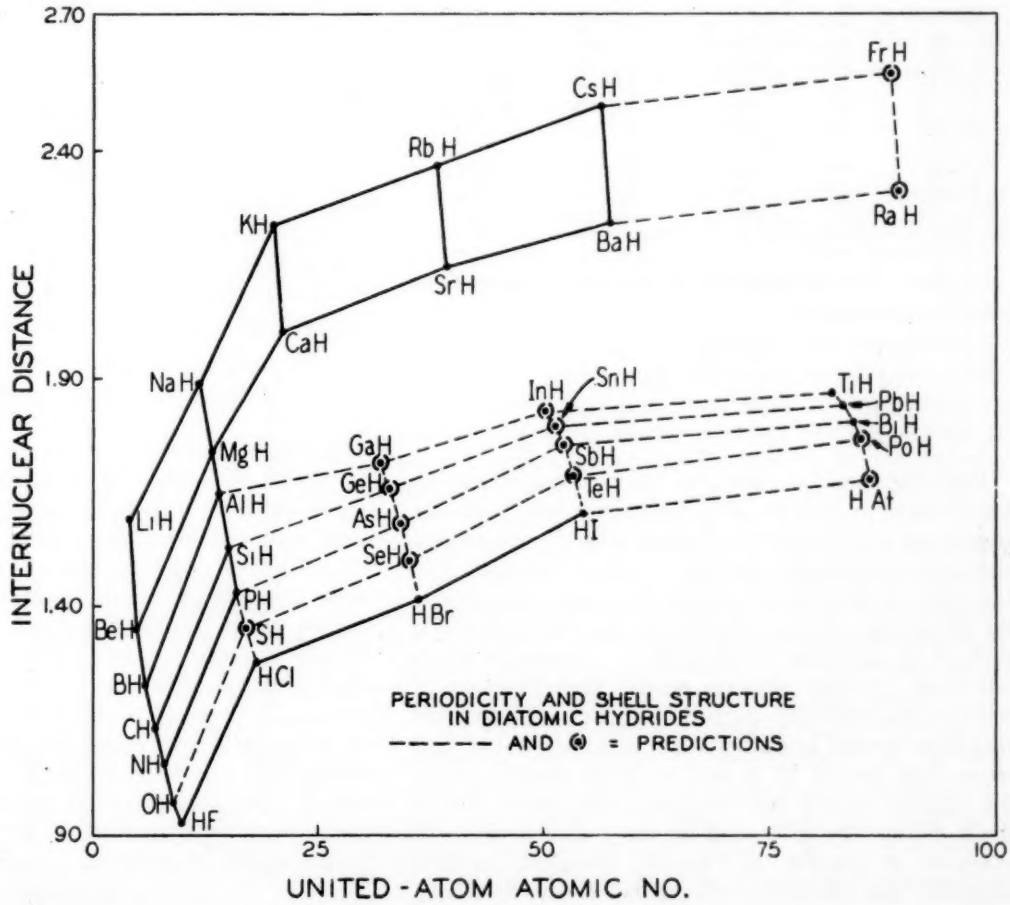

FIG. 2. Interatomic distance of diatomic hydrides plotted against the atomic number of the "united atom."

[12] G. Herzberg, *Molecular Spectra and Molecular Structure* (Prentice-Hall, Inc., New York, 1939). Herzberg has plotted the force constants of all available hydrides *versus* the atomic number.

TABLE I. Force constants of HA diatomic molecules.

Diatomic molecule	Electronic ground state	ω_e	μ	Force constant (10^5 dynes/cm)
Ag−H	$^1\Sigma^+$	1760.0	0.99888	1.8219
Al−H	$^1\Sigma^+$	1682.57	0.97200	1.6203
Au−H	$^1\Sigma^+$	2305.01	1.00287	3.1375
Ba−H	$^2\Sigma^+$	1172.	1.00099	0.8096
Be−H	$^2\Sigma^+$	2058.5	0.90688	2.2628
B−H	$^1\Sigma^+$	2366.	0.92362	3.0445
Bi−H	$^1\Sigma^+$	1689.9	1.00329	1.7051
Ca−H	$^2\Sigma^+$	1299.	0.98333	0.97702
Cd−H	$^2\Sigma^+$	1430.7	0.99917	1.2043
C−H	$^2\Pi_r$	2824.	0.93002	4.3673
Co−H	$^3\phi_4$	(1890)?	0.99118	(2.0848)
Cs−H	$^1\Sigma^+$	890.7	1.00054	0.46740
Cu−H	$^1\Sigma^+$	1940.4	0.99224	2.1999
H−H	$^1\Sigma^+$	4405.3	0.50000	5.7137
H−Br	$^1\Sigma^+$	2649.67	0.99557	4.1157
H−Cl	$^1\Sigma^+$	2988.95	0.97989	5.1547
H−F	$^1\Sigma^+$	4141.305	0.95752	9.6697
H−I	$^1\Sigma^+$	2309.53	1.00036	3.1419
Hg−H	$^2\Sigma^+$	1387.09	1.00327	1.1366
K−H	$^1\Sigma^+$	983.3	0.98289	0.55959
Li−H	$^1\Sigma^+$	1405.65	0.88164	1.0258
Mg−H	$^2\Sigma^+$	1494.9	0.96764	1.2733
Mn−H	?	(1580)?	0.99014	(1.4555)
N−H	$^3\Sigma^-$	(3300)?	0.94060	(6.0314)
Na−H	$^1\Sigma^+$	1170.8	0.96596	0.77970
Ni−H	$^2\Delta_{5/2}$	(1926.6)?	0.99128	(2.1666)
O−H	$^2\Pi_i$	3727.95	0.94837	7.7608
P−H	$^3\Sigma^-$	(2380)?	0.97653	(3.2571)
Pb−H	$^2\Sigma$	1565.2	1.00345	1.4425
Rb−H	$^1\Sigma^+$	936	0.99648	0.51406
Si−H	$^2\Pi_r$	(2080)?	0.97324	(2.4793)
Sr−H	$^2\Sigma^+$	1206.2	0.99688	0.85401
Tl−H	$(^1\Sigma^+)$?	1390.7	1.00338	1.1426
Zn−H	$^2\Sigma^+$	1607.6	0.99300	1.5111

Gaydon[13] lists the dissociation energies of the various hydrides as follows:

MnH	less than 2.4 ev
NiH	2.6±0.3 ev
CuH	2.7±0.3 ev
ZnH	0.845±0.02 ev

Both the force constant and the dissociation energy trend seem to indicate that there is a bond stability connected with creating a "united atom" with enough electrons to complete one-half or all of the *d* shell in the atom to which the hydrogen is bonded. Apparently the disruption of the complete or one-half complete *d* shell of an atom by bonding it to a hydrogen which interposes another electron results in a decrease of relative bond stability. Accordingly, it can be predicted that there should be a double discontinuity in the log*Z* *versus* log*k* plot of all *d* shell hydrides resulting from the stability of the half filled and completely filled *d* shells. Since very little data on the *d* shell hydrides is available at present, but should ultimately become available, the validity of this prediction may be tested.

[13] A. G. Gaydon. *Dissociation Energies* (John Wiley and Sons, Inc., New York, 1947).

TABLE II. Predictions of force constants of diatomic hydrides.

Periodic table group	Molecule	Force constant (10^5 dynes/cm)
Group VI	SH	4.15
	SeH	3.18
	TeH	2.53
	PoH	2.10
Group V	AsH	2.43
	SbH	2.05
Group IV	GeH	1.87
	SnH	1.61
Group III	GaH	1.31
	InH	1.17

TABLE III. Predicted interatomic distances.

	Predicted from graph	Comparison with sums of Gordy's covalent radii*
FrH	2.57	
RaH	2.31	
PoH	1.77	1.83
HAt	1.68	
SH	1.35	1.41
GaH	1.72	1.63
InH	1.83	1.81
GeH	1.66	1.59
AsH	1.58	1.58
SeH	1.50	1.54
SnH	1.80	1.77
SbH	1.76	1.78
TeH	1.69	1.74

* W. Gordy, Phys. Rev. **69**, 606 (1946).

4. Prediction of the force constants. Since there is such a pronounced periodicity especially in the *s* and *p* shells, it appears possible to predict the force constants for a number of the diatomic hydrides by extrapolating trends or interpolating between neighboring trends.

Accordingly, predictions are made for the force

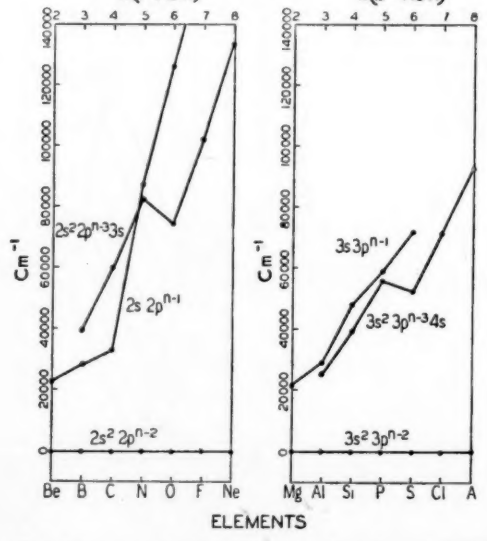

FIG. 3. Low lying atomic energy levels plotted against the first two short rows of elements periodically arranged.

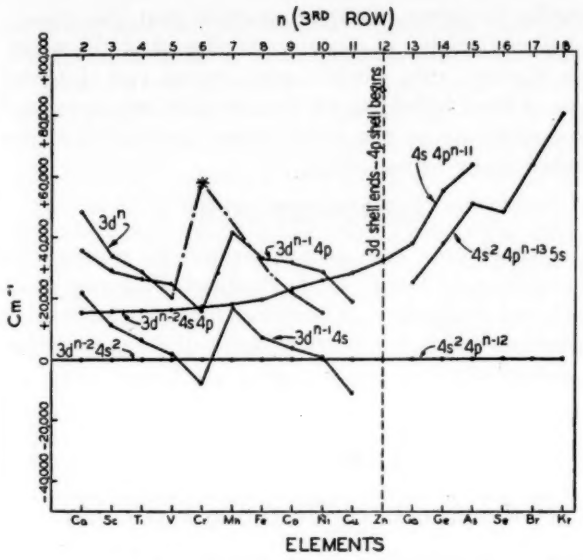

FIG. 4. Low lying atomic energy levels plotted against the third row of elements periodically arranged.

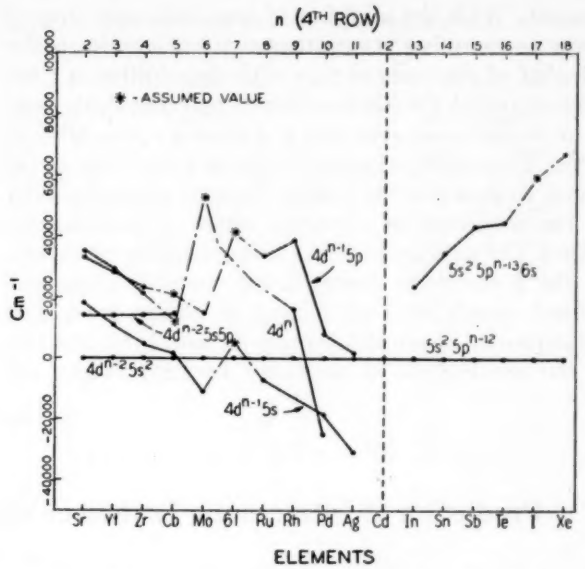

FIG. 5. Low lying atomic energy levels plotted against the fourth row of elements periodically arranged.

constants of ten diatomic hydrides in their ground electronic states in Table II. It is probable that many of the force constants predicted in Table II will become available in the near future so that the validity of the predictions may be tested.

INTERATOMIC DISTANCES

Since there is such a distinct periodicity in the force constants indicating a "united atom," it is reasonable to expect a similar periodicity for the interatomic distances. Accordingly in Fig. 2 the interatomic distances of all the available *s* and *p* shell diatomic hydrides[12] are plotted *versus* the atomic number of the "united atom." Herzberg[12] has also plotted the interatomic distances of the hydrides against the atomic number. However, his plot does not suggest the remarkable periodicity shown in Fig. 2 with the following characteristics:

1. A distinct shell structure is observed. Thus the interatomic distance decreases monotonously from LiH to HF and then jumps discontinuously to a new high value at NaH. This discontinuity which occurs with the completion of a shell is observed four times in Fig. 2.

2. The rate of increase of interatomic distance with "united atom" atomic number is fairly constant over a range of atomic number but changes abruptly twice. This change is most obvious in groups I and II and occurs at KH, CaH and CsH, BaH. In each case it would appear that this change in rate of increase of interatomic distance was the result of adding an inner shell to the atom to which the H was bonding. In the first case it would be the addition of the 3*d* shell and in the second, the addition of the 4*f* shell. This behavior is again reminiscent of atomic behavior.

3. Since there is such a pronounced shell structure and periodicity especially in the *s* and *p* shells, it would again seem valuable to attempt the prediction of 13 missing hydride interatomic distances. These predictions are listed in Table III along with the sums of the appropriate covalent radii of Gordy. It is probable that most of these interatomic distances will be observed experimentally so that these predictions can be checked with experiment.

DISCUSSION

Both force constant considerations and interatomic distances seem to indicate with the coarse features of the periodicity that the atom of the next higher element is a close approximation to the hydride.

However, there are certain of the finer features of the periodicity which do not appear to be internally consistent and which are somewhat at variance with atomic periodicity. Thus, the plot of the log of the force constant *versus* the atomic number is approximately a linear function for *p* shells but for *d* shells this linearity fails completely. Furthermore there is an internal trend in the *d* shell associated with the "united atom" being half-filled which does not occur in the *p* shell. Since we have shown a strong similarity to exist between appropriate atoms and hydrides, it is possible that the energy states of the atoms might indicate the source of these seeming inconsistencies in hydride periodicity by the bond hybridization trends which they initiate.

Accordingly in Figs. 3, 4, and 5 the term values of all the lowest lying states of the elements[14] of the two short rows and the first two long rows of the periodic table are plotted. The figures show that there is a gradual increase in the bonding of 3*d* or 4*d* electrons over 4*s* and 5*s* electrons as we progress from element to

[14] R. F. Backer and S. Goudsmit, *Atomic Energy States* (McGraw-Hill Book Company, Inc., New York, 1932).

element. With the addition of one, two, and three d electrons there is a strong tendency to complete half a sub-shell of electrons so that with the addition of a 4th electron one of the electrons which had previously been in an s shell goes over into a d state to give $3d^5 4s$ or $4d^5 5s$. This mixing of states occurs in two trends in the d shell as shown in the figures. No such anomalies exist in the sequences of elements where p electrons are added. The analogy in Fig. 1 is immediately perceived. In the p shells the energy levels continue along well defined trends with no mixing of energy levels and consequently no abrupt changes in bond hybridization. If our assumption of similarity between atoms and hydrides is correct, we may conclude that the strange d shell periodicity is due to a mixing of states which goes through two minima and creates two different types of bond hybridization trends which are connected discontinuously at the point where the d shell of the "united atom" is half-filled.

ACKNOWLEDGMENT

In conclusion the author wishes to express his appreciation to Dr. C. C. J. Roothan, Professor J. R. Platt, and Professor R. S. Mulliken for many interesting discussions which were very valuable in the preparation of this paper.

THE JOURNAL OF CHEMICAL PHYSICS VOLUME 18, NUMBER 7 JULY, 1950

Prediction of Interatomic Distances and Force Constants in Diatomic Hydrides

JOHN R. PLATT
Physics Department, University of Chicago, Chicago, Illinois
(Received March 24, 1950)

The interatomic distance in hydrides is roughly the radius in the united atom at which $Z_{eff}=1.0$. The force constant is roughly $4\pi\rho e^2$ where ρ is the electron density at this radius. These results are justified by a perturbation treatment. The best fit to experimental values is obtained using Hartree wave functions. Slater functions account for the general trends and breaks in the curves of distance and force constant *vs.* atomic number, and for the anomalous values noted by the Sheline in the transition elements.

THIS paper examines the following pair of hypotheses concerning interatomic distances and force constants in diatomic hydrides, MH:

(1) the interatomic distance, d is near $r_{1.0}$, the radius in the neutral united atom $(M+1)$ at which the effective nuclear charge is unity. This is the radius beyond which lie a total number of 1.0 electrons;

(2) the force constant, k, is approximately given by

$$k=4\pi e^2\rho_{1.0},$$

where $\rho_{1.0}$ is the density of electrons in the united atom at radius $r_{1.0}$.

These hypotheses may be justified by a crude application of perturbation theory. For, starting with the united atom, suppose we remove one proton from the nucleus, keeping the electronic charge density fixed, as though this were a small perturbation. If the proton is now placed outside $r_{1.0}$, it will be attracted by the excess negative charge. Inside $r_{1.0}$ it will be repelled. Therefore $r_{1.0}$ will equal d, the equilibrium internuclear distance, to a first approximation.

A small displacement, dx, outward from this position, $r_{1.0}$, will subject the proton to the attraction of the added shell of charge,

$$dF=-4\pi r^2\rho_{1.0}e^2dx/r^2,$$

so that $k(=-dF/dx)$ has the value given above. This value can also be written as

$$k=\frac{e^2}{a_0^3}\frac{q_{1.0}}{z_{1.0}^2}=(15.62\times10^5 \text{ dynes/cm})\frac{q_{1.0}}{z_{1.0}^2},$$

where

$$q=4\pi r_{1.0}^2\rho_{1.0}a_0$$

is the radial electron density in atomic units, and

$$z_{1.0}=r_{1.0}/a_0$$

is the radius in atomic units. In Hartree calculations, q is often written as $-dZ/dr$, or in the present notation, $-dZ/dz$.

Two values of k may be computed: k_t, at the radius $r_{1.0}$ given by hypothesis (1); and k_0, at a radius equal to the observed interatomic distance, d. The first value will compound the errors of the hypotheses and the second, semi-empirical, value will give a more valid test of hypothesis (2) alone.

The success actually attained by the force-constant predictions from this kind of perturbation argument was unexpected. The assumptions seem to go exactly counter to the Born-Oppenheimer approximations, since they seem to imply that the electrons remain almost fixed in position while the protons oscillate in their field, instead of *vice-versa*. Perhaps the results can be justified in some other way.

Certain parameters familiar to chemists and commonly used in empirical formulas for force constants and distances, such as the electronegativity of the heavy atom, or the percent ionic character of the bond, do not need to be introduced separately in the present predictions since they are implicit in the electronic wave functions.

The values of $r_{1.0}$ and k_0 computed using these hypotheses are compared with the observed values in Table I and in Figs. 1 and 2. The observed values are taken from

Herzberg[1] and Sheline.[2] The wave functions used for the computations were (a) Hartree wave functions without exchange, where available;[3] (b) compound Slater orbitals fitted by Shull to the Hartree functions for some second-row elements;[4] and (c) simple Slater orbitals.[5]

Normalized spherically symmetric functions were used. For some atoms, the effective nuclear charge has not been tabulated with the other Hartree parameters in the literature, and so $r_{1.0}$ has not been determined here. Hartree functions with exchange seemed to give slightly poorer agreement with the observed values than those without exchange, so computations based on them contribute nothing new to the comparisons and are omitted here.

The determination of $r_{1.0}$ from the Slater functions requires solution of explicit but unpleasant transcendental equations of many terms. These were solved by trial. The values in Table I are accurate to one or two units in the last decimal place, which is sufficient for testing our hypotheses.

The contributions of the d-electrons to the force constants, Δk_d, and to the distances, Δr_d, are shown by separate columns in the table and by the shaded areas in the figures. The curves marked "ns^2" in the figures show the contributions of the outer s-electrons alone; these contributions are of course influenced by the presence of the d-electrons through their screening factors. This separation of the s- and d-contributions is helpful in understanding the d-shell anomalies to which Sheline has called attention.[2]

A constant outer s^2 configuration was used throughout each d-shell and rare-earth group in the computations. This was done to permit examination of general trends without the disturbance introduced by changing valence states. No doubt the irregularities in the observed properties in the iron group are due to changing valence. In the method of computation used here, irregularities in the observed distances, d, produce irregularities in the computed semi-empirical k_0, as may be seen in the iron group.

Several general results emerge from the comparisons. First, the absolute values computed for the radius and force constant agree rather well with the observed values. Note that there were no adjustable parameters in this treatment. Second, the Slater orbital computations account for the general trends and gross breaks in the curves quite well but are affected by large systematic deviations. The Hartree and Shull functions, which are closer to the true wave functions, predict the diatomic properties more accurately. It is not possible to determine whether the remaining errors of the predictions are due to remaining inaccuracies in the wave functions, or to second-order corrections to the first-order perturbation theory we have used, or to the inadequacy of the united-atom approximation, or to the crudity of the assumption that perturbation theory can be used at all. The good agreement may be partly due to mutual cancellation of some of these factors.

The predictions for k_0 seem generally more successful than those for $r_{1.0}$. The predicted radius for H_2 is especially bad, as might be expected for this extreme case. Probably the force constant agreement for H_2 is fortuitous.

TABLE I. Predicted and observed distances and force constants.

Hydride	Slater Δr_d	Slater $r_{1.0}$	Shull $r_{1.0}$	Hartree $r_{1.0}$	Obs. d	Slater Δk_d	Slater k_0	Shull k_0	Hartree k_0	Obs. k
	Angstroms					$\times 10^5$ dynes/cm				
HH		0.42		0.43	0.74		5.21		5.40	5.71
LiH		1.27		1.39	1.60		0.93		1.02	1.03
BeH		1.13			1.34		2.01		2.13	2.26
BH		1.01	1.18		1.23		2.65	3.04	3.04	3.04
CH		0.90	1.04		1.12		3.35	3.87	4.36	4.37
NH		0.82	0.97		1.04		3.82	5.13	5.63	(6.03)
OH		0.75		0.93	0.97		4.17		7.10	7.76
FH		0.69		0.87	0.92		4.22		7.82	9.67
NaH		1.86			1.89		0.72			0.78
MgH		1.78			1.73		1.35			1.27
AlH		1.65			1.65		1.84			1.62
SiH		1.49			1.52		2.58			(2.48)
PH		1.38			1.44		3.01			(3.26)
SH		1.27			(1.36)		3.51			—
ClH		1.18			1.27		4.30		5.12	5.15
KH		2.77		2.30	2.24	0.00	0.38		0.44	0.56
CaH	0.12	2.77			2.00	0.29	0.81			0.98
—										
TiH	0.06	2.46								
—										
MnH	0.02	2.15			(1.58)	0.89	1.80			(1.46)
FeH	0.01	2.06			1.48	1.09	2.12			—
CoH	0.00	1.96			1.54	0.44	1.55			(2.08)
NiH		1.89			1.48	0.41	1.64			(2.17)
CuH		1.83			1.46	0.26	1.61			2.20
ZnH		1.83			1.59	0.02	1.99			1.51
—										
GeH		1.67								
—										
BrH		1.41			1.41		4.27			4.12
RbH		3.24			2.37		0.26			0.51
SrH	0.30	3.37			2.15	0.22	0.52			0.85
—										
ZrH	0.24	3.02								
—										
MoH	0.12	2.68								
—										
RuH	0.07	2.43								
—										
AgH	0.02	2.12			1.62	1.30	1.98			1.82
CdH	0.00	2.11			1.76	0.24	1.81			1.20
—										
SnH		1.91								
—										
IH		1.60			1.60		3.06			3.14
CsH		3.51			2.49		0.20			0.47
BaH	0.41	3.75			2.23	0.15	0.37			0.81
—										
EuH	0.41	3.75								
—										
TmH	0.41	3.75								
—										
HfH	0.30	3.35								
—										
WH	0.18	2.96								
—										
OsH	0.13	2.64								
—										
AuH	0.05	2.36		1.91	1.52	4.16	4.85		3.02	3.14
HgH	0.03	2.36			1.74	0.78	2.18			1.14
TlH	0.01	2.23			1.87	0.14	1.76			1.14
—										
BiH		1.97			1.81	0.03	2.49			1.71
—										
AtH		1.75								

[1] G. Herzberg, *Molecular Spectra and Molecular Structure. I. Diatomic Molecules* (Prentice-Hall, Inc., New York, 1939).

[2] R. K. Sheline, J. Chem. Phys. **18**, 927 (1950).

[3] He: D. R. Hartree, Proc. Camb. Phil. Soc. **24**, 111 (1928).
Be, Ca, Hg: D. R. Hartree and W. Hartree, Proc. Roy. Soc. (London) **A149**, 210 (1935).
B, C, N: Brown, Bartlett, and Dunn, Phys. Rev. **44**, 296 (1933).
C: C. C. Torrance, Phys. Rev. **46**, 388 (1934).
O: D. R. Hartree and M. M. Black, Proc. Roy. Soc. (London) **A139**, 311 (1933).
F, Ne: F. W. Brown, Phys. Rev. **44**, 214 (1933).
A: D. R. Hartree and W. Hartree, Proc. Roy. Soc. (London) **A150**, 9 (1935).

[4] I am indebted to Dr. Harrison Shull for communicating some of his results to me in advance of publication.

[5] J. C. Slater, Phys. Rev. **36**, 57 (1930).

The Slater function computations account for the breaks in the internuclear-distance curves after completion of a d-shell. The break is not so marked in the computed as in the observed curves, but this may be due to the systematic errors of the Slater functions. Approximate constancy of distance is predicted for the rare-earth hydrides and of course is expected empirically from the constancy of rare-earth radii in other compounds.

The Slater functions exaggerate the contribution of the d-electrons to the internuclear distance in the transition elements. Their direct contribution, aside from their screening effect on the s^2 electrons, is evidently negligible.

On the other hand, their contribution to the force constants is large, both as predicted and as observed. The difference in their contribution to $r_{1.0}$ and to k_0 is due to the fact that k_0 depends on the charge density near $r_{1.0}$ while $r_{1.0}$ itself depends on the integrated charge outside. The d-orbitals are in a stronger field with higher Z_{eff} than the outer s-orbitals and so they decrease faster with distance. As a result they may and apparently do contribute much to the density though they contribute little to the integrated charge outside. The rules-of-thumb relating distances and force constants in other molecules may consequently be hard to generalize to compounds of the transition elements.

The predicted force constants are very successful for the hydrides through HCl. Even the alternation in groups I to IV is reproduced, though of course it simply reflects the alternation introduced by use of empirical distances in the calculation. Sheline has inferred from this empirical alternation, or weak break in the curves, whichever it is, that the s and p electrons are not as nearly equivalent as the Slater wave functions would have us assume.

The large force constants found for the transition elements are predicted qualitatively quite well by the Slater functions. The breaks in the curves after completion of a d-shell are not due to the commencement of a p-shell as were the corresponding breaks in the distance curves. They are due instead to the fairly sudden exponential decrease of the d-shell contribution to the charge density with increasing atomic number. The Slater functions underestimate this drop-off after Cu, but give about the right value after Au. It would be interesting to determine the force constants for the platinum group hydrides just before Au to see if the abnormally high values indicated by the Slater calculations in this region are also correct.

The Slater functions predict the same force constants for all rare-earth hydrides in the same valence state, which is again an empirically expected result. The f-electrons are buried too deeply in the atoms to contribute much to either $r_{1.0}$ or to k_0.

The method used here may be valuable as a teaching device, to give a general understanding of the electronic

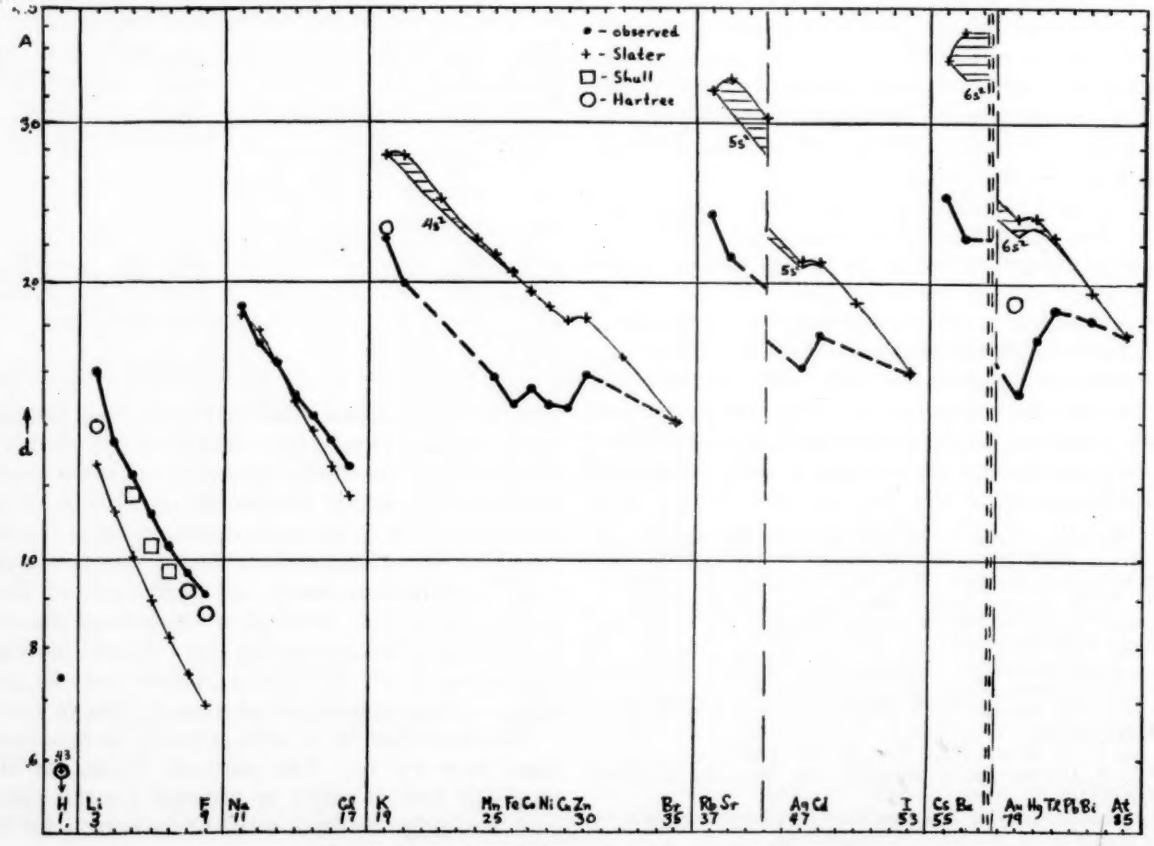

FIG. 1. Comparison of observed d with computed $r_{1.0}$.

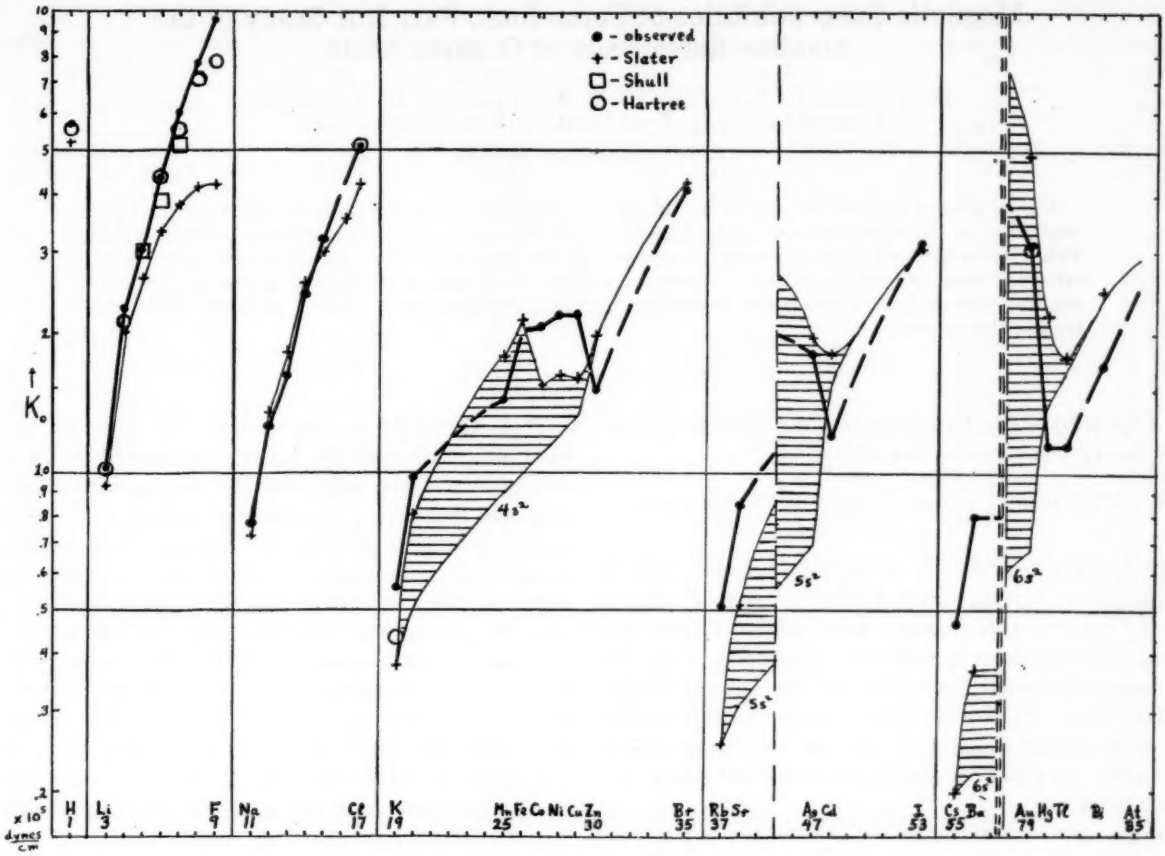
● - observed
+ - Slater
□ - Shull
○ - Hartree
K_e
$4s^2$
$5s^2$
$5s^2$
$6s^2$
$6s^2$
H Li F Na Cl K Mn Fe Co Ni Cu Zn Br Rb Sr Ag Cd I Cs Ba Au Hg Tl Bi At
1 3 9 11 17 19 25 30 35 37 47 53 55 79 85
$\times 10^5$ dynes/cm

FIG. 2. Comparison of observed k with computed k.

factors affecting atomic bond radii and molecular force constants. It may be useful for computing unknown force constants or distances if the systematic deviations of the Slater functions can be determined and compensated for, or if better convenient wave functions become available throughout the Periodic Table.

Several improvements in the general approach also suggest themselves.

First, the calculations might be carried out using the negative atomic ion, M^-, as the basis for the perturbation treatment instead of the neutral united atom, $M+1$. This would probably overemphasize the ionic character of the hydride, much as the present calculations overemphasize its united-atom character. The first-order truth should lie in between. Neither approximation takes the atomic-orbital character of the wave-functions sufficiently into account. As a result perhaps this general approach cannot be justifiably extended to molecules other than hydrides.

A second improvement might be the use of wave functions with angular dependence.

Another would be the examination of the effect of the valence state on the predictions for the transition elements and rare earths.

The method might be tried on the more complicated problem of excited states.

Further examination will show whether it can lead to any new rules-of-thumb for predicting or relating force constants and distances.

ACKNOWLEDGMENT

Coulson used a similar approach in discussing CH_4 from a united-atom point of view.[6] Mulliken and others have treated hydrides, and H_2O, NH_3 and CH_4 extensively from this point of view[7] but without applying perturbation theory to make specific predictions such as those given here. The prediction of proton position from the unperturbed electron density distribution was suggested by Longuet-Higgins' predictions of substitution position in aromatic hydrocarbons from the unperturbed electron density distribution.[8]

I am especially indebted to Dr. Ray K. Sheline for bringing the hydride data and the d-shell anomalies to my attention.

Note added in proof.—L. Pauling, Proc. Roy. Soc. **A114**, 181 (1927), used the same method and criterion used here for predicting distances in HF, HCl, and HBr. His wave functions and consequently his predicted distances were not as accurate as those given here. He did not predict force constants.

[6] C. A. Coulson, Trans. Faraday Soc. **33**, 388 (1937).
[7] R. S. Mulliken, Rev. Mod. Phys. **4**, 1 (1932); J. Chem. Phys. **1**, 492 (1933).
[8] H. C. Longuet-Higgins, J. Chem. Phys. **18**, 283 (1950).

Magnetic Susceptibilities of Some Ions. Part I. A Study of the Alkaline Earth Salts of Organic Acids

MATA PRASAD, C. R. KANEKAR, S. P. WALVEKAR, AND D. D. KHANOLKAR
Chemical Laboratories, Royal Institute of Science, Bombay, India

(Received February 20, 1950)

A linear relation between the molar susceptibility (χ_m) and the number of electrons in the cation has been established for the organic salts of (i) Mg, Zn, and Cd, and (ii) Ca, Sr, and Ba, containing a common anion. This relation has been successfully used to evaluate (a) the susceptibilities of anions in combination with cations of these two subgroups and (b) the susceptibilities of the cations themselves. It has been pointed out that this method of evaluation of ionic susceptibilities enables one to predict unknown cases with considerable accuracy.

ACCORDING to Langevin,[1] the susceptibility of an ion (χ_a) is given by the expression:

$$\chi_a = -(Ne^2/6mc^2)\sum_n\langle\gamma^2\rangle = -2.832\times10^{10}\sum_n\langle\gamma^2\rangle \text{ e.m.u.},$$

where $\sum_n\langle\gamma^2\rangle_{Av}$ is the sum of the mean-square radii of all electronic orbits. Several workers (cf. Pauling,[2] Stoner,[3] Slater,[4] and Angus[5]) have used certain theoretical considerations to calculate the values of $\sum_n\langle\gamma^2\rangle$ and hence evaluated the values for the susceptibilities of many ions. These calculated values not only differ from one another quite often, but are also not in agreement with the experimental values of several ions given in the literature.

So far, the experimental values of the ionic susceptibilities have been deduced from the observed values of the molar susceptibilities of salts on two assumptions: (i) the molar susceptibility of a heteropolar salt is the sum of the susceptibilities of the constituent ions, that is $\chi_m=\chi_{\text{cation}}+\chi_{\text{anion}}$, and (ii) the susceptibility of some ion has been fixed as standard on the basis of either theoretical considerations or otherwise [cf. Joos,[6] Ikenmeyer,[7] Brindley,[8] Brindley and Hoare,[9] Trew,[10] Reicheneder,[11] and Weiss[12]], and these values have been employed to deduce the susceptibilities of other ions. The result has been that in most cases several values widely different from one another have been found for the same ion. Such differences, in some cases, also arise from the fact that the values of the molar susceptibilities reported in the literature for the same salt by various workers are also often widely different.

It is therefore necessary that the problem of the ionic susceptibilities be attempted afresh with a view to obtain correct values of the susceptibilities of the ions and thereby to examine the accuracy of the theoretical calculations. For this purpose it is necessary, in the first instance, to check the values of the molar susceptibilities of salts already available in the literature by measuring very carefully the susceptibilities of these salts of known purity. The next problem is the selection of the value of the susceptibility of an ion which should be undoubtedly correct. This cannot be done with the values available at present. In order to overcome this difficulty and to obviate errors due to the arbitrariness involved in the assumptions made by various workers in choosing certain values of ions as standard, Bhatnagar and co-workers[13] and Prasad and co-workers[14] followed a statistical method in which they subtracted all the known values of the susceptibilities of anions from the molar susceptibilities of a number of salts of a cation and took the arithmetical mean of the values thus obtained as the correct value of the susceptibility of the cation. Although this procedure improves matters to some extent, it cannot be said to be entirely satisfactory because the values obtained by this method are also not free from the errors inherent in the reported values.

It is, therefore, necessary that the ionic susceptibilities be deduced by a method which does not involve the use of any of the values reported in the literature and whose accuracy will depend only on the accuracy of the experimental data of the molar susceptibilities of salts. Rudiments of such a method appear in the work of Kido[15] who observed a linear relation between the molar susceptibilities of salts of (i) alkali and (ii) alkaline earth metals containing a common anion and the number of electrons in the cations. Joos,[6] and Iken-

[1] P. Langevin, Ann. Chim. Phys. **5**, 70 (1905).
[2] L. Pauling, Proc. Roy. Soc. **114A**, 181 (1927).
[3] E. C. Stoner, Proc. Leeds, Phil. Soc. **1**, 484 (1927); *Magnetism and Matter* (Methuen and Company, Ltd., London (1934).
[4] J. C. Slater, Phys. Rev. **36**, 57 (1930).
[5] W. R. Angus, Proc. Roy. Soc. **136A**, 569 (1932).
[6] G. Joos, Zeits. f. Physik **19**, 347 (1923).
[7] K. Ikenmeyer, Ann. d. Physik **1**, 169 (1929).
[8] G. W. Brindley, Phil. Mag. **11**, 786 (1931).
[9] G. W. Brindley and F. E. Hoare, Proc. Roy. Soc. **152A**, 342 (1935); **159A**, 395 (1937).
[10] V. C. G. Trew, Trans. Faraday Soc. **32**, 1658 (1936); **37**, 476 (1941).
[11] K. Reicheneder, Ann. d. Physik **3**, 58 (1929).
[12] P. Weiss, J. de phys. et. rad. **1**, 185 (1930).
[13] S. S. Bhatnagar *et al.*, Curr. Sci. **4**, 153, 234 (1935); Phil. Mag. **18**, 449 (1934); J. Ind. Chem. Soc., **13**, 273 (1936); **12**, 799 (1935); **13**, 329 (1936); Proc. Ind. Acad. Sci. **9A** (1939).
[14] Prasad, Dharmatti, and Kanekar, Proc. Ind. Acad. Sci. **10A**, 307 (1942); and S. V. Gokhale, *ibid.* **20A**, 224 (1944); and H. V. Amin, *ibid.* **24A**, 312 (1947); and D. D. Khanolkar, *ibid.* **24A**, 328 (1947).
[15] K. Kido, Sci. Rep. Tohoku, Imp. Univ. **21**, 149, 288, 869 (1932); **22**, 835 (1933).

TABLE I.

Compound	χ_s	χ_m and χ_{ms}
Mg formate, 2 H_2O	0.464	69.74
		43.82
Ca formate	0.348	45.30
Zn formate, 2 H_2O	0.400	76.63
		50.71
Sr formate	0.339	60.30
Cd formate, 2 H_2O	0.336	80.90
		54.98
Ba formate	0.325	73.70
Mg acetate, 4 H_2O	0.567	116.2
		64.36
Ca acetate	0.433	68.40
Zn acetate, 2 H_2O	0.460	100.9
		74.98
Sr acetate, ½ H_2O	0.318	87.70
		81.20
Cd acetate	0.363	83.66
Ba acetate	0.390	99.49
Mg propionate, H_2O	0.527	99.30
		86.34
Ca propionate	0.539	100.4
Zn propionate	0.470	99.40
Sr propionate	0.462	107.9
Cd propionate	0.437	109.3
Ba propionate, H_2O	0.453	136.5
		123.5
Mg butyrate	0.558	110.6
Ca butyrate	0.558	119.5
Zn butyrate	0.499	119.5
Sr butyrate, H_2O	0.510	142.6
		129.6
Cd butyrate, H_2O	0.473	144.0
		131.0
Ba butyrate	0.468	145.6
Mg palmitate	0.705	376.8
Ca palmitate	0.707	389.1
Zn palmitate	0.673	387.0
Sr palmitate	0.675	403.3
Cd palmitate	0.645	401.6
Ba palmitate	0.645	417.4
Mg stearate	0.718	423.9
Ca stearate	0.721	436.7
Zn stearate	0.692	436.6
Sr stearate	0.677	444.0
Cd stearate	0.650	440.6
Ba stearate	0.654	460.0
Mg oxalate, 2 H_2O	0.455	67.60
		41.68
Ca oxalate	0.346	44.30
Zn oxalate, 2 H_2O	0.410	77.60
		51.68
Sr oxalate, H_2O	0.349	67.60
		54.64
Cd oxalate	0.265	53.10
Ba oxalate	0.287	64.80
Mg malonate, H_2O	0.475	68.50
		55.54

TABLE I.—(*Continued*)

Compound	χ_s	χ_m and χ_{ms}
Ca malonate	0.440	62.40
Zn malonate, H_2O	0.405	75.00
		62.04
Sr malonate	0.353	66.90
Cd malonate, 2 H_2O	0.370	92.75
		66.83
Ba malonate	0.340	81.30
Mg succinate, 3 H_2O	0.532	103.4
		64.52
Ca succinate, 3 H_2O	0.446	93.70
		54.82
Zn succinate	0.403	73.20
Sr succinate	0.381	71.50
Cd succinate	0.363	83.77
Ba succinate	0.385	97.60
Mg tartrate, 5 H_2O	0.505	132.5
		67.70
Ca tartrate, 4 H_2O	0.508	132.1
		80.26
Zn tartrate, 2 H_2O	0.424	105.9
		79.98
Sr tartrate, 4 H_2O	0.457	140.5
		88.66
Cd tartrate	0.369	96.10
Ba tartrate, H_2O	0.410	117.1
		104.1
Mg benzoate, 3 H_2O	0.573	183.4
		144.5
Ca benzoate, 3 H_2O	0.565	189.9
		151.0
Zn benzoate	0.498	153.2
Sr benzoate, H_2O	0.517	179.7
		166.7
Cd benzoate, 2 H_2O	0.476	186.1
		160.2
Ba benzoate, 2 H_2O	0.489	203.2
		177.3
Mg salicylate, 4 H_2O	0.558	206.5
		154.7
Ca salicylate, 2 H_2O	0.546	200.9
		162.0
Zn salicylate, 3 H_2O	0.512	201.5
		162.6
Sr salicylate, 2 H_2O	0.508	202.0
		176.1
Cd salicylate, H_2O	0.455	183.8
		170.8
Ba salicylate, H_2O	0.468	201.0
		188.0

meyer[7] have also shown that a linear relation exists between the susceptibilities of ions of chemically related elements belonging to the same group of the Periodic Table and their atomic numbers. Pascal[16] also obtained a linear relation between atomic susceptibility and the atomic number for elements belonging to one group in the periodic table. These observations are in accordance with the periodic law and only confirm the expectation of the group behavior of chemically related elements. Kido employed the linear relation for the calculation of susceptibilities of the constituent cations and the anions of the salts of alkali and alkaline earth metals. This method of the evaluation of ionic susceptibilities has been questioned by Trew[17] and Selwood[18] on the ground that it is open to theoretical objection, although both of them find that the values obtained by this method are fairly satisfactory. In some of the previous investigations of the authors, Kido's method has given very satisfactory results. In this investigation, the authors have therefore attempted to examine Kido's suggestion in the case of a large number of salts of alkaline earth metals with organic acids whose susceptibilities have been measured very carefully for this purpose.

[16] P. Pascal, Rev. Gen. Sci. **34**, 388 (1923); Chem. Abs. **17**, 344 (1923).

[17] V. C. G. Trew, Trans. Faraday Soc. **32**, 1658 (1936); **37**, 476 (1941).

[18] P. W. Selwood, *Magnetochemistry* (Interscience Publishers, Inc., New York, 1943).

EXPERIMENTAL

All the compounds used in this investigation were prepared in the laboratory in a chemically pure state by standard methods and were analyzed for their purity. Their susceptibilities were measured on a modified form of Gouy balance by the method followed by Prasad, Dharmatti and Gokhale.[14] The magnet was specially designed to give a fairly moderate field with a low current, so that the errors due to the heating of the coils were practically avoided. The yoke of the magnet was made of the best quality dynamo steel of low hysteresis. The current fed was 0.7 amp. from 230 d.c. mains. It was observed that the magnet showed no rise of temperature for half an hour's continuous run when kept open in a room, but when enclosed in a case, the temperature rose by 0.1°C. The field in the pole gap of about 1 cm was found to be 7300 gauss. Arrangements were made to keep the current, feeding the electromagnet, constant. The analytical balance had an accuracy of 0.0001 g in weight measurements. The tube containing the specimen was of uniform bore and made of Pyrex glass. When suspended in the pole gap, the lower end of the tube always lay exactly in the center of the field while the upper end was in a region where the field was almost negligible. Care was taken to see that the tube was always placed in the same position for all the measurements which were made relative to KCl as a standard ($\chi_{KCl}=-0.516\times10^{-6}$). Since the experimental method demands a mathematically continuous medium to be placed in the field, precautions were taken to pack the substances in the specimen tube as tightly and as uniformly as possible. To average errors due to (i) packing of the substances and (ii) non-uniformity, if any, of the specimen tubes, measurements were made on two specimen tubes with three separate fillings of the same substance in each tube. The average of the six closely agreeing values thus obtained was taken to be the correct value of the susceptibility of the substance. This arrangement and procedure gave fairly reproducible results.

The results obtained are given in Table I, in which χ_a represents the specific susceptibility, χ_m the molar susceptibility, and χ_{ma} the molar susceptibility of the anhydrous salt. χ_{ma} is obtained by subtracting the susceptibility for the molecules of water of crystallization ($\chi_{H_2O}=-12.96\times10^{-6}$) from the molar susceptibility of the hydrated salt on the assumption of the additivity law. Although this procedure is not strictly correct, for the present purpose it is quite satisfactory. The values of χ_m and χ_{ma} are given one below the other. The observed values of susceptibilities are expressed in the units of -1×10^{-6}. (A few of these values were used to evaluate the ionic susceptibilities of mercury in a previous communication.[19]

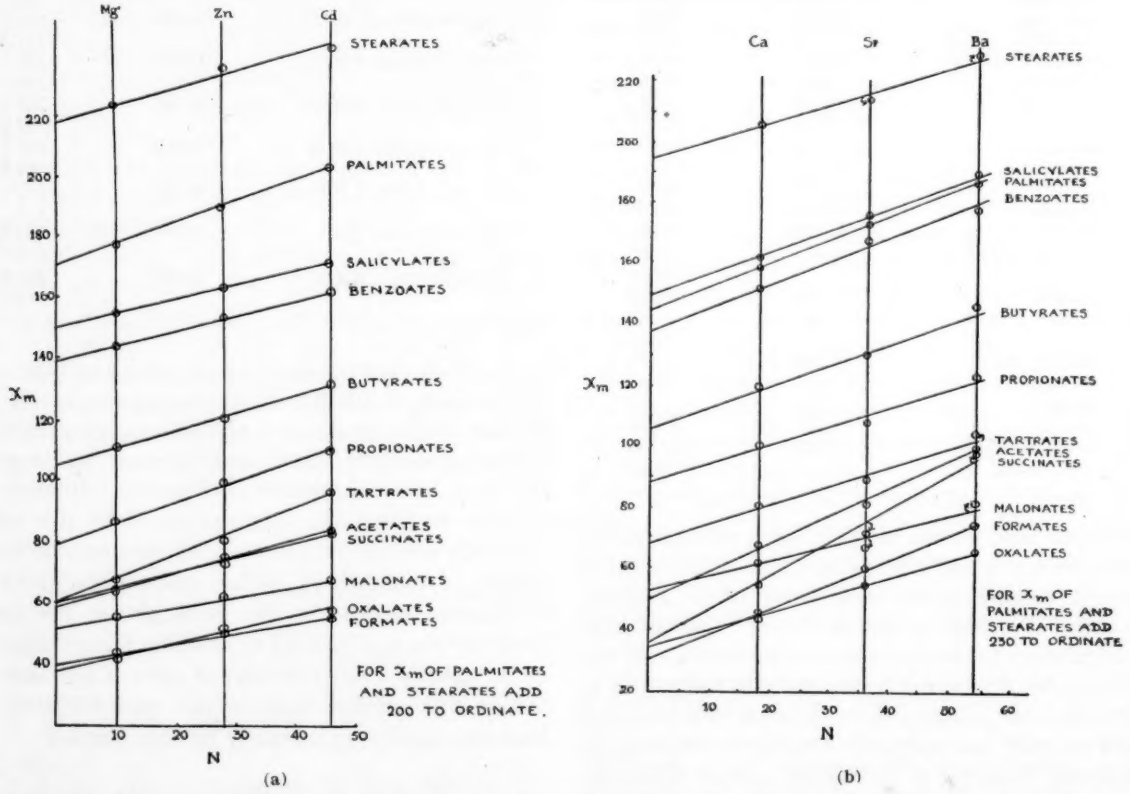

FIG. 1. Values of molar susceptibilities plotted against number of electrons in the cation. (a) Mg, Zn, and Cd. (b) Ca, Sr, and Ba.

[19] Prasad, Dharmatti, and Ghose, J. Chem. Phys. 17, 819 (1949).

TABLE II. Values of χ_{anions}.

Anions	χ_{anion} Mg-Zn-Cd	Ca-Sr-Ba	χ_{anion} (Pascal)
Formate	20.0	15.0	16.90
Acetate	29.5	25.0	28.76
Propionate	39.75	44.0	40.62
Butyrate	52.50	52.5	52.48
Palmitate	185.00	187.5	194.80
Stearate	209.00	212.0	218.52
Benzoate	70.00	68.5	67.72
Salicylate	75.50	74.5	73.93
Oxalate	38.00	34.0	27.94
Malonate	52.00	53.0	39.80
Succinate	60.00	36.0	51.66
Tartrate	60.00	68.0	60.88

DISCUSSION OF RESULTS

The values of the molar susceptibilities of salts of (i) Mg, Zn, and Cd, and (ii) Ca, Sr, and Ba containing a common anion have been plotted against the number of electrons in the cation. The plotted points lie on a series of straight lines [Fig. 1(a) and (b), respectively], which are different for the salts containing cations belonging to the two groups mentioned above. The straight lines have been extrapolated to the χ_m-axis and the values of the slope and the intercept for each line have been determined. The values of χ_m for the plotted points have been calculated from the values of the slopes and the intercepts, and the agreement, within the limits of experimental error, between the values thus obtained and the observed values, establishes that the relation between the χ_m of salts of (i) Mg, Zn, and Cd, and (ii) Ca, Sr, and Ba having the same anion, and the number of electrons (N) in the cation is definitely linear, that is,

$$\chi_m = (\delta\chi_m/\delta N)N + \text{intercept}$$

It must be remembered that this relation is true only for the plotted points; other points on the straight lines have no physical significance. These observations are in agreement with those of Kido.

Significance of $\chi_m - N$ Relations

The linear relation discussed previously indicates that (i) the magnetic behavior of the cations Ca, Sr, and Ba is similar, and the same is the case with the cations Mg, Zn, and Cd, and (ii) magnetically, the ions belonging to the two subgroups behave in a distinctly different manner. Chemically, although Mg for most purposes is similar to Ca, Sr, and Ba, magnetically it appears that its behavior is similar to that of Zn and Cd. This observation is in accordance with the expectations based on the periodic law.

When two ions combine there is every likelihood of a deformation taking place in both the ions. The existence of the linear relation between χ_m and N indicates that, possibly in combination with the same anion, the deformation caused by the group of chemically related cations appears to be very nearly the same, although one might have anticipated a greater effect in the case of the smaller cations.

The slopes ($\delta\chi_m/\delta N$) of the straight lines shown in Fig. 1 represent the susceptibility contribution per electron of the cation to the molar susceptibility of the salt. The intercept of these straight lines on the χ_m-axis represents a hypothetical condition, namely the χ_m of a salt when the number of electrons (N) in the cation is zero, and hence twice the susceptibility of the anion itself when combined with a particular group or subgroup of cations.

This interpretation of the intercept is very different from that of Kido who included in his plot not only the molar susceptibilities of the alkali salts containing the same anion but also the molar susceptibilities of the corresponding acids, against the number of electrons in the cation (N for H^+ ion being zero). The intercepts obtained by Kido, therefore, represent the molar susceptibilities of the acids and not the ionic susceptibility of the anion. In order to calculate the susceptibilities of the anions, Kido had to assume that the susceptibility of H^+ ion is zero, which may or may not be correct; because all organic acids are far from being electrovalent compounds. However, the intercepts obtained in this paper give the susceptibilities of the anions directly. It must be noted, however, that these intercepts have only a hypothetical significance and no physical significance can be ascribed to them.

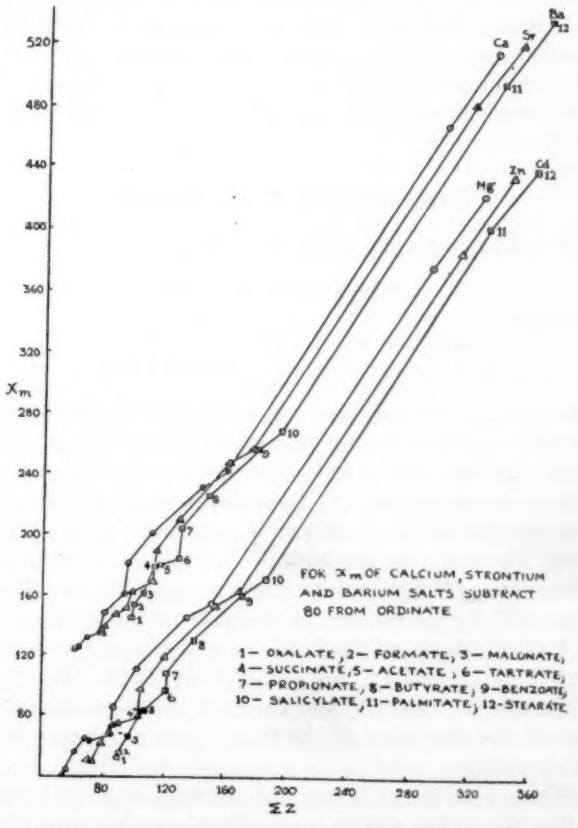
Ba
Ca
Sr
Mg
Zn
Cd
FOR χ_m OF CALCIUM, STRONTIUM AND BARIUM SALTS SUBTRACT 80 FROM ORDINATE
1- OXALATE, 2- FORMATE, 3- MALONATE, 4- SUCCINATE, 5- ACETATE, 6- TARTRATE, 7- PROPIONATE, 8- BUTYRATE, 9- BENZOATE, 10- SALICYLATE, 11- PALMITATE, 12- STEARATE
χ_m
Σz

FIG. 2. Values of molar susceptibilities plotted against total number of electrons.

TABLE III.

Series	$\chi_{cations}$ for Mg^{++}		Zn^{++}		Cd^{++}		Ca^{++}		Sr^{++}		Ba^{++}	
	χ_a	χ_b	χ_a	χ_b	χ_a	χ_b	χ_a	χ_b	χ_a	χ_b	χ_a	χ_b
Formate	3.44	3.50	10.70	9.80	14.98	16.10	15.30	14.99	30.30	29.99	43.70	44.98
Acetate	5.36	5.50	15.98	15.40	24.66	25.30	18.40	16.56	31.22	33.12	49.49	49.68
Propionate	6.86	6.50	19.93	18.20	29.80	29.90	12.37	11.39	19.92	22.79	35.51	34.18
Butyrate	5.62	5.60	14.54	15.68	26.08	25.76	14.45	13.32	24.64	26.64	40.60	39.96
Palmitate	6.80	6.90	16.99	19.32	31.57	31.74	14.12	14.04	28.20	28.08	42.44	42.12
Stearate	5.85	5.60	18.59	15.68	22.62	25.76	12.73	11.88	19.97	23.76	35.95	35.64
Benzoate	4.52	4.25	13.20	11.90	21.10	19.55	14.02	14.04	29.74	28.08	40.28	42.12
Salicylate	3.66	4.36	11.66	12.21	19.80	20.06	13.02	13.05	27.08	26.10	39.04	39.15
Oxalate	3.67	3.80	13.44	10.64	15.13	17.48	10.30	9.90	21.45	19.80	30.85	29.70
Malonate	3.53	3.50	10.06	9.80	14.83	16.10	9.43	9.00	13.93	18.00	28.27	27.00
Succinate	4.52	5.10	13.14	14.28	10.87	23.46	18.86	18.90	35.48	37.80	61.59	56.70
Tartrate	7.70	7.55	19.90	21.14	21.24	34.73	12.32	12.24	20.66	24.48	36.14	36.72
Average (1)	5.13	5.18	14.84	14.50	21.06	23.83	13.77	13.28	25.21	26.55	40.32	39.83
Average (2) from organic salts (Prasad and co-workers)	7.04		17.01				12.33		26.36		42.47	

The susceptibilities of the anions obtained from the intercepts are given in Table II.

Table II brings out very clearly that the susceptibility values of the anions deduced from the salts of Mg, Zn, and Cd are distinctly different from those deduced from the salts of Ca, Sr, and Ba. This means that the susceptibility of an anion is a fixed quantity only for cations of a particular subgroup in the periodic table. A mean of the values obtained for these anions from the two subgroups approximates the values calculated from Pascal's data. However, it is apparent from the above discussion that this method of assigning anion values permits a much more accurate prediction of an unknown case if two salts containing cations of the same column of the periodic table have been previously measured.

Susceptibilities of the Cations

It follows from the above discussion that

$$\chi_m = (\delta\chi_m/\delta N)N + 2\chi_{anion}.$$

Further,

$$\chi_m = \chi_{cation} + \sum \chi_{anion} \quad \text{(Pascal's law)},$$

where χ_{anion} has a definite value for salts of chemically related elements having the same anion. These relations can be used to calculate the susceptibility of a cation in two ways: (1) By subtracting the value of the susceptibility of an anion (intercept on χ_m-axis) from the molecular susceptibility of the salt containing the anion. (2) By multiplying the value of the slope $(\delta\chi_m/\delta N)$ by the number of electrons in the cation.

Values calculated by both these methods are designated as χ_a and χ_b, respectively, in Table III. The difference between the two values is, of course, a measure of the deviation of the point from a straight line relationship.

Table III further brings out the important fact that when the anion values are assigned in this way, the susceptibility of a cation is not a constant quantity but is different in combination with different organic anions; these differences are quite large in some cases and small in others. An average value has been calculated and given in row (1) at the bottom of the table only as an *ad hoc* measure to ascertain how far such average values obtained by a graphical method agree with the average values calculated by Prasad and co-workers[14] for these cations from salts of organic acids by the method of averages [row (2) at the bottom of the table]. The two sets of values are distinctly different in all cases, excepting Sr, though they are of the same order.

Ikenmeyer's Relation

Ikenmeyer observed a linear relation when the molar susceptibilities (χ_m) of alkaline earth halides determined from aqueous solutions were plotted against the total nuclear charge ($\sum z$) or the total number of electrons in the molecule and expressed it mathematically as:

$$\chi_m = C_1 \sum z + C_2$$

where C_1 is a general constant, while C_2 is a constant specific for a given series of salts. Trew[17] applied this relation to susceptibilities of thallium salts of various organic and inorganic acids and found that it holds with a few exceptions. Prasad and co-workers[14] have, however, shown that the relation is definitely non-linear for salts of inorganic and organic acids containing a common cation. These workers have further observed that by plotting the molar susceptibilities of salts containing the same cation against $\sum z$, a pattern is obtained which is characteristic of the group or subgroup in the periodic table to which that cation belongs. Thus, the patterns obtained by plotting the χ_m of corresponding salts of Ca, Sr, and Ba are strikingly similar to one another but differ, to a marked extent, from the patterns obtained for those of Mg, Zn, and Cd or of the elements of the other groups in the periodic table.

Such graphs obtained by plotting the χ_m of corresponding salts of (i) Ca, (ii) Sr, (iii) Ba, (iv) Mg,

(v) Zn, and (vi) Cd with organic acids against $\sum z$ are shown in Fig. 2.

SUMMARY

Magnetic susceptibilities of a large number of alkaline earth salts of organic acids have been measured by a modified form of Gouy's balance.

A linear relation between χ_m and the number of electrons in the cations has been established for the salts of chemically related elements, (i) Mg, Zn, and Cd, and (ii) Ca, Sr, and Ba, containing a common anion. This relation has been used to evaluate (a) the susceptibilities of anions in combination with the two subgroups of cations and (b) the susceptibilities of cations in combination with various organic anions. It has been pointed out that this method of evaluation of ionic susceptibilities enables one to make predictions in an unknown case with a much greater accuracy than by any other method.

The values obtained by the graphical method for the susceptibilities of organic anions indicate that formally the susceptibility of an organic anion is a fixed quantity only for cations of a particular subgroup in the periodic table. The susceptibility of a cation is also different in combination with different organic anions when the data are treated by this method.

Ikenmeyer's relation is not obeyed by these salts. The patterns obtained by plotting χ_m against $\sum z$ are strikingly similar for corresponding salts of (a) Mg, Zn, and Cd, and (b) Ca, Sr, and Ba.

THE JOURNAL OF CHEMICAL PHYSICS VOLUME 18, NUMBER 7 JULY, 1950

Magnetic Susceptibilities of Some Ions. Part II. A Study of Alkali Salts of Organic Acids

M. PRASAD, S. S. DHARMATTI, C. R. KANEKAR, AND D. D. KHANOLKAR
Chemical Laboratories, Royal Institute of Science, Bombay, India

(Received February 20, 1950)

The molar susceptibilities of a number of alkali salts of organic acids have been examined and a linear relation between the molar susceptibility and the number of electrons in the cation has been found. This behavior is similar to that of the group two elements discussed previously and enables one to extend the tabulation of ionic susceptibilities by the authors' graphical method.

IN Part I of this series the authors have shown that of all the various methods available for the tabulating of susceptibilities of ions, the graphical methods developed by Prasad and co-workers[1] is the most suitable one. In this paper the authors have extended its application to alkali salts of organic acids.

EXPERIMENTAL RESULTS

All the salts used in this investigation were prepared from pure materials and their purity tested by standard methods of analysis. The Gouy technique described in the previous paper was used for measuring the susceptibilities of these salts. The values of susceptibilities of the salts are given in Table I, in which the notations used are the same as in Part I.

DISCUSSION OF RESULTS

A series of straight lines shown in Fig. 1 are obtained by plotting the molar susceptibilities of the alkali salts containing the same anion against N. The intercepts of the straight lines on the χ_m-axis are the susceptibilities of the anions in combination with the alkali ions as discussed in Part I. These values are given in Table II along with those calculated by using Pascal's atomic constants and those obtained by the authors from the study of salts of alkaline earth metals. An examination of Table II reveals that the anion values determined from salts of alkali metals are distinctly different from Pascal's values and also from those deduced from the salts of alkaline earth metals. This is in agreement with the observation made by the authors in the case of salts of alkaline earth metals.

Susceptibilities of the Cations

From the considerations discussed in Part I, it is possible to deduce the susceptibilities of Li, Na, and K ions by two methods: (i) by subtracting the susceptibility value of the anion from the molecular susceptibility of the salt, and (ii) by multiplying the slopes $(\delta\chi_m/\delta N)$ of straight lines by the number of electrons in the cation.

The values calculated in this manner are given in Table III and are designated as χ_a and χ_b, respectively, and their difference is a measure of the deviation of the experimental points from a straight line.

It will be clear from Table III that the susceptibility values of the same alkali ion are different when it combines with different anions. This means that an alkali ion does not have a fixed value of susceptibility but a particular value is true only for its combination with a particular anion.

[1] Prasad, Dharmatti, and Kanekar, Proc. Ind. Acad. Sci. **10A**, 307 (1942). Prasad, Dharmatti, and Gokhale, *ibid.* **20A**, 224 (1944). Prasad, Dharmatti, and Amin, *ibid.* **24A**, 312 (1947). Prasad, Dharmatti, and Khanolkar, *ibid.* **24A**, 328 (1947).

TABLE I.

Substance	χ_a	χ_m and χ_{ma}
Lithium salts		
Formate, 1 H_2O	0.494	34.57
		21.61
Acetate	0.533	35.20
Propionate	0.573	45.90
Butyrate	0.608	57.20
Palmitate	0.730	191.4
Stearate	0.721	209.1
Oleate	0.692	199.4
Oxalate	0.378	38.00
Malonate	0.424	49.20
Succinate	0.478	62.20
Tartrate	0.448	72.60
Citrate, 4 H_2O	0.488	137.7
		85.86
Benzoate	0.577	73.90
Salicylate	0.573	82.50
Cinnamate	0.593	91.40
Hippurate, 1 H_2O	0.562	114.2
Sodium salts		
Formate	0.360	24.50
Acetate, 3 H_2O	0.574	78.10
		39.22
Propionate	0.509	48.90
Butyrate	0.560	61.60
Palmitate	0.706	196.4
Stearate	0.279	223.1
Oleate	0.690	210.1
Oxalate	0.382	51.20
Malonate	0.418	61.80
Succinate, 3 H_2O	0.535	115.7
		76.82
Tartrate, 2 H_2O	0.512	117.9
		91.98
Citrate, $\frac{1}{2}$ H_2O	0.439	117.2
		110.7
Benzoate	0.539	77.60
Salicylate	0.536	85.70
Cinnamate	0.580	98.70
Hippurate	0.556	111.8
Potassium salts		
Formate	0.370	31.10
Acetate	0.454	44.60
Propionate	0.510	57.20
Butyrate	0.555	70.00
Palmitate	0.700	205.9
Stearate	0.720	232.3
Oleate	0.672	215.2
Oxalate, 1 H_2O	0.427	78.60
		65.64
Malonate	0.405	73.00
Succinate, 3 H_2O	0.518	128.5
		89.62
Tartrate, $\frac{1}{2}$ H_2O	0.464	109.0
		102.5
Citrate, 1 H_2O	0.443	143.6
		130.6
Benzoate, 3 H_2O	0.567	121.5
		82.62
Salicylate	0.532	93.70
Cinnamate	0.591	110.0
Hippurate	0.554	120.2

A close examination of χ_a and χ_b values brings out very clearly that the values of susceptibilities of the alkali ions in combination with large anions like palmitate, stearate, oleate, cinnamate, etc., are higher than those in combination with smaller anions like formate, acetate, propionate, and butyrate. This observation is in conformity with that made by Trew[2] and Prasad and co-workers[1] who have tried to show that the susceptibility of a cation in combination with organic anions increases with the increase in the number of carbon atoms in the anion. The agreement between the cation values obtained from benzoates and salicylates on the one hand and from formates and acetates on the other suggests that formally benzoates and salicylates resemble formates and acetates in their behavior. But the uncertain effect of an aromatic system makes it difficult to interpret this behavior at the present stage.

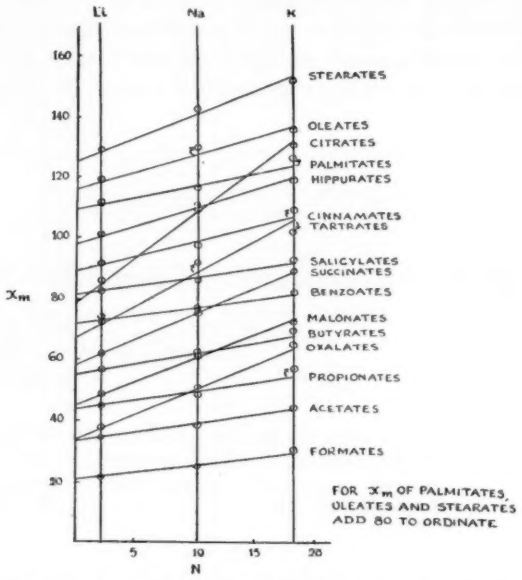

FIG. 1. Values of molar susceptibilities plotted against number of electrons in the cation.

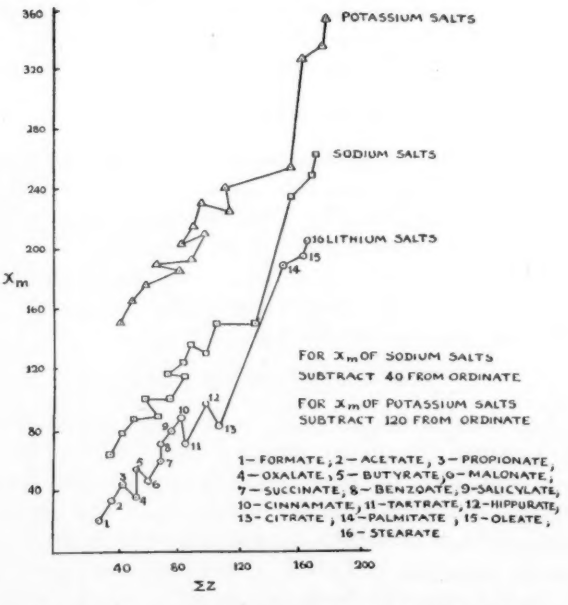
POTASSIUM SALTS
SODIUM SALTS
LITHIUM SALTS
FOR χ_m OF SODIUM SALTS SUBTRACT 40 FROM ORDINATE
FOR χ_m OF POTASSIUM SALTS SUBTRACT 120 FROM ORDINATE
1- FORMATE, 2- ACETATE, 3- PROPIONATE, 4- OXALATE, 5- BUTYRATE, 6- MALONATE, 7- SUCCINATE, 8- BENZOATE, 9- SALICYLATE, 10- CINNAMATE, 11- TARTRATE, 12- HIPPURATE, 13- CITRATE, 14- PALMITATE, 15- OLEATE, 16- STEARATE
χ_m
ΣZ

FIG. 2. Values of molar susceptibilities plotted against total number of electrons.

[2] V. C. G. Trew, Trans. Faraday Soc. **32**, 1658 (1936); **37**, 476 (1941).

TABLE II.

Anions	χ_{anion} Graphical (Li-Na-K)	Pascal	Graphical (Mg-Zn-Cd)	Graphical (Ca-Sr-Ba)
Formate	20.50	16.90	20.00	15.00
Acetate	34.00	28.76	29.50	25.00
Propionate	44.00	40.62	39.75	44.00
Butyrate	55.50	52.48	52.50	52.50
Palmitate	189.0	194.8	185.0	187.5
Stearate	206.0	218.5	209.0	212.0
Oleate	197.0	207.9	—	—
Oxalate	34.40	27.94	38.00	34.00
Malonate	45.50	39.80	52.00	53.00
Succinate	58.80	51.66	60.00	36.00
Tartrate	68.00	60.88	60.00	68.00
Citrate	79.50	79.17	—	—
Benzoate	72.50	67.72	70.00	68.50
Salicylate	81.00	73.93	75.50	74.50
Cinnamate	89.00	80.03	—	—
Hippurate	98.50	92.35	—	—

TABLE III.

Series	χ_{Li^+} χ_A	χ_B	χ_{Na^+} χ_A	χ_B	χ_{K^+} χ_A	χ_B
Formate	1.10	1.0	3.97	5.00	10.62	9.00
Acetate	1.18	1.14	5.19	5.70	10.55	10.26
Propionate	1.87	1.26	4.90	6.30	13.23	11.34
Butyrate	1.65	1.54	6.10	7.70	14.54	13.86
Palmitate	2.40	1.74	7.40	8.70	16.90	16.66
Oleate	2.40	2.24	13.10	11.20	18.20	20.16
Stearate	3.10	3.06	17.10	15.30	26.30	27.54
Benzoate	1.36	1.06	5.07	5.30	10.12	9.54
Salicylate	1.49	1.24	4.74	6.20	12.65	11.16
Cinnamate	2.39	2.14	9.65	10.70	21.70	19.26
Hippurate	2.74	2.54	13.30	12.70	21.00	22.86
Oxalate	1.81	1.70	8.40	8.50	15.62	15.30
Malonate	1.84	1.60	8.15	8.00	13.75	14.40
Succinate	1.70	1.75	9.01	8.75	15.40	15.75
Tartrate	2.29	2.10	11.99	10.50	17.26	18.90
Citrate	2.12	1.96	10.40	9.8υ	17.05	17.64

Ikenmeyer's Relation

Ikenmeyer's relation[3] has been examined in the case of alkali salts of organic acids and the graphs obtained are shown in Fig. 2. These curves show none of the linearity which is obtained by the authors' method of plotting. There is, however, a general similarity between the curves for each element of a group in the periodic table.

[3] K. Ikenmeyer, Ann. d. Physik **1**, 169 (1929).

SUMMARY

The linear relation between χ_m and the number of electrons in the cations established in Part I of this paper was observed to hold good for the alkali salts containing a common organic anion. From this relation, values have been calculated for the susceptibilities of the cations and anions in these salts.

The authors are grateful for a very helpful discussion with Dr. W. K. Wilmarth of the University of Southern California in this series of papers.

THE JOURNAL OF CHEMICAL PHYSICS VOLUME 18, NUMBER 7 JULY, 1950

Bipyramidal Heptacovalent Bond Orbitals

GEORGE H. DUFFEY
Chemistry Department, South Dakota State College, Brookings, South Dakota

(Received April 6, 1950)

A set of seven orthogonal bond orbitals of symmetry D_{5h} is considered. The orbitals are of type sp^3d^3. When the attached groups are all equivalent (such as in the bipyramidal AB_7 structure), the equatorial orbitals *and* the axial orbitals are strong. In general, the composition of an axial orbital differs considerably from the composition of an equatorial orbital. The discussion supports the view that IF_7 has a pentagonal bipyramidal structure.

SEVERAL arrangements of seven groups around a central atom are possible. Kimball[1] considered the ZrF_7^{-3} and TaF_7^{-2} structures. Recently, evidence[2] supporting a pentagonal bipyramidal structure for IF_7 has been presented.

In this paper the method of directed valence bonds[3] is used in discussing the pentagonal bipyramidal structure of symmetry D_{5h}. The fivefold axis is assumed to lie on the Z axis. The s, p, and d wave functions are defined in the same way as in previous papers[4] by the author.

The five equivalent bonds lying in the xy plane, separated by angles of $2\pi/5$, may be represented by the functions

$$\psi_1=\{[1/(5)^{\frac{1}{2}}]\sin\alpha\}s+[\sqrt{2}/(5)^{\frac{1}{2}}]p_x - \{[1/(5)^{\frac{1}{2}}]\cos\alpha\}d_z+[\sqrt{2}/(5)^{\frac{1}{2}}]d_{xy}, \quad (1)$$

$$\psi_2=\{[1/(5)^{\frac{1}{2}}]\sin\alpha\}s+\{[\sqrt{2}/(5)^{\frac{1}{2}}]\cos 72°\}p_x +\{[\sqrt{2}/(5)^{\frac{1}{2}}]\sin 72°\}p_y-\{[1/(5)^{\frac{1}{2}}]\cos\alpha\}d_z +\{[\sqrt{2}/(5)^{\frac{1}{2}}]\cos 144°\}d_{xy} +\{[\sqrt{2}/(5)^{\frac{1}{2}}]\sin 144°\}d_{x+y}, \quad (2)$$

[1] G. Kimball, J. Chem. Phys. **8**, 188 (1940).
[2] Lord, Lynch, Schumb, and Slowinski, J. Am. Chem. Soc. **72**, 522 (1950).
[3] L. Pauling, *The Nature of the Chemical Bond* (Cornell University Press, Ithaca, New York, 1940).
[4] See G. H. Duffey, J. Chem. Phys. **17**, 196 (1949).

TABLE I. Results of calculations on pentagonal bipyramidal orbitals.

Function maximized	Amount[a] of s in an equatorial orbital	S_1, Strength of an equatorial orbital	Amount[a] of s in an axial orbital	S_6, Strength of an axial orbital
$5S_1+2S_6$	0.1311	2.976	0.1723	2.920
S_1	0.0889	2.991	0.2778	2.806
S_6	0.1667	2.933	0.0833	2.957

[a] Note that the p content of any equatorial orbital is $\frac{2}{3}$; the p content of any axial orbital is $\frac{1}{3}$.

$$\psi_3=\{[1/(5)^{\frac{1}{2}}]\sin\alpha\}s+\{[\sqrt{2}/(5)^{\frac{1}{2}}]\cos144°\}p_x+\{[\sqrt{2}/(5)^{\frac{1}{2}}]\sin144°\}p_y-\{[1/(5)^{\frac{1}{2}}]\cos\alpha\}d_z+\{[\sqrt{2}/(5)^{\frac{1}{2}}]\cos72°\}d_{xy}-\{[\sqrt{2}/(5)^{\frac{1}{2}}]\sin72°\}d_{x+y}, \quad (3)$$

$$\psi_4=\{[1/(5)^{\frac{1}{2}}]\sin\alpha\}s+\{[\sqrt{2}/(5)^{\frac{1}{2}}]\cos144°\}p_x-\{[\sqrt{2}/(5)^{\frac{1}{2}}]\sin144°\}p_y-\{[1/(5)^{\frac{1}{2}}]\cos\alpha\}d_z+\{[\sqrt{2}/(5)^{\frac{1}{2}}]\cos72°\}d_{xy}+\{[\sqrt{2}/(5)^{\frac{1}{2}}]\sin72°\}d_{x+y}, \quad (4)$$

$$\psi_5=\{[1/(5)^{\frac{1}{2}}]\sin\alpha\}s+\{[\sqrt{2}/(5)^{\frac{1}{2}}]\cos72°\}p_x-\{[\sqrt{2}/(5)^{\frac{1}{2}}]\sin72°\}p_y-\{[1/(5)^{\frac{1}{2}}]\cos\alpha\}d_z+\{[\sqrt{2}/(5)^{\frac{1}{2}}]\cos144°\}d_{xy}-\{[\sqrt{2}/(5)^{\frac{1}{2}}]\sin144°\}d_{x+y}. \quad (5)$$

In testing these functions for orthogonality and in determining their composition, use the relation

$$\cos144°+\cos72°=-\tfrac{1}{2}. \quad (6)$$

This relation can be proved with the help of well-known trigonometric identities.

If it is assumed that the maxima of the p and d functions for the axial bonds lie on the Z axis[4] and that the orbitals are of symmetry D_{5h}, the axial bonds may be represented by the functions

$$\psi_6=\{[1/\sqrt{2}]\cos\beta\}s+(1/\sqrt{2})p_z+\{[1/\sqrt{2}]\sin\beta\}d_z, \quad (7)$$

$$\psi_7=\{[1/\sqrt{2}]\cos\beta\}s-(1/\sqrt{2})p_z+\{[1/\sqrt{2}]\sin\beta\}d_z. \quad (8)$$

Let

$$\beta=\alpha, \quad (9)$$

so that these seven functions form an orthogonal set. Their over-all composition is sp^3d^3.

Two functions orthogonal to $\psi_1\cdots\psi_7$ can be set up as follows:

$$\psi_8=d_{x+z}, \quad (10)$$

$$\psi_9=d_{y+z}. \quad (11)$$

Let the maximum value of ψ_1 be called S_1, and the maximum value of ψ_6, S_6. Consider molecules or ions of type AB_7. Assume the energy of each A-B bond is given by Eq. (13) in "Hexacovalent bond orbitals III."[5] In general, W for an axial bond differs from W for an equatorial bond. However, if the degree of ionic character of an axial bond and of an equatorial bond are assumed to be equal and constant, the sum of the W's and, incidentally, the sum of the R's over all bonds in AB_7 are not changed when α is changed. Then the value of α giving the largest sum of the bond energies is found by maximizing $5S_1+2S_6$. The results are given in the first row of Table I. Note that the composition of an axial bond orbital is near the composition of a cylindrical octahedral bond orbital.

When a molecule AB_7 assumes the pentagonal bipyramidal structure, one might expect considerable repulsion to exist between the five equatorial B's. It is of interest to compare this structure with the dodecahedral structure[3,6] as assumed by $Mo(CN)_8^{-4}$. Since in the dodecahedral structure there are fourteen angles equal to about 73°40′, one would expect that a radius ratio which was favorable to the formation of a dodecahedral structure would probably be favorable to the formation of the pentagonal bipyramidal structure.

In $Mo(CN)_8^{-4}$ the ratio of the covalent radius[3] of carbon to the covalent radius of molybdenum is 0.56. In IF_7 the ratio of the covalent radius of fluorine to the covalent radius of iodine is about 0.50, a more favorable value. The pentagonal bipyramidal structure for IF_7 uses one $5s$, three $5p$, and three $5d$ orbitals of the iodine atom, the orbitals most readily available for hybridization in heptacovalent iodine. From Table I the strength of an equatorial orbital is 2.976 and the strength of an axial orbital is 2.920. We tentatively conclude that the pentagonal bipyramidal structure is a reasonable structure for IF_7.

In each of the metal atoms of ZrF_7^{-3}, CbF_7^{-2}, and TaF_7^{-2} there are no unshared electrons in the valence shells and the p orbitals are more unstable than the s or d orbitals. Hence each tends to use a heptacovalent configuration approaching type spd^5 rather than sp^3d^3, the type which might yield the bipyramidal structure.

The other results recorded in Table I are of some interest. For instance, in a pentagonal plane molecule of type AB_5, $\psi_1\cdots\psi_5$ are used as the bond orbitals, and the best value of α is found by maximizing S_1 if the s and d orbitals are of equal stability.

[5] G. H. Duffey, J. Chem. Phys. **18**, 510 (1950).
[6] J. L. Hoard and H. H. Nordsieck, J. Am. Chem. Soc. **61**, 2853 (1939).

A Modification of the Theory of the Thermal Diffusion Column

H. G. DRICKAMER, E. W. MELLOW,* AND L. H. TUNG
Department of Chemistry, University of Illinois, Urbana, Illinois

(Received March 9, 1950)

Thermal diffusion measurements were made for the system argon-neon over a pressure range from 4–108 atmospheres. It is found that the classical theory of Furry, Jones, and Onsager is inadequate to describe the results obtained on a series of carefully constructed thermal diffusion columns. A modification of their theory, based on a more complete picture of the behavior of the column, is developed which fits the data satisfactorily. It is predicted and confirmed by experiment that even though turbulence occurs over part of the gap, a separation will occur, and may even be enhanced by this turbulence.

THERMAL diffusion, being the most sensitive of the transport properties to the molecular model chosen, offers an unusual opportunity to study the effect of temperature and pressure on molecular interaction. The difficulty arises that the effect is small, particularly at low temperatures, so that either very large temperature differences must be used, or one must resort to the use of a thermal diffusion column.

The first alternative essentially eliminates an accurate study of temperature dependence. The objection to the second alternative is that the column hydrodynamics are rather complex, and involve the knowledge of a variety of the physical properties of the system. Furry, Jones, and Onsager[1] and later Furry and Jones[2] have worked out a somewhat simplified picture which is a most satisfactory starting basis, but which does not seem to fit completely the data obtained in this laboratory for a variety of columns and gas systems.

Furry, Jones, and Onsager pictured a column with the following characteristics:

(1) A layer of hot gas of width one-half the annular gap rises on the hot wall.

(2) A layer of cold gas of the same width descends on the cold wall.

(3) The vertical velocity v_z depends on X (the horizontal coordinate) only and is independent of column height.

(4) There is no horizontal convective mixing between the hot and cold streams in the ideal case. The sole effect of such mixing when it does occur is to reduce the separation.

Based on this picture the three processes occurring are horizontal thermal diffusion and diffusion, vertical convection, and vertical diffusion. The equation obtained for the separation factor q is:

$$\ln q=\frac{H}{K_c+K_d}=\frac{63}{2}\frac{L\alpha D\eta}{\beta g w^4 T}\left[\frac{1}{1+5670(D\eta\Delta T/\beta w^3 g)^2}\right], \quad (1)$$

where

$$H=\frac{w^3\rho\alpha g\beta(\Delta T)^2 B}{90\eta T}, \quad (2)$$

$$K_c=\frac{w^7\rho g^2\beta^2 B(\Delta T)^2}{2835\eta^2 D}, \quad (3)$$

$$K_d=2w\rho DB. \quad (4)$$

Here H is concerned with horizontal diffusion and thermal diffusion, K_c is the vertical convection factor, and K_d the vertical diffusion factor.

On solving (1) for α one obtains:

$$\alpha=\ln q\frac{2\beta g w^4 T}{63LD\eta}\left[1+5670\left(\frac{D\eta\Delta T}{w^3\beta g}\right)^2\right]. \quad (5)$$

From Eq. (1) it can be seen that the separation will be small at low density or ΔT, limited by vertical diffusion (K_0), will increase to a maximum at the optimum density, and then decrease limited by vertical convective mixing (K_c).

Work in this laboratory, in part reported earlier,[3] in part reported in this paper, and in part to be reported later, has shown that even at high temperatures and/or low pressures where the classical kinetic theory should hold, Eq. (5) gives values of α which are too low at low densities (below the optimum) and too high at high

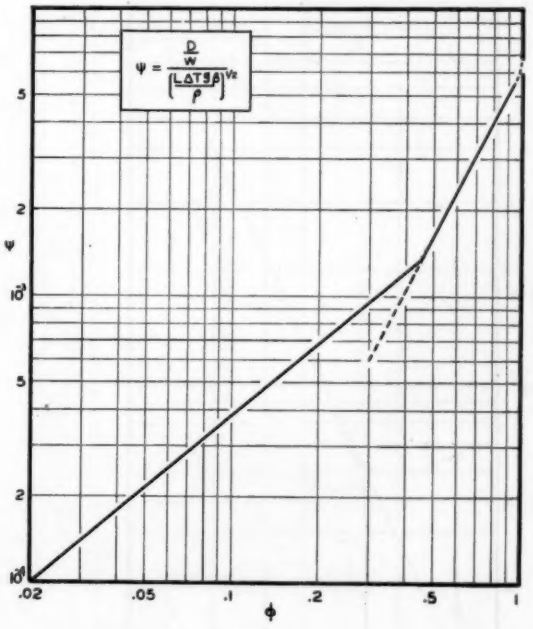

FIG. 1.

* Present address: University of Missouri, Columbia, Missouri.

[1] Furry, Jones, and Onsager, Phys. Rev. **55**, 1083 (1939).

[2] W. H. Furry and R. C. Jones, Rev. Mod. Phys. **18**, 151 (1946).

[3] Drickamer, O'Brien, Bresee, and Ockert, J. Chem. Phys. **16**, 122 (1948).

TABLE I.

Column	w	Length	Chamber volume	Pressure range
I	0.0508 cm	40 cm	4.6 cc (each)	3.7– 60 atmos.
II	0.0254 cm	41.6 cm	7.8 cc (each)	10.7–108 atmos.

densities. Furthermore the thermal diffusion ratios calculated for two carefully constructed columns (with different values of w) operated on the same gas system failed to check.

There appear to be no hydrodynamical studies of convection between two vertical parallel plates, one heated and one cold; however, Schmidt and Beckmann[4] have made a thorough investigation of convection near a single heated plate. While their findings are not directly applicable, it is possible to use certain of their results, namely that the maximum vertical velocity at any height is proportional to $[(h\beta\Delta Tg)/\rho]^{\frac{1}{2}}$, and that the degree of entrainment from the cold air to the rising stream is roughly proportional to this maximum vertical velocity.

The data from a number of different columns and a variety of gas systems yield consistent and reasonable values of α using the following modified column theory.

It is presumed that the equation of Furry, Jones, and Onsager gives an idealized picture of column operation essentially satisfactory near the optimum operating conditions, but that the relationship is not quantitative at densities very far removed from the optimum.

At low densities or ΔT's (i.e., low convection rates) only a fraction φ' of the half-gap w is in vertical convection in the sense defined by Furry, Jones, and Onsager. This fraction becomes unity before the optimum density is reached and remains there at higher convection rates.

At high convection rates, due to entrainment between the streams only a fraction φ of the gap is available for horizontal diffusion and thermal diffusion. This fraction will approach one near optimum operating conditions and remain there at lower convection rates.

It is presumed that the entire gap width is always available for vertical diffusion.

Equation (5) can then be written:

$$\alpha=\ln q\frac{2\beta g w^4 T(\varphi')^3\varphi}{63LD\eta}\left[1+\frac{5670}{\varphi}\left(\frac{D\eta\Delta T}{w^2\beta g\varphi'^3}\right)^2\right]. \quad (5a)$$

Further it seems reasonable that φ' should depend on some form of the Grashof number, the standard group for correlating convection along a vertical heated plate. φ will depend on the ratio between the horizontal diffusional transport rate D/W and the horizontal convective transport, which is presumed to be proportional to $[L\beta\Delta Tg/\rho]^{\frac{1}{2}}$.

From Eq. (5a) and from this discussion it can be seen that under some circumstances the effect of a certain degree of turbulence is to increase the net separation. This is more reasonable than it seems at first, since the effect of convective heat and mass transfer in the center of the gap is to increase the temperature gradient in the non-turbulent part (for fixed wall temperatures) and to decrease the path length for thermal diffusion, thus increasing its importance relative to the other processes occurring.

Data obtained on three different columns and with four different gas systems have been correlated using the relationships for φ and φ' shown in Eqs. (6)–(8) and Figs. 1 and 2.

$$\varphi'=1.00 \qquad Gr>1.2\times10^5 \quad (6a)$$

$$\varphi'=0.576[Gr]^{0.0486} \qquad 1.2\times10^5>Gr>6\times10^3 \quad (6b)$$

$$\varphi'=0.866 \qquad Gr<6\times10^3 \quad (6c)$$

$$\varphi=1260(\psi)^{1.2} \qquad \psi<1.35\times10^{-3} \quad (7a)$$

$$\varphi=13.6(\psi)^{0.512} \qquad 6.3\times10^{-3}>\psi>1.35\times10^{-3} \quad (7b)$$

$$\varphi=1.00 \qquad \psi>6.3\times10^{-3} \quad (7c)$$

$$Gr=\frac{\rho\beta g\Delta T w^2 L}{\eta^2} \quad (8a)$$

$$\psi=\left[\frac{D^2\rho}{w^2L\beta\Delta Tg}\right]^{\frac{1}{2}}. \quad (8b)$$

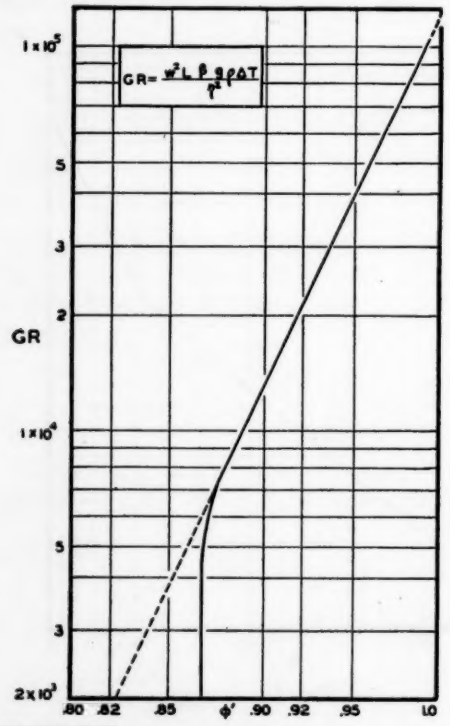

FIG. 2.

EXPERIMENTAL DATA AND RESULTS

Previous data have been reported[3] on the system $CO_2-C_3H_8$ using a column 244 cm long with $w=0.154$

[4] E. Schmidt and W. Beckmann, Tech. Mech. and Therm., 341, 391 (1930).

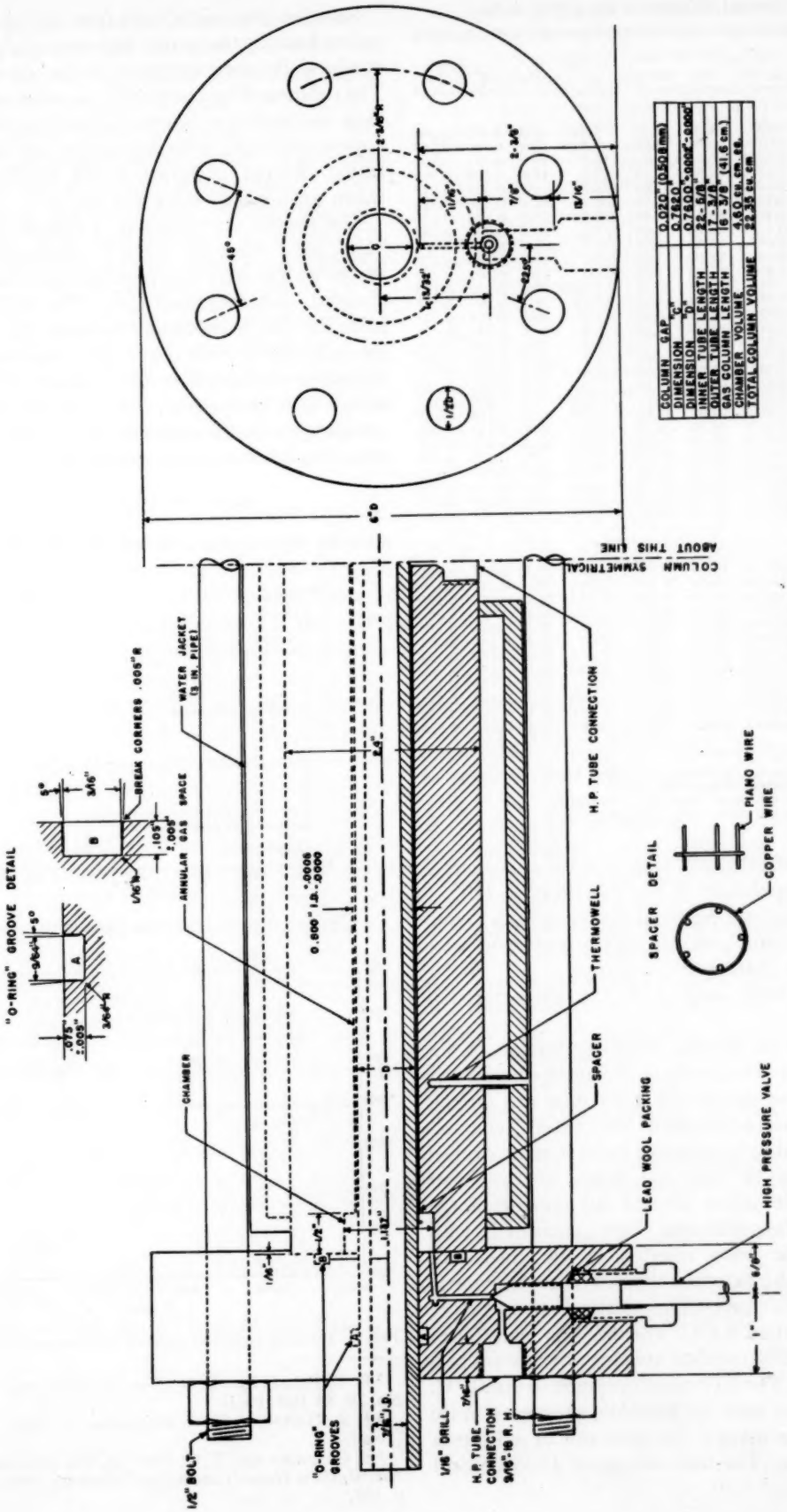

FIG. 3. Thermal diffusion column. Material: cold-rolled steel.

TABLE II. Thermal diffusion in the system A-Ne.

Run No.	T (°K)	P (atmos.)	(g/ml)	Percent neon top	Percent neon bottom	q	T (°C)	α'	α
Column II									
1	302.6	29.5	0.0373	61.35	26.15	4.483	19.8	0.177	0.209
2	302.5	15.78	0.0199	48.72	41.00	1.416	19.4	0.149	0.213
3[a]	302.2	103.2	0.1304	86.25	5.05	117.9	19.9	0.327	0.201
4	302.6	102.2	0.1291	79.40	1.80	210.3	19.6	0.329	0.208
5	302.6	102.2	0.1291	81.60	1.95	223.0	19.2	0.335	0.213
6	327.5	107.9	0.1247	82.30	1.70	268.9	20.4	0.336	0.228
7	327.3	104.3	0.1207	82.50	1.40	332.0	20.7	0.328	0.226
8	327.5	99.6	0.1152	82.20	1.05	435.2	20.6	0.331	0.238
9	327.6	82.5	0.0957	83.40	1.25	396.9	20.9	0.280	0.229
10	303.1	79.6	0.1005	87.60	1.95	355.2	18.9	0.296	0.228
11	303.0	81.0	0.1023	87.90	1.70	420.1	19.3	0.305	0.230
12	303.7	15.64	0.0197	46.85	39.75	1.336	20.0	0.121	0.173
13	303.7	40.9	0.0515	72.20	12.50	18.18	20.1	0.191	0.203
14	303.7	39.3	0.0496	74.20	12.60	19.95	20.3	0.208	0.224
15	303.8	60.4	0.0768	88.80	2.60	297.0	20.2	0.252	0.226
16	303.7	58.6	0.0739	89.95	2.40	364.0	20.1	0.266	0.246
17	325.8	59.6	0.0698	86.85	4.40	143.5	21.8	0.234	0.222
18	325.8	59.0	0.0691	85.80	4.65	123.9	21.8	0.224	0.214
19[b]	302.2	58.3	0.0739	67.50	21.10	7.767	10.6	0.234	0.243
20[b]	302.0	57.5	0.0755	52.95	35.55	2.040	5.7	0.239	0.274
21	325.1	32.8	0.0385	64.65	26.55	5.059	22.6	0.173	0.203
22	324.9	16.59	0.0195	48.20	40.15	1.387	22.4	0.145	0.209
23	324.9	10.53	0.0124	46.10	42.55	1.155	22.4	0.151	0.216
24	324.3	10.67	0.0126	45.05	41.75	1.144	22.5	0.135	0.208
25	322.3	10.67	0.0126	46.80	41.30	1.250	28.0	0.141	0.217
26	322.2	10.67	0.0127	46.60	41.20	1.246	28.7	0.132	0.202
27	322.1	10.67	0.0127	47.15	41.15	1.276	29.0	0.143	0.220
28	324.7	16.72	0.0195	48.10	40.05	1.387	22.4	0.147	0.213
Column I									
29	303.7	60.0	0.0757	54.05	28.15	3.003	20.2	0.353	0.195
30	303.7	58.2	0.0734	53.60	27.50	3.046	20.2	0.337	0.189
31	303.7	41.3	0.0521	61.20	20.96	5.970	20.2	0.284	0.198
32	303.7	40.6	0.0512	62.45	20.65	6.391	20.1	0.287	0.202
33	303.5	31.4	0.0396	69.65	18.65	10.22	20.4	0.248	0.220
34	303.5	30.2	0.0380	69.90	18.15	10.47	20.4	0.241	0.203
35[a]	303.6	15.98	0.0201	59.60	25.30	4.356	20.5	0.173	0.194
36	303.6	15.24	0.0192	59.00	25.35	4.238	20.5	0.183	0.207
37	303.6	10.40	0.0131	51.45	34.00	2.057	20.4	0.175	0.227
38	303.6	10.37	0.0131	50.85	34.55	1.960	20.5	0.164	0.212
39[b]	303.7	5.65	0.0071	45.05	40.30	1.215	20.4	0.158	0.242
40[b]	303.7	3.72	0.0047	43.95	41.95	1.085	20.4	0.153	0.235

Note.—α' calculated by the equations of Furry, Jones, and Onsager; α calculated by the equations in this paper.
[a] Steady state not yet obtained—separation increasing.
[b] Steady state not yet obtained—separation decreasing.

cm over a range of pressures from 0.3–1.8 atmospheres at an average temperature of 380°K with $\Delta T = 180°$.

In this paper data are reported for the system argon-neon. The gases were spectroscopically pure and were obtained from the Matheson Company.

Two columns were used with the characteristics shown in Table I.

Figure 3 shows the details, including tolerances, for one of the columns. The inside of the outer column was honed, while the outside of the inner tube was ground and lapped. Gas was admitted at the center. Temperatures were obtained by circulating water from controlled temperature baths through the inside of the inner column and in the jacket around the outside of the outer column. Temperatures were measured with thermocouples, one being inserted in the inner wall opposite each of the external thermowells. A Type K potentiometer was used. The vertical temperature gradient was less than 0.1°C. The ΔT was maintained fairly low (about 20°C) so that average physical properties would be used. The ΔT was maintained to ±0.05°C. The pressures were read on bourdon gauges accurate to ±0.2 psia in the range 0–200 psia and to ±1.5 psia above this pressure. The feed contained 43.55 percent neon.

Samples were withdrawn from the chambers through valves built in the heads, and were analyzed by thermal conductivity measurements as described previously.[5,6] The columns were operated on a series of ascending and then descending pressures so that the steady state was approached both with increasing and decreasing separation. Except as noted in the results samples were taken until steady state was reached.

The results are shown in Table II and Fig. 4. The value of α (denoted by α') calculated from Eq. (5) varies widely with the pressure, and between columns at fixed operating conditions. The value α calculated from Eq. (5a) is consistent between the columns within the accuracy of the data and shows only the slight variation with pressure to be expected at higher pressures. The theoretical values shown in Fig. 4 were calculated from the equations of Chapman and Cowling[7] using the Lennard-Jones potential,

$$E = -4\epsilon[(r_0/r)^6 - (r_0/r)^{12}], \tag{9}$$

and the integrals tabulated by Hirshfelder, Bird, and

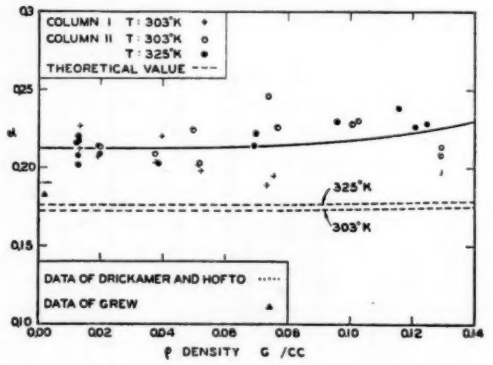

FIG. 4. Thermal diffusion ratio of the system A-Ne.

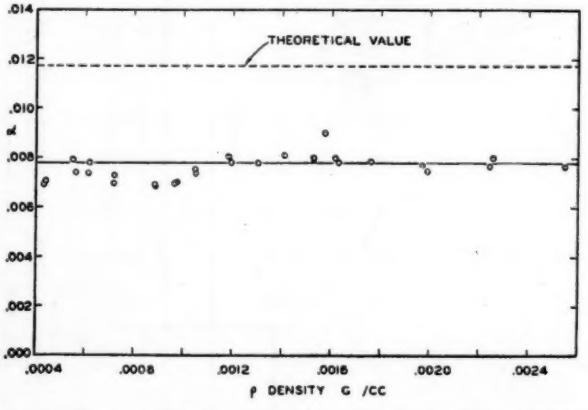

FIG. 5. Thermal diffusion ratio of the system CO_2-C_3H_8 at 380°K.

[5] P. E. Palmer and E. R. Weaver, Tech. Pap. Bur. Stand. **18**, No. 29, 35–100 (1924).
[6] J. R. Hofto and H. G. Drickamer, J. Chem. Phys. **17**, 1165 (1949).
[7] S. Chapman and T. G. Cowling, *The Mathematical Theory of Non-Uniform Gases* (Cambridge University Press, London, 1939), p. 167.

Spotz.[8] At the higher densities Thorne's[9] modification of Enskog's dense gas theory was used. The results as calculated from Eq. (5a) are about 25 percent higher than the theoretical value and some 10–15 percent higher than the experimental values found for two-bulb systems.[6,10] It is felt that this discrepancy is probably due to the large vertical concentration gradient which results in a large vertical density and viscosity gradient.

In order to use Eqs. (5) and (5a) it is necessary to know or to calculate the coefficient of ordinary diffusion D_{12}, the viscosity η, the density ρ and $\partial\rho/\partial T$.

The viscosity at atmospheric pressure was taken from Trautz and Kapphan[11] for argon-neon mixtures. This was corrected for density using Enskog's[12] dense gas theory. ρ and β were evaluated from p-v-t data.[13] The diffusion coefficients were calculated from the theory of Chapman and Cowling[14] using the Lennard-Jones potential.

Table III and Fig. 5 show the results for the system CO_2-C_3H_8. The theoretical values and the gas properties were calculated as above, using the viscosity data of Trautz and Kurz.[15] The experimental and theoretical values agree as well as might be expected, as in this temperature region the calculated α depends strongly on the value of the interaction energy assumed for unlike molecules. This was here assumed to be the geometric mean of the interaction energy for like molecules.

The fit obtained using Eq. (5a) and the above data has been confirmed with further data on a variety of other systems which will be published in following articles. It might be mentioned here that the columns have been operated in the region where the heat transfer is definitely turbulent. A separation was obtained and could be correctly predicted using the above correlation.

It appears now to be possible to measure and correlate thermal diffusion ratios and to predict interaction energies for dense gases and possibly liquids.

The authors wish to acknowledge the assistance of N. C. Pierce with the design and construction of the equipment.

TABLE III. Thermal diffusion in the system CO_2-C_3H_8.

Run no.	T=380°K P (atmos.)	ρ (g/ml)	T=180°C q	α'[a]	α[b]
1	1.116	0.001578	5.01	0.01350	0.00896
2	0.836	0.001181	4.58	0.00987	0.00804
3	0.845	0.001192	4.41	0.00967	0.00780
4	0.625	0.000883	2.91	0.00730	0.00690
5	0.631	0.000892	2.94	0.00733	0.00686
6	0.397	0.000561	1.69	0.00649	0.00740
7	0.390	0.000551	1.70	0.00689	0.00790
8	0.998	0.001410	4.60	0.01120	0.00809
9	0.682	0.000965	3.24	0.00765	0.00695
10	0.686	0.000970	3.32	0.00778	0.00700
11	1.410	0.001991	3.06	0.01330	0.00749
12	1.395	0.001970	3.18	0.01356	0.00770
13	0.510	0.000720	2.22	0.00673	0.00697
14	0.510	0.000720	2.30	0.00703	0.00730
15	0.744	0.001050	3.90	0.00866	0.00752
16	0.744	0.001050	3.72	0.00845	0.00735
17	1.593	0.002252	2.82	0.01529	0.00796
18	1.590	0.002246	2.70	0.01468	0.00768
19	1.248	0.001761	3.67	0.01276	0.00785
20	1.247	0.001760	3.79	0.01305	0.00787
21	0.312	0.000441	1.35	0.00581	0.00710
22	0.309	0.000436	1.32	0.00560	0.00692
23	1.805	0.002550	2.35	0.01594	0.00766
24	1.805	0.002550	2.31	0.01566	0.00752
25	1.153	0.001630	3.96	0.01203	0.00781
26	1.143	0.001617	4.09	0.01219	0.00799
27	1.082	0.001530	4.33	0.01179	0.00801
28	1.082	0.001530	4.25	0.01165	0.00791
29	0.924	0.001303	4.42	0.01022	0.00779
30	0.433	0.000612	1.85	0.00664	0.00734
31	0.439	0.000620	1.97	0.00713	0.00783

[a] α' calculated by the equations of Furry, Jones, and Onsager.
[b] α calculated by the equations in this paper.

NOMENCLATURE

B average circumference
D_{12} coefficient of ordinary diffusion
D_T coefficient of thermal diffusion
g acceleration of gravity
h height to any point on a vertical plate
L height of the column
n_{10} mole fraction of component one
n_{20} mole fraction of component two
p pressure in atmospheres
q separation factor
T absolute temperature
ΔT temperature difference between the hot and cold plate
w one-half the annular spacing
α thermal diffusion ratio
$\beta = -(\partial\rho/\partial T)_p$
η coefficient of viscosity
ρ density
φ fraction of w available for diffusion
φ' fraction of w in convection.

[8] Hirschfelder, Bird, and Spotz, J. Chem. Phys. **16**, 968 (1948).
[9] Reference 7, p. 293.
[10] K. E. Grew, Proc. Roy. Soc. **189** (1947).
[11] M. Trautz and G. Kapphan, Ann. d. Physik **2**, 737 (1929); **5**, 561 (1930).
[12] Reference 7, p. 288.
[13] Holborn and Otto, Ann. d. Physik **63**, 674 (1920); Zeits. f. Physik **10**, 367 (1922); **38**, 359 (1926).
[14] Reference 7, p. 292.
[15] M. Trautz and F. Kurz, Ann. d. Physik **9**, 981 (1931).

Thermal Diffusion in the Critical Region. I

N. C. PIERCE,* R. B. DUFFIELD,† AND H. G. DRICKAMER
Department of Chemistry, University of Illinois, Urbana, Illinois
(Received March 9, 1950)

Thermal diffusion data in the critical region have been obtained for the system ethane-xenon using very low xenon concentrations and Xe^{133} as a tracer. The results indicate that even at pressures as low as four atmospheres and temperatures twenty degrees above the critical, the simple kinetic theory of gases is not adequate to explain thermal diffusion. In the critical region evidence is found for the existence of clusters of ethane.

THERMAL diffusion is the most sensitive of the transport quantities to the mechanism of molecular interaction. Accordingly, the measurement of the thermal diffusion ratio in the critical region should give considerable insight into the difference between the mechanism of molecular motion in the gas and in the liquid state. The present paper presents the results of an exploratory investigation in this region.

EXPERIMENTAL APPARATUS AND PROCEDURE

The following factors were considered in the selection of a gas system:

1. The system should have a narrow phase envelop in order to permit varied operation in and near the critical region within a reasonable range of temperature and pressure.
2. The critical temperature and pressure should be within a range of accurate experimental measurement and control.
3. The system should be capable of rapid and accurate analysis.
4. The physical properties of the mixture must be well known in the critical region.
5. The gases must be obtainable in a state of high purity.
6. The gases should be such that they will give a reasonable separation by thermal diffusion.
7. The molecules of the mixture should be as symmetrical as possible, and they should be chemically inert under all phases of operation.

The system ethane-xenon was chosen as representing a suitable compromise of the restrictions listed above. Ethane of 99.9 mole percent purity whose most probable impurity was propane was purchased from the Phillips Petroleum Company. Spectroscopically pure xenon was purchased from the Matheson Company. Ethane has a critical temperature of 32.28°C, and a critical pressure of 48.7 atmospheres. Xenon has a critical temperature of 16.6°C, and a critical pressure of 58.2 atmospheres.

The radioactive tracer used was the 5.3-day Xe^{133} which decays by the emission of 0.33-Mev beta-ray and 0.085-Mev gamma-ray. This was produced by neutron irradiation of 40 cc of xenon at 60 cm pressure in the heavy water pile at the Argonne National Laboratory. The specific activity used was approximately one millicurie per millimole of xenon.

A mixture of ethane and irradiated xenon containing 0.18 mole percent xenon was then used in the work. At this dilution the p-v-t data for pure ethane could be used within the accuracy of the measurements.

EQUIPMENT AND OPERATION

The column used for this study was column II described in the previous paper.[1] The temperature control and measurement were the same as discussed there. The pressures were measured on bourdon gauges giving the accuracies shown in Table I.

Samples were taken to a glass cell with a mica (or alternatively aluminum foil) window. The cell was fixed to maintain constant geometry with respect to a thin window Geiger-Müller counter. The counts were then corrected for the temperature and pressure of the gas in the cell and for the decay of the xenon. The corrected ratio of the counts was then taken as the separation factor "q."

CALCULATION AND DISCUSSION OF RESULTS

As discussed in the previous paper[1] the thermal diffusion ratio can be calculated from the separation obtained in a column from the equation

$$\alpha=\ln q\frac{2\beta g w^4 T(\varphi')^3\varphi}{63LD\eta}\left[1+5670\frac{D^2\eta^2(\Delta T)^2}{w^6g^2\beta^2\varphi(\varphi')^6}\right], \quad (1a)$$

which may be written

$$\alpha=\ln q\frac{(\varphi')^3\varphi}{A\Gamma}\left[1+\frac{B\Gamma^2}{\varphi(\varphi')^6}\right], \quad (1b)$$

where

$$A=\frac{63L}{2gw^4T} \quad (2)$$

$$B=\frac{5670(\Delta T)^2}{w^6g^2} \quad (3)$$

$$\Gamma=D\eta/\beta. \quad (4)$$

A and B depend only on the column and operating conditions, while Γ is a property of the gas. As discussed in the previous paper φ and φ' depend on both

* Present address: Nylon Division, E. I. du Pont de Nemours, Wilmington, Delaware.
† R. B. Duffield is also in the Department of Physics.

[1] Drickamer, Mellow, and Tung, J. Chem. Phys. 18, 945 (1950).

the column and the gas. The physical properties needed are ρ, β, η, and D. ρ and β were evaluated from p-v-t data.[2,3] The viscosities were a combination of measured values[4] and values calculated from the theory of non-uniform gases[5] using Enskog's dense gas correction.[6] The Lennard-Jones potential for molecular interaction

$$E=-4\epsilon[(r_0/r)^6-(r_0/r)^{12}] \quad (5)$$

was assumed to apply at atmospheric pressure. The integrals of Hirschfelder, Bird, and Spotz[7] were used. Both the Lennard-Jones potential at atmospheric pressure[7] and the dense gas correction[6,8] have been shown to hold quite accurately for gases in the critical region, and even for liquids near the critical, in so far as viscosity is concerned, so no great error should arise from their use in calculating viscosity. The diffusion coefficients were also calculated using the Lennard-Jones potential and Thorne's[9] dense gas correction. The Lennard-Jones potential fits experimental data at atmospheric pressure quite closely, but no experimental corroboration of the dense gas theory for diffusion is yet available, and this may be the source of considerable error. Measurements of diffusion in dense gases are now under way in this laboratory.

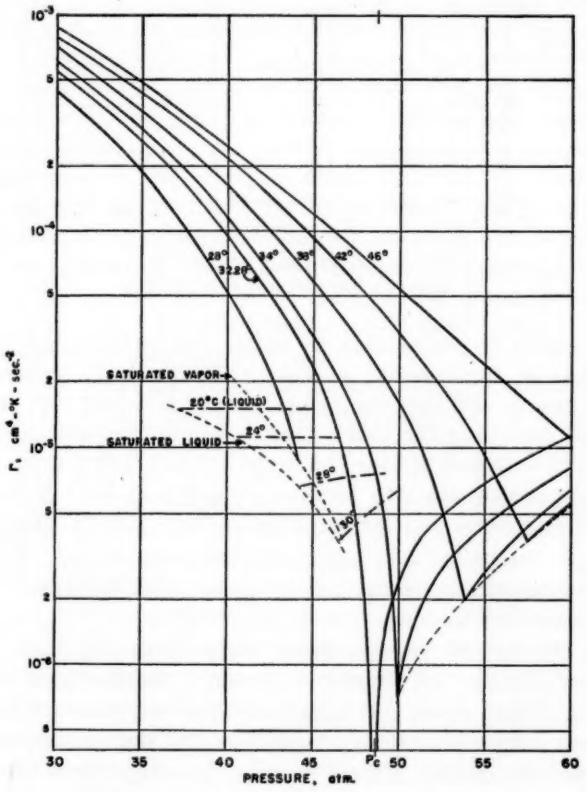

FIG. 1. Values of Γ for xenon-ethane.

TABLE I.

Range
0– 200 psig±0.2 psia
200– 500 psig±1.5 psia
500– 800 psig±0.5 psia
800–1500 psig±1.5 psia

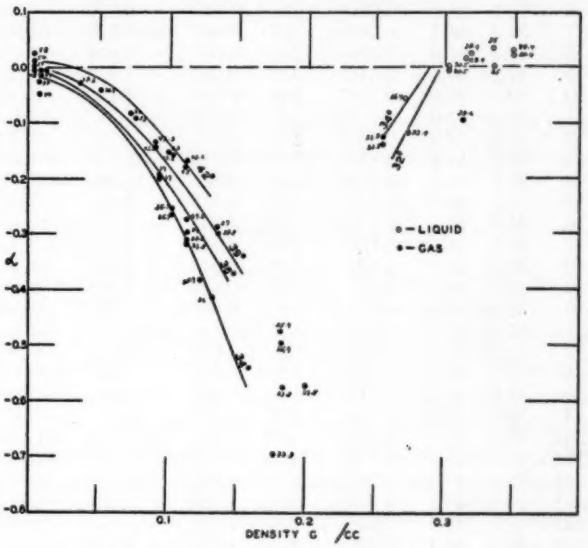

FIG. 2.

Since most gas properties vary rapidly near the critical point, very low ΔT's were maintained, often below 2°C.

Γ is plotted as a function of temperature and pressure in Fig. 1. Near the critical point it varies rapidly and irregularly over even a one degree ΔT. An integrated average Γ was used. The accuracy of this procedure was checked by numerically integrating the original differential equations of Furry, Jones, and Onsager[10] for several points using appropriate values of φ and φ'. The use of an integrated average Γ checked this more accurate method within four percent. The data and results are presented in Table II and Fig. 2. All runs except the starred ones were made in duplicate to insure that the steady state had been obtained.

The data are not sufficiently complete to allow for very general conclusions; nevertheless, several rather remarkable points can be made. In the first place, α very definitely depends on pressure, even at pressures as low as four atmospheres. This is not predicted by theory, nor does it occur at temperatures sufficiently far above the critical.[1] The change of sign with temperature is predicted by the theory using the Lennard-Jones model,

[2] B. Sage and N. Lacey, Ind. Eng. Chem. **28**, 931 (1937).
[3] Barkelew, Valentine, and Hurd, Chem. Eng. Progress **43**, 25 (1947).
[4] T. Titani, Bull. Inst. Phys. Chem. Research (Japan) **8**, 433 (1929).
[5] S. Chapman and T. G. Cowling, *Mathematical Theory of Non-Uniform Gases* (Cambridge University Press, London, 1939) p. 164.
[6] Reference 5, p. 288.
[7] Hirschfelder, Bird, and Spotz, J. Chem. Phys. **16**, 968 (1948).
[8] Comings, Mayland, and Egly, Univ. of Ill. Eng. Expt. Station Bulletin 354 (1944).
[9] Reference 5, p. 293.
[10] Furry, Jones, and Onsager, Phys. Rev. **55**, 1083 (1939).

TABLE II.

Run No.	Temp. °C	Press. atmos.	Density ρ	ΔT°C	q	α'[a]	α[b]
1	43.2	51.8	0.1160	3.6	0.660	− 1.50	−0.168
2	43.2	51.6	0.1150	3.5	0.645	− 1.53	−0.176
3	43.0	49.7	0.1041	3.9	0.623	− 1.155	−0.162
4	42.6	49.2	0.1026	4.2	0.617	− 1.105	−0.155
5	42.3	46.7	0.0921	3.8	0.608	− 0.728	−0.145
6	42.0	46.6	0.0918	3.3	0.634	− 0.670	−0.145
7	39.2	46.1	0.0945	2.2	0.643	− 0.826	−0.195
8	39.2	46.0	0.0944	2.1	0.641	− 0.819	−0.198
9	39.2	49.6	0.1148	2.0	0.630	− 1.920	−0.275
10	39.0	49.6	0.1151	2.0	0.608	− 2.13	−0.302
11	39.0	52.0	0.1376	1.8	0.709	− 3.24	−0.286
12	38.8	52.0	0.1395	1.9	0.711	− 3.42	−0.294
13	35.9	51.6	0.1855	1.8	0.756	−14.54	−0.473
14	35.9	51.6	0.1855	1.8	0.745	−15.32	−0.499
15	35.9	49.1	0.1258	1.65	0.651	− 3.41	−0.382
16	36.0	49.7	0.1330	1.55	0.644	− 4.53	−0.426
17	35.7	46.7	0.106	2.00	0.649	− 1.530	−0.253
18	35.9	46.9	0.107	1.9	0.646	− 1.610	−0.266
19	33.6	46.9	0.116	2.1	0.636	− 2.84	−0.307
20	33.8	46.6	0.113	1.9	0.629	− 2.37	−0.308
21	33.8	49.7	0.1850	1.8	0.731	−22.3	−0.568
22	33.85	49.7	0.1783	1.8	0.667	−27.0	−0.690
23	33.8	51.2	0.256	1.8	0.878	− 6.31	−0.129
24	33.8	51.2	0.256	1.9	0.881	− 6.17	−0.126
25	33.8	49.6	0.180	1.8	0.484	−48.3	−1.22
26*L*	20.4	42.1	0.3545	4.35	1.182	+ 1.062	+0.0237
27*L*	20.4	43.5	0.356	4.3	1.176	+ 1.031	+0.021
28*L*	25.0	47.1	0.339	3.9	0.994	− 0.056	−0.001
29*L*	25.0	46.3	0.3378	3.9	1.150	+ 1.289	+0.032
30*L*	28.4	48.9	0.324	2.0	1.070	+ 0.843	+0.024
31*L*	28.4	48.4	0.3192	2.1	1.060	+ 0.740	+0.021
32*L*	30.5	49.5	0.3075	2.2	0.983	− 0.264	−0.007
33*L*	30.5	49.5	0.3075	2.1	1.000	0	0.0
34*L*	32.0	49.6	0.2765	2.35	0.912	− 3.28	−0.055
35	32.4	49.6	0.2757	1.9	0.882	− 6.51	−0.130
36	33.7	49.8	0.202	2.0	0.729	−27.6	−0.575
37	33.6	58.4	0.3165	2.25	1.016	+0.216	+0.0074
38	31.6	38.9	0.0748	8.8	0.579	− 0.460	−0.081
39	31.6	39.9	0.0783	8.8	0.590	− 0.583	−0.088
40*	33.9	32.6	0.0540	19.9	0.518	− 0.150	−0.039
41*	38.3	26.2	0.0385	28.4	0.536	− 0.056	−0.027
42*	38.7	7.69	0.0095	28.4	0.787	− 0.021	−0.027
43*	34.0	5.01	0.0063	20.3	0.920	− 0.031	−0.046
44	49.8	4.60	0.0054	20.0	0.988	− 0.007	−0.012
45	49.7	4.67	0.0055	20.3	1.003	+ 0.002	+0.003
46*	58.6	7.37	0.0086	17.0	0.992	− 0.003	−0.004
47*	58.9	4.82	0.0055	16.7	1.006	+ 0.007	+0.010
48*	58.7	4.14	0.0047	17.0	1.018	+ 0.025	+0.040
49*	57.7	7.88	0.0093	17.2	0.993	− 0.002	−0.003

[a] α'—calculated by the method of Furry, Jones, and Onsager.
[b] α—calculated by the method of Drickamer, Mellow, and Tung.

but at a considerably lower temperature. Figure 3 shows the theoretical values of α. At atmospheric pressure the sign change obtained experimentally may occur at a considerably lower temperature. For the calculation of the theoretical α the interaction energy was chosen as the geometric mean of those of the pure components. A change in the assumed interaction energy would change the calculated temperature of sign change considerably.

The large negative values for α near the critical

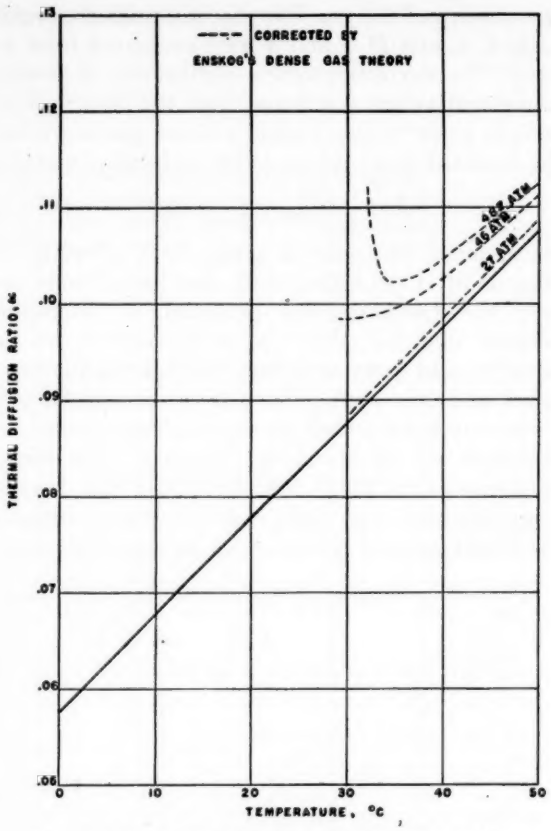

FIG. 3. The thermal diffusion ratio for xenon-ethane based on the Lennard-Jones model.

density (corresponding to xenon concentrating at the top of the column) indicate that ethane is forming clusters, and that these clusters have sufficient stability to constitute the major source of molecular motion of ethane in this region. The surprising fact is that clusters apparently start to form at pressures as low as four atmospheres and temperatures as high as 50°C. There are no indications from measurements of the other transport properties that the assumption of molecular chaos breaks down at such low densities.

It appears from a single point (Run 37) that at sufficiently high densities α becomes positive again. In the liquid phase α is apparently positive, although the exact temperature and density of the sign change are not determined. A more complete investigation of these points, and a discussion of their meaning will be presented in a further paper.

The authors wish to acknowledge the assistance of E. W. Mellow in the construction of the equipment.

The cooperation of the Argonne National Laboratory of the AEC made this work possible.

The Vapor Pressure of Americium*

N. D. ERWAY† AND O. C. SIMPSON
Argonne National Laboratory, Chicago, Illinois

(Received February 21, 1950)

The vapor pressure of americium from a dilute solution in plutonium has been measured by a modification of the Knudsen effusion method. The resulting vapor pressure for pure americium in the temperature range 1450°K to 1820°K is given by the equation $\log_{10}p_{mm}=7.02-(11,300)/T$. The vapor pressures are probably accurate to a factor of two or three. Relative values are much more precise.

INTRODUCTION

IN the Knudsen[1] effusion method for the determination of vapor pressures the substance to be studied is placed in an oven having a small thin-edged orifice. The oven is maintained at constant known temperature in a vacuum and measurement is made of the amount of vapor effusing from the orifice in a known period of time. The rate of effusion of vapor is a function of the partial pressure of vapor in the oven, the size of the orifice, the oven temperature, and the molecular weight of the vapor molecule. In order that the partial pressure of vapor in the oven be equal to the saturation vapor pressure at the oven temperature, it is essential that the evaporation surface be very large compared to the total area of the orifice and any leaks in the oven. Since the orifice must be large enough to permit effusion of a measurable amount of vapor and since there is also a lower limit to the size of orifice which may be used in practice, it is in general desirable to have at least a few milligrams of material available for vapor pressure measurements.

When only tracer amounts of material are available, it is possible to meet the above requirement of large evaporation surface by using a dilute solution of the desired material in a second substance. If the two substances are sufficiently similar, it may be assumed that an ideal solution is formed. Thus a large evaporation surface may be obtained and the vapor phase in the oven will be saturated with respect to each component of the solution. The desired vapor pressure may be calculated from the measured partial pressure and the mole fraction of the constituent in the solution.

The relatively short[2] half-life of Am^{241} with its correspondingly high specific activity permits the detection and measurement of very small amounts of this isotope. Therefore it is possible to measure very small partial pressures of americium by the effusion method and consequently to use very dilute solutions of americium to charge the effusion oven.

In this investigation plutonium metal was used as the solvent for the tracer amount of americium. Since these two metals are neighboring elements in the actinide series, it is reasonable to assume the applicability of perfect solution laws.

APPARATUS

To prevent oxidation of the surface of the metal sample it was desirable that the apparatus permit the sample to be kept in a high vacuum throughout the entire series of measurements. The apparatus which was used is shown in Fig. 1. Except for the type of oven and oven support, this apparatus is similar to that described by Phipps, Sears, Seifert, and Simpson.[3] In this apparatus a calculable fraction of the vapor which effuses from the orifice passes through a collimator and is collected on a cooled platinum target.

The oven and oven support are shown in detail in Fig. 2. The oven was machined from 0.75-in. tantalum rod. The fact that molten metals will creep over hot, clean tantalum surfaces is an advantage in that the resulting thin layer of metal offers a large evaporation surface. However, the creepage may be a disadvantage if it occurs to too great an extent. In such a case the oven orifice may be partially closed or some metal may even creep onto the outside of the orifice plate. To combat this possibility, the oven had a set of two nested cups. To utilize the hindering effect that sharp edges have on creepage, each cup had a sharp upper edge. The sample was placed in the innermost cup.

The oven orifice was formed at the center of a disk of 0.005-in. tantalum foil, which was then spot-welded to the top of the oven. The top section of the oven was force-fitted to the bottom section by a perfect fitting taper joint. At the oven temperatures used, the two pieces cohered strongly to each other, thereby preventing any leakage of vapor. The lower section of the oven had a threaded 0.15-cm hole drilled in its center. This hole was of the proper depth and diameter to simulate blackbody conditions. The temperature of the oven was determined by observation of this "blackbody" hole with a calibrated Leeds and Northrup optical pyrometer.

The oven was supported by three 0.040-in. tungsten legs, spaced equilaterally in its base. These three legs rested respectively in a conical hole, a V-groove, and a

* This investigation was carried out under Contract No. W-7401-eng-37 for the Manhattan Project at the Metallurgical Laboratory, University of Chicago.

† Present address: 155 Lincoln Avenue, Oregon, Wisconsin.

[1] M. Knudsen, Ann. d. Physik **29**, 179 (1909).

[2] G. T. Seaborg, Chem. and Eng. News **25**, 358 (1947).

[3] Phipps, Sears, Seifert, and Simpson, J. Chem. Phys. **18**, 713 (1950).

flat-bottom groove, which were ground to equal depth in the quartz oven support. This type of support gave a definite reproducible position for the oven. Also supported on the quartz table and concentric with the oven was a two-walled quartz radiation shield. The shield had sections of 1-mil platinum foil between its walls. As the oven was heated by induction, the sections of platinum foil were separated by small gaps in order to decrease the power loss in the radiation shield. The hole at the center of the quartz table and the optical Pyrex window at the bottom of the apparatus made it possible to observe the oven with the pyrometer.

Platinum targets (0.75 in. diameter×0.005 in.) were mounted in aluminum holders as previously described.[3] Fifty target holders were stacked in the cassette magazine (Fig. 1) with the target side facing the collimator. As previously described,[3] a shutter was provided to interrupt the beam of vapor molecules passing from the orifice through the collimator and an ejector rod was provided to push the bottom target across the ejection table. A Pyrex tube with several flat "seal-off" constrictions was provided to collect the ejected targets and permit their removal from the apparatus.

The apparatus was attached to a vacuum line which had sufficient pumping speed to maintain a pressure of less than 10^{-6} mm of Hg in the apparatus while the oven was at its highest temperature.

PROCEDURE

A 66.97-mg sample of plutonium metal was used, which was prepared to contain tracer amounts of Pu^{241} and Am^{241}.[2] A tracer amount of Pu^{238} was also present. The sample was homogeneous, since the tracer isotopes

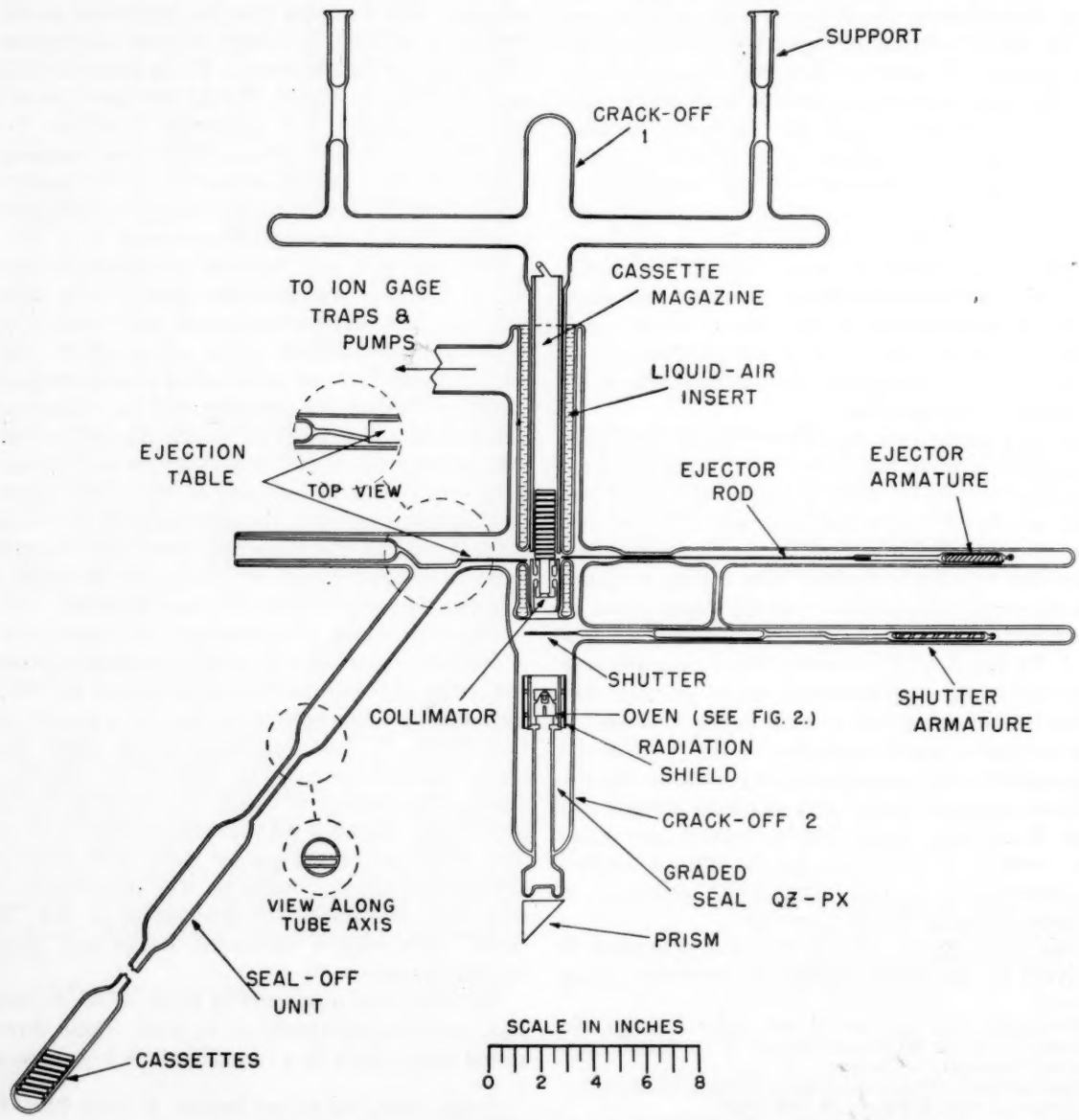

FIG. 1. Apparatus for the measurement of the vapor pressure of americium metal.

were present in the plutonium sample when it was reduced to metal. The cleaned sample of metal was sealed in an evacuated ampoule until the time it was placed in the oven.

The two sections of the oven were thoroughly outgassed by induction heating in an auxiliary vacuum system to a temperature of 2000°C for a period of 10 hr. After the oven was outgassed by this treatment, the vacuum in the system was broken with helium which had been dried by passage through a liquid air cooled trap. The oven was then removed and loaded in a stream of helium. After the charge had been placed in the oven base, the top section was forced on with a hydraulic press at a pressure of 2000 lb in^{-2}. While the oven was being loaded, the vapor pressure vacuum system, which had previously been evacuated and thoroughly torched, was opened at "crack-off 1" (Fig. 1) and dried helium was allowed to flow through the system. The oven was placed in position on the quartz table and the target magazine was replaced above it. The system was evacuated to a pressure of 8×10^{-7} mm of Hg. During the initial heating of the oven the temperature was raised slowly, so as to maintain a low pressure in the system.

With liquid nitrogen in the "liquid air insert" (Fig. 1) and the shutter in place under the collimator, the oven was heated by induction to a constant temperature. Then the shutter was opened and the target was exposed to effusing vapor for a measured length of time. The oven temperature was determined every 30 sec. during the exposure. At the end of the exposure the shutter was closed and the power output of the induction heater was altered to raise or lower the temperature of the oven for the exposure of the next target. The exposed target was ejected as previously described[3] and the next target was allowed to fall into position. After a desired number of targets had been exposed, they were removed from the apparatus by sealing off the compartment of the "seal-off unit" (Fig. 1) which contained the exposed targets. The exposed targets were removed from the aluminum holders and the amount of americium deposited on each was determined by radiochemical assay.

The analysis involved the determination of the total alpha-activity on the platinum targets by counting in a standard parallel plate alpha-chamber and a determination of the percentage of the total activity which was due to the Am^{241} alpha-particles. The latter determination was made in an alpha-pulse analyzer.[4]

The small amount of Pu^{238} which was present in the oven charge made necessary a small correction on the measurement with the pulse analyzer, since the range of the alpha-particles[5] from Pu^{238} is sufficiently near the range of alpha-particles from Am^{241} that the pulse analyzer did not distinguish between the particles originating from these two isotopes. The range of the Pu^{239} alphas[5] is sufficiently less than that of the other alpha-particles to permit good separation by the pulse analyzer method. Since the percentage of Pu^{238} in the plutonium was known, it was possible to correct for its presence and to obtain an accurate value for the Am^{241} activity on each target.

The greatest uncertainty was in the determination of the Am-Pu composition in the oven at the time of each exposure. The amount of each isotope removed from the oven during each exposure could be calculated very accurately from the analysis of the material on the target and the geometry of the apparatus. However, that removed during the intervals between exposures had to be estimated. The periods of time involved were known. However, the temperature of the oven was being changed between exposures. The temperature of the oven was measured frequently during these intervals and the total period of time between exposures was kept small compared to the length of the exposures. As a result it was possible to determine within one or two percent the total amount of each isotope removed from the oven prior to each exposure.

Corrections were made for the growth of americium from Pu^{241} [6] during the experiment, which covered a period of several days. Thus the net loss of each isotope from the oven prior to the midpoint of each exposure was known. The average mole fraction of americium in the oven during each exposure could then be calculated if the initial mole fraction were known.

The initial mole fraction of americium in the metal sample could not be obtained with accuracy from analysis of a sample of the original mixture of salts because of the uncertainty as to relative loss of americium and plutonium by volatilization during reduction to metal. Loss by volatilization during the reduction step or during a remelting of the sample would result

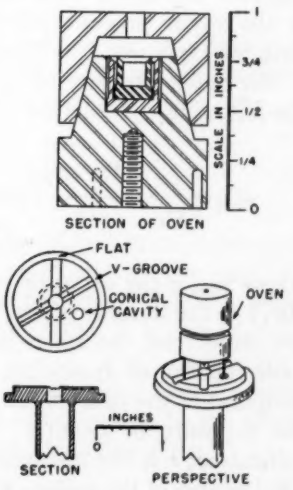

FIG. 2. Tantalum effusion oven and quartz support.

[4] Ghiorso, Weissbourd, and Robinson, "The multi-channel pulse analyzer," MDDC-23, Technical Information Division, Oak Ridge, Tennessee.

[5] Chamberlain, Gofman, Segrè, and Wahl, Phys. Rev. **71**, 529 (1947).

[6] G. T. Seaborg, Chem. and Eng. News **26**, 1902 (1948).

TABLE I. The vapor pressure of americium metal.

Target No.	Temp. T°K	Exposure time τ(min.)	Registered disintegrations of Am c(dis./min.)	Mole fraction of Am $N\times10^5$	Vapor pressure p(mm Hg)	Recip. temp. $\frac{1}{T}\times10^3$
1	1412	30.00	14.9	1.90	0.0301	70.8
2	1462	150.00	300	1.90	0.123	68.4
3	1500	65.00	308	1.78	0.316	66.7
4	1565	25.00	193	1.55	0.603	63.9
5	1614	10.00	113	1.43	0.977	62.0
6	1666	5.00	95.4	1.31	1.82	60.0
7	1709	3.00	82.7	1.19	2.95	58.5
8	1761	2.00	47.2	0.69_5	4.37	56.8
9	1818	1.00	15.8	0.32_7	6.31	55.0
10	1454	150.00	80.7	0.29_4	0.214	68.8
11	1810	1.00	13.6	0.28_8	6.17	55.3
12	1501	65.00	46.0	0.26_6	0.316	66.6

in a surface concentration of americium which was different from that in the body of the metal sample. Therefore it was not possible to obtain a truly representative sample of the reduced metal.

The initial mole fraction of americium was therefore determined by observing the partial pressure of americium above the solution for the same oven temperature at two widely separated times during the series of measurements. The ratio of observed partial pressure of americium vapor to the mole fraction of americium in the solution should be constant at a given oven temperature. A simple calculation gives a value for that initial mole fraction of americium which, when combined with the data for the net loss of all isotopes prior to the two exposures, results in the same value for the ratio of observed pressure to mole fraction for each exposure.

RESULTS

Sixteen exposures were made, during which time 5.53×10^{-9} mole of americium was removed from the oven. The last four exposures gave amounts of americium too low to detect accurately with the pulse analyzer and hence these exposures were not included in the vapor pressure calculations. The experimental data for exposures 1 to 12 are given in Table I.

The vapor pressure of americium was calculated by the following equation (cf. Eq. (4) of reference 3).

$$p_{\text{mm}}=\frac{c}{N\tau}\cdot\frac{(D^2+4r^2)}{aD^2}(2\pi MRT)^{\frac{1}{2}}\frac{10^{-6}}{s(241)60(1333)}, \quad (1)$$

where p_{mm} is the vapor pressure of americium in mm of Hg; c is the number of registered alpha-disintegrations per minute for the americium on the target; N is the mole fraction of americium in the oven charge at the midpoint of the time of the exposure; τ is the length of the exposure in minutes; D is the diameter of the collimator; r is the distance from orifice to collimator; a is the area of the orifice; M is the molecular weight of the americium vapor molecule; R is the molar gas constant; T is the absolute temperature of the oven; and s is the number of registered alpha-disintegrations per minute per microgram of americium under the counting conditions used. The americium vapor was assumed to be monatomic, so that M was taken to be 241. s had the value 3.45×10^6 registered disintegrations per minute per microgram. At 25°C the experimental values of D, r, and a were, respectively, 0.5333 cm, 9.921 cm, and 2.41×10^{-4} cm². The slight change in value of r and a with oven temperature was neglected, since the resulting error was negligible compared to other uncertainties. Equation (1) then reduces to the experimental equation

$$p_{\text{mm}}=\frac{3.067\times10^{-8}c(T)^{\frac{1}{2}}}{N\tau}, \quad (2)$$

which was used to calculate the values of p in Table I for pure americium.

The initial mole fraction of americium was calculated from the experimental data for targets 3 and 12, which were exposed at the same oven temperature within the experimental error of the temperature measurement. Unfortunately the experimental error in the analysis of the deposit on targets 13 to 16 was too great to permit this same calculation to be made with other pairs of exposures. The value arrived at by use of targets 3 and 12 was consistent with the value obtained from the initial composition of the mixture of isotopes if the history of the mixture prior to these measurements was considered.

The vapor pressure data of Table I are shown graphically in Fig. 3. The experimental points are numbered in the order in which measurements were made. The vapor pressures given by targets 1 and 2 are apparently low. This probably resulted from a lower concentration of reduced americium atoms in the surface of the sample than in the body of the sample. Equilibrium was soon attained either by diffusion or by molten metal breaking through the surface skin and spreading over the surface of the tantalum cup. The line in Fig. 3 is the most probable line as given by a least-squares calculation utilizing the data for targets

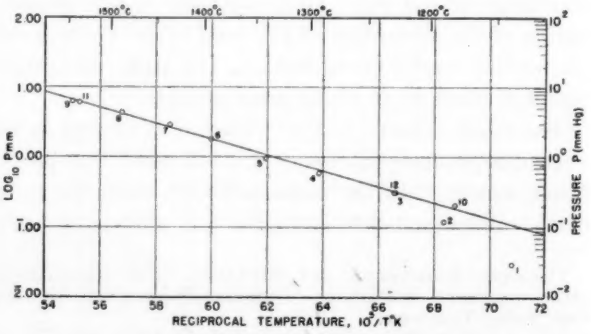

FIG. 3. Vapor pressure of americium metal.

3 to 12. The equation for this experimental vapor pressure curve is

$$\log_{10} p_{\text{mm}} = 7.02 - (11{,}300/T) \qquad (3)$$

for the temperature range 1450°K to 1820°K.

The probable error in values of p calculated by Eq. (3), within the given temperature range, is less than two percent as determined by the residuals of the experimental points from the most probable line. However, the uncertainties in the initial concentrations of Am^{241} and Pu^{238} and in possible deviations from ideal solution laws may make the results in error by as much as a factor of 2 or 3.

On the basis of Eq. (3) the molar heat of vaporization of americium is 51.7 kcal./mole; the normal boiling point is 2460°C; and the molar entropy of vaporization at the normal boiling point is 18.9 cal./deg. mole.

ACKNOWLEDGMENT

The authors wish to express their appreciation to Dr. Ralph L. Seifert for his interest and help in carrying out the investigation and in preparing the manuscript.

THE JOURNAL OF CHEMICAL PHYSICS VOLUME 18, NUMBER 7 JULY, 1950

Internal Motion and Molecular Structure Studies by Electron Diffraction. II. Interpretation and Method*

J. KARLE AND I. L. KARLE
U. S. Naval Research Laboratory, Washington, D. C.
(Received March 10, 1950)

The application of a recently developed objective procedure to the analysis of electron diffraction photographs from more complex molecules is discussed in terms of the further development of the details of some of the theoretical and experimental aspects of the procedure. The topics discussed are the physical significance of measured vibrational amplitudes, the method for drawing a background line, the calibration of photographic plates, and the computation of intensity curves by means of IBM machines.

THE theory and procedure for determining molecular structure and internal motion by an objective analysis of electron diffraction photographs have been presented in a previous paper.[1] The diffraction photographs are obtained with a rotating sector and are analyzed by means of a microphotometer. A procedure was developed for treating the molecular scattering data so that the equilibrium distances and vibrational motion can be computed directly from these data. This paper discusses refinements in interpretation and procedure which increase the accuracy and facilitate the extension of the method to the analysis of more complex molecules. The topics to be considered are the physical significance of the measured vibrational amplitude, the method for choosing the best background line representing the background scattering, a simple and accurate method for calibrating photographic plates, and the computation of intensity curves by means of IBM machines.

VIBRATIONAL MOTION, INTERPRETATION

The contribution of internal motion to scattering by gases has been evaluated in a very fine paper by R. W. James.[2] A brief derivation will be repeated here since the treatment differs from that given by James in a way which clarifies the physical significance of the final result. In James' treatment, the ξ-axis of a rectangular coordinate system, ξ, η, ζ, was always placed along the line joining the pair of atoms whose motion was being considered. In the treatment to be presented, a general rectangular coordinate system is established without any restriction on its orientation and a more general expression is obtained which is suitable for application to any interatomic distance in a molecule. There may also be some advantage in having the general expression for use with spectroscopic data since it obviates the necessity for transforming the coordinate system for each pair of atoms in a molecule.

We start with the expression for the contribution to the intensity of scattering from a pair of vibrating atoms (omitting scattering factors),

$$I(s) = \int_0^\infty P(r) \frac{\sin sr}{sr} dr, \qquad (1)$$

where $P(r)dr$ is the probability of finding an interatomic distance between r and $r+dr$ and $s=(4\pi \sin\theta/2)/\lambda$ where θ is the angle of scattering and λ is the wavelength of the radiation. We define a rectangular coordinate system ξ, η, ζ so that ξ^i, η^i, ζ^i are the equilibrium components of the ith atom and ξ_i, η_i, ζ_i represent its deviations from equilibrium due to the vibrational motion of the molecule. It is found that

$$r = [(\xi_i + \xi^i - \xi_j - \xi^j)^2 + (\eta_i + \eta^i - \eta_j - \eta^j)^2 + (\zeta_i + \zeta^i - \zeta_j - \zeta^j)^2]^{\frac{1}{2}} \qquad (2)$$

* Presented at the Pittsburgh Diffraction Conference, November 7–8, 1949.

[1] I. L. Karle and J. Karle, J. Chem. Phys. **17**, 1052 (1949).

[2] R. W. James, Physik. Zeits. **33**, 737 (1932).

which becomes from application of the binomial expansion

$$r=r_{ij}+[\xi_{ij}(\xi_i-\xi_j)+\eta_{ij}(\eta_i-\eta_j)+\zeta_{ij}(\zeta_i-\zeta_j)]/r_{ij} +f(\xi_i^2,\eta_i^2,\zeta_i^2,\xi_j^2,\eta_j^2,\zeta_j^2)+\cdots, \quad (3)$$

where r_{ij} is the equilibrium distance between the ith and jth atoms, $\xi_{ij}=\xi^i-\xi^j$, $\eta_{ij}=\eta^i-\eta^j$, $\zeta_{ij}=\zeta^i-\zeta^j$ represent the components of r_{ij} along the ξ, η, ζ axes, and f is the quadratic term in the expansion. Following the notation of James, the transformation to the $3N$ normal coordinates p_n (where N is the number of atoms in the molecule in question) is

$$\xi_i=\sum_{n=1}^{3N}\alpha_{in}p_n, \quad \eta_i=\sum_{n=1}^{3N}\beta_{in}p_n, \quad \zeta_i=\sum_{n=1}^{3N}\gamma_{in}p_n, \quad (4)$$

where the α, β, γ are transformation constants. By means of (4), the variable interatomic distance r, given by (3), may be expressed in terms of the normal coordinates,

$$r=r_{ij}+\sum_{n=1}^{3N}c_np_n+\sum_{n=1}^{3N}\sum_{m=1}^{3N}k_{nm}p_np_m, \quad (5)$$

where

$$c_n=[\xi_{ij}(\alpha_{in}-\alpha_{jn})+\eta_{ij}(\beta_{in}-\beta_{jn}) +\zeta_{ij}(\gamma_{in}-\gamma_{jn})]/r_{ij} \quad (6)$$

and the k_{nm} are rather involved functions of ξ_{ij}, η_{ij}, ζ_{ij} and the α, β, γ. These functions are readily derived but need not be known for the physical interpretation of the final result.

The probability function describing normal vibrations was shown by Bloch[3] from quantum mechanical considerations to have the form,

$$W(p_1,p_2,\cdots p_{3N})=\prod_{n=1}^{3N}\left(\frac{B_n}{\pi}\right)^{\frac{1}{2}}\exp(-B_np_n^2) \quad (7)$$

where

$$B_n=\frac{4\pi^2\nu_n}{h}tgh\frac{h\nu_n}{2kT}. \quad (8)$$

The quantity ν_n is the frequency of the nth normal vibration, h is Planck's constant, k is Boltzmann's constant and T is the absolute temperature. Note that

$$\langle p_n^2\rangle_{Av}=1/(2B_n). \quad (9)$$

Instead of evaluating (1), we have the following expressions to integrate over all normal coordinate space,

$$I=\int\int_{-\infty}^{\infty}\cdots\int W(p_1,p_2,\cdots p_{3N}) \times\frac{\sin[sr(p_1,p_2,\cdots p_{3N})]}{sr(p_1,p_2,\cdots p_{3N})}dp_1dp_2\cdots dp_{3N}. \quad (10)$$

On substituting (5) into the argument of the sine in (10), we have to a very good approximation, because of the very small magnitude of the contribution from the quadratic term[4] in (5),

$$\sin[sr(p_1,p_2,\cdots p_{3N})]\sim\sin(sr_{ij}+s\sum_n c_np_n) +s\sum_n\sum_m k_{nm}p_np_m\cos(sr_{ij}+s\sum_n c_np_n). \quad (11)$$

The contribution of the first term on the right of (11) will be considered first. On substituting it into (10) we have the following expression to integrate[5]

$$I_1=(i.p.)\left(\frac{B_1}{\pi}\right)^{\frac{1}{2}}\left(\frac{B_2}{\pi}\right)^{\frac{1}{2}}\cdots\left(\frac{B_{3N}}{\pi}\right)^{\frac{1}{2}}\frac{\exp(isr_{ij})}{sr_{ij}} \times\int\int_{-\infty}^{\infty}\cdots\int\exp(-B_1p_1^2-B_2p_2^2-\cdots B_{3N}p_{3N}^2) \times\exp[is(c_1p_1+c_2p_2+\cdots+c_{3N}p_{3N})] \times dp_1dp_2\cdots dp_{3N} \quad (12)$$

where $(i.p.)$ stands for imaginary part. By expanding $\exp(isc_1p_1)$ in (12), the integral with respect to p_1 may be written

$$\int_{-\infty}^{\infty}\exp(-B_1p_1^2)\cos(sc_1p_1)dp_1, \quad (13)$$

bearing in mind that the integrand containing $\sin(sc_1p_1)$ is odd and its contribution to the integral is therefore zero. We obtain for (13)

$$\left(\frac{\pi}{B_1}\right)^{\frac{1}{2}}\exp(-s^2c_1^2/4B_1). \quad (14)$$

Each integration proceeds like the one for p_1 and, hence, the final answer becomes[6]

$$I_1=\exp\left(-s^2/2\sum_{n=1}^{3N}c_n^2/2B_n\right)\sin sr_{ij}/sr_{ij}. \quad (15)$$

The second term in (11) may be inserted into (10) and we obtain for the integral I_2 by steps similar to those in (12) to (15),

$$I_2=\left\{\sum_{n=1}^{3N}\frac{k_{nn}}{B_n}\left(\frac{1}{2}-\frac{s^2c_n^2}{4B_n}\right)\exp(-s^2c_n^2/4B_n) -\sum_{n=1}^{3N}\sum_{m=1}^{3N}k_{nm}\frac{s^2c_nc_m}{4B_nB_m}\exp\left(-\frac{s^2c_n^2}{4B_n}-\frac{s^2c_m^2}{4B_m}\right)\right\} \times\frac{\cos sr_{ij}}{r_{ij}}. \quad (n\neq m) \quad (16)$$

[3] F. Bloch, Zeits. f. Physik **74**, 295 (1932).

[4] The quadratic term may be large for a molecule undergoing restricted internal rotation. This case has been treated by J. Karle and H. Hauptman, J. Chem. Phys. **18**, 875 (1950).

[5] In the denominator of (12), r has been replaced by its equilibrium value, r_{ij}. This introduces a negligible error in the region of interest.

[6] This result is the same as James' if the ξ axis lies in r_{ij}. For this special choice of axes, c_n is equal to $(\alpha_{in}-\alpha_{jn})$ according to (6).

We consider first the physical significance of the summation in the exponent of (15), since it is this quantity which is measured in diffraction experiments. This term may be written, by means of (9),

$$\sum c_n^2/2B_n=\sum c_n^2\langle p_n^2\rangle_{Av}. \tag{17}$$

Note that

$$\sum c_n^2\langle p_n^2\rangle_{Av}=\langle\sum c_n^2p_n^2\rangle_{Av}. \tag{18}$$

Now

$$\langle(\sum c_np_n)^2\rangle_{Av}=\langle\sum c_n^2p_n^2\rangle_{Av}+\langle\sum\sum c_nc_mp_np_m\rangle_{Av}. \quad (n\neq m) \tag{19}$$

The second term on the right in (19) is expressible in terms of $3N$ integrals from $-\infty$ to ∞ whose integrands are odd and, therefore, this term is identically zero. Thus the combination of (17), (18) and (19) gives

$$\langle(\sum c_np_n)^2\rangle_{Av}=\langle\sum c_n^2p_n^2\rangle_{Av}=\sum c_n^2/2B_n. \tag{20}$$

The problem is now resolved to the point where it is necessary to consider the meaning of $\sum c_np_n$. A comparison of (3) and (5) shows that

$$\sum_{1=n}^{3N} c_np_n=\frac{\xi_{ij}}{r_{ij}}(\xi_i-\xi_j)+\frac{\eta_{ij}}{r_{ij}}(\eta_i-\eta_j)+\frac{\zeta_{ij}}{r_{ij}}(\zeta_i-\zeta_j). \tag{21}$$

The quantities $(\xi_i-\xi_j)$, $(\eta_i-\eta_j)$ and $(\zeta_i-\zeta_j)$ are the instantaneous displacements along the coordinate axes. The quantities ξ_{ij}/r_{ij}, η_{ij}/r_{ij}, and ζ_{ij}/r_{ij} *project* these displacements in the direction of r_{ij}, the line connecting pairs of atoms at equilibrium. Therefore, it is seen from (20) and (21) that the physical significance of the summation in the exponent of (15) is that it represents the *average of the square of the amplitudes projected on the line joining the pair of atoms in their equilibrium position*. This quantity has been erroneously interpreted as the average of the square of the amplitudes. If we denote the instantaneous projected amplitude by l_{ij}, (15) assumes its well-known form,

$$I_1=\exp(-s^2\langle l_{ij}^2\rangle_{Av}/2)\sin sr_{ij}/sr_{ij}. \tag{22}$$

The quantities in (16) may also be expressed in terms of the average values of the linear and quadratic terms in (3). The following approximation is made,

$$(-\tfrac{1}{2}+1-s^2c_n^2/4B_n)\sim-\tfrac{1}{2}+\exp(-s^2c_n^2/4B_n) \tag{23}$$

which is ordinarily quite good for $0\leq s\leq 20$. The quantity in the exponent is small and may be replaced by an average value,

$$\exp(-s^2c_n^2/4B_n)\sim\exp\left(-\frac{s^2}{6N}\sum c_n^2/2B_n\right)=\exp\left(-\frac{s^2}{6N}\langle l_{ij}^2\rangle_{Av}\right). \tag{24}$$

Substituting (24) into (16) gives,

$$I_2=\left[\exp\left(-\frac{s^2}{3N}\langle l_{ij}^2\rangle_{Av}\right)\left\{\sum_{n=1}^{3N}k_{nn}/B_n-s^2\sum_{m=1}^{3N}\sum_{n=1}^{3N}k_{nm}c_nc_m/4B_nB_m\right\}-\exp\left(-\frac{s^2}{6N}\langle l_{ij}^2\rangle_{Av}\right)\sum_{n=1}^{3N}k_{nn}/2B_n\right]\times\cos sr_{ij}/r_{ij} \quad (n\neq m) \tag{25}$$

which becomes, using (3), (5) and (9),

$$I_2=\left[\exp\left(-\frac{s^2}{3N}\langle l_{ij}^2\rangle_{Av}\right)\left\{2\bar{f}-\frac{s^2}{2}(\langle l_{ij}^2f\rangle_{Av}-\langle l_{ij}^2\rangle_{Av}\bar{f})\right\}-f\exp\left(-\frac{s^2}{6N}\langle l_{ij}^2\rangle_{Av}\right)\right]\cos sr_{ij}/r_{ij}. \tag{26}$$

The bracket in (26) is seen to be in terms of average values of the projected amplitudes and the quadratic term in (3). The expression (26) which has been derived from the second term on the right in (11) may ordinarily be neglected as compared to (22).

By taking the Fourier sine transform of (22), it is possible to find, to a good approximation, the probability function, $P(r)$, as expressed in (1), which describes the motion of a pair of atoms. We have from (1)

$$\frac{P(r)}{r}=\frac{2}{\pi}\int_0^\infty sI(s)\sin sr\,ds. \tag{27}$$

If (22) is substituted for $I(s)$, then

$$\frac{P(r)}{r}=\frac{2}{\pi}\int_0^\infty\exp(-s^2\langle l_{ij}^2\rangle_{Av}/2)\frac{\sin sr_{ij}}{r_{ij}}\sin sr\,ds \tag{28}$$

$$=\frac{1}{r_{ij}(2\pi\langle l_{ij}^2\rangle_{Av})^{\frac{1}{2}}}\{\exp[-(r_{ij}-r)^2/2\langle l_{ij}^2\rangle_{Av}]-\exp[-(r_{ij}+r)^2/2\langle l_{ij}^2\rangle_{Av}]\}. \tag{29}$$

In the vicinity of $r=r_{ij}$, the second term in the braces of (29) is negligible and $r/r_{ij}\sim 1$, giving

$$P(r)\sim\frac{1}{(2\pi\langle l_{12}^2\rangle_{Av})^{\frac{1}{2}}}\exp[-(r_{ij}-r)^2/2\langle l_{ij}^2\rangle_{Av}]. \tag{30}$$

If the mean square projected amplitude is expressed as

$$\langle l_{ij}^2\rangle_{Av}=1/(2h_{ij}), \tag{31}$$

then

$$P(r)\sim\left(\frac{h_{ij}}{\pi}\right)^{\frac{1}{2}}\exp[-h_{ij}(r_{ij}-r)^2]. \tag{32}$$

It is seen that (32) is a Gaussian probability distribu-

tion in r whose damping constant h is related by (31) to the *mean square projected amplitude*. Expression (32) is the basis for formula (5), reference 1.

BACKGROUND LINE

One of the steps in the procedure for extracting the molecular scattering from the total scattering involves drawing a background line through the oscillations of the curve representing the total intensity.[1] The total intensity is then divided by this background line and yields the molecular scattering curve. Dividing the total intensity curve by the background line not only eliminates the atomic scattering but replaces by constants to a good approximation, except at low s values, the variable coefficients in the molecular scattering expression. It is not possible to use theoretical values for the background shape since these values are not sufficiently accurate. The best possible background line which may be drawn is one which produces a molecular scattering curve whose Fourier sine transform (called the radial distribution curve) is essentially positive everywhere. This is because the Fourier transform represents a series of probability functions which describe the vibrational motion of pairs of atoms in the molecule. In actual practice the molecular scattering is multiplied by a factor e^{-as^2} to assure convergence of the sine transform. The criterion of positiveness, however, is in no way altered since a transform computed using the damping factor must be positive if the corresponding transform without the damping factor is positive. A method of successive approximations will now be described for choosing the best background line.

The experimental intensity curve in the region of s from zero to four or five is replaced by a curve for an assumed model computed with constant coefficients. A preliminary radial distribution curve is then computed using the function[7]

$$f(r)=\sum_{s=0}^{s_{\max}} s_n I(s_n)\exp(-as_n^2)\sin s_n r\Delta s, \qquad (33)$$

where $\Delta s=0.2$, $s_{\max}\sim 25-35$, and $a\sim 0.0057$. The summation (33) represents the numerical integration of an integral whose integrand is the same as that of (27) with an additional damping function e^{-as^2}. The first radial distribution curve, $RD(a)$, which was computed in a study of the CH_2CF_2 molecule is shown in Fig. 1. Extraneous oscillations in the base line are quite apparent especially in the region below 1A and between the two large peaks. Aside from experimental inaccuracies, these oscillations may arise from two causes. There may be some errors in the assumed model used for the inner portion of the intensity curve and in addition the background line drawn through the oscillations of the total scattering curve may be misplaced in some regions. It should be noted that even with these difficulties, the positions of the maxima of the radial distribution curve are very nearly correct and only the shapes of the peaks and the areas under the peaks are in error. It has been found that if the extraneous oscillations in radial distribution curves are roughly fitted with a sum of $\sin\alpha r$ curves, the values of α are the values of s at which there are difficulties in the background line.[8] For instance, the extraneous oscillations in $RD(a)$ are mostly $\sin 10r+\sin 3r$. Accordingly, the background line was raised in the region $s=7.5$ to 12.5, a new intensity curve was computed for the s region 0

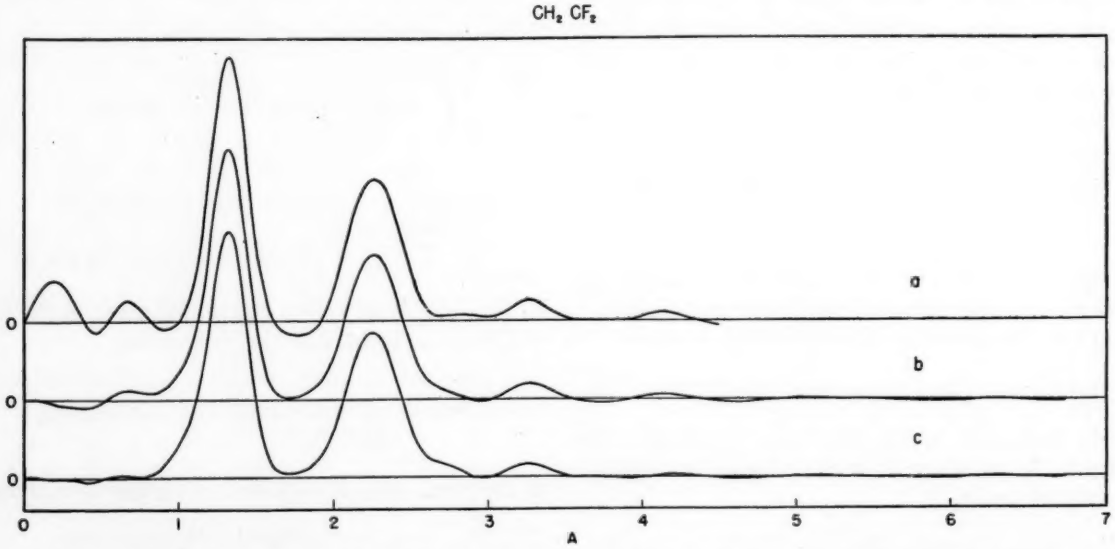

FIG. 1. Three radial distribution curves for CH_2CF_2 computed from experimental intensity data showing the successive improvements which resulted from adjusting the background line on the total intensity curve. The small peaks at $r\sim 2.7$ and 3.3 represent the H–F distances in the molecule.

[7] This function is computed in our laboratory by means of IBM punch cards prepared at the California Institute of Technology. Shaffer, Schomaker, and Pauling, J. Chem. Phys. **14**, 659 (1946).

[8] If the error is approximated by a bell shape, the Fourier transform of the error is roughly a damped sine curve.

to 4 from a model whose interatomic distances were consistent with the values indicated by $RD(a)$, and a second radial distribution curve, $RD(b)$, was computed. The positions of the maxima remained the same and the extraneous oscillations were much smaller than in $RD(a)$. A further improvement in the background line was made by fitting the extraneous oscillations in $RD(b)$ with $\sin 11r - \sin 7.5r - \sin 17r$. Accordingly, the background was raised around s equal to 11, lowered at s between 7 and 8 and at s between 15 and 20. The third computation gave a curve $RD(c)$ which was essentially zero everywhere except in the vicinities of interatomic distances. The remaining oscillations about the zero line were small and irregular and could be due to small uncertainties in the experimental intensity curve.

The process of successive approximations produces a good radial distribution curve in very few steps. The various changes in the background line which were made to compute the three radial distribution curves are illustrated in Fig. 2. It should be noted that the background line was always kept smooth and that no sudden changes occurred in the curvature.

CALIBRATION OF PHOTOGRAPHIC DENSITY

A calibration of the photographic density as read on a microphotometer as a function of the incident electron intensity may be obtained from two photographs of different exposure. It is not necessary to know how the exposures differ and the photographs to be used are conveniently those of the substance whose structure is being studied. For low exposures with fast electrons, the photographic density D is directly proportional to the exposure E. In addition, it is always possible to interpret the difference in two exposures as due to differences in electron intensity at constant time. Since $E \propto I$, we have $D \propto I$ for low exposures, or $D=I$ on an arbitrary scale.

Figure 3a shows the density as a function of the distance R from the center of the pattern for two traces of different exposure. At low densities, from R_a to R_b, it is found that $D_1/D_2=k$, a constant. Since $D=I$ (scale arbitrary) in this region, the D *vs.* I plot in Fig. 3b is a straight line from $D=0$ to D_b. From R_b to R_c, densities for the curve (1) lie below D_b, hence $D_1=I_1$ while $D_2 \neq I_2$. However, use of the relation $I_2=I_1/k$ permits the evaluation of the I_2 corresponding to the D_2 in the range R_b to R_c and, therefore, we have the relationship between D and I for D values D_b to D_c. From R_c to R_d, D_1 values are converted to I_1, making use of Fig. 3b from D_b to D_c, I_2 is again obtained from the relation $I_2=I_1/k$, and the measured D_2 values up to D_d are plotted *versus* the computed I_2 values. The preceding step is repeated until a complete calibration curve is obtained. The calibration may be checked by repeating the process with two other exposures. It is found that the separate calibration curves differ from each other by less than two percent.

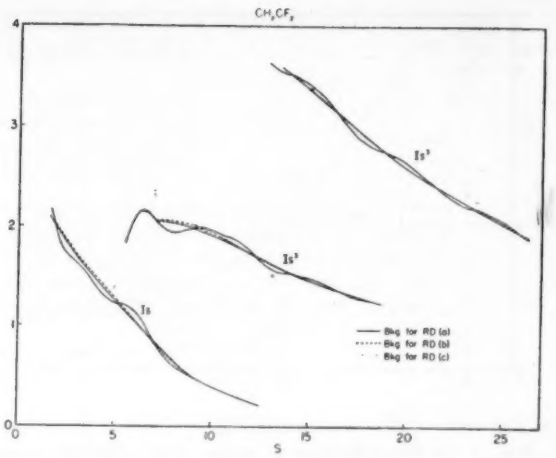

FIG. 2. The total intensity of scattering obtained through an s sector (Is) and multiplied by an additional $s^2(Is^3)$. The two lower curves are from the same exposure and the upper one is from a heavier exposure. The various changes which were made in the background line to compute the radial distribution curves in Fig. 1 are illustrated.

COMPUTATION OF INTENSITY CURVES

The intensity of molecular scattering obtained by the procedure described previously[1] is given by,[9]

$$I_m(s)=\sum_{i=1}^{N}\sum_{j=1}^{N} c_{ij}\exp(-s^2\langle l_{ij}^2\rangle_M/2)\sin sr_{ij}/sr_{ij} \quad (34)$$

where N is the number of atoms in the molecule being studied and c_{ij} is a constant equal approximately to the product of the atomic numbers z_iz_j, the accuracy of the approximation depending upon the spread of atomic numbers among the atoms present.

A procedure for computing (34) with the aid of IBM punch cards has been worked out with the invaluable help of Mr. B. F. Cheydleur of the Naval Ordnance Laboratory. The calculation is performed with two decks. One deck consists of the function $\sin sr/sr$ which we call deck I and the other deck consists of the function $\exp(-s^2\langle l_{ij}^2\rangle_M/2)$ which we call deck II.

Deck I consists of 101 cards for each value of r. The interval on r is 0.01 and the maximum value of r is 6.00. The range and interval of s may be expressed in terms of n where $s=0.05\pi n$. The value of n varies from 0 to 200 in steps of one. It is seen, therefore, that on each of the 101 cards for a particular r, there are two values of $\sin sr/sr$ except on the last card which has one value, $\sin 10\pi r/10\pi r$. The value of r is punched in columns 4–6, the value of n is punched in columns 7–9, and the values of $\sin 0.05\pi nr/0.05\pi nr$ and $\sin 0.05\pi(n+1)r/0.05\pi(n+1)r$ appear in columns 31–35 and 61-65, respectively.

Deck II consists of 101 cards for each value of $(\langle l^2\rangle_M)^{\frac{1}{2}}$ which ranges from 0.02 to 0.22 in steps of 0.002. The variation with n is the same as that for deck I. Therefore, each of the 101 cards for a particular value of

[9] In cases of internal rotation, see reference 4.

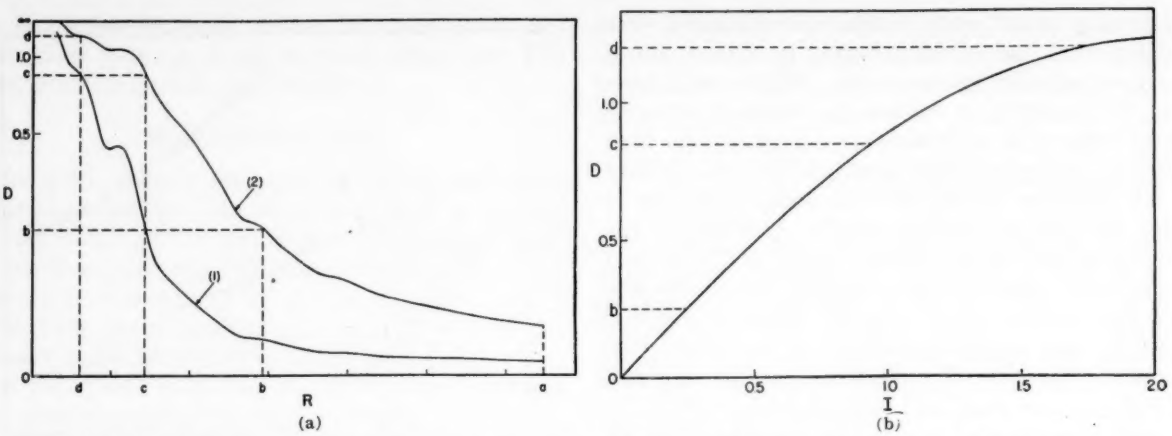

FIG. 3. (a) Microphotometer traces of two different exposures of the same substance. (b) Typical D *vs.* I calibration curve.

$(\langle l^2\rangle_{Av})^{\frac{1}{2}}$ has two values of the function $\exp(-s^2\langle l^2\rangle_{Av}/2)$ except the last card which has only the value of $\exp(-100\pi^2\langle l^2\rangle_{Av}/2)$. The value of n is punched in columns 7–9, the value of $10\langle l^2\rangle_{Av}/2$ is punched in columns 10–14 and the values of $\exp[-(0.05\pi n)^2\langle l^2\rangle_{Av}/2]$ and $\exp[-(0.05\pi(n+1))^2\langle l^2\rangle_{Av}/2]$ appear in columns 21–24 and 51–54, respectively.

PROCEDURE

1. At the beginning of each computation a set of cards is prepared, one for each interatomic distance, on which are key-punched r_{ij} in columns 4–6, $10\langle l_{ij}^2\rangle_{Av}/2$ in columns 10–14 and the coefficient c_{ij} in columns 15–18.

2. Sets of cards are drawn from deck I corresponding to each interatomic distance in the molecule. Each set is reproduced and the values from the card with the same r value, prepared in step 1, are simultaneously gang-punched into each reproduced set. These cards are called answer cards.

3. Sets of cards are drawn from deck II corresponding to the $10\langle l^2\rangle_{Av}/2$ values used for each r value in the molecule. These cards are merged with the answer cards.

4. The values from the exponential deck are multiplied by the values of c and $\sin sr/sr$ on the answer cards using a 604 electronic computing punch. The result is punched in columns 41–45 and 71–75 on the answer cards.

5. The exponential cards are sorted out and the answer cards are grouped according to corresponding values of n.

6. The results on the answer cards are tabulated and summed on a 405 tabulator. The total operation time for computing five intensity curves consisting of eight different interatomic distances is about three hours.

The purpose in computing intensity curves is to determine the range of uncertainty in the structure parameters as obtained from the radial distribution curve. Small variations are made on the structure parameters and the resulting intensity curves are compared with the original experimental curve.

Announcement on Binding Journals

From time to time, the Institute has received inquiries from subscribers for information as to where and how they may have their copies bound. After investigation the Institute has found that this may be best accomplished by selecting a capable bindery that will work to our specifications and produce a well-bound volume at as low a price as possible. The necessary arrangements have been completed with the Book Shop Bindery, 308 West Randolph Street, Chicago 6, Illinois.

The volumes will be bound in the best grade of washable buckram with facsimile gold stamping on the spine and the subscriber's name in gold on the front cover. A distinctive color for each of the Journals has been selected as listed below. Advertising matter and covers are removed before binding. The price of $3.00 per volume applies to any of these journals regardless of size. Issues, comprising complete volumes, should be sent by prepaid express or parcel post to the Book Shop Bindery. Bound volumes will be shipped approximately 30 days after receipt. Return transportation will be prepaid when remittance accompanies order.

No deviation in color or specification can be allowed in view of the favorable price.

Physical Review	Green
Reviews of Modern Physics	Orange
Journal of the Optical Society	Brown
Journal of the Acoustical Society	Orange
American Journal of Physics	Black
Review of Scientific Instruments	Grey
Journal of Chemical Physics	Blue
Journal of Applied Physics	Red
Physics Today	Purple

Internal Motion and Molecular Structure Studies by Electron Diffraction. III. Structure of CH_2CF_2 and CF_2CF_2*

I. L. KARLE AND J. KARLE
U. S. Naval Research Laboratory, Washington, D. C.
(Received March 10, 1950)

The interatomic distances and vibrational amplitudes projected on the lines connecting pairs of atoms at equilibrium have been determined for CH_2CF_2 and CF_2CF_2 by an objective procedure for analyzing electron diffraction photographs. Distances involving hydrogen atoms have been evaluated and the procedure for resolving radial distribution peaks involving more than one distance is illustrated. The effects on the accuracy of the method of various characteristics such as sample spread and multiple scattering have been analyzed.

IN previous papers,[1,2] an objective procedure was described for obtaining quantitative intensity data from electron diffraction photographs of gases and for using this data to compute radial distribution curves. These curves are related analytically by means of the folding theorem to the probability of the occurrence of the interatomic distances in a molecule. It is, therefore, possible to determine not only the equilibrium distances but also the displacements from the equilibrium positions due to vibrations in the molecule. The application of this method to the molecules CH_2CF_2 and CF_2CF_2 is of interest for several reasons in addition to the inherent interest in the values of the structural parameters. It affords an opportunity to compare the results of this method with those obtained by means of microwave spectra since a microwave study has been made of CH_2CF_2 by Roberts and Edgell.[3] It also permits a comparison of the magnitude of the vibrational amplitudes in similar molecules and an evaluation of the extent to which restricted internal rotation in ethylene type structures influences the scattering patterns. The two molecules to which the new procedure has already been applied, CCl_4 and CO_2, were quite simple and the peaks in the radial distribution curves corresponding to the interatomic distances were well separated. When several interatomic distances contribute to a peak in the radial distribution curve, it is necessary to resolve the composite peak into the individual curves corresponding to each of the distances. The method for performing the decomposition of a composite peak is illustrated in the determination of the structures of CH_2CF_2 and CF_2CF_2. The range of uncertainty of the values for the structure parameters is obtained from a comparison of the experimental intensity curves with computed theoretical intensity curves.

PROCEDURE

Electron diffraction photographs of CH_2CF_2 and CF_2CF_2[4] were taken through an s sector with a wavelength near 0.06A and a specimen to plate distance near 11 cm. The rotating sector whose center acts as a beam stop was placed 1 cm from the photographic plates. A timing device to control the exposure was used which could be activated when the stopcock was turned to admit the gas sample. The beam was focused by a focusing grid and two magnetic lenses. Photographs of the beam alone with the sector in place were blank indicating the absence of extraneous scattering. Photographs of the beam without the sector show the mean cross section of the beam to be less than 0.1 mm.

The photographic plates were rotated rapidly about the center of the diffraction pattern while being scanned by a microphotometer in order to smooth the irregularities due to graininess in the emulsion.[5] A circular light beam of 0.01 mm radius was used in the microphotometer to obtain good resolution. The microphotometer readings as a function of the radius were obtained by measuring these traces with an instrument constructed for this purpose. It readily measures differences in density of 0.001 and differences in radii of 0.01 mm. These readings were then converted to relative intensities,[2] which were plotted *versus* the variable s. Several months later, new photographs were taken and the whole procedure was repeated. The results did not change.

The total intensity of scattering is composed of a steeply falling background due to atomic scattering upon which is superimposed an oscillating curve due to molecular scattering. Since an s sector was used, the photographs register the total intensity, I, multiplied by s. It was convenient to multiply Is by s^2 for s values greater than 5 or 6 to accentuate the oscillations. A smooth background line was drawn through the oscillations and the molecular scattering curve was obtained by dividing the total intensity curve by the background line. This process not only eliminated the atomic scattering, but replaced by constants to a good approximation, except at low s values, the variable coefficients in

* Presented at the meeting of the American Society for X-Ray and Electron Diffraction, Philadelphia, December 1–3, 1949.
[1] I. L. Karle and J. Karle, J. Chem. Phys. **17**, 1052 (1949).
[2] J. Karle and I. L. Karle, J. Chem. Phys. **18**, 957 (1950).
[3] A. Roberts and W. F. Edgell, Phys. Rev. **76**, 178 (1949).
[4] These compounds were obtained from Dr. W. S. Murray of the Jackson Laboratory, DuPont Company. The specially purified sample of CF_2CF_2 was the same as that used in the infra-red and Raman investigation by Nielsen, Claassen, and Smith, J. Chem. Phys. **18**, 485 (1950).
[5] Karle, Hoober, and Karle, J. Chem. Phys. **15**, 765 (1947).

the molecular scattering expression. The location of the best position for the background line and the subsequent computation of radial distribution curves was described for the CH_2CF_2 molecule in the preceding paper.[2] The same procedure was used for the scattering data from CF_2CF_2. The difference in amplitude between adjacent maxima and minima of the molecular intensity curve could be measured from several photographs with better than 7 percent average deviation in the range $4 \leq s \leq 20$.

The function $f(r)$ used for computing the radial distribution curve was

$$f(r)=\int_0^{s_{\max}} sI_m(s)\exp(-as^2)\sin sr ds, \quad (1)$$

where I_m is the molecular scattering intensity, a is a number (usually 0.0057) chosen to make the integrand of (1) converge rapidly, $s_{\max}=27$, and $s=(4\pi\sin\theta/2)/\lambda$ where θ is the angle of scattering and λ is the wave-length of the electron beam. The desired probability distribution function, $D(r)$, may be obtained from the computed radial distribution function $f(r)$. $D(r)$ is defined by[1]

$$D(r)=\frac{\pi}{2}\sum_{i=1}^{n}\sum_{j=1}^{n}c_{ij}\frac{P_{ij}(r)}{r_{ij}}=\int_0^{\infty} sI_m(s)\sin sr ds \quad (i\neq j), \quad (2)$$

where $P_{ij}(r)$ is the probability distribution for the distance between the ith and jth atoms, c_{ij} is proportional to the product of the atomic numbers for the ith and jth atoms and n is the number of atoms in the molecule. The relation between $f(r)$ and $D(r)$ is given by

$$f(r)=\frac{1}{2(\pi a)^{\frac{1}{2}}}\int_{-\infty}^{\infty} D(\rho)\exp[-(r-\rho)^2/4a]d\rho. \quad (3)$$

It is found from (3) that if $f(r)$ has the Gaussian form,

$$f(r)=\sum_i\sum_j c_{ij}(\pi h_{ij})^{\frac{1}{2}}\exp[-h_{ij}(r-r_{ij})^2/(4ah_{ij}+1)]/2r_{ij}(4ah_{ij}+1)^{\frac{1}{2}}, \quad (4)$$

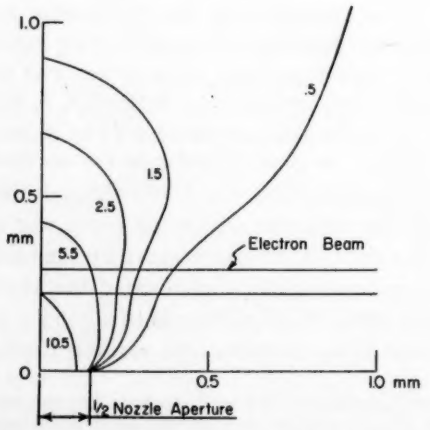

FIG. 1. Diagram of density contours of a jet of gas issuing from a nozzle into a vacuum. Density values are on an arbitrary scale. The position of the electron beam as it strikes the gas is indicated.

then $D(r)$ has the Gaussian form

$$D(r)=\sum_i\sum_j c_{ij}(\pi h_{ij})^{\frac{1}{2}}\exp[-h_{ij}(r-r_{ij})^2]/2r_{ij}, \quad (5)$$

which is expected from theoretical considerations.[2,6] The fitting of Gaussian peaks to the function $f(r)$ gives a value for the damping constant

$$H_{ij}=h_{ij}/(4ah_{ij}+1). \quad (6)$$

Since a has the value chosen for the computation of (1), the h_{ij} may be determined and inserted into (5). It has been shown[2] that

$$1/2h_{ij}=\langle l_{ij}^2\rangle_{Av}$$

is the *mean square amplitude of vibration projected on the line connecting a pair of atoms at equilibrium.*

In practice the peaks of the computed $f(r)$ curves, Eq. (1), often are composed of peaks for several distances. The two criteria used to decompose composite peaks into individual peaks for each distance are that the peaks should be Gaussian in shape, Eq. (4), and that the areas under the peaks multiplied by their respective equilibrium distances should be proportional to the scattering powers of the pairs of atoms involved. These criteria are found to be quite restrictive.

CAMERA CHARACTERISTICS AND ACCURACY

The procedure outlined above is based upon an ideal experiment in which the data which are obtained result from primary scattering from a point source. It is the purpose of this section to analyze the features of an actual electron diffraction experiment and to show that the above procedure applied to experimental data is suitable with very minor modification for giving accurate results for both interatomic distances and vibrational amplitudes.

The experimental difficulties which have been considered are the focusing of the beam, shadows cast by the sector and nozzle, the effect of the spreading of the gas sample in the camera and multiple scattering.

Focus, Shadows

The electron beam was collimated by a hole of 0.1 mm diameter before passing through the lens which focussed it on the photographic plate. Its mean diameter at the photographic plate was less than 0.1 mm and there were no shadows cast by the nozzle or the sector on photographs of the beam alone. Diffraction photographs taken with the sector in place (1 cm from the photographic plate), but not rotating, showed that there was no measurable spray directed from the sector edges. This may be determined by tracing with a microphotometer across the edge of the sector outlined on the photograph. The traces showed a sharp drop to zero density as the microphotometer passed from the region of scattering in the sector opening across the edge and into the region shielded by the sector. No corrections

[6] R. W. James, Physik. Zeits. **33**, 737 (1932).

were therefore required for the action of the sector. In addition, a beam diameter of less than 0.1 mm is sufficiently small to make corrections for the finite beam width negligible.

Finite Sample Size

The spread of the gas about the nozzle was investigated with CH_2CF_2 at a pressure of ~100 mm (the same pressure used for taking the diffraction photographs). Ordinarily, when taking diffraction photographs, the gas issuing from the nozzle was directed toward a liquid air trap. However, for convenience in investigating the spread of gas, the conditions for condensing the gas were not as favorable since the superstructure on the nozzle was cut away leaving a gap of several centimeters in which the gas could diffuse through the camera. A shadow microscope photograph was taken of the gas jet for ½ second exposure.[7] The contour map of the gas density on a relative scale is plotted in Fig. 1. It was found that the main portion of the gas is well confined at the point where the beam strikes the jet; however, it was difficult to estimate from the photographs how much gas had diffused through the camera due to poor condensation. Another experiment was performed in which controlled diffraction photographs were taken with the electron beam displaced known distances from the orifice of the gas nozzle. This was accomplished by attaching a shield to the top of a nozzle, Fig. 2, with 0.4 mm apertures located at 0, 1.0, 2.5 and 5.0 mm to the side of the gas jet. From the intensity of the resulting diffraction photographs it was found that the gas distribution about the nozzle could be expressed by a function of the type

$$A\exp(-ax^2)+B\exp(-bx^2) \tag{8}$$

where $A=0.9$, $B=0.1$, $a=3$ and $b=0.2$ and x is expressed in mm.

The effect of a gas sample of this form on the shape of the background may be evaluated from

$$\frac{a^{\frac{1}{2}}b^{\frac{1}{2}}}{\pi^{\frac{1}{2}}(Ab^{\frac{1}{2}}+Ba^{\frac{1}{2}})}\int_{-\infty}^{\infty}\frac{L^3}{k^3}(A\exp[-a(L-L_0)^2] +B\exp[-b(L-L_0)^2])dL, \tag{9}$$

where the background function has been approximated by $1/s^3\cong L^3/k^3$. L is the distance from the point of scattering to the photographic plate, L_0 is the distance from the nozzle aperture to the plate, and $k=2\pi R/\lambda$ where R is the radius of the diffraction pattern and λ is the electron wave-length. The evaluation of (9) gives

$$\frac{L_0^3}{k^3}+\frac{3L_0}{2k^3}\left|\frac{Ab^{\frac{1}{2}}+Ba^{\frac{1}{2}}}{ab(Ab^{\frac{1}{2}}+Ba^{\frac{1}{2}})}\right|\cong\frac{1}{s^3}\left(1+\frac{3}{2L_0^2}C\right). \tag{10}$$

where the first term is the original background function and the second term is of the order of 10^{-4} smaller. Thus not only the shape but also the magnitude of the background function are preserved even though the scattering does not take place from a point source.[8]

The effect of a gas jet of form (8) on the shape of each term of the molecular intensity,

$$I_m(s)=\sum_{i=1}^{n}\sum_{j=1}^{n}c_{ij}\exp(-\langle l_{ij}^2\rangle_{Av}s^2/2)\sin sr_{ij}/sr_{ij}\ (i\neq j), \tag{11}$$

may be evaluated from

$$\frac{a^{\frac{1}{2}}b^{\frac{1}{2}}}{\pi^{\frac{1}{2}}(Ab^{\frac{1}{2}}+Ba^{\frac{1}{2}})}\int(A\exp[-a(L-L_0)^2] +B\exp[-b(L-L_0)^2])\exp[-mG^2/L^2]\frac{\sin G/L}{G/L}dL \tag{12}$$

where $G/L=2\pi Rr/\lambda L\cong sr$ and $mG^2/L^2\cong\langle l^2\rangle_{Av}s^2/2$. The value of (12) is

$$\exp(-\langle l^2\rangle_{Av}s^2/2)\frac{\sin sr}{sr}\left\{\left[\frac{A}{a^{\frac{1}{2}}}\exp(-s^2r^2/4aL_0^2) +\frac{B}{b^{\frac{1}{2}}}\exp(-s^2r^2/4bL_0^2)\right]\frac{a^{\frac{1}{2}}b^{\frac{1}{2}}}{Ab^{\frac{1}{2}}+Ba^{\frac{1}{2}}}\right\}. \tag{13}$$

As the scattering volume is decreased to approach a point source, a and b become large and (13) reduces to the desired function, $\exp(-\langle l^2\rangle_{Av}s^2/2)(\sin sr/sr)$. The damping of the molecular curve caused by a spreading gas sample is selective and increases for larger s values and larger interatomic distances.

If it were assumed that the value of the brace in (13) was unity, as would have been the case in an ideal experiment, the value for $(\langle l^2_{F-F}\rangle_{Av})^{\frac{1}{2}}$ obtained from our experiments with CF_2CF_2 would have been 0.117A. For an interatomic distance of $r=3.50$A and the values of the parameters, $A=0.9$, $B=0.1$, $a=3$ and $b=0.2$,

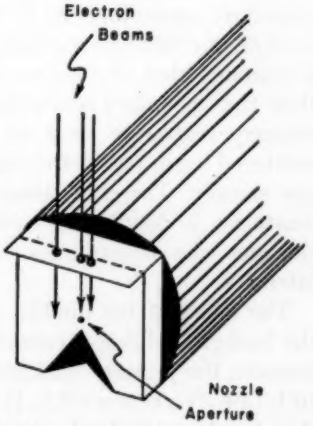

FIG. 2. Diagram of a nozzle used for the experiment to determine the spread of gas about the nozzle aperture. The shield above the nozzle aperture has several apertures to direct the electron beam various distances away from the nozzle aperture.

[7] A very nice microscope photograph of a gas jet may be found in a paper by H. Boersch, Zeits. f. Physik **107**, 493 (1937).

[8] Figure 20d in a report by Bauer, Keidel, and Harvey, "An Evaluation of Quantitative Procedures for the Estimation of Intensities of Diffracted Electrons," Contract No. N6 ori-213, Task Order I, NR052-040(1949), computed graphically using theoretical scattering functions may be compared with this result.

TABLE I. The effect of secondary scattering on a theoretical background shape.

s	Prim. scat. Eq. (14)	Sec. scat. Eq. (16)	85% Prim. +15% Sec. / 100% Prim.
0	11	3.7	0.90
1	0.592	0.888	1.08
2	0.054	0.120	1.18
5	1.56×10^{-3}	3.48×10^{-3}	1.18
10	1×10^{-4}	2.14×10^{-4}	1.17
20	6.25×10^{-6}	12.77×10^{-6}	1.16
30	1.23×10^{-6}	2.49×10^{-6}	1.15

the corrected value from (13) is 0.114A. Although the damping due to sample spread appears important in (13) at first sight, the effect of the vibrational motion is considerably more important as may be observed from the detailed computation. Therefore the spread of sample leads to a minor correction. For smaller r values, the correction amounts to 0.001–0.003A. These corrections have been taken into account in reporting the final results. It should be noted that these corrections are extreme since they were derived from a jet shape determined under unfavorable conditions of vapor condensation.

Multiple Scattering

The evaluation of the effect of multiple scattering is complicated by the fact that the electron scattering function is not known for very small values of s. In order to avoid this difficulty the following treatment was made. It was assumed that all electrons within a circle of 0.1 mm radius about the center of the main beam constituted the undeviated beam. It was then possible to measure the fraction of the main beam scattered beyond the circle of 0.1 mm radius and treat this as the total scattered intensity. This was found to be of the order of 25 percent for CH_2CF_2 under the conditions similar to those of our diffraction experiment. The total scattering is composed of primary scattering, secondary scattering, etc. If the total scattering is equal to 0.25, the tertiary scattering may be neglected. If it is assumed that the gas sample is of uniform density, then the secondary scattering is equal to 0.125 of the primary scattering since on the average the primary scattered beam passes through half the thickness of the gas sample. Therefore about 13 percent of the total scattering is doubly scattered. It is now of interest to consider the contribution of this doubly scattered intensity.

The effect of the double scattering on the shape of the background line is considered first. In the region of interest, the primary background function is very close to $1/(a+s^3)$ where $a\sim0.1$. It is not convenient to study this function. Instead, the background was assumed to be

$$1/(b+s^2)^2 \qquad (14)$$

where $b\sim0.3$. This function drops off somewhat faster than $1/(a+s^3)$ in the region where its values are important but is sufficiently similar to permit a rough estimate of the effect of the multiple scattering on the background line.

The multiple scattering integral which must be evaluated is

$$\frac{b}{\pi}\int_{-\infty}^{\infty}\int \frac{1}{[b+\xi^2+\eta^2]^2}\,\frac{1}{[b+(x-\xi)^2+(y-\eta)^2]^2}\,d\xi d\eta, \qquad (15)$$

where $s\cong(\xi^2+\eta^2)^{\frac{1}{2}}$ and b/π is a normalization factor. The result which is a new function of s, since $s\cong(x^2+y^2)^{\frac{1}{2}}$, is $1/3b^2$ for $s=0$ and

$$\frac{2(s^2-2b)}{s^2(s^2+4b)^2}+\frac{4b(s^2+b)}{s^3(s^2+4b)^{5/2}} \times\log\left\{\frac{s^2(s^2+4b)^{\frac{1}{2}}+s(s^2+4b)}{b(s^2+4b)^{\frac{1}{2}}-bs}+1\right\} \qquad (16)$$

for $s\neq0$. A comparison of (14) and (16) is shown in Table I. The intensity at the origin has been reduced by a factor of 3. As a result of the decrease in intensity about the origin, the remainder of the background from $s=2$ to ∞ is increased by about a factor of 2. It may be seen from column 4, which is the ratio of 85 percent primary scattering plus 15 percent secondary scattering to 100 percent primary scattering, that the change in shape of the background line is very small except for very low s values. It is interesting to notice however, that the level of the background is increased by about 17 percent in the region of interest ($2<s<30$). This is of no significance in our procedure for studying molecular structure or vibrational amplitudes since the only feature of importance is the shape of the background line.

An evaluation was made of the effect of the double scattering on the molecular intensity. For this purpose the background function was assumed to have the form $A\exp(-ks^2)$. For some choice of k it is possible to have this function agree fairly well in shape with (14)

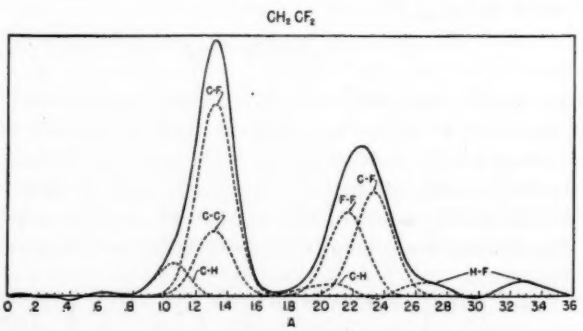

Distance	C-H	C-C	C-F	C-H	F-F	C-F	H-F	H-F
nZ_iZ_j	4	12	36	4	27	36	6	6
Actual Area	4.2	12.1	36.0	4.1	27.2	36.0	5.4	7

FIG. 3. The solid line is the computed radial distribution curve, $f(r)$, for CH_2CF_2. The dashed lines indicate the individual peaks for each interatomic distance.

for small values of s which is the region making the major contribution. The exponential ultimately decreases too rapidly and therefore the results obtained from this function indicate a somewhat more favorable situation than is actually the case. The integral which must be evaluated is

$$\frac{k^{\frac{1}{2}}}{\pi^{\frac{1}{2}}}\int_{-\infty}^{\infty}\int \exp\{-k[(x-\xi)^2+(y-\eta)^2\} \times\exp\{-M(\xi^2+\eta^2)\}\frac{\sin r(\xi^2+\eta^2)^{\frac{1}{2}}}{r(\xi^2+\eta^2)^{\frac{1}{2}}}d\xi d\eta, \quad (17)$$

where $s\cong(\xi^2+\eta^2)^{\frac{1}{2}}$, $M=\langle l^2\rangle_{Av}/2$, and r is an interatomic distance. A portion of this integral merely contributes to the background, whereas the remainder leads to the expression

$$\exp(-\langle l^2\rangle_{Av}s^2/2)\exp(-r^2/4k)\left\{\frac{\sin sr}{sr}-\frac{r}{4ks}\frac{\cos sr}{sr}\right\}. \quad (18)$$

The main consequence of the double scattering is that the molecular terms are reduced by a factor $\exp(-r^2/4k)$, as a function of r, the interatomic distance, but uniformly for all s. However, for small s values, phase shifting also plays some role. A reasonable value for k is about 2, hence for distances of about 1.3A the scattering coefficient is reduced by 2.5 percent whereas for distances of about 3.5A the scattering coefficient is reduced by 10 percent for 13 percent double scattering.

The decrease of the scattering factors because of multiple scattering has a small effect upon the shape of the measured experimental molecular intensity curves in these experiments and may be ignored in computing the theoretical curves. It is noted that the difference in the reduction of the scattering coefficients for shorter and longer distances is about eight percent. The longer distances contribute less than the shorter ones to the molecular intensity, for comparable scattering factors, because of the increased damping in the denominator of (18) and also because of the larger l associated with larger r. Therefore, the shape of the measured molecular intensity curve would differ from the ideal by about two percent for s values around four and approach the ideal as s increases. In our method a theoretical curve is attached to the experimental curve in the region $0<s<3$ or 4. Ideal scattering factors are used for this curve which is computed in the final step of a successive approximation procedure[2] from correct structural parameters. It will be seen that the areas under the final distribution curve yield ideal scattering factors indicating that the parameters of the attached inner region are essentially consistent with the experimental curve.

General Conclusions

On the basis of the study of the camera characteristics, the following remarks apply to this investigation and may readily be extended to those involving other molecules.

TABLE II. Equilibrium distances and average displacements from equilibrium as determined from the radial distribution curves for CH_2CF_2.

	r, A	$(2k)^{-\frac{1}{2}}$, A
C−H	1.07	0.05, assumed
C−C	1.31	0.03, assumed
C−F	1.32	0.043
C=H	~2.05	0.065, assumed
F=F	2.16	0.063
C=F	2.33	0.063
H=F	2.65	0.08, assumed
H=F	3.27	0.10, assumed

1. The diameter of the main beam was sufficiently small to behave like one of infinitesimal thickness.

2. No extraneous shadows or spray were obtained from the gas nozzle or sector.

3. The spread of sample caused no change in the background line and introduced a small increase in the measured vibrational amplitudes which could be easily corrected.

4. Double scattering caused a negligible change in the shape of the background line although it raised its level in the region of interest by about 17 percent. Double scattering also caused a decrease in the scattering factors for longer distances relative to shorter ones by amounts of the order of eight percent.

ANALYSIS AND RESULTS

CH_2CF_2

The first peak for the CH_2CF_2 molecule, Fig. 3, is composed of three distances, the C−C, the bonded C−F, and the bonded C−H. It did not appear likely

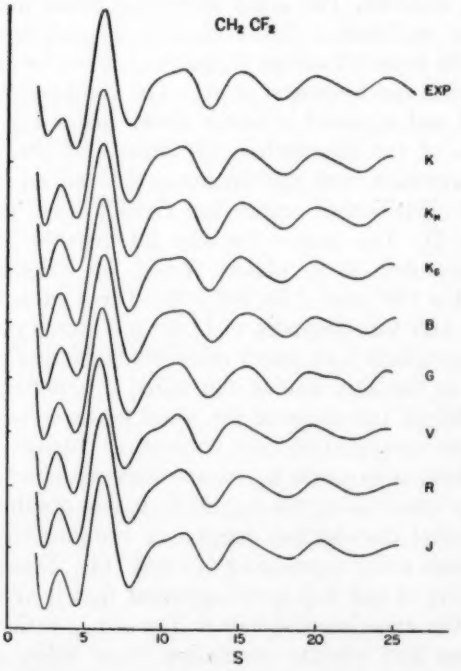

FIG. 4. The experimental and computed molecular intensity curves for CH_2CF_2.

TABLE III. Equilibrium distances and average displacements from equilibrium as determined from the radial distribution curve for CF_2CF_2.

	r, A	$(2h)^{-\frac{1}{2}}$, A
C−C	1.315	0.03, assumed
C−F	1.315	0.057
F=F	2.20	0.097
C=F	2.30	0.089
F=F	2.74	0.093
F=F	3.485	0.117

that any contribution from the C−H distance would affect the right side of the peak; hence the right side was fitted by trial and error with the function

$$\frac{c_1 H_1^{\frac{1}{2}}}{r_1}\exp[-H_1(r-r_1)^2]+\frac{c_2 H_2^{\frac{1}{2}}}{r_2}\exp[-H_2(r-r_2)^2], \quad (19)$$

where r_1 and r_2 are the equilibrium C−C and C−F distances, H_1 and H_2 are related to the projected amplitudes for C−C and C−F by means of (6) and (7) and c_1 and c_2 are 1×6×6 and 4×6×9. The curve which fit the right side of the peak almost exactly was subtracted from the peak and the remaining area formed a smooth curve about $r=1.07$A which was attributed to the C−H distance. The three components of the first peak of the curve for CH_2CF_2 are illustrated in Fig. 3.

The second peak of the $f(r)$ curve was decomposed in a similar fashion into four peaks for C=H, F=F, C=F, and H=F, where the C=H and H=F peaks were obtained by subtraction. The third peak of the radial distribution curve represented only the longer H=F distance. The areas under the peaks multiplied by the equilibrium distances were in good agreement with the expected values (equal to c_{ij}) even for distances involving the hydrogen atoms. The comparison of the actual and expected values is shown below Fig. 3. The values of the equilibrium distances and the average displacements from equilibrium as determined from the radial distribution curve for CH_2CF_2 are listed in Table II. The values for the interatomic distances corresponded to a planar model of CH_2CF_2 with $\angle FCF=110°$ and $\angle HCH\cong 120°$. The h values for the C−C and the distances to hydrogen atoms could not be determined with much certainty since small oscillations in the zero line of the radial distribution curve can change the shape of the small peaks considerably. For the computation of a theoretical intensity curve, therefore, reasonable h_{ij} values were assumed. An intensity curve using the r_{ij} and h_{ij} values obtained from the radial distribution curve was computed on IBM machines using expressions (7) and (11). This curve is K in Fig. 4 and it is quite apparent that it agrees well with the experimental curve. The s/s_{exp} ratio for the maxima and minima (excluding those below $s=4$) is 1.001 ± 0.006 and the ratio of the intensities for the maxima and minima for the two curves are within ± 3 percent (excluding the region below $s=4$). As mentioned in the section on Procedure, the intensities of the maxima and minima are measured from several photographs with about 7 percent average deviation.

It is possible to vary somewhat some of the r_{ij} values along with the companion h_{ij} values without having too large a discrepancy with the radial distribution curve. In order to determine the range of uncertainty of the various parameters, a number of intensity curves were computed based on assumed models. One set of curves was computed for planar models with C_{2v} symmetry where the C−F distance was kept at 1.32A while the C−C and F−F distances assumed the values indicated in the parameter chart in Fig. 5, and the h_{ij} values were chosen to be as consistent as possible with the radial distribution curve. The $\angle HCH$ was kept at 120°. Some of the computed curves are reproduced in Fig. 4.

The computed intensity curves have features which are sensitive to small changes in the parameters. Each dotted or dashed line in Fig. 5 denotes when a particular feature in a computed curve becomes sufficiently different from the experimental curve to be considered unacceptable.[9] The arrows indicate the direction in which models become more unacceptable. The —·—· line concerns the shape of the maximum at $s=10$–11. Curves B, V, and R illustrate unacceptable shapes for this feature. The —— line concerns the difference in intensity from the maximum at $s=11$ to the minimum at $s=13$. Curve B is unacceptable in this respect since this intensity difference differs from that in the experimental curve by 13 percent. The – – – – line concerns the difference in intensity from the minimum at $s=13$ to the maximum at $s=15$. In curve B, this feature

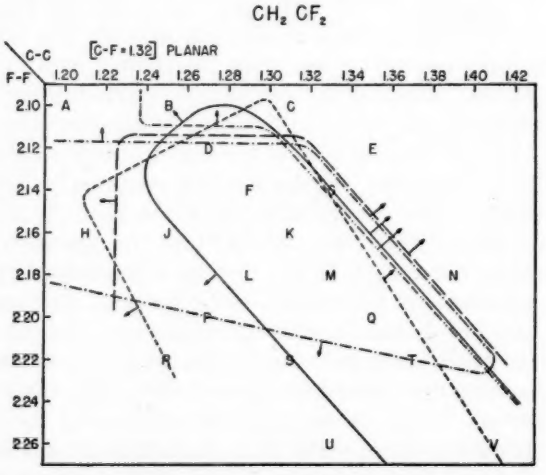

FIG. 5. Parameter chart for CH_2CF_2. The positions of the letters indicate the parameters of the models for which intensity curves were computed. The dashed and dotted lines indicate when particular features of the intensity curves were sufficiently different from the experimental curve to make them unacceptable.

[9] Each of the various dashed lines which denote curves with acceptable features should form a closed region. It was considered unnecessary to compute more curves to extend the map since those curves would necessarily be unacceptable.

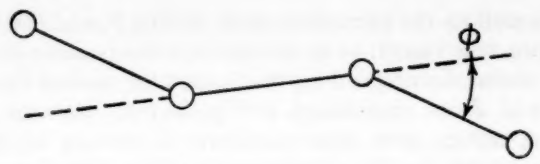

FIG. 6. Edgewise view of a bent configuration. Angle ϕ measures the deviation from coplanarity.

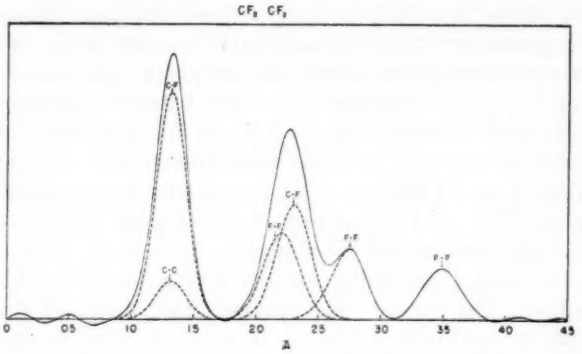

Distance	C-F	C-C	F-F	C-F	F-F	F-F
nZ_iZ_j	36	6	27	36	27	27
Actual Area	35.9	6.0	27.2	36.1	26.8	27.0

FIG. 7. The solid line is the computed radial distribution curve, $f(r)$, for CF_2CF_2. The dashed lines indicate the individual peaks for each interatomic distance.

differs by 14 percent from the experimental curve, whereas in curves *G*, *V*, and *R* the difference is of the order of 10 percent and these models are on the borderline of acceptability for this particular feature. The - - - · line concerns the position of the maximum at $s=15$. Curves *B* and *G* illustrate how this maximum can be misplaced. The solid line concerns the shape and position of the maximum at $s=20$. In curves *B* and *G*, this maximum has the wrong shape and in curves *R* and *J* this maximum is misplaced.

Curves *B*, *G*, *V*, *R* and *J* were chosen to illustrate how some of the features change with a change of the parameters of a planar molecule. Curves for models *A*, *C*, *E*, *H*, *N*, *P*, *S*, *U* have similar and even more serious difficulties. Curves for models *D*, *F*, *K*, *L*, *M*, *Q*, and *T* are in an acceptable region. Model *K* is the one most consistent with the results from the radial distribution curve and the experimental intensity curve. Accordingly, the deviation from the average s/s_{exp} value for the maxima and minima becomes larger in the directions of *D*, *T* and *L*. The acceptable area is somewhat smaller than that indicated in the parameter chart since the scale factor s/s_{exp} must be taken into consideration.

Good agreement with the radial distribution curve and the experimental intensity curve is obtained with a planar model having a HCH angle of 120°. Investigations were made of the effect of changing the HCH angle and of twisting the molecule about the C−C axis. In the first case, the only distances which are affected are the longer C=H and the two H=F. They are fairly sensitive to a change in angle becoming larger when the HCH angle is decreased and vice versa. Although they contribute only about 12 percent to the total molecular scattering, the effect on the computed intensity curve is considerable since they all change in the same direction. The feature which is affected most is the maximum at $s=10$–11. Three curves were computed for the same parameters as in model *K* except that the HCH angle was 105°, 110° and 130°. For the curve with the 130° angle, the peak at $s=10$–11 appeared like the peak in curve *R* and hence an HCH angle as large as 130° is improbable. Curve *K* is the curve for the 110° angle and the small minimum near $s=10$ puts this model on the borderline. For the curve with the 105° angle, the minimum near $s=10$ becomes sufficiently deep to make this curve unacceptable. Hence it is concluded that the HCH angle is about 117°±7°.

Twisting the molecule about the C−C axis affects only the two H=F distances. The changes in the magnitudes of these distances are small for angles of rotation up to 45°. Moreover, the two distances change in opposite directions, so that the changes compensate each other and have little effect on the intensity curves. Hence, electron diffraction data are inconclusive about the possibility of the existence of a twist about the C−C axis up to 45°. For angles of rotation of 45° and greater, the intensity curve is affected in the region of $s=10$–11. This peak assumes an undesirable shape similar to that in curve *V*.

Another type of non-planar molecule may be possible in which the configuration shown in Fig. 6 is assumed. It is possible to obtain such a model from a planar model by lengthening the C−C distance and keeping

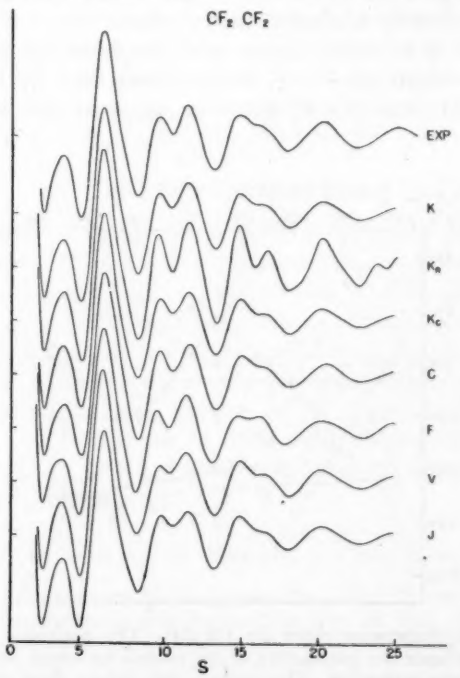

FIG. 8. The experimental and computed molecular intensity curves for CF_2CF_2.

all other interatomic distances practically the same. Curve K_C was obtained in this way from model K and thus the C−C distance increased from 1.31 to 1.36A and angle ϕ was 26°. This curve is unacceptable in the region of $s=10$–11 since the maximum is too flat. However, configurations with angle ϕ up to 20° cannot be excluded on the basis of intensity curves. The increase in the C−C distance required for angle ϕ to be as large as 20° is contained in the uncertainty placed on this distance for planar models.

CF_2CF_2

The radial distribution curve for CF_2CF_2 is shown in Fig. 7. The composite peaks were resolved in the manner described for the CH_2CF_2 molecule and the comparison of expected and actual areas under the peaks is shown beneath the figure. The values for the equilibrium distances and average displacements from equilibrium as determined from the radial distribution curve are shown in Table III. These distances are compatible with a planar model with V_h symmetry and an FCF angle of 114°. An intensity curve, K, computed for this model is compared to the experimental curve in Fig. 8. The s/s_{exp} ratio for the maxima and minima (excluding those below $s=4$) is 1.002 ±0.003 and the ratios of the intensities of the maxima and minima of the two curves are within ±3 percent in the region $4\leq s\leq 20$. An intensity curve, K_R, computed for a rigid model with the same interatomic distances as in K, illustrates the importance of including the vibrational motions in the computation of intensity curves. Not only the magnitudes of the peaks are changed, but the actual shapes of the maxima can be considerably altered at high s values.

A set of intensity curves was computed for planar models where the C−F distance was kept at 1.31A, the C−C and F=F distances assumed the values

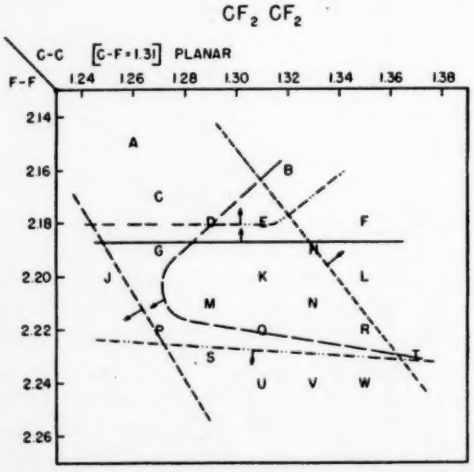

FIG. 9. Parameter chart for CF_2CF_2. The positions of the letters indicate the parameters of the models for which intensity curves were computed. The dashed and dotted lines indicate when particular features of the intensity curves were sufficiently different from the experimental curve to make them unacceptable.

indicated on the parameter chart in Fig. 9, and the h_{ij} values were chosen to be as consistent as possible with the radial distribution curve. Curves for models C, F, V, and J are reproduced in Fig. 8. Four features of these curves were quite sensitive to changes in the parameters. In the experimental curve, the descent from the large maximum at $s=6$ to the third minimum is concave in shape. In curves C and F, the descent in this region is almost a straight line. The solid line on the parameter chart separates the curves which are concave from those which are straight in this region. The – – · · line concerns the height between the minimum and maximum at $s=8$–9. As for instance, the height in curve C is 11 percent greater and that in curve V is 12 percent less than in the experimental curve. The — — line concerns the relative heights of the two maxima and the minimum at $s=9$–12. Curves C, V and J illustrate various difficulties with this feature. The – – – – line concerns the shape of the peak at $s=15$–16. Curve F is representative of one type of unacceptable shape and curve J is representative of another type of unacceptable shape for this feature.

Curves for models K, M, N, and R reproduce the experimental curve fairly well. Model K is most consistent with the values from the radial distribution curve and the experimental intensity curve. The average deviation from the average s/s_{exp} value ranges from ±0.003 for K up to ±0.005 for H, Q, and R. The s/s_{exp} scale factor reduces the size of the acceptable region somewhat.

A considerable number of models were computed with the configuration shown in Fig. 6, in which the center of symmetry is preserved. The principal effect of this change on the intensity curves was to make the two peaks at $s=9$–12 more nearly equal in size and to decrease the size of the satellite on the peak at $s=15$. An example of this is curve K_C which represents a model where ϕ is 24°, the C−C distance is 1.35A, and the two C−F and the short F−F distances are the same as in model K. It is possible to make angle ϕ as large as 24° without being able to rule out the model with electron diffraction data. The changes in the interatomic distances for angle ϕ to be 24° are contained in the uncertainties placed on the distances for a planar model.

A twist about the C−C axis has an effect on the two longer F−F distances. The *trans* F−F distance is at its maximum and the *cis* F−F distance is at its minimum when the molecule is planar. A twist about the C−C axis brings the value of these two distances closer together. The values which are derived from the radial distribution curve for these two indicate that a twist of ~15° is possible. An intensity curve computed for model K with a twist of 15° is entirely compatible with the experimental curve while one with a twist of 30° is unacceptable since it has features similar to those in curve F. It is more likely that the molecule may be oscillating about the C−C axis within an angle of

$\sim 30°$. The equilibrium value of the *trans* F−F distance in the planar model is ~ 0.02A larger than the position of the maximum of the F−F peak in the radial distribution curve. Likewise, the equilibrium value of the *cis* F−F distance in the planar model is about the same amount smaller. This is in qualitative agreement with theoretical expectations[10] for oscillation about the C−C bond but is not a strong enough effect to permit quantitative analysis.

The structures of CH_2CF_2 and CF_2CF_2 as obtained using quantitative electron diffraction data are given in Table IV.

DISCUSSION

The procedure used in this determination of molecular structure is entirely mechanized except for drawing a background line to represent the atomic scattering. The placement of the background line is subject to a very restrictive criterion, namely, that the resultant radial distribution curve is essentially zero everywhere except in the vicinities of the interatomic distances and that the background line be smooth. The background lines determined in this fashion for the two molecules studied are in good agreement with the theoretical values, except at small scattering angles where the theoretical values for the light atoms involved in these molecules are not known accurately. The criteria for good data in general are that the areas under all the peaks in the radial distribution curve are in proper ratios to each other, that the equilibrium interatomic distances indicated in the radial distribution curve form a consistent model, and that, in general, the amplitudes of vibration increase with longer interatomic distances. It has been found in this experiment that even distances involving H atoms obey these criteria quite well. The purpose in computing theoretical intensity curves has been to place limits of uncertainty upon the values for the structure parameters as obtained from the radial distribution curves.

The C−C and C−F distances in CH_2CF_2 and CF_2CF_2 are essentially the same. The main difference in the two structures is the $\angle$FCF which is about 4° larger in CF_2CF_2 than in CH_2CF_2. The results for CH_2CF_2 are in excellent agreement with those obtained from an investigation of its microwave rotational spectrum[3] and in addition the electron diffraction data permit an evaluation of the $\angle$HCH. The C−F values in this experiment have been found to be near 1.32A. This can be compared to the C−F values in CH_2F_2 and CHF_3 (more than one F atom attached to a C atom) obtained from infra-red and microwave spectroscopy[11–13] which are consistently near 1.32A. The moments of inertia of CH_2CF_2 and CF_2CF_2 are consistent with the interpretation of the infra-red and Raman spectra.[4,14] Small alterations in the parameters of CH_2CF_2 could destroy this consistency.

It was found that the average vibrational amplitudes (along the lines joining two atoms at equilibrium) were about 50 percent larger in CF_2CF_2 than in CH_2CF_2. It would be worthwhile to perform detailed computations of the amplitudes from spectroscopic data to compare to the electron diffraction data.

TABLE IV. Equilibrium distances and average displacements from equilibrium obtained from quantitative electron diffraction data.

	CH_2CF_2*	
	r, A	$\langle l^2\rangle_{Av}^{\frac{1}{2}}$, A
C−F	$1.321+a$	0.042 ± 0.005
C−C	1.311 ± 0.035	
C−F	2.335 ± 0.009	$0.060+d$
F−F	$2.162+b$	$0.060+d$
C−H	$1.07\ \pm0.02$	
C−H	$2.06\ \pm0.04$	
H−F	$2.61\ \pm0.05$	
H−F	$3.29\ \pm0.03$	
$\angle$FCF $=110°+c$		where $b\leq\pm0.026$
$\angle$HCH $=117°\pm7°$		and $a=-0.015b/0.026$
		$c=3b/0.026$
		$d=0.01b/0.026\pm0.003$

	CF_2CF_2†	
	r, A	$\langle l^2\rangle_{Av}^{\frac{1}{2}}$, A
C−F	1.313 ± 0.010	0.056 ± 0.005
C−C	1.313 ± 0.035	
C−F	2.306 ± 0.014	0.087 ± 0.01
F−F	2.204 ± 0.022	0.095 ± 0.01
F−F	2.737 ± 0.029	0.090 ± 0.01
F−F	3.515 ± 0.011	0.114 ± 0.01
$\angle$FCF $=114°\pm2°$		

* Extent of oscillation about the C−C axis relatively indeterminate (less than 60°). Possible bending (angle ϕ in Fig. 6) up to 20°.
† Possible oscillation about the C−C axis within 30°. Possible bending (angle ϕ in Fig. 6) up to 25°.

ACKNOWLEDGMENT

We wish to thank Dr. W. S. Murray of the Jackson Laboratory (E. I. Du Pont de Nemours and Company) for making available to us samples of CH_2CF_2 and CF_2CF_2, Dr. V. S. Schomaker of the California Institute of Technology for making available a set of IBM punched cards used for the $f(r)$ computations, the Mechanized Analysis Section of the Naval Ordnance Laboratory for the use of their computation facilities, and Dr. D. C. Smith of the Naval Research Laboratory for helpful discussions.

[10] J. Karle and H. Hauptman, J. Chem. Phys. **18**, 875 (1950).

[11] H. J. Bernstein and G. Herzberg, J. Chem. Phys. **16**, 30 (1948).
[12] H. B. Stewart and H. H. Nielsen, Phys. Rev. **75**, 640 (1949).
[13] Gilliam, Edwards, and Gordy, Phys. Rev. **75**, 1014 (1949).
[14] Smith, Claassen, and Nielsen, J. Chem. Phys. **18**, 326 (1950).

Hydrogen Peroxide in the Thermal Hydrogen Oxygen Reaction. II. Reaction of Hydrogen Peroxide with Hydrogen and Chain Initiation in the Hydrogen Oxygen Reaction

C. K. McLane*
Lyman Laboratory of Physics, Harvard University, Cambridge, Massachusetts
(Received March 20, 1950)

The reaction between hydrogen peroxide and hydrogen has been studied in the temperature range 470 to 500°C. The dependence of reaction rate on concentrations is rather complicated for hydrogen, and is between first and second order for hydrogen peroxide. The evidence presented favors the conclusion that the reaction proceeds by a chain mechanism involving no direct reaction between hydrogen and hydrogen peroxide molecules, at least at low hydrogen concentrations.

It was found that hydrogen oxygen mixtures undergo appreciable reaction at temperatures where the rate of reaction is normally very small if small amounts of hydrogen peroxide are first added.

I. INTRODUCTION

In a recent paper,[1] a kinetic study of the decomposition of hydrogen peroxide vapor in boric acid treated vessels was reported. The work was done in a flow system to permit observations to be made to 540°C, where the reaction proceeds with a half-life of less than half a second in the presence of one atmosphere of oxygen. Hydrogen peroxide is, under certain conditions, an important intermediate in the hydrogen oxygen reaction,[2,3] when the latter occurs in the region near the third explosion limit; therefore, considerable interest may be associated with the reaction of hydrogen peroxide with hydrogen under these or similar conditions. This reaction, and the part it plays in chain initiation in the hydrogen oxygen reaction, form the subject of this communication.

The present study was made with precisely the same flow system which was employed for the investigation of hydrogen peroxide decomposition.[1] As might reasonably be expected, a much more rapid disappearance of hydrogen peroxide was found when the reaction occurred in the presence of hydrogen than when it occurred in the presence of an inert gas. It is immediately apparent that there are (at least) two factors which make it impossible for this approach to yield unambiguous and complete information on the mechanism of the reaction of hydrogen peroxide with hydrogen. These are: (1) The participation of hydrogen *atoms* will now undoubtedly be involved. The rate of diffusion of these will be so great that diffusion is not likely to be negligible, even in the narrower vessels (made from 8 mm O.D. Pyrex tubing). This means that results obtained with the different sized vessels will have no simple connection with the extent to which surface reaction occurs. (2) The average duration of a reaction chain may exceed the time required for the gaseous mixture to flow an appreciable distance.

II. MATHEMATICAL PART

Our procedure will be as follows: We start from the assumption that longitudinal diffusion may be neglected in the reaction vessels, but that lateral diffusion is rapid enough so as not to be a limiting factor on any surface reaction which may be occurring. We then derive rate equations for first- and second-order dependence of the rate on hydrogen peroxide concentration and find by experiment which best fits the observed facts. Dependences of reaction rates on hydrogen concentration and surface area are also investigated.

In all the experiments described here, the concentration of hydrogen was so large in comparison with that of hydrogen peroxide that it could be considered constant throughout the progress of the reaction. To see if the reaction rate was first order with respect to peroxide concentration, an attempt was made to fit the data with the following equation:

$$\ln c_f/c_i = -Kt_r + \text{constant}, \qquad (1)$$

where c_i and c_f are the peroxide concentrations in the gas streams entering and leaving the furnace, and t_r is a "reaction time" defined as the total volume of the reaction vessel divided by the gas flow rate corrected from room temperature, where it is measured, to furnace temperature. Here K will be the product of the rate constant and the function of hydrogen concentration on which the rate depends.** This functional de-

* Present address: Department of Physics, University of Wisconsin, Madison, Wisconsin.

[1] C. K. McLane, J. Chem. Phys. **17**, 379–385 (1949). A flow system was used in this work. Hydrogen peroxide concentrations were determined by measuring the optical transmission (at 2537A) of a six-foot layer of the gas before and after the passage through the reaction vessel in the furnace.

[2] See, for example, G. von Elbe and B. Lewis, J. Chem. Phys. **10**, 366 (1942).

[3] Presence of hydrogen peroxide in the reacting mixture was shown spectroscopically by R. B. Holt and O. Oldenberg, Phys. Rev. **71**, 479 (1947).

** The rate of reaction will, of course, be represented by the following differential equation if it is of the first order with respect to hydrogen peroxide concentration: $dc/dt = -kf(H_2)c$. Here c represents hydrogen peroxide concentration, k is the rate constant, and $f(H_2)$ gives the dependence of the rate on hydrogen concentration. Since $f(H_2)$ may be considered constant in performing the integration, Eq. (1) follows. It is the product $kf(H_2)$ which is designated by K in Eq. (1). The additive constant appears as a correction for reaction occurring in the inlet and outlet tubes of the reaction vessel (see reference 1).

pendence will be investigated by studying the dependence of K on hydrogen concentration (Fig. 3).

Use will also be made of the second-order counterpart of Eq. (1), derived in an exactly similar fashion:

$$1/c_f - 1/c_i = K_2 t_r + \text{constant}. \quad (2)$$

This may be expressed in terms of optical transmissions thus:

$$Q \equiv 1/\log T_i - 1/\log T_f = 2.3K_2 t_r/\alpha l + \text{constant}, \quad (3)$$

where the T's are optical transmissions of the peroxide vapor before and after its passage through the furnace, α is the absorption coefficient of the vapor, and l is the length of the absorption path. If a plot of Q *versus* the reaction time should prove to be linear, a second-order dependence of the rate on peroxide concentration would be indicated.

Data obtained with the lower surface vessels[1] (surface to volume ratio approximately 3 cm^{-1}) will be treated by means of the first-order equation only (number 10 of reference 1). This equation assumes uniform composition of the gaseous mixture in the reaction zone:

$$K = (c_f/c_i)^{-1}[(c_f/c_i)_0 - (c_f/c_i)]F_0 T_F/VT_R. \quad (4)$$

Here F_0 is volume flow rate measured at room temperature, T_F and T_R are temperatures of furnace and room, respectively, V is the volume of the reaction vessel *excluding* entrance and exit tubes, and the concentration ratio indicated with subscript '0' is measured with a vessel identical to the first, but in which the volume V is zero. Measurements with this latter vessel provide a correction for the reaction taking place in the inlet and outlet tubes of the first vessel.

III. EXPERIMENTAL PART

A series of experimental runs was made with various concentrations of hydrogen (designated by the mole fraction, f_{H_2}, of hydrogen in the gaseous mixture) in the higher surface vessels (surface to volume ratio about 7 cm^{-1}). These were constructed of 8 mm O.D. Pyrex,[1] and coated on the interior with boric acid. Representative data from these runs are plotted according to the first-order equation, (1), in Fig. 1 and according to the second-order equation, (3), in Fig. 2. First-order rate constants are summarized in Fig. 3.

A decision as to which of these orders best fits the observed data is made very difficult by large scatter of experimental points. However, over-all comparison of Figs. 1 and 2 (and the balance of similar figures, omitted here to conserve space) seems to indicate that the first-order plots fit the observed data somewhat better, particularly at the lower hydrogen concentrations. An ambiguity as to order is not unexpected, since

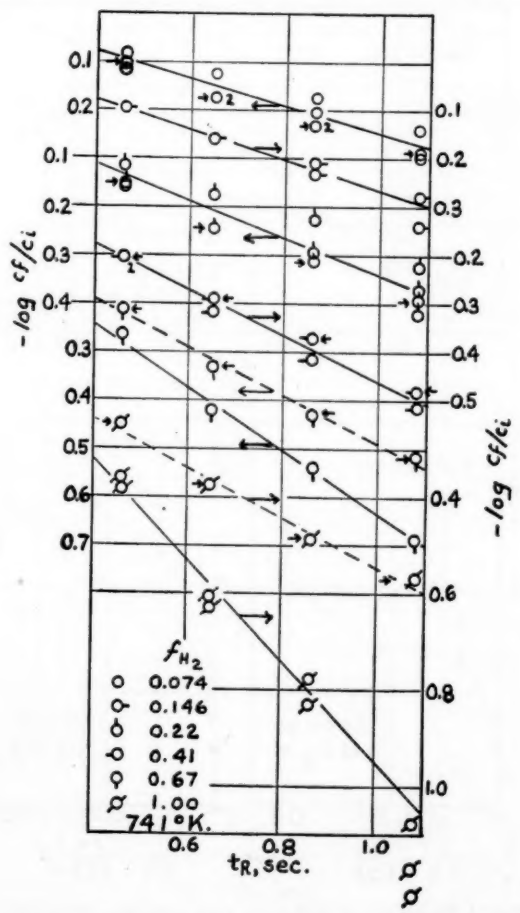

FIG. 1. Typical first-order rate plots of the experimental data on the reaction of hydrogen peroxide with hydrogen.

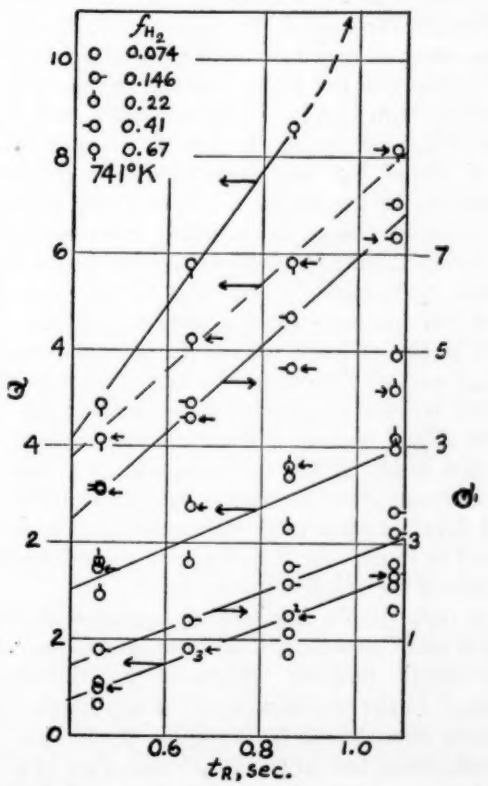

FIG. 2. Typical second-order rate plots of the experimental data on the reaction of hydrogen peroxide with hydrogen.

TABLE I. Study of effect of gas flow rate on hydrogen peroxide hydrogen reaction in vessels with lower S/V ratio. Furnace temperature, 740°K. Room temperature, 300°K. Nitrogen used as inert diluent.

Flow rate, l/min.	f_{H_2}	K sec.$^{-1}$
0.25	0.37	1.44
0.33	0.40	1.54
0.43	0.42	1.55
0.49	0.41	1.45
0.61	0.41	1.45

a simple mechanism to be discussed in Part IV would give rise to an order between the first and second.

Certain of the points, which are indicated by small arrows in these figures, lie on rate curves different from the balance of those taken under the same conditions. These points represent data taken in a series of runs (numbered 30–33) in which the same vessels were coated by exactly the same procedure employed in all other runs. After unusual results were obtained on the hydrogen peroxide hydrogen reaction with the vessels, their performance in the decomposition of hydrogen peroxide in the presence of an inert gas was checked. The mean absolute deviation of the results obtained differed from the best previous data by an average of less than 2 percent. Since the vessels as prepared for this series of runs could differ only in the character of their surface, the hydrogen peroxide hydrogen reaction must have greater sensitivity, or sensitivity of a different sort, to surface conditions than the decomposition of hydrogen peroxide in the absence of hydrogen.

The effect of flow rate on the observed (first-order) rate constant in the higher surface vessels with about 40 percent hydrogen in nitrogen at 740°K was found to be small but not negligible. The data are presented in Fig. 4. (Some, but only a small part, of the observed change can be accounted for by a slight variation in the hydrogen concentration during these experiments.) The change in the rate constant is in the wrong direction to allow explanation by induction period, carry-over of active radicals from the hot zone to continue the reaction in the cold exit tube of the reaction vessel, or a surface reaction limited by the rate of lateral diffusion. It is not possible to say what some combination of these effects might lead to without making a much more complete study of the rate constant as a function of flow rate and vessel geometry. Such an elaborate treatment does not seem to be warranted, as it is not likely to lead to much new knowledge of a fundamental nature about the reaction mechanism.

The only simple, immediately apparent explanation of this small dependence on flow rate is provided by longitudinal diffusion (enhanced by turbulence, if present). In the previous paper,[1] it was shown that this diffusion effect would be negligible in the ideal case of no turbulence, but larger in hydrogen than in a heavier gas (because of the larger diffusion coefficient in hydrogen). It is possible that the large concentration gradient, which may exist in a rapidly reacting mixture of hydrogen peroxide and hydrogen, leads to a diffusion effect large enough to account for the observed small dependence of rate constant on flow rate.

The reaction of hydrogen peroxide with hydrogen was also studied in the vessels of lower surface to volume ratio (3 cm^{-1}). These are the vessels in which uniform composition is assumed to be obtained in the reaction zone by mixing. The data obtained with these vessels are also included in Fig. 3. The constants have been calculated on the assumption of the first order with respect to hydrogen peroxide concentration, using Eq. (4).

As pointed out in the previous paper,[1] the assumption of uniform composition in the lower surface vessel must be tested by seeing whether or not the rate constant depends on gas flow rate. The data in Table I show that no significant variation was observed from 0.25 liter/minute, where the effluent concentration was only 16 percent of the feed concentration, to 0.61 liter/minute, where 37 percent of the hydrogen peroxide survived. That the reaction rate is less dependent on flow rate here than in the case of the narrower vessels may probably be attributed to the increased diffusion rates in hydrogen. This will aid in the achieve-

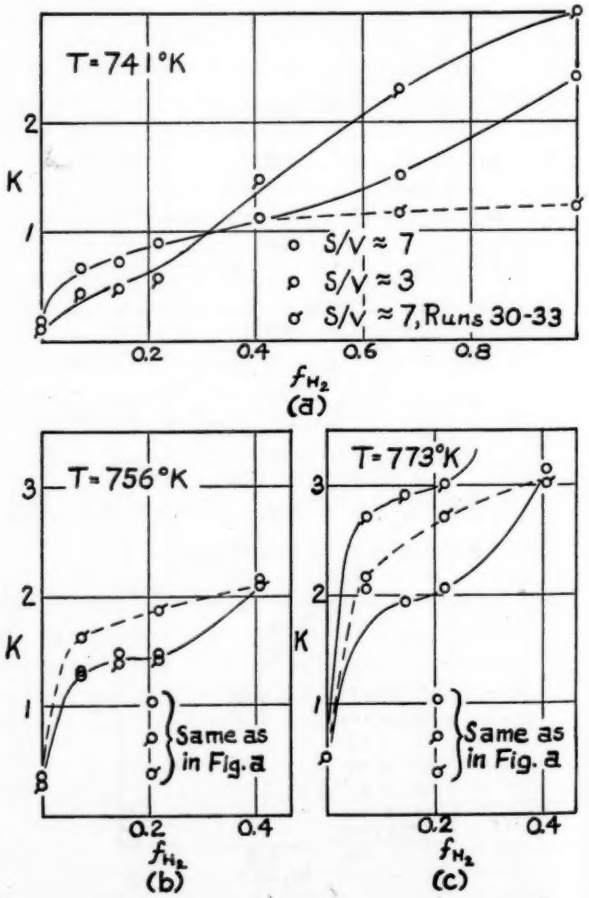

FIG. 3. Summary of first-order rate constants obtained for the reaction of hydrogen peroxide with hydrogen, showing the dependence of these constants on the mole fraction of hydrogen.

ment of uniform composition throughout the vessel, hence making the reaction in the vessel conform more closely to the equation derived for it.

The data in Fig. 3 show that the surface effect is dependent on temperature and hydrogen concentration. The reaction seems to be accelerated by the surface at low hydrogen concentrations and surface decelerated at higher hydrogen concentrations at the lowest temperature (740°K). At 757°K, there seems to be little if any surface effect in the range of hydrogen concentrations studied. At 773°K the effect of vessel size corresponds to a surface decelerated reaction, even at the lowest hydrogen concentrations which were used here.

It is necessary to postulate a chain mechanism to fit the observed dependence of rate on surface to volume ratio. Under some conditions (low temperature, high hydrogen concentration and high temperature, all hydrogen concentrations studied) the surface had a decelerating effect on the reaction. This could occur only if reaction chains were being terminated by the surface. The curious behavior observed in experimental runs 30 through 33 might then have been caused by an unusually high efficiency of the surface for breaking chains. This chain breaking efficiency of a surface would have to be entirely distinct from its catalytic activity for the decomposition of hydrogen peroxide in order to account for the low surface activity of the vessel coatings used in runs 30 through 33 for the decomposition of hydrogen peroxide in the absence of hydrogen.

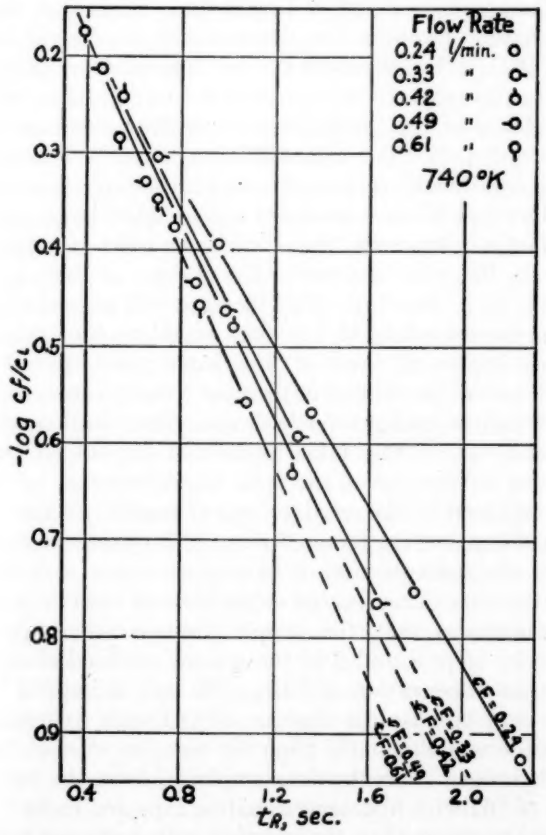

FIG. 4. The effect of flow rate on the first-order rate plot obtained for the reaction of hydrogen peroxide with hydrogen.

TABLE II. Apparent activation energy of $H_2O_2-H_2$ reaction

f_{H_2}	Apparent activation energy, E, kcal./mole $S/V\sim7$ cm^{-1}	$S/V\sim3$ cm^{-1}
0.074	41	64
0.146	35	63
0.22	30	57
0.41	37	54

IV. ENERGY OF ACTIVATION AND MECHANISM

The rate constants obtained with both surface to volume ratios were used to derive the apparent energy of activation for the hydrogen peroxide hydrogen reaction. (Of course, the result obtained may not be the energy of activation for any single step of the chain reaction.) The values obtained for the energy of activation are recorded in Table II.

As was observed in the case of the decomposition of hydrogen peroxide in the absence of hydrogen, the activation energies obtained with the low surface vessels are considerably larger. Assuming the results obtained with the low surface vessels to be reliable, this fact indicates that there may be two rate controlling mechanisms proceeding simultaneously, one of which occurs on the surface with a lower activation energy. As the surface to volume ratio is lowered, the observed activation energy should then tend to increase toward the value for the gas phase reaction.

Another fact worth noting is the tendency for the activation energy to decrease as the hydrogen concentration is increased. Without a detailed mechanism, which, unfortunately, cannot be derived from the data presented here, it is not possible to state the exact significance of this. If it is assumed that the measured activation energy is that of the rate controlling step, it might be concluded that one such step is operative at low hydrogen concentrations, and that this is supplanted by another, involving the hydrogen molecule, as the hydrogen concentration is increased. It might also be concluded that this decrease should be attributed to the effect of hydrogen concentration on the progress of reaction chains which follow the initiating step. The similarity in activation energies obtained at low hydrogen concentrations for this reaction and for the simple decomposition reaction described earlier[1] makes it seem reasonable that the same initiating step may be operative in both cases.

Further than this, it is difficult to go. If the initiating step is assumed to be decomposition to two hydroxyl radicals, and all conceivable subsequent steps are included, a final rate equation is obtained which is far too complicated to yield any useful information here. If the reaction:

$$OH+H_2O_2=H_2O+HO_2$$

TABLE III. Initiation of chains in the hydrogen oxygen reaction with hydrogen peroxide in higher surface vessel. Contact time about 1 sec.**

Conditions	T, °K	Run no.	c_f*	c_i*	c_f/c_i
0.5 l/min. N_2 Sat. H_2O_2	771	19.2-I	2.55	5.96	0.43
	773	34.1	2.80	5.13	0.55
	779	34.6	2.61	5.10	0.51
	785	34.11	2.28	5.20	0.44
0.16 l/min. N_2 Sat. H_2O_2 0.34 l/min. H_2	771	19.2-II	0.12	1.88	0.06
	773	34.2	0.09	1.66	0.05
	779	34.7	0.09	1.68	0.05
	785	34.12	0.0	1.70	—
0.16 l/min. O_2 Sat. H_2O_2 0.34 l/min. H_2	771	19.2-III	1.63	1.91	0.85
	773	34.3	1.58	1.70	0.93
	779	34.8	1.74	1.72	1.01
	785	34.13	1.66	1.71	0.97
0.16 l/min. O_2 Not sat. H_2O_2 0.34 l/min. H_2	771	19.2-IV	0	0	—
	773	34.4	0.05	0.08	—
	779	34.9	0.05	0.06	—
	785	34.14	0.02	0.06	—
0.5 l/min. N_2 Sat. H_2O_2	771	19.2-V	2.51	5.78	0.43
	773	34.5	2.91	5.23	0.56
	779	34.10	2.53	5.22	0.49
	785	34.15	2.25	5.29	0.43

* Units are molecules per cc $\times 10^{-16}$.
** All flow rates given here and in Table IV are measured at room temperature.

is considered to be negligible as compared with

$$OH+H_2=H_2O+H,$$

then HO_2 is removed from the reaction scheme and the latter is enormously simplified.[4] This assumption seems reasonable since the concentration of hydrogen is always about thirty times greater than the concentration of hydrogen peroxide in these experiments.

A reaction mechanism subject to the above conditions, and including no steps of the second order in chain carriers, could be represented by:[5]

(1) $H_2O_2+M=2OH+M$
(2) $H_2O_2 \xrightarrow{\text{wall}} 2\delta OH$***
(3) $OH+H_2=H_2O+H$
(4) $H+H_2O_2=H_2O+OH$
(5) Rate of destruction of H at wall $=k_5[H]$
(6) Rate of destruction of OH at wall $=k_6[OH]$.

The inclusion of reaction 6 is necessary to get a sufficiently strong dependence of the rate on hydrogen concentration. If reaction 6 were omitted, this would have the same effect as setting k_6 equal to zero in the rate equations, (5), (5′), and (5″). It will be noted that this would cause the denominator of the factor, B, to become always proportional to the concentration of hydrogen. This would cancel the important, direct dependence of reaction rate on hydrogen concentration.

The following rate equations follow from the above scheme:

$$d[H_2O_2]/dt=-A[H_2O_2]-B[H_2O_2]^2 \quad (5)$$

where

$$A=\{k_1[M]+k_2\} \quad (5')$$

and

$$B=\{2k_1[M]+2k_2\delta\}\frac{k_3k_4[H_2]}{k_3k_5[H_2]+k_4k_6[H_2O_2]+k_5k_6}. \quad (5'')$$

These equations represent the dependence of the rate of reaction on hydrogen concentration as shown in Fig. 3 in several important qualitative characteristics.

First, the rate will be of the first order in peroxide at low hydrogen concentrations, if the rates of steps 5 and 6, chain breaking, are small compared to the chain continuing steps 3 and 4. Under these conditions, the dominating term in the denominator of B will be $k_4k_6[H_2O_2]$. It follows that the denominator, being practically proportional to peroxide concentration, will cancel one of the $[H_2O_2]$ factors in the second order term of Eq. (5). The rate will be expected to increase quite rapidly with hydrogen concentration, because the product k_3k_4 in the numerator will be quite large, and the factor in braces will be of the same order of magnitude as the rate constant in the absence of hydrogen (factor A in Eq. (5)). This increase will be retarded when the term $k_3k_5[H_2]$ in the denominator of B becomes important—and at the same time, the dependence on peroxide will increase toward the second order and dependence on hydrogen concentration will decrease. *When* this takes place will depend on the relative efficiencies of the wall for destruction of H and OH, and on the relative rates of reactions 3 and 4.

Furthermore, the factor B (Eq. (5″)) reduces to zero when the concentration of hydrogen is zero, and the rate becomes that expected in the absence of hydrogen. This assumes that the simple decomposition takes place by steps 1 and 2 of the scheme outlined above. Complete destruction of OH at the wall is implied in this case, because the reaction of OH with hydrogen peroxide was eliminated from the reaction scheme. At the hydrogen concentrations employed here, the reaction of OH with hydrogen would be expected to be far more important than the reaction with hydrogen peroxide. At low hydrogen concentrations, however, the

[4] The very successful use of this reaction in treating the vapor phase photo-decomposition of hydrogen peroxide by D. H. Volman (J. Chem. Phys. **17**, 947–950 (1949)) should be noted. The reaction is omitted here for simplicity. Though it was found by Volman to be very important in the low temperature photo-decomposition of hydrogen peroxide, it seems reasonable to assume that it may be less important here because of the competition with the reaction of OH with H_2. We can give no quantitative confirmation that this assumption is valid: in fact, the mechanism outlined here is by no means proven. However, it does show a qualitative agreement with the observed dependence of rate on hydrogen concentration. Direct reaction of hydrogen peroxide with hydrogen would not show such qualitative agreement.

[5] This reaction scheme was selected on the basis of the discussions of the mechanism of the hydrogen oxygen reaction given by von Elbe and Lewis (see reference 2) and by A. H. Willbourn and C. N. Hinshelwood, Proc. Roy. Soc. **A185**, 353–369 (1946).

*** Of the hydrogen peroxide molecules decomposing at the wall, a fraction, δ, is assumed to provide two hydroxyl radicals per molecule which add to the supply of gas phase chain carriers. The balance, a fraction, $1-\delta$, is assumed to produce no active chain carriers.

hydrogen peroxide might successfully compete with hydrogen for reaction with the OH radicals. This would introduce HO_2 into the scheme, which would thereby become much more complicated. A detailed study of the reaction at low hydrogen concentrations might prove to be interesting.

This scheme is, of course, very incomplete. Nothing has been said of the further increase after the leveling of the rate which occurs at hydrogen concentrations from ten to thirty percent. This might be caused by an effect of hydrogen on the character of the adsorbed gas film at the surface, or could be due to the inception of some new chain propagating step involving the hydrogen molecule.

V. INITIATION OF CHAINS IN THE HYDROGEN OXYGEN REACTION BY INTRODUCTION OF HYDROGEN PEROXIDE

A considerable interest is connected with the ability of decomposing hydrogen peroxide to cause initiation of chains in the hydrogen oxygen reactions for two reasons. First, if such initiation were found, it would prove that active radicals are produced in the decomposition of hydrogen peroxide. Second, it would substantiate the view first expressed by von Elbe and Lewis[2] that the reaction chains in a reacting mixture of hydrogen and oxygen may be initiated by the hydroxyl radicals produced (directly or indirectly) by the decomposition of hydrogen peroxide. That this compound is present in a reacting mixture of hydrogen and oxygen was shown by the observations of Holt and Oldenberg.[3]

In the experiments to be described here, the same flow system was used as for the work on the decomposition of hydrogen peroxide and on the reaction of this compound with hydrogen. The flow rate used for all the work was 0.5 liter/minute, and the temperature was so low that no appreciable reaction took place in a stoichiometric mixture of hydrogen and oxygen in the absence of hydrogen peroxide with the short contact times used in this system. With the apparatus available, it was convenient to use the hydrogen peroxide concentration in the effluent gas stream as a measure of the degree of reaction. This provided only a lower limit, since hydrogen peroxide is not a stable product of the hydrogen oxygen reaction, and hence its concentration cannot exceed a certain equilibrium value for each particular set of experimental conditions.

The quantities measured are the feed concentration, c_i, and effluent concentration, c_f, of hydrogen peroxide: from these the ratio, c_f/c_i, was obtained.

In a typical set of experiments, the ratio c_f/c_i was first determined with 0.5 liter/minute of nitrogen saturated with hydrogen peroxide. This measurement gave the rate of decomposition of peroxide in the vessel, and hence, also, an index of its surface condition (excluding, of course, the part played by adsorbed gas films. These will change with changing mixture). The same was then repeated with a 2:1 mixture of hydrogen and nitrogen. The minor gaseous constituent of the mixture (in this case, nitrogen) was saturated with hydrogen peroxide and the hydrogen introduced just before the gas entered the reaction vessel. This was primarily a safety measure to prevent a possible explosion from traveling back to the saturators, which were filled with 90 percent hydrogen peroxide, but also served the purpose of permitting work with low concentrations of hydrogen peroxide in the feed mixture.

TABLE IV. Initiation of chains in the hydrogen oxygen reaction with hydrogen peroxide in low surface vessel. Contact time about 1 sec.

Conditions	T, °K	f_{H_2}	c_f*	c_i*	c_f/c_i
0.5 l/min. N_2 Sat. H_2O_2	772	0.0	3.25	5.54	0.59
0.16 l/min. N_2 Sat. H_2O_2 0.34 l/min. H_2	772	0.68	0.35	1.81	0.19
0.08 l/min. O_2 Sat. H_2O_2 0.42 l/min. H_2	772	0.84	1.15	0.94	1.23
0.12 l/min. O_2 Sat. H_2O_2 0.38 l/min. H_2	772	0.76	1.42	1.39	1.02
0.16 l/min. O_2 Sat. H_2O_2 0.34 l/min. H_2	772	0.68	1.72	1.83	0.94
0.18 l/min. O_2 Sat. H_2O_2 0.32 l/min. H_2	772	0.64	1.95	2.09	0.93
0.16 l/min. O_2 Not sat. H_2O_2 0.34 l/min. H_2	772	0.68	0.08	0.06	—
0.5 l/min. N_2 Sat. H_2O_2	772	0.0	3.11	5.64	0.55

* Units are molecules per cc $\times 10^{-16}$.

The measurement with 2:1 hydrogen and nitrogen showed to what extent hydrogen peroxide would survive in a mixture differing from the reacting gas mixture only in the substitution of nitrogen for oxygen. It is to be remembered that oxygen is practically as inert as nitrogen insofar as hydrogen peroxide decomposition is concerned. This was followed by a measurement with the stoichiometric mixture, first with, then without, hydrogen peroxide introduction. Finally, the decomposition of hydrogen peroxide mixed with nitrogen was checked to detect any alteration in experimental conditions which might have occurred.

The first two sets of measurements were made with a vessel of surface to volume ratio 7 cm^{-1}, and volume of 22.2 cc. The relevant data are recorded in Table III. It is apparent that the surface coating was more active in catalytic decomposition of hydrogen peroxide in the experimental runs numbered 19.2. This effect was accompanied by a lower yield of hydrogen peroxide

(observed in the $2H_2$ plus O_2 mixture with H_2O_2 initiation) than in the experiments of run 34 where a surface of lower activity was achieved. Therefore, it seems reasonable to infer that the surface decomposition yields fewer radicals capable of initiating reaction chains in the hydrogen oxygen reaction than the gas phase decomposition does.

In Table IV are the results of a series of experiments with the vessel of surface to volume ratio 3 cm^{-1} and volume 24 cc. In this series, the ratio of hydrogen to oxygen and the hydrogen peroxide content of the mixture were simultaneously varied.

The variation of the observed c_f/c_i value with the concentration of hydrogen is in the direction expected if formation of hydrogen peroxide is due to the reaction:

$$HO_2+H_2=H_2O_2+H.$$

A similar variation of peroxide yield with hydrogen concentration in the thermal reaction below the third explosion limit in hydrogen and oxygen mixtures was found by Pease[6] and by Holt and Oldenberg.[7]

It would be desirable to set some limit on the rate at which hydrogen peroxide is consumed by decomposition and reaction with the various atomic and molecular species present in the reacting hydrogen oxygen mixture at near third limit temperatures. Such is the complexity of the chain mechanisms which have been postulated for the reaction of hydrogen with oxygen and those which seem likely to apply to the reaction of hydrogen peroxide with hydrogen alone, that any attempt to extrapolate the reaction rates observed here to near third limit temperatures would be entirely without significance.

It is a pleasure for me to thank Professor O. Oldenberg for suggesting this problem and for his continuing interest and helpful advice, both in the experimental work and in the preparation of the manuscript. I also wish to express my appreciation to the National Research Council for the grant of a predoctoral fellowship which made this work possible. The financial support of the Rumford Fund of the American Academy of Arts and Sciences is gratefully acknowledged. The Buffalo Electrochemical Company generously supplied the 90 percent hydrogen peroxide used, and provided valuable information on the properties and safe handling of this material.

[6] R. N. Pease, J. Am. Chem. Soc. **52**, 5106–5110 (1930).
[7] R. B. Holt, Ph.D. Thesis, Harvard University (1947).

THE JOURNAL OF CHEMICAL PHYSICS VOLUME 18, NUMBER 7 JULY, 1950

Electrostatic Interaction in Hydrogen Bonding

NORMAN D. COGGESHALL
Gulf Research and Development Company, Pittsburgh, Pennsylvania
(Received March 20, 1950)

An attempt has been made to calculate the frequency shift, the intensity of absorption, and the energy of association of a hydroxyl group which is a participant in a hydrogen-bonded complex. When a term expressing the polarization energy of a hydroxyl group due to electrostatic interaction is added to the Morse function, the Schrödinger equation may be solved. The calculated wave-length of maximum absorption agrees with the experimental value fairly well for benzyl alcohol and exactly for catechol. Agreement between calculated and observed absorption intensity is satisfactory. The association energy, calculated on the linear polymer model, agrees quite well with the experimental results reported by Mecke.

SINCE the hydrogen bond was first recognized some thirty years ago there has been an increasing interest in it due to its great importance in the physical and chemical behavior of many polar materials. A voluminous literature dealing with the qualitative aspects has accumulated whereas the quantitative aspects have received much less attention. However, at the present time it is necessary to obtain a fuller understanding of the quantitative aspects of the phenomenon in order to further utilize the data. The present material reports upon some calculations of the fundamental stretching frequency of a hydroxyl group attendant to participation in a hydrogen bond.

THE NATURE OF THE BOND

From the x-ray studies of strongly bonded crystalline materials[1] it is known that the hydrogen bonds are of the general type shown in Fig. 1. Here the proton of one hydroxyl group is electrostatically attracted to the oxygen of another. This model is consistent with the statistical analysis of Kempter and Mecke[2] who showed that the dependence of degree of association of phenol on concentration cannot be explained by the dimer model wherein hydroxyl groups are bonded together through dipole-dipole attraction. It is clear that in an attempt to calculate the stretching frequency due to a hydrogen-bonded hydroxyl group the exact force conditions would be difficult to describe. In addition to the electrostatic effects of the nearest oxygen and proton atoms there are the van der Waals interactions between various members. Furthermore, by virtue of the relatively loose coupling of the hydrogen bonds, the

[1] L. Pauling, *The Nature of the Chemical Bond* (Cornell University Press, Ithaca, New York, 1944), Chapter IX.

[2] H. Kempter and R. Mecke, Zeits. f. physik. Chemie **46B**, 229 (1941).

molecules cannot be regarded as independent of one another.

In order to make the problem tractable we shall use a simplified force field situation. The hydroxyl frequencies are independent of the remainder of the molecule to a first approximation. Further, let us consider a diatomic group possessing a dipole moment immersed in a constant electric field. There will be an interaction energy depending upon the dipole moment, the angle of orientation, and the electric field. This will not be evidenced in the transition energies for the vibrational states of the group as they will all be shifted the same amount. There will be, however, a change of potential energy of the diatomic group due to polarization. This will be $-qE_pz$, where q is the charge unbalance for the group, E_p is the electric field component parallel to the direction of the valence bond, and z is the internuclear displacement from equilibrium. This change of potential energy will be evidenced in changes in the transition energies.

THE HARMONIC OSCILLATOR MODEL

When we apply the new energy term $-qE_pz$ to the Schrödinger equation there results a shift of all the energy levels for this model but no changes in the transition energies. This is readily seen from Eq. (1) which is the Schrödinger equation applied to the harmonic oscillator with the added energy term.

$$\frac{d^2\Psi}{dz^2}+\frac{8\pi^2\mu}{h^2}\left\{W-\frac{kz^2}{2}+qE_pz\right\}\Psi=0. \quad (1)$$

Here μ is the reduced mass for the oscillator and k is the force constant. It is obvious that a linear transformation of the displacement variable will restore the equation to its original form, i.e., without the new energy term, and with the only change being in the constant term W. This results in an equal shift of all the levels.

DIATOMIC GROUP WITH MORSE FUNCTION

The Schrödinger equation for the diatomic group with a Morse potential energy function and with the new term will be:

$$\frac{d^2\Psi}{dz^2}+\frac{8\pi^2\mu}{h^2}\{W-D(1-e^{-az})^2+qE_pz\}\Psi=0. \quad (2)$$

If we let $x=e^{-az}$ and expand $\log x$ in terms of $x-1$, dropping cubic and higher order terms, Eq. (2) becomes:

$$\frac{d^2\Psi}{dx^2}+\frac{d\Psi}{xdx}+\frac{8\pi^2\mu}{a^2h^2}\times\left\{\frac{W-D-C_0}{x^2}+\frac{2D-C_1}{x}-D-C_2\right\}\Psi=0, \quad (3)$$

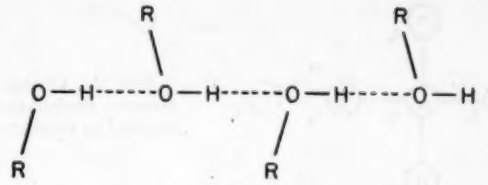

FIG. 1. Schematic linear model of hydrogen bonding; electrostatic interaction is along dashed lines.

where:

$$C_0=-(3qE_p)/2a$$

$$C_1=(2qE_p)/a$$

and

$$C_2=-(qE_p)/2a.$$

If we use the transformation:

$$\Psi(x)=e^{-y/2}y^{b/2}F(y),$$

where

$$y=2dx$$

$$d^2=(8\pi^2\mu/a^2h^2)(D+C_2)$$

and

$$b^2=-(32\pi^2\mu/a^2h^2)(W-D-C_0).$$

Equation (3) may be readily solved[3] and the energy levels become:

$$W(v)=W^1+\frac{ah(D-qE_p/a)}{\pi(2\mu)^{\frac{1}{2}}(D-qE_p/2a)^{\frac{1}{2}}}(v+\tfrac{1}{2})-\frac{a^2h^2}{8\pi^2\mu}(v+\tfrac{1}{2})^2 \quad (4)$$

where v is the vibrational quantum number and W^1 is given by:

$$W^1=D+C_0-(D-C_1/2)^2/(D+C_2).$$

Equation (4) is to be compared to the energy expression for the same diatomic group without the perturbing field, namely,

$$W(v)=\frac{ah}{\pi}\left(\frac{D}{2\mu}\right)^{\frac{1}{2}}(v+\tfrac{1}{2})-\frac{a^2h^2}{8\pi^2\mu}(v+\tfrac{1}{2})^2. \quad (5)$$

The result is thence a shifting of all levels with a decrease in the transition energies. A comparison with experimental results may now be made if values for q, E_p and a are chosen.

COMPARISON WITH EXPERIMENT

In order to compare the results of Eq. (4) with experimental values we may evaluate the unbalanced charges by the relation $\mu=qd$ where μ is the dipole moment for a diatomic group, q is the unbalanced charge, and d is the internuclear distance. We shall

[3] See, for example, L. Pauling and E. B. Wilson, *Introduction to Quantum Mechanics* (McGraw-Hill Book Company, Inc., New York, 1935), Chapter X.

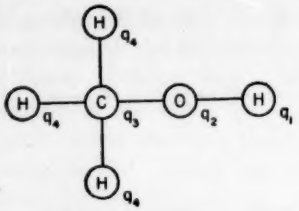

FIG. 2. Charge unbalance designations as applied to methanol.

evaluate q_1, the charge on the hydrogen atoms, and q_2, the charge on the oxygen atom from a consideration of methanol and then assume the same values hold for the higher alcohols. Let us consider Fig. 2 where q_1 and q_2 are the unbalanced charges as above and q_3 and q_4 are the unbalanced charges on the carbon atom and on the other hydrogen atoms. From Pauling's tabulations[4] of covalent radii and of dipole moments we have:

$$d(\text{O}-\text{H})=0.96\text{A},\quad d(\text{C}-\text{H})=1.07\text{A},\quad d(\text{C}-\text{O})=1.43\text{A}$$
$$\mu(\text{O}-\text{H})=1.51\times10^{-18}\text{e.s.u.},\quad \mu(\text{C}-\text{H})=0.4\times10^{-18}\text{e.s.u.}$$
$$\mu(\text{C}-\text{O})=0.8\times10^{-18}\text{e.s.u.}$$

We may evaluate q_1, q_4, and (q_2-q_3) directly from $\mu=qd$ obtaining $q_1=1.57\times10^{-10}$e.s.u., $9_4-0.37\times10^{-10}$ e.s.u., and $(q_2-q_3)=0.56\times10^{-10}$e.s.u. When these results are combined with the equation

$$q_1+3q_4+q_2+q_3=0,$$

we obtain $q_2=-1.62\times10^{-10}$ e.s.u. To evaluate E_p we use 2.70A for the O—H---O distance. The value of E_p at the center of the O—H bond is then 6.47×10^5 e.s.u. This is due to the contributions from the oxygen on one side and the hydrogen on the other The constant a may be evaluated by using Eq. (5) for a non-hydrogen-bonded hydroxyl group. For this we consider benzyl alcohol and use 2.77μ for the "free hydroxyl absorption."[5] For the dissociation energy D, the value of 110.2 kcal./mole may be used.[6] When this is done we obtain $a=2.30\times10^8$ cm^{-1}. To evaluate the term qE_p/a, the charge unbalance on the hydrogen atom, namely 1.57×10^{-10} e.s.u. is used with the above values for E_p and a to yield $qE_p/a=4.42\times10^{-13}$ erg. This is then used with the above value for a in Eq. (4) to calculate the transition energy between the ground and first excited state. From this the wave-length of maximum absorption λ_0 for the hydrogen bonded hydroxyl is determined to be $\lambda_0=2.92\mu$.

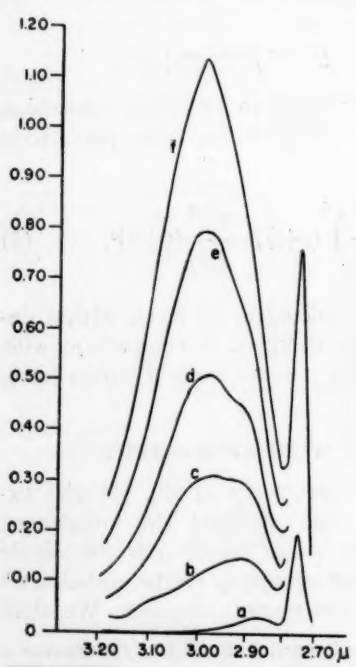

FIG. 3. Plot of optical density *versus* wave-length for benzyl alcohol in carbon tetrachloride solution at concentrations (a) 0.0486 mole/liter, (b) 0.0972 mole/liter, (c) 0.155 mole/liter, (d) 0.194 mole/liter, (e) 0.243 mole/liter, and (f) 0.278 mole/liter.

A comparison with experimental results may be obtained through Fig. 3. It shows the optical density plotted *versus* the wave-length for several concentrations of benzyl alcohol, ranging from 0.024 to 0.277 mole/liter. The non-bonded hydroxyl absorption occurring at about 2.77μ is shown for the extreme concentrations whereas the absorption in the bonded region, i.e., from 2.85 to 3.10μ is displayed for all.

It is seen that the wave-length of maximum absorption varies with concentration. This is consistent with the explanation of Kempter and Mecke[2] wherein the distribution of bonded molecules among the various n-fold complexes is a function of the total concentration. It is to be noticed in Fig. 3 that the lower concentrations exhibit a band maxima at about 2.89μ. The shape of the curves for heavier concentrations suggests that they are superpositions of a maximum at about 3.00μ and the maximum at 2.89μ. We thenceforth assume that the 2.89μ point is characteristic of molecules bonded in dimer form and the 3.00μ point is characteristic of molecules bonded in the higher order complexes. Since we used an O—H---O distance from crystal data we should therefore expect our calculated λ_0 to be characteristic of the higher order complexes rather than of the dimer form.

The calculated value of 2.92μ is thence of the correct order of magnitude but is some 0.08μ lower than the observed value. This is perhaps good when it is considered that the perturbation scheme used does not consider van der Waals forces, the polarization of the electron clouds, nor the resonance effects whereby the oxygen is rendered more negative by extraction of electrons from the remainder of the molecule. It must also be borne in mind that the values used for q and E_p are approximate rather than exact.

Catechol provides a simple molecule of well-known structure for a rather direct test of Eq. (4). Overtone data for this material have been published by Wulf and Liddel.[7] From their Fig. 2 the value of 7060 cm^{-1} may be assigned to the "free" hydroxyl absorption and 6970 cm^{-1} to the bound hydroxyl. The latter value will be compared to one calculated from Eq. (4).

In Fig. 4 are given the geometrical conditions used

[4] See reference 1, Chapters II and V.

[5] J. J. Fox and A. E. Martin, Proc. Roy. Soc. (London) **162**, 419 (1937).

[6] See reference 1, Chapter II.

[7] O. R. Wulf and U. Liddel, J. Am. Chem. Soc. **57**, 1464 (1935).

to evaluate E_p. The first step is to determine the O---H distance and angle between O—H and O---H. These values were first determined directly from the accepted bond distances and angles. However, that is not sufficient as a correction must be made for the bending of the O—H bond due to the attraction along the O---H line. In order to do this the force constant for O—H bending was evaluated using the value of $\nu=1340$ cm^{-1} for the O—H bending frequency.[8] This provides a value of $k=9.98\times10^4$ dynes cm^{-1}. When this is used the O---H distance becomes 2.19A and the angle between O—H and O---H becomes 61°57′. Using this geometry the value of E_p at the center of the O—H bond is evaluated to be 1.59×10^5 e.s.u. In this the repulsion effect of the unbound proton is neglected in view of the large distance between it and the bound hydroxyl. Equation (5) may be used with the value of 7060 cm^{-1} for the first overtone of the free hydroxyl to obtain $a=2.31\times10^8$ cm^{-1}.

When these values are utilized in Eq. (5) we obtain $\nu=6970$ cm^{-1} as the calculated frequency of the first overtone for the bound hydroxyl. Such excellent agreement with the observed value of 6970 cm^{-1} seems fortuitous in view of the poorer agreement for benzyl alcohol.

IONIC BOND STRENGTH CONSIDERATIONS

It is interesting to observe that a rather simple consideration based on the partial ionic and covalent characteristics of the hydroxyl group also yields frequencies in fair agreement with experiment. Using the postulate of additivity of energies of normal covalent bonds[9] and the known energies of the O—O and H—H bonds we arrive at the energy of 41.1 kcal./mole as that portion of the hydroxyl bond energy due to the ionic character. Referring back to Fig. 1 we see that in the bonded polymer the oxygen and hydrogen atoms of a particular hydroxyl group are attracted toward neighboring molecules along the dashed lines. This is equivalent to reducing the electrostatic attraction, due to the charge inequality, within the hydroxyl group. A reduction in the electrostatic attraction will reduce the ionic bond character and the dissociation energy. When the dissociation energy is reduced the absorption frequencies are reduced as per Eq. (5). Thence we may calculate the absorption frequency for the bonded hydroxyl if we evaluate the reduction in ionic bond character. In this we assume that the covalent nature of the bond is essentially unaffected by the magnitude of electric field experienced.

For small vibrations the fractional reduction in ionic bond character will just be the ratio between the electrostatic force on a proton due to hydrogen bonding and that due to the charge inequality within the parent hydroxyl group. To calculate these the values of above

[8] G. Herzberg, *Infrared and Raman Spectra* (D. Van Nostrand Company, Inc., New York, 1945), p. 335.
[9] See reference 1, p. 47.

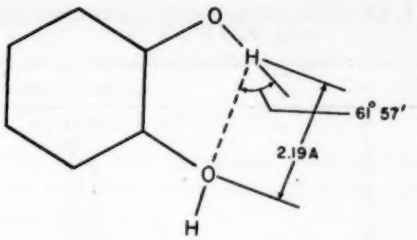

FIG. 4. Distance and angle arrangement as used for catechol calculations.

for q_1, q_2 and the interatomic spacings are used. Thus F_1 the electrostatic force on a proton due to hydrogen bonding and F_2 the electrostatic force due to the charge inequality in the hydroxyl group are calculated to be:

$$F_1=(1.57\times1.62\times10^{-20})/(1.73\times10^{-8})^2 =8.50\times10^{-5}\text{ dyne}$$

$$F_2=(1.57\times1.62\times10^{-20})/(0.97\times10^{-8})^2 =27.0\times10^{-5}\text{ dyne.}$$

The fractional decrease of ionic bond character F_1/F_2 is thence 0.315. The new dissociation energy D' is then

$$D'=110.2-0.315\times41.1=97.2\text{ kcal./mole.}$$

When this value of D' and the value of a obtained above are used in Eq. (5) we obtain $\lambda=2.96\mu$ for the bound hydroxyl in a simple alcohol. This is in better agreement with the observed value of $\lambda=3.00\mu$ than the value obtained by the perturbation method. However, no correction for the constant a as appears in the Morse function was made.

We may now apply the same considerations to catechol, using the geometry and the value of a given above in connection with Eq. (5). When this is done it is found that $F_1/F_2=0.0921$ and this leads to a predicted value of 6970 cm^{-1} for the frequency of the first overtone of the bound hydroxyl This is the same as the observed value.

INTENSITY OF ABSORPTION

There exists a fairly widespread notion that when a hydroxyl group becomes hydrogen bonded the intensity of absorption is enhanced. This may be theoretically checked by solving Eq. (2) and making a comparison with the results for an unperturbed Morse function. This is done by a direct comparison of the squares of matrix elements of the dipole moment for the two cases. The data given in Fig. 3 then may be used as a check on the calculations.

If the earlier calculations are completed for the two cases we get the set of general results given below. The ground and first excited eigenfunctions are:

$$\Psi_0=a_0e^{-y/2}y^{b_0/2}$$

$$\Psi_1=a_1e^{-y/2}y^{b_0/2}\left(\frac{1}{y}-\frac{1}{b_0-1}\right)$$

TABLE I. ΔE values corresponding to increasing polymer order from n to $n+1$.

n	ΔE (kcal./mole)
1	3.94
2	4.39
3	4.52
4	4.58
5	4.60
6	4.61

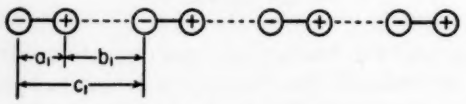

FIG. 5. Simplified model of hydrogen-bonded dipole polymer used in calculating association energy.

where

$$a_0=(a)^{\frac{1}{2}}/B, \quad a_1=(ab_0-2a)^{\frac{1}{2}}(b_0-1)/B$$

and

$$B=\int_0^\infty e^{-y}y^{(b_0-1)}dy.$$

The matrix element, $P(0, 1)$, of the dipole moment for the transition between the ground and first excited state calculates to be:

$$P(0, 1)=(b_0-2)^{\frac{1}{2}}/a(b_0-1). \tag{6}$$

For the unperturbed Morse function:

$$b_0=[4\mu(2\mu D)^{\frac{1}{2}}/ah]-1 \tag{7}$$

and for the perturbed Morse function:

$$b_0=\frac{4\mu(2\mu)^{\frac{1}{2}}(D-qE_p/a)}{ah(D-qE_p/2a)^{\frac{1}{2}}}-1. \tag{8}$$

As qE_p/a goes to zero, Eq. (8) reduces to Eq. (7). Also the derivatives of $P(0, 1)$ with respect to qE_p/a is positive. Hence the induced transition probability for the case of the perturbed Morse function is greater than for the unperturbed case.

To make a comparison with experiment through Eq. (6) we shall assume that the value of qE_p/a used earlier was too small. This is based on the fact that it did not give as large a shift of the wave-length of maximum absorption as was observed. We shall evaluate an essentially empirical value of qE_p/a through the use of the observed data and Eq. (4). This is then incorporated in Eqs. (6)–(8) to predict a ratio of absorption intensities. When this is done we obtain:

$$P^2(0, 1)\text{ (perturbed)}/P^2(0, 1)\text{ (unperturbed)}=1.16. \tag{9}$$

In the data of Fig. 3 the solution of 0.243 mole/liter, i.e., curve e, was chosen for comparison because of the optimum values of optical density. At higher concentrations accurate optical density values are difficult to obtain and at the lower concentrations the absorption band of the bound hydroxyl does not demonstrate the maximum shift.

The optical density $\bar{D}$ is given by:

$$\bar{D}=\log I_0/I=\alpha cl,$$

where I_0 and I are incident and transmitted energy, respectively, α is the extinction coefficient, c is the concentration in moles/liter and l is the length of the absorption cell. The extinction coefficient may be evaluated through the use of dilute concentrations such that appreciable bonding does not occur. When this is done it is found that $(\alpha l)=5.40$ liter/moles. For curve e the 0.243-mole/liter concentration is thus divided between 0.126 mole/liter of non-bonded hydroxyls and 0.117 mole/liter of bonded material. The predicted optical density for the bonded material is thence:

$$1.16\times 0.117\times 5.40=0.732$$

which compares to the observed value of 0.795 with a reasonably good agreement, in view of the assumptions involved.

ASSOCIATION ENERGY

We may make a simple calculation of the approximate energy per hydrogen bond using the polymer model as seen in Fig. 1. In Fig. 5 the same model is simplified for the purpose at hand. Here we have replaced each alcohol molecule with a dipole with electrostatic interaction along the dashed lines. Since the length of the hydroxyl dipole is of the order of one-third the O—H---O distance the association must be calculated as the sum of the electrostatic interactions between individual charges rather than as a sum of dipole interactions. If we consider a polymer formed of n interacting dipoles the decrease of potential energy ΔE resulting from adding another dipole to form a polymer of $n+1$ members calculates to be:

$$\Delta E=q_1q_2\sum_{m=1}^{n}\left\{\frac{1}{mc_1+a_1}+\frac{1}{mc_1+b_1-c_1}-\frac{2}{mc_1}\right\}. \tag{10}$$

If we let $a_1/c_1=g$, Eq. (10) reduces to:

$$\Delta E=\frac{q_1q_2}{c_1}\sum_{m=1}^{n}\frac{2g^2}{m^3-mg^2}. \tag{11}$$

In Table I may be seen the values of ΔE in kcal./mole for successive values of n. Here we have used the same values of q_1, q_2, a_1, b_1, and c_1 as above for benzyl alcohol.

The largest change in ΔE occur for the first few members and it is to be seen that for $n>3$ there is relatively little change. For $n>2$ the values of Table I agree quite closely with the value of 4.60 kcal./mole for benzyl alcohol in carbon tetrachloride reported by Mecke.[10] This is to be expected if there are negligible volume changes attendant to the bond formation.

[10] R. Mecke, Zeits. f. Electrochemie **52**, 269 (1948).

Mecke's values were calculated from data for the free hydroxyl absorption band as a function of temperature and concentration.

By the use of the above equations a relation between ΔE and $\Delta\gamma$, i.e., the frequency shift between the free and bonded hydroxyl may now be calculated. From Eqs. (4) and (5) we obtain the approximate expression:

$$\Delta\nu(\text{cm}^{-1})=\frac{3q_1E_p}{4\pi c(2\mu)^{\frac{1}{2}}(D)^{\frac{1}{2}}} \tag{12}$$

wherein terms involving quadratic and higher order terms in $(q_1E_p/a(D)^{\frac{1}{2}})$ have been neglected. Equation (12) may now be rewritten as:

$$\Delta\nu=\frac{3q_1(q_1+q_2)}{4\pi c(2\mu)^{\frac{1}{2}}(D)^{\frac{1}{2}}(b_1+a_1/2)^2},$$

from which we may obtain b_1 as:

$$b_1=(H/(\Delta\nu)^{\frac{1}{2}}-a_1/2) \tag{13}$$

where

$$H=[3q_1(q_1+q_2)/4\pi c(2\mu)^{\frac{1}{2}}(D)^{\frac{1}{2}}]^{\frac{1}{2}}.$$

If we use Eq. (13) with the above relations between a_1, b_1, and c_1 in Eq. (11), we obtain ΔE in terms of $\Delta\nu$ by the following expression:

$$\Delta E=\frac{2q_1q_2a_1^2(H/(\Delta\nu)^{\frac{1}{2}}-a_1/2)^{-2}}{(H/(\Delta\nu)^{\frac{1}{2}}+a_1/2)}\times\sum_{m=1}^{n}\frac{1}{m^3-ma_1^2(H/(\Delta\nu)^{\frac{1}{2}}-a_1/2)^{-2}}.$$

Acknowledgment is made to Dr. Paul D. Foote, Executive Vice-President of Gulf Research and Development Company, for permission to publish this material.

THE JOURNAL OF CHEMICAL PHYSICS VOLUME 18, NUMBER 7 JULY, 1950

Vibrational Intensities. I. Theory of Diatomic Infra-Red Bands*

BRYCE L. CRAWFORD, JR. AND H. L. DINSMORE†
School of Chemistry, University of Minnesota, Minneapolis, Minnesota
(Received March 27, 1950)

A rigorous treatment of the intensities of vibration-rotation absorption spectra of diatomic molecules is given, leading to explicit expressions relating the observed intensities of the fundamental and first two overtones to the appropriate coefficients in the expansions of the potential energy and the dipole moment.

AN approximate model conveniently employed in treating the nuclear energy problem of a diatomic molecule is that of a pair of nuclei which execute small (Hooke's-law) vibrations in the average potential field of the electrons with an accompanying electric moment linear in the displacement coordinate $(r-r_e)$, this model also partaking of free rotation in space. This simple picture fails to account for observed frequency and intensity features of diatomic infra-red spectra. In particular the presence of overtone bands shows the existence of appreciable anharmonic influences. These may be of two sorts: mechanical anharmonicity, arising from higher order terms in the potential energy, and electrical anharmonicity, deriving from higher order terms in the dipole moment. When such improvements are made the theory satisfactorily accounts for overtone transitions of appreciable intensity. An important question is the comparative importance of each of these types of anharmonicity in actual spectra. Fortunately accurate term analysis of line frequencies is sufficient to determine completely the mechanical anharmonicity. Since the line intensities represent the combined contribution of both types of anharmonicity, there is the possibility of estimating the relative importance of each effect from study of adequate frequency and intensity data.

In the present paper we present a complete and rigorous derivation of explicit expressions giving the intensities of the fundamental and the first two overtone diatomic infra-red bands in terms of suitable mechanical and electrical anharmonic coefficients. From a theoretical standpoint the only previous work having a similar objective and approach is that of J. L. Dunham,[1] who derived the matrix elements for the vibrational transitions $0\rightarrow1$, $0\rightarrow2$, $0\rightarrow3$ of a diatomic vibrator in terms of mechanical and electrical anharmonic coefficients. We have included several refinements heretofore disregarded; namely (1) the rigorous treatment of the rotational problem, in which the correct frequency-variation over the vibration-rotation band is considered in the intensity summation over all rotational components, (2) the summation of the contributions of all vibrational transitions $v\rightarrow v+n$ which result in essentially the same frequency, $\omega_{o,n}$. The resulting formulas, while quite simple, contain several new terms, involving the vibrational and rotational partition functions, and are, we believe, presented for the first time. Other pertinent theoretical studies, especially as re-

* From a thesis submitted to the Graduate Faculty of the University of Minnesota by H. L. Dinsmore, in partial fulfillment of the requirements for the Ph.D. degree.

† Predoctoral Fellow of National Research Council (1946–49); now at Metcalf Research Laboratory of Brown University.

[1] J. L. Dunham, Phys. Rev. **34**, 438 (1929); **35**, 1347 (1930).

garding the absorption laws, are the papers by Bourgin,[2] Dennison,[3] Matheson,[4] Nielsen,[5] and Wilson and Wells,[6] which treat the theory of line shapes and of intensity measurement.

THEORY OF LIGHT ABSORPTION

When monochromatic light of frequency ν and intensity I_ν is passed through an infinitesimal thickness dx of absorbing medium the basic law of light absorption is

$$-(1/I_\nu)(dI_\nu/dx)=\alpha_\nu, \tag{1}$$

and states that the fractional decrease in light intensity is proportional to the sample thickness. The constant of proportionality α_ν is called the absorption coefficient and is proportional to the molecular concentration of absorbing material.

These ideas may readily be expressed on a quantum-mechanical basis. Let us designate by A, B different energy levels and by a, b the individual degenerate states having these energies. All transitions between the levels A, B give a single spectral line of frequency

$$\nu=\nu_A{}^B=(E_B-E_A)/h; \tag{2}$$

transitions between any two states a, b give a component of this line. In accord with Einstein's theory the probability that a transition will take place, with photons of energy $h\nu=E_B-E_A$ transferring their energy to molecules in a lower state a and raising them to an excited state b, is $\pi_a{}^b=B_a{}^b\rho_\nu$, where ρ_ν is the energy density and is related to the energy flux I_ν by

$$I_\nu=c\rho_\nu. \tag{3}$$

If the population of the initial level is N_A and its multiplicity is g_A, the rate of energy absorption from the beam is

$$-(dI_\nu)_a{}^b=(h\nu)(N_A dx/g_A)(B_a{}^b I_\nu/c). \tag{4}$$

For all transitions from the lower to the upper level the total energy absorption is

$$-dI_\nu=\sum_{a,\,b}(-dI_\nu)_a{}^b=(h\nu)(N_A dx/g_A)(B_A{}^B I_\nu/c), \tag{5}$$

where

$$B_A{}^B=\sum_{a,\,b}B_a{}^b \tag{6}$$

is the total probability coefficient for absorption.‡ Simple rearrangement of (5) immediately gives

$$\alpha_\nu=-(1/I_\nu)(dI_\nu/dx)=(h\nu/c)(N_A/g_A)B_A{}^B. \tag{7}$$

At this point the derivation may be criticized on the ground that molecules in exicted states are returning to lower states, so that the net absorption is somewhat less than that in Eq. (5). However, such re-emission of energy is isotropic, while the removal is from a directed beam. Accordingly only a minute fraction of the energy returned should be regarded as lying in the small solid angle necessary for light passing through the spectrometer. For this reason Eq. (7) is much more appropriate than the equation

$$\alpha_\nu=(h\nu/c)(N_A/g_A)B_A{}^B(1-e^{-h\nu/kT}) \tag{7'}$$

frequently given in the literature.

In order to introduce the electrical nature of light absorption we employ the quantum-mechanical result

$$B_A{}^B=(8\pi^3/3h^2)S_A{}^B, \tag{8}$$

where

$$S_A{}^B=\sum_{a,\,b}S_a{}^b=\sum_{a,\,b}|(b|\mathbf{p}|a)|^2 \tag{9}$$

is known as the line-strength, $\mathbf{p}$ being the electric moment. Combined use of (7) and (8) gives

$$\alpha_\nu=(8\pi^3\nu_A{}^B/3hc)(N_A/g_A)S_A{}^B. \tag{10}$$

This is the basic relationship between molecular theory and experimentally observable absorption.

DIATOMIC INFRA-RED SPECTRA

In order to specialize our problem to that of a diatomic molecule, the initial step is the solution of the energy problem in order to obtain the conditions of quantization, characteristic energies, and wave functions appropriate to nuclear vibration and rotation (in the ground electronic state). The details of this problem are lucidly presented by Kronig in his book *Band Spectra and Molecular Structure*. In terms of the nuclear coordinates r, θ, φ, the angular and radial problems are formally separable as

$$\left\{\frac{1}{\sin\theta}\frac{\partial}{\partial\theta}\left(\sin\theta\frac{\partial}{\partial\theta}\right)+\frac{1}{\sin^2\theta}\left(\frac{\partial}{\partial\phi}-i\lambda\cos\theta\right)^2+\frac{2\mu r^2}{\hbar^2}E'_{\rm rot}\right\}L(\theta,\phi)=0 \tag{11}$$

and

$$\left\{\frac{1}{r^2}\frac{d}{dr}\left(r^2\frac{d}{dr}\right)+\frac{2\mu}{\hbar^2}[E-E'_{\rm rot}+U(r)]\right\}R(r)=0, \tag{12}$$

where λ is different from zero only if there is a resultant electronic angular momentum, as in the case of NO.

The solution of (11) is well known: the rotational energies (in cm^{-1} unit) are

$$E_{\rm rot}'/hc=G_j=(h/8\pi^2c\mu r^2)[j(j+1)-\lambda^2], \quad j=\lambda,\ \lambda+1,\ \lambda+2,\ \cdots, \tag{13}$$

and have the usual $(2j+1)$-fold m-degeneracy. For solution of the radial problem it is customary to approximate the potential energy by the series

$$U(\xi)/hc=V(\xi)=(\omega_e/2\gamma^2)(\xi^2+a_1\xi^3+a_2\xi^4+\cdots), \tag{14}$$

where

$$\xi=(r-r_e)/r_e \tag{15}$$

and

$$\gamma^2=(h/4\pi^2c\omega_e\mu r_e^2)=(2B_e/\omega_e). \tag{16}$$

[2] D. G. Bourgin, Phys. Rev. **29**, 794 (1927); **32**, 237 (1928).
[3] D. M. Dennison, Phys. Rev. **31**, 503 (1928).
[4] L. A. Matheson, Phys. Rev. **40**, 813 (1932).
[5] J. R. Nielsen, Rev. Mod. Phys. **16**, 307 (1944).
[6] E. B. Wilson and A. J. Wells, J. Chem. Phys. **14**, 578 (1946).

‡ In terms of this definition the total probability coefficients obey the same interrelationships as do the simple coefficients, namely,

$$B_A{}^B=B_B{}^A=(c^3/8\pi h\nu^3)A_B{}^A.$$

Also r^{-2} which occurs in E_{rot}' may be expanded as

$$r^{-2}=r_e^{-2}(1-2\xi+3\xi^2-\cdots). \tag{17}$$

If the new variables

$$q=\gamma^{-1}\xi \tag{18}$$

and

$$r\cdot R(r)=F(r)\sim F(q) \tag{19}$$

are employed, the various orders of approximation are conveniently indicated by powers of γ, with the zeroth-order problem being simply that for the harmonic vibrator. By standard perturbation treatment, the higher order effects are then included to give the familiar energy formula (in cm^{-1})

$$G_{v,j}=(v+\tfrac{1}{2})\omega_e[1-x_e(v+\tfrac{1}{2})] +j(j+1)[(B_v-j(j+1)D_e], \quad v=0, 1, 2\cdots, \tag{20}$$

with

$$B_v=B_e-\alpha_e(v+\tfrac{1}{2}). \tag{21}$$

Here x_e expresses the anharmonic nature of the potential energy U, while α_e expresses the effect of rotational-vibrational interaction in terms of a vibrational dependence in the rotational "constant" B.

In practice, term analysis of highly resolved spectra affords values of ω_e, B_e, x_e, and α_e,¶ and from these the mechanical anharmonic parameters a_1 and a_2 in Eq. (14) can be deduced:

$$x_e=(3/4)\gamma^2[a_2-(5/4)a_1^2], \tag{22}$$

$$-\alpha_e=3\gamma^2B_e(a_1+1). \tag{23}$$

The general frequencies of transitions between stable energy states may now be written down:

$$\overset{v',j'}{\omega}_{v,j}=\omega_{\text{vib}}+\omega_{\text{rot}} =\omega_e(v-v')[1-x_e(v'+v+1)] +[B_{v'}j'(j'+1)-B_vj(j+1)]. \tag{24}$$

These will subsequently be limited by selection rules. At present we can say that because of the much closer spacing of rotational levels the spectral appearance will be that of a band of rotational lines accompanying any particular vibrational frequency. Applied to this problem, Eqs. (9) and (10) give for the absorption coefficient of one of these fine-structure lines $v, j\rightarrow v', j'$

$$\overset{v',j'}{\alpha}_{v,j}=(8\pi^3\overset{v',j'}{\omega}_{v,j}/3hc)(N_{v,j}/g_j)\overset{v',j'}{S}_{v,j}, \tag{25}$$

where

$$\overset{v',j'}{S}_{v,j}=\sum_{m,m'}\overset{v',j',m'}{S}_{v,j,m} =\sum_{m,m'}|(v', j', m'|p(r,\theta,\phi)|v, j, m)|^2. \tag{26}$$

For comparison with experiment we require the total intensity[6] of this entire vibration-rotation band, regarded as the integral, over the band, of the absorption coefficient α in Eq. (1) with respect to the frequency:

$$A=\int_{\text{and}}\alpha(\omega)d\omega. \tag{27}$$

Theoretically this will be the sum of all fine-structure components,

$$A_v{}^{v'}=\sum_{j,j'}\overset{v',j'}{\alpha}_{v,j}=(8\pi^3N_v/3hcZ)\sum_{j,j'}\overset{v',j'}{\omega}_{v,j}e^{-E_j/kT}\overset{v',j'}{S}_{v,j}; \tag{28}$$

here Boltzmann statistics have been used, with Z being the rotational partition function

$$Z=\sum_{j=0}^{\infty}g_je^{-E_j/kT} \tag{29}$$

and N_v the total molecular concentration in the lower vibrational level. Further, the fact that the radial and angular problems are separable permits factoring of the line strengths

$$\overset{v',j'}{S}_{v,j}=\overset{v'}{S}_v\overset{j'}{S}_j, \tag{30}$$

where the first factor involves only the magnitude of the dipole moment as a function of internuclear distance, and the second involves only the direction-cosines whereby $\mathbf{p}$ is resolved into its components in a space-fixed Cartesian frame.

ROTATIONAL INTENSITIES

The computation of direction-cosine matrices for the space-rotator, or for the symmetrical-top rotator if $\lambda>0$, is a familiar procedure; the results follow readily from recurrence formulas for the (orthogonal) wave functions, or may alternatively be deduced from commutation rules. Rademacker and Reiche[7] have derived the selection rules and the line-component strengths $\overset{j',\lambda',m'}{S}_{j,\lambda,m}$ for the symmetrical-top rotator, and from these the results for a diatomic molecule easily follow. The usual case $\lambda=0$ has also been given directly by Mensing.[8] The selection rules are familiar: $\Delta m=0, \pm1$ and $\Delta j=\pm1$, with the additional transition $\Delta j=0$, when $\lambda\neq0$. From these the frequencies, by Eq. (24), are

$$\overset{v',j'}{\omega}_{v,j}=\omega_v{}^{v'}+2\bar{B}M+(B_{v'}-B_v)M^2, \tag{31}$$

where $M=(j+1)$ for the R branch, $(-j)$ for the P branch, and 0 for the Q branch ($\lambda\neq0$), and

$$2\bar{B}=B_{v'}+B_v=2B_e-\alpha_e(v'+v+1), \quad B_{v'}-B_v=-\alpha_e(v'-v). \tag{32}$$

The line strengths turn out to be

$$\overset{j'}{S}_j=\sum_{m,m'}\overset{j',m'}{S}_{j,m}=\frac{\lambda^2(2j+1)}{j(j+1)}\delta_{j,j'}+\frac{(j+\lambda)(j-\lambda)}{j}\delta_{j',j-1} +\frac{(j+1+\lambda)(j+1-\lambda)}{(j+1)}\delta_{j',j+1}. \tag{33}$$

¶ The second-order rotational effect $D_e=4B_e^3/\omega_e^2$ is usually negligible.

[7] H. Rademacker and F. Reiche, Zeits. f. Physik. **41**, 453 (1927).
[8] L. Mensing, Zeits. f. Physik **36**, 814 (1926).

From these and the frequencies the absorption coefficient expression (25) follows at once.

The sums over j, j' are then carried out to give the total band intensities (28). When $\lambda=0$ the important steps are:

$$\sum_{j'} \alpha_{v,j}^{v',j'} = [f(v,v')/Z]\{\omega_v^{v'}[(j+1)+(j)] + 2\bar{B}[(j+1)^2-(j)^2]+(B_{v'}-B_v)[(j+1)^3 + (j)^3]\}\cdot e^{-E_j/kT} = [f(v,v')/Z]\{\omega_{\text{vib}}+2\bar{B} + (B_{v'}-B_v)(j^2+j+1)\}g_j e^{-E_j/kT}, \quad (34)$$

where

$$f(v,v') = (8\pi^3 N_v/3hc)S_v^{v'}. \quad (35)$$

On carrying out the remaining sum over j the first two terms of (34) simply contain $\sum_j g_j \exp(-E_j/kT)=Z$ as a common factor, which serves to cancel the Z in the denominator. The third term reduces to $(B_{v'}-B_v)\times(1+Z)$ since

$$(1/Z)\sum_j (j^2+j)g_j e^{-E_j/kT} = (G_{\text{rot}}/B)_{\text{Av}} = kT/hcB = Z, \quad (36)$$

G_{rot} being the average (thermodynamic) rotational energy in cm^{-1} per molecule. Accordingly the result is,

$$A_v^{v'} = \sum_{j,j'} \alpha_{v,j}^{v',j'} = (8\pi^3 N_v/3hc)\{\omega_{\text{vib}} + 2\bar{B}+(B_{v'}-B_v)(1+Z)\}S_v^{v'}. \quad (37)$$

The work for the case $\lambda\neq 0$ is more involved but leads to precisely the same results. The rotational terms in the band intensity formula (37) have, to the best of our knowledge, not been derived heretofore. Although the practical contribution of the rotational part is nearly negligible compared to ω_{vib}, it is satisfying to see that the result comes out so neatly when the usual approximation

$$\omega_{v,j}^{v',j'} = \omega_{\text{vib}}$$

is not made. If the vibrational dependence of the rotational constants is neglected, the simpler formula

$$A_v{}^{v'} = (8\pi^3 N_v/3hc)(\omega_{\text{vib}}+2B_e)S_v{}^{v'} \quad (38)$$

is obtained.

VIBRATIONAL INTENSITIES

The vibrational-intensity factors $S_v{}^{v'} = (v|p(r)|v')^2$ corresponding to fundamental and overtone transitions can be evaluated in successive orders of approximation by matrix perturbation methods. Depending on the order of approximation to be considered, the matrix elements for the actual (perturbed) problem will be related to those for the zeroth-order problem by the unitary transformation

$$\mathbf{p} = \bar{\mathbf{C}}\,(\mathbf{p})^0\,\mathbf{C}, \quad (39)$$

where $\mathbf{C}$ is a unitary matrix which renders the Hamiltonian diagonal to the chosen approximation and $\bar{\mathbf{C}}$ is its transpose. The various-order effects in evaluation of Eq. (39) can be separated formally by employing the expansions

$$\mathbf{C} = \mathbf{C}^0+\gamma\mathbf{C}^I+\gamma^2\mathbf{C}^{II}+\gamma^3\mathbf{C}^{III}+\cdots \quad (40)$$

and

$$\mathbf{p} = \mathbf{p}^0+\gamma\mathbf{p}^I+\gamma^2\mathbf{p}^{II}+\gamma^3\mathbf{p}^{III}+\cdots. \quad (41)$$

Actually the coefficients $\mathbf{C}$, which reflect the various-order effects in the potential energy (15) come out quite naturally in the form (40) with γ having the definition previously assigned it. The dipole moment may be written as a Taylor series in $\xi=(r-r_e)/r_e$:

$$p(\xi) = p_e+p_e'\xi+(1/2!)p_e''\xi^2+(1/3!)p_e'''\xi^3+\cdots. \quad (42)$$

On evaluation in terms of the coordinate q the matrix element $(v|p|v')$ is,

$$(v|p|v') = p_e\cdot\delta_{v,v'}+\gamma p_e'(v|q|v') + (\gamma^2/2!)p_e''(v|q^2|v')+(\gamma^3/3!)p_e'''(v|q^3|v')+\cdots \quad (43)$$

an equation which is of the form (41). Separation of the various orders of approximation in (39) now gives

$$\mathbf{p}^0 = p_e\cdot\mathbf{1}, \quad (44a)$$

$$\mathbf{p}^I = p_e'\cdot(\mathbf{q})^0, \quad (44b)$$

$$\mathbf{p}^{II} = (1/2!)p_e''\cdot(\mathbf{q}^2)^0+p_e'\cdot[\bar{\mathbf{C}}^I(\mathbf{q})^0+(\mathbf{q})^0\mathbf{C}^I], \quad (44c)$$

$$\mathbf{p}^{III} = (1/3!)p_e'''\cdot(\mathbf{q}^3)^0+(1/2!)p_e''\cdot[\bar{\mathbf{C}}^I(\mathbf{q}^2)^0+(\mathbf{q}^2)^0\mathbf{C}^I] + p_e'\cdot[\bar{\mathbf{C}}^{II}(\mathbf{q})^0+\bar{\mathbf{C}}^I(\mathbf{q})^0\mathbf{C}^I+(\mathbf{q})^0\mathbf{C}^{II}]. \quad (44d)$$

These equations apply respectively to the constant-dipole-moment, fundamental, first-overtone, and second-overtone effects. Since the mechanical anharmonicity enters as the coefficients $\mathbf{C}^I$, $\mathbf{C}^{II}$, while the electrical anharmonicity enters as the coefficients p_e'', p_e''', the formal manner in which overtone intensities depend on each effect is clear.

The actual evaluation of Eqs. (44) is elementary matrix multiplication, though the work becomes tedious for the higher order cases. Hutchisson[9] has given the coefficients $\mathbf{C}$, while the coordinate matrices $(\mathbf{q}^k)^0$ have the well-known harmonic-oscillator values. The results (for absorption) are tabulated.

$$\mathbf{p}^I_{v,v+1} = (2)^{-\frac{1}{2}}(v+1)^{\frac{1}{2}}\cdot p_e' \quad (45a)$$

$$\mathbf{p}^{II}_{v,v+2} = (4)^{-1}[(v+2)(v+1)]^{\frac{1}{2}}\cdot(p_e''+p_e'\cdot a_1) \quad (45b)$$

$$\mathbf{p}^{III}_{v,v+3} = (2)^{-\frac{1}{2}}(4)^{-1}[(v+3)(v+2)(v+1)]^{\frac{1}{2}}\cdot[(\tfrac{1}{3})p_e''' + p_e''\cdot a_1+p_e'\cdot(\tfrac{1}{2}a_2+\tfrac{3}{8}a_1^2)] \quad (45c)$$

$$\mathbf{p}^{III}_{v,v+1} = (2)^{-\frac{1}{2}}(v+1)^{\frac{1}{2}}[(1/2)p_e'''-(5/2)p_e''\cdot a_1+p_e'\cdot(11a_1^2/8-3a_2/8)]. \quad (45d)$$

The fourth result above is, of course, a second-order correction to the fundamental band intensity.

The intensities $A_v{}^{v'}$ in Eq. (37) may now be written down (through the second-overtone transition). On

[9] E. Hutchisson, Phys. Rev. **37**, 45 (1930).

introducing the abbreviations

$$\bar{\omega}_v{}^{v'}=\omega_v{}^{v'}+2\bar{B}+(B_{v'}-B_v)(1+Z) \quad (46)$$

$$\rho_e''=p_e''/p_e',\ \rho_e'''=p_e'''/p_e' \quad (47)$$

$$\Delta=(1/2)\rho_e'''-(5/2)\rho_e''a_1+(11/8)a_1{}^2-(3/2)a_2 \quad (48)$$

we have:

Fundamental:

$$A_v{}^{v+1}=(4\pi^3N_v/3hc)\bar{\omega}_v{}^{v+1}\gamma^2p_e'{}^2(v+1)\times[1+\gamma^2(v+1)\Delta]. \quad (49)$$

First overtone:

$$A_v{}^{v+2}=(4\pi^3N_v/3hc)\bar{\omega}_v{}^{v+2}\gamma^4p_e'{}^2\times[(v+2)(v+1)/8](\rho_e''+a_1)^2. \quad (50)$$

Second overtone:

$$A_v{}^{v+3}=(4\pi^3N_v/3hc)\bar{\omega}_v{}^{v+3}\gamma^6p_e'{}^2[(v+3)(v+2)(v+1)/16]\times[(\tfrac{1}{3})\rho_e'''+\rho_e''a_1+(\tfrac{1}{2})a_2+(\tfrac{3}{8})a_1{}^2]^2. \quad (51)$$

When we set $v=0$, these formulas are consistent with the results of Dunham.[1]

TOTAL BAND INTENSITIES

In order to obtain the total intensity of the nth-harmonic vibrational band, observed at approximately $\omega_0{}^n$, the intensities $A_v{}^{v+n}$ for individual transitions must be summed over all values of v:

$$A^{(n)}=\sum_{v=0}^{\infty}A_v{}^{v+n}=(8\pi^3N/3hcQ)\sum_{v=0}^{\infty}[\bar{\omega}_v{}^{v+n}(v|p|v+n)^2e^{-\beta v}]. \quad (52)$$

Here N_v has been expressed by Boltzmann statistics in terms of the total molecular concentration N and the vibrational partition function

$$Q=\sum_{v=0}^{\infty}e^{-E_v/kT}=\sum_{v=0}^{\infty}e^{-(hc\omega_0/kT)v}=(1-e^{-\beta})^{-1},\quad \beta=hc\omega_0/kT. \quad (53)$$

The sums in (52) are somewhat complicated by the fact that the variable v occurs not only in the matrix elements $(v|p|v+n)$ but also in the frequency factors $\bar{\omega}_v{}^{v+n}$. The latter dependency is easily expressed as

$$(\bar{\omega}_v{}^{v+n}/\bar{\omega}_0{}^n)=1-2vY_n, \quad (54)$$

where $Y_n=(nx_e\omega_e+\alpha_e)/\bar{\omega}_0{}^n$. Inspection of the intensity factors $(v|p|v+n)^2$ shows that we can write (for the cases studied here)

$$A_v{}^{v+n}=A_0{}^n\cdot\frac{(v+n)!}{n!v!}e^{-\beta v}[1-v(2Y_n-\delta)]. \quad (55)$$

Here the quantity δ is included to cover terms in v which may arise from second-order corrections to the intensity factors $(v|p|v+n)^2$. In the cases studied here the only such correction occurs for the fundamental, and it is easily shown that in this case $\delta=\gamma^2\Delta$. By use of the series-identities

$$\sum_{v=0}^{\infty}\frac{(v+n)!}{n!v!}e^{-\beta v}=Q^{n+1} \quad (56a)$$

$$\sum_{v=0}^{\infty}\frac{v(v+n)!}{(n+1)n!v!}e^{-\beta v}=\sum_{v=0}^{\infty}\frac{(v+n)!}{(n+1)!(v-1)!}e^{-\beta v}=(Q-1)Q^{n+1} \quad (56b)$$

the summations (55, 52) give

$$A^{(n)}=\sum_v A_v{}^{v+n}=A_0{}^n\cdot Q^{n+1}[1-(n+1)(Q-1)(2Y_n-\delta)], \quad (57)$$

where

$$A_0{}^n=(8\pi^3N/3hcQ)(\mathbf{p}_0{}^n)^2[\omega_0{}^n+2\bar{B}_0{}^n+(B_n-B_0)(1+Z)]. \quad (58)$$

The various quantities in (58) obtained from the analogous general formulas by setting $v=0$, are

$$\begin{aligned}&\omega_0{}^n=n\omega_e[1-x_e(n+1)]\\&\bar{B}_0{}^n=B_0+B_n=2B_e-\alpha_e(n+1)\\&(B_n-B_0)=-\alpha_en\\&\mathbf{p}_0{}^1=(2)^{-\frac{1}{2}}\gamma p_e'(1+\tfrac{1}{2}\gamma^2\Delta)\\&\mathbf{p}_0{}^2=(8)^{-\frac{1}{2}}\gamma^2p_e'(\rho_e''+a_1)\\&\mathbf{p}_0{}^3=(3)^{\frac{1}{2}}(4)^{-1}\gamma^3p_e'[(\tfrac{1}{3})\rho_e'''+\rho_e''a_1+(\tfrac{1}{2})a_2+(\tfrac{3}{8})a_1{}^2].\end{aligned} \quad (59)$$

Although the formulas (55) and (57) have been worked out only through the second-overtone (third-harmonic) case, the results have a regularity which would appear to be general.

It comes as somewhat of a surprise that the final result (57), based on a rigorous analysis, is so simply expressed in terms of the ground-transition result (58) and the vibrational partition function Q. Since $A_0{}^n$ contains Q^{-1} the total intensity $A^{(n)}$ actually involves Q^n. The fact that the correction term comes out having $(Q-1)$ as a factor is especially pleasing, since $(Q-1)$ is normally of the order of 10^{-3} while x_e, α_e, δ are themselves second-order corrections ($\sim10^{-2}$).

In applications the observables in (57), (58) will be the intensities and frequencies, in terms of which the dipole-moment factors $(\mathbf{p}_0{}^n)^2$ are to be studied. In these the mechanical anharmonicity and electrical anharmonicity enter explicitly as the quantities a_1, a_2 and ρ_e'', ρ_e''', respectively. Since a_1 and a_2 will be known quantities, the actual unknowns are ρ_e', ρ_e'', ρ_e''' (or p_e', p_e'', p_e'''). The fact that these enter quadratically will lead to a number of alternative solutions for the higher order terms, as well as to ambiguities of sign in general. On the basis of such values, however, some ideas of the mechanical and electrical anharmonicities present in diatomic molecules can be hopefully expected, if reliable intensity data on fundamental and first- and second-overtone bands are obtainable.

We are indebted to Professor E. L. Hill for helpful discussions concerning several points.

Financial aid in part of this research was received from the ONR through Contract N5ori-147, T.O. II.

Letters to the Editor

THIS section will accept reports of new work, provided these are terse and contain few figures, and especially few half-tone cuts. The Editorial Board will not hold itself responsible for opinions expressed by the correspondents. Contributions to this section should not exceed 600 words in length and must reach the office of the Managing Editor not later than the 15th of the month preceding that of the issue in which the letter is to appear. No proof will be sent to the authors. The usual publication charge ($8.00 per page) will not be made and no reprints will be furnished free.

The Electronic Structure of Di-*p*-Xylene

L. L. INGRAHAM*
Berkeley, California
May 22, 1950

THE apparently highly strained molecule di-*p*-xylene[1] has recently been reported as a pyrolysis product of paraxylene. D. J. Cram and H. Steinberg[2] of the University of California at Los Angeles have been investigating the synthesis of this and analogous compounds to determine whether or not there is any stabilization of the molecule due to $2p\sigma$-type bonds between the benzene rings.

It is of interest to determine what can be predicted from the valence bond (V.B.) and molecular orbital (L.C.A.O.) approximations. (Table I.)

Twenty resonance structures were considered in the valence bond treatment, three structures each of types I, II and III, six each of types IV and V, and one of type VI. Dashed lines indicate bonds on the lower benzene ring and dots indicate $2p\sigma$-bonds between rings. (See Fig. 1.)

The assumption of D_6 symmetry**,[3] greatly simplifies the resulting secular equations. Six wave functions are of class A_1, one of class B_1, three of class B_2, four of class E_1 and six of class E_2. The single exchange integrals (α') of the $2p\sigma$-bonds are estimated from the corresponding overlap integrals[4] at 3A°.[1]

In the L.C.A.O. treatment D_{6h} symmetry was assumed which allows the following molecular orbitals:

$$(a_{1g})^2(a_{2u})^2(b_{1u})^2(b_{2g})^2(e_{1g})^4(e_{1u})^4(e_{2g})^4(e_{2u})^4.$$

The filled levels are:

$$(a_{1g})^2(a_{2u})^2(e_{1g})^4(e_{1u})^4.$$

Overlap integrals were neglected. The exchange integral β' corresponds to α'.

Both the valence bond method and the molecular orbital (L.C.A.O.) method predict no stabilization with respect to two benzene rings infinitely separated. Although the valence bond method predicts 4.00 kcal. more resonance energy for di-*p*-xylene than for two infinitely separated benzene rings, due to repulsions it still requires 16.00 kcal. to bring two benzene rings to 3A° apart from infinite separation.

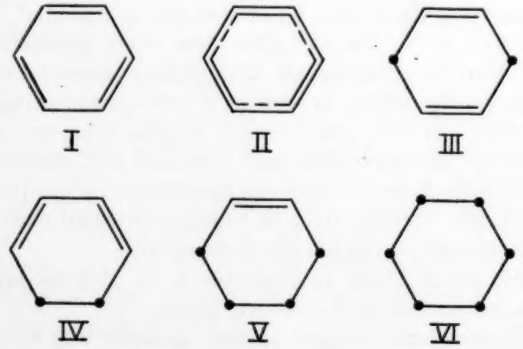

FIG. 1. Resonance structures.

TABLE I. Energies of π-electrons in kcal. for various states and separations.

Separation→	∞	3A°
	Valence bond	
No resonance Kekule form	0.00†	+20.00
Ground state (A_1) Structures I–II Structures I–VI	−72.00 −72.40	−52.00 −56.40
Excited state (B_2) Structures I–II Structures I–VI	+24.00 +23.60	+44.00 +41.60
$A_{1g}-B_{2u}$ band[5]	297 mμ	291 mμ
	Molecular orbital	
Kekule form Ground state	0.00† −80.0	0.00 −80.0

† Energies are relative to Kekule structures at infinity. $\alpha=40$ kcal., $\beta=20$ kcal., $\alpha'=\beta'=0$ for infinite separation. $\alpha'=\alpha/6$ and $\beta'=\beta/6$ for separation of 3A°.

The L.C.A.O. method, due to its neglect of repulsive forces, predicts the same energy as that of two benzene rings completely separated. If the e_{1u} level were missing one or two electrons, i.e., if one or both rings were phenyl radicals, there would be attractions of β' or $2\beta'$, respectively, between rings. Similar to α', $\beta'=\beta/6$ or about 3 kcal. at 3A°.

The valence bond method indicates a slight shift of the 2600A° benzene band ($A_{1g}-B_{2u}$)[5] to shorter wave-lengths. (Due to the approximations made, the values given are only qualitatively correct.) This slight shift is probably minor compared to effects that have been neglected.**

The results obtained demonstrate the fallibility of the rough rule "the more resonance forms the more stabilization."

* Present address: Western Regional Research Laboratory, 800 Buchanan Street, Albany 6, California.
[1] Brown and Farthing, Nature **164**, 915 (1949).
[2] D. J. Cram, private communication.
** Effects due to the dimethylene chain and the non-planarity of the benzene rings (see reference 1) are neglected.
[3] Herzberg, *Infra-Red and Raman Spectra* (D. Van Nostrand Company, Inc., New York, 1945).
[4] R. S. Mulliken, (to be published in J. Am. Chem. Soc.). The author is indebted to Professor Mulliken for seeing a copy of the manuscript before publication.
[5] Craig, Proc. Roy. Soc. **200A**, 401 (1950); Sklar, J. Chem. Phys. 5, 669 (1937).

On Generalizations of the Quasi-Chemical Equilibrium Approximation in Statistical Mechanics

TERRELL L. HILL
Naval Medical Research Institute, Bethesda, Maryland
May 12, 1950

THE writer has just noticed a recent paper by Li[1] on a generalization (from pairs of sites to larger groups of sites) of the quasi-chemical (hereafter *q-c*) approximation. The method applies to the order-disorder transition in alloys, regular solutions, adsorption, ferromagnetism, etc. Since we have been developing the same method independently[2] but in a more general way in one respect, a few remarks may be in order. We shall use adsorption language for convenience.

Our point of view has been: (a) by assuming a *q-c* equilibrium among larger groups of sites than pairs, not only can one obtain (in principle) convergence to exact results but also this procedure

Type of square	0	1	2′	2″	3	4
Number of equivalent arrangements	1	4	4	2	4	1
Number of squares of this type	N_0	N_1	N_2'	N_2''	N_3	N_4
Energy of each square	0	0	w	w'	$2w+w'$	$4w+2w'$

FIG. 1.

allows taking into account *second, third, etc. neighbor interactions* in addition to first neighbor interactions; (b) an approximate treatment of higher neighbor interactions may be as important in the interpretation of some experimental data as an *exact* treatment of the first neighbor problem; (c) the adsorption of ions and molecules on the *non-overlapping* groups of sites presented by, for example, protein molecules in solution is a related problem; and (d) since the q-c assumption using pairs of sites is *exact* in the one-dimensional first neighbor problem (Chang[2]), a strictly intuitive generalization is that the use of a square of four sites for a simple quadratic lattice and a cube of eight sites for a simple cubic lattice *might* be exact for these latter problems.

We conclude with an example: The first and second neighbor problem for a simple quadratic lattice using squares of four sites. Let N molecules be distributed on B sites. There are B (overlapping) squares of sites, of which N_i contain i molecules (Fig. 1):

$$N_0+N_1+N_2'+N_2''+N_3+N_4=B, \tag{1}$$

$$N_1+2N_2'+2N_2''+3N_3+4N_4=4N. \tag{2}$$

Let $y=\exp(-w/kT)$ and $t=\exp(-w'/kT)$, where w and w' are the first and second neighbor interaction energies. Let $g(N_2', N_2'', N_3, N_4, N, B)$ be the number of ways of putting N molecules on B sites so that there are N_2' squares of type $2', \cdots, N_4$ of type 4 (Fig. 1). Then the grand partition function is

$$\Xi=\sum_N \sum_{N_2'} \cdots \sum_{N_4} g y^{(N_2'+2N_3+4N_4)/2} t^{N_2''+N_3+2N_4} (a^0\lambda)^N, \tag{3}$$

where a^0 is the partition function of an isolated adsorbed molecule and λ is the absolute activity. As an approximation we now use

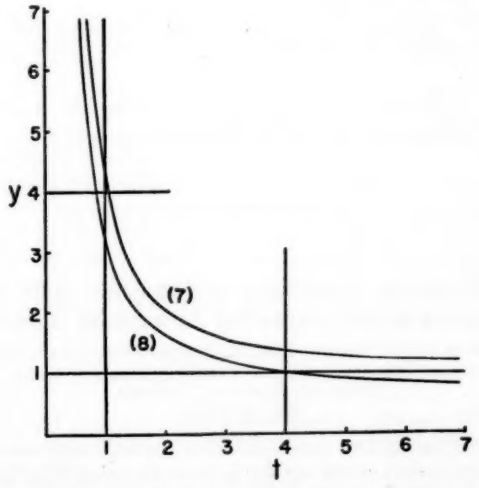

FIG. 2. Relation between y and t at critical point, according to Eqs. (7) and (8). For both curves, $t\to 0$ as $y\to\infty$. For Eq. (8): $y\to\frac{1}{2}$ as $t\to\infty$. For Eq. (7): $y\to 1$ as $t\to\infty$; also, near $t=1$,

$$-w/kT_c=1.44365\,[1-1.3416(w'/w)+2.2519(w'/w)^2-\cdots].$$

that g which leads to a q-c equilibrium[3] between $N_0, \cdots, N_4$ when[4] $w'=0$, namely $g=P^{\frac{1}{4}}Q^{\frac{1}{4}}$, with

$$P=\frac{(B-N)!N!}{N_0![(N_1/4)!]^4[(N_2'/4)!]^4[(N_2''/2)!]^2[(N_3/4)!]^4N_4!}, \qquad Q=\frac{(B-N)!N!}{B!}, \tag{4}$$

where N_0 and N_1 are to be eliminated by use of Eqs. (1) and (2). The maximum term in Ξ is found by differentiating $\ln\Xi$ with respect to $N_2', \cdots, N_4, N$. The N differentiation produces the adsorption isotherm

$$a^0\lambda=\alpha^2(1-\theta)/\theta, \qquad \theta=N/B, \quad \alpha=N_1/4N_0. \tag{5}$$

The other differentiations, when combined with Eqs. (1) and (2), lead to

$$4\theta=\frac{4\alpha+8\alpha^2y+4\alpha^2t^2+12\alpha^3y^2t^2+4\alpha^4y^4t^4}{1+4\alpha+4\alpha^2y+2\alpha^2t^2+4\alpha^3y^2t^2+\alpha^4y^4t^4}, \tag{6}$$

which gives $\alpha=\alpha(\theta, y, t)$ for use in Eq. (5). From Eqs. (5) and (6) one finds the critical point to be at $\theta=\frac{1}{2}$, $a^0\lambda=1/y^2t^2$ and a critical temperature determined by

$$y=(1/t)\{(1/t)+1+[(1+(1/t))^2+t^2]^{\frac{1}{2}}\}. \tag{7}$$

When $w'=0$, this reduces to Yang's[1,5] result $y=4.236$.

For completeness we have carried through the analogous treatment based on the less accurate (near $t=1$, the region of main interest) approximation of using in Eq. (3) that g which leads to a q-c equilibrium between $N_0, \cdots, N_4$ when[4] $w=0$, namely $g=PQ^2$. One finds the critical conditions $\theta=\frac{1}{2}$, $a^0\lambda=1/y^2t^2$,

$$t^{\frac{1}{2}}=\{y^{\frac{1}{2}}+[y+8y^{\frac{1}{2}}(2y-1)]^{\frac{1}{2}}\}/2(2y-1). \tag{8}$$

Equations (7) and (8) are plotted in Fig. 2.

[1] Y. Y. Li, Phys. Rev. **76**, 972 (1949). See also the earlier work of C. N. Yang, J. Chem. Phys. **13**, 66 (1945).
[2] We found the same combinatorial expression as Li by generalizing T. S. Chang's result for pairs of sites (Proc. Camb. Phil. Soc. **35**, 265 (1939)).
[3] For example, $N_0^2(N_2/4)/(N_1/4)^2=y^2$.
[4] On account of a lack of symmetry in this example (notice the factor $\frac{1}{2}$ in Eq. (3), which arises because each first neighbor pair is counted in two squares), it is not possible to write a g which will give $q-c$ equilibrium equations with *both* $w\neq 0$ and $w'\neq 0$. The unknown *exact* g is of course independent of the values of w and w'.
[5] In connection with (d) above ($w'=0$), the $q-c$ pair approximation gives $y=4$ and Kramer's and Wannier's (Phys. Rev. **60**, 252, 263 (1941)) presumably exact treatment gives $y=5.829$ (so the "intuitive generalization" in (d) is wrong).

Atomic Space-Lattice and the Metallic State

T. A. HOFFMANN
Physical Institute of the Technical University, Budapest, Hungary
May 12, 1950

A SIMPLE linear model for a metal has been developed by Hoffmann and Kónya on the basis of the molecular orbital method.[1] Now these results are extended to the space model by some mathematical results of Rutherford.[2] Provisionally this method has been applied for metals of simple cubic lattice structures for the case of a very large lattice-constant.

The determinant equation occurring in the space problem is of the form (taking into account a simple cubic crystal of l, m, n atoms in three mutually perpendicular dimensions):

$$\begin{vmatrix} (1) & L_m(x) & I_{mn} & & & & \\ (2) & I_{mn} & L_m(x) & I_{mn} & & & \\ (3) & & I_{mn} & L_m(x) & & & \\ \cdot & & & & \cdot & & \\ \cdot & & & & & \cdot & \\ \cdot & & & & & & \\ (l-1) & & & & L_m(x) & I_{mn} & \\ (l) & & & & I_{mn} & L_m(x) & \end{vmatrix} =0,$$

where I_{mn} is the unit matrix of mn rows and columns and $L_m(x)$ is a matrix:

$$L_m(x)=\begin{array}{c}(1)\\(2)\\(3)\\\cdot\\\cdot\\\cdot\\(m-1)\\(m)\end{array}\left\|\begin{array}{ccccccc}M_n(x) & I_n & & & & & \\ I_n & M_n(x) & I_n & & & & \\ & I_n & M_n(x) & & & & \\ & & & \cdot & & & \\ & & & & \cdot & & \\ & & & & & M_n(x) & I_n \\ & & & & & I_n & M_n(x)\end{array}\right\|,$$

and similarly $M_n(x)$ is a matrix:

$$M_n(x)=\begin{array}{c}(1)\\(2)\\(3)\\\cdot\\\cdot\\\cdot\\(n-1)\\(n)\end{array}\left\|\begin{array}{ccccc}x & 1 & & & \\ 1 & x & 1 & & \\ & 1 & x & & \\ & & & \cdot & \\ & & & & \cdot \\ & & & & x \quad 1 \\ & & & & 1 \quad x\end{array}\right\|.$$

Here x is, in the case of neglected overlap integrals,

$$x=W/\beta=(Q-E)/\beta,$$

where Q is the Coulomb integral and β the exchange integral of two neighboring atoms,[1] and E is the energy eigenvalue. If we do not neglect the overlap integrals of two neighboring atoms, S, we have

$$x=W/\beta'=(Q-E)/(\beta-SE).$$

Applying Rutherfords results,[2] we obtain for the roots of the determinant equation

$$x=2\left(\cos\frac{\lambda\pi}{l+1}+\cos\frac{\mu\pi}{m+1}+\cos\frac{\nu\pi}{n+1}\right)$$

($\lambda=1, 2, \cdots, l$; $\mu=1, 2, \cdots, m$; $\nu=1, 2, \cdots, n$). Thus in the case of neglected overlap integrals we have

$$E=Q-2\beta\left(\cos\frac{\lambda\pi}{l+1}+\cos\frac{\mu\pi}{m+1}+\cos\frac{\nu\pi}{n+1}\right),$$

and with the overlap integral S:

$$E=\frac{Q-2\beta\left(\cos\frac{\lambda\pi}{l+1}+\cos\frac{\mu\pi}{m+1}+\cos\frac{\nu\pi}{n+1}\right)}{1-2S\left(\cos\frac{\lambda\pi}{l+1}+\cos\frac{\mu\pi}{m+1}+\cos\frac{\nu\pi}{n+1}\right)}.$$

In the case of $S=0$ one can see that—treating metals with one valence electron only—the filled part of the band of width 12β are those states in which

$$\cos\frac{\lambda\pi}{l+1}+\cos\frac{\mu\pi}{m+1}+\cos\frac{\nu\pi}{n+1}<0.$$

FIG. 1. Space covered by the range of integration.

If $l, m, n\to\infty$, we have a continuous band from $Q+6\beta$ to $Q-6\beta$, which is filled from $Q+6\beta$ to Q. One can obtain the average energy, if one integrates

$$\frac{2}{\pi^3}[Q+2\beta(\cos x+\cos y+\cos z)]$$

in the (x, y, z)-space closed by the six planes $x=0$, $y=0$, $z=0$, $x=\pi$, $y=\pi$, $z=\pi$, further by the surface

$$\cos x+\cos y+\cos z=0.$$

The space which is covered by this integration is sketched in Fig. 1.

We can transform this integral finally to an integral which involves in the integrand the normal elliptic integral of the first kind. This integral can be simply evaluated and so we get

$$\bar{E}_{sp}=Q+1945\beta.$$

This means a considerable gain in stability against the linear chain,[1] which gives

$$\bar{E}_{lin}=Q+1273\beta.$$

In a similar way one can calculate the plane structure too, which gives

$$\bar{E}_{pl}=Q+1621\beta.$$

The increasing stability as the structure becomes of more dimensions gives a rough explanation of Kossel's theory concerning crystal growth, namely, if on the surface of a crystal there is begun a new row or a new plane, there will be no atom beginning another row or plane until the first row or plane is accomplished in the neighborhood of the point considered, since the more condensed (more dimensional) structures are energetically favorized.

The calculations are somewhat more tedious if we take into account the overlap integral. In this case we treat only the case $S<\frac{1}{6}$.

The average energy for one electron will be in this case

$$\bar{E}=(\beta/S)+[Q-(\beta/S)]f(S),$$

where $f(S)$ is a function of the overlap integral only, it is the average of

$$1/[1-2S(\cos x+\cos y+\cos z)].$$

This average as a series in S begins

$$f(S)=1-1945S+\cdots.$$

The calculation of $f(S)$ makes necessary the evaluation of integrals involving certain elliptic normal integrals. $f(S)$ can be given in integral form or in a table.

Detailed investigations and applications of the preceding theory will be published in a forthcoming paper in the *Hungarica Acta Physica*.

[1] T. A. Hoffmann and A. Kónya, J. Chem. Phys. **16**, 1172 (1948); Hungarica Acta Physica (to be published).
[2] D. E. Rutherford, Proc. Roy. Soc. Edinburgh **62A**, 229 (1947).

The Molecular Structure of Isocyanic Acid from Microwave and Infra-Red Absorption Spectra

L. H. JONES,* J. N. SHOOLERY, R. G. SHULMAN,** AND DON M. YOST
Gates and Crellin Laboratories of Chemistry, California Institute of Technology, Pasadena, California
May 22, 1950

EXPERIMENTAL investigations of the infra-red† and microwave spectra of the slightly asymmetric rotor, HNCO, have been made, and the structure of the molecule has been determined. The molecular constants computed from the microwave absorption frequencies of the $J=0\to1$ rotational transitions in the ground vibrational state, and from the resolved infra-red hybrid band of

TABLE I. Rotational molecular constants for HNCO.

	Microwave absorption frequencies ($J=0\rightarrow1$) Mc/sec.	$B_0+C_0/2$ cm^{-1} from microwaves	$A_0-B_0+C_0/2$ cm^{-1} from the infra-red
$H^1N^{14}C^{12}O^{16}$	21,981.7	0.36664	30.30±0.1
$H^1N^{15}C^{12}O^{16}$	21,323.5	0.35566	
$H^2N^{14}C^{13}O^{16}$	20,394.7	0.34017	

the first overtone of the N−H stretching vibration, ν_1, are listed in Table I.

On the assumption that the −NCO group is linear and that the molecule is HNCO and not HOCN, the four remaining structural parameters (three interatomic distances and one angle) have been evaluated. The linearity of the −NCO group is shown by the electron diffraction investigation of Eyster, Gillette, and Brockway,[1] which yielded equal N−C and C−O distances of 1.19A in accord with the following reasonable resonating structures, all of which contribute to a linear configuration.

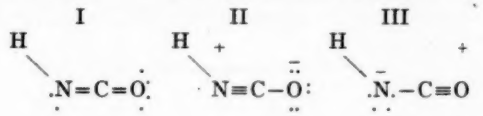

Measured values of the stretching frequencies associated with hydrogen valence forces in HNCO and HNCS are listed in Table II, along with characteristic values for other relevant bonds. Although the hydrogen valence frequency in isocyanic acid is high in comparison with the value usually attributed to N−H vibrations, the practical identity of this frequency in HNCO and HNCS can leave little doubt but that in both cases it results from an NH vibration, and that isocyanic and isothiocyanic acids are predominantly, if not exclusively, present.

TABLE II. Hydrogen stretching frequencies.

	Fundamental cm^{-1}	First overtone cm^{-1}
HNCO	3538	6915
HNCS	3530	6903
H−N<	3350[a]	—
H−O−	3680[a]	—
H−S−	2750[a]	—

[a] See reference 2, p. 195.

Since the force constant for the NH bond is unusually high in isocyanic acid, as shown by the stretching frequency, Badger's rule suggests that the length of the bond will be shortened from the value of 1.014A found in NH_3[2] to 0.987A. This is indeed found to be the case.

Effective values of the calculated structural parameters in the ground vibrational state are listed in Table III.

Equations expressing A_0 and C_0 for the various isotopic species in terms of the molecular parameters were solved numerically by the Newton-Raphson approximation method to the nearest 0.001A. The isotopic substitutions of deuterium for hydrogen and N^{15} in place of N^{14} lead to an uncertainty of about 0.005A in the N−O distance and 0.01A in the N−H distance. In spite of the accuracy of the N−O distance there is an uncertainty of 0.01A in the N−C and C−O distances, because the proximity of the carbon to the center of mass makes the calculation insensitive to its exact position. Excellent agreement is obtained with the total N−O distance determined by electron diffraction.

TABLE III. Structural parameters for HNCO.

	Spectroscopic HNCO parameters distances in A	Electron[a] diffraction values distances in A
C−O distance	1.171±0.01	1.19±0.03
N−C distance	1.207±0.01	1.19±0.03
N−H distance	0.987±0.01	1.01 (estimated)
N−O distance	2.378±0.005	2.38±0.03
H−N−C angle	128° 5′±30′	125° (estimated)

[a] See reference 1.

We wish to thank Professors W. H. Pickering, and H. V. Neher, and Mr. Bart Locanthi for invaluable counsel concerning electronic problems. We also greatly appreciate several very helpful discussions with Professor R. M. Badger. The work was supported in part by a grant from the Research Corporation, to whom we wish to express our gratitude here.

* AEC Predoctoral Fellow.
** AEC Postdoctoral Fellow.
† In some of the infra-red bands interesting perturbations were observed which will be discussed in a later paper.

[1] Eyster, Gillette, and Brockway, J. Am. Chem. Soc. **62**, 3236 (1940).
[2] G. Herzberg, *Infra-Red and Raman Spectra* (D. Van Nostrand Company, Inc., New York, 1947), third printing, p. 439.

Remarks on the Surface Tension of Small Droplets

FRANK P. BUFF* AND JOHN G. KIRKWOOD
Gates and Crellin Laboratories of Chemistry, California Institute of Technology, Pasadena, California
May 4, 1950

IN two recent communications to this Journal, LaMer and Pound[1,2] have reported estimates of the surface tension of very small drops based upon the Becker-Döring[3] theory of nucleation and measurements of the critical supersaturation pressure leading to the rapid production of a fog in certain vapors. Using the data of Volmer and Flood,[4] they concluded that the surface tension is independent of radius, in apparent conflict with predictions of Tolman's[5] quasi-thermodynamic theory and our statistical mechanical theory[6] of surface phases. Later calculations based on the data of Sander and Damköhler[7] yielded values of the surface tension which decreased with increasing drop curvature, in agreement with the predictions of both theories.

It is our purpose in the present note to make a few critical remarks concerning the significance of calculations of the sort carried out by LaMer and Pound. The conclusion that surface tension decreases with increasing curvature, reached both by Tolman and by us, does not seem to be open to doubt. However, it must be emphasized that the magnitude of the predicted effect becomes significant only for drops so small that the application of macroscopic thermodynamic concepts becomes ambiguous. In other words, the theory states that there is no sensible effect of curvature on surface tension in the macroscopic domain. Since the critical "droplet" of nucleation theory is in representative cases a cluster of about 100 molecules of radius of the order of 10A, it is definitely outside the domain of applicability of macroscopic thermodynamic concepts, and it is with the "surface tension" of such droplets that LaMer and Pound are concerned.

The Becker-Döring theory of the dynamics of nucleation extrapolates macroscopic concepts into the microscopic domain and is therefore subject to the ambiguities to which we have called attention. By this remark, we do not intend to depreciate the value of the Becker-Döring theory as an extraordinarily useful approximation. On the contrary, we believe that it should be exploited to the fullest extent. We are, however, inclined to doubt whether it is sufficiently refined to decide the rather delicate point in question, that is the dependence of surface tension on radius of curvature. We shall discuss some of the ambiguities which arise when it is used for this purpose.

Nucleation in a supersaturated vapor is initiated by statistical density fluctuations giving rise to molecular clusters, which decay unless they exceed a critical size. Cluster embryos exceeding the critical size serve as nuclei for the new phase through growth by accretion of molecules from the vapor. In the Becker-Döring theory, the clusters are idealized as minute spherical droplets possessing the properties of the liquid phase in bulk with a vapor pressure determined by the Gibbs-Thompson formula. The work of

formation of a droplet of radius r, and surface tension γ is estimated by the Gibbs formula as $4\pi\gamma r^2/3$. Similar approximations are made in Band's[8] equilibrium theory of condensation, which bears the same relation to the exact theory of Mayer[9] that the Becker-Döring theory bears to an exact dynamic theory of condensation, which awaits future development.

We do not propose to discuss here the ambiguities arising from applying the Gibbs-Thompson formula for the vapor pressure and the Gibbs formula for the work of formation to drops containing a small number of molecules of radii comparable to the range of intermolecular force. We shall limit ourselves to a few remarks concerning the definition of drop radius in the Becker-Döring theory under the temporary hypothesis that these relations can still be applied. In order to define the drop size, it is necessary to select a Gibbs dividing surface. If the mass of the drop in moles is equated to $4\pi R^3/3v$, v being the molal volume of the liquid phase, the radius R evidently refers to the dividing surface which makes the Gibbs superficial density of matter, Γ, vanish. On the other hand, if the work of formation W of the drop is equated to $4\pi\gamma r^2/3$, the radius r and the surface tension γ evidently refer to the surface of tension. In the Becker-Döring theory these two radii r and R are treated as identical, an assumption which is unjustified when both are small. The difference $R-r$ is in fact the quantity δ which determines the dependence of surface tension on the radius of curvature r of the surface of tension by the Gibbs-Tolman formula,

$$\frac{d\log\gamma}{dr}=\frac{[2\delta/r^2][1+\delta/r+\frac{1}{3}(\delta/r)^2]}{1+2(\delta/r)[1+\delta/r+\frac{1}{3}(\delta/r)^2]} \qquad (1)$$
$$R=r+\delta.$$

In a future publication, it will be shown by one of us (F.P.B.) that the Gibbs formula and the Gibbs-Thompson formula can be written for an incompressible fluid in the alternative forms,

$$W=\frac{4\pi r^2\gamma}{3}=\frac{4\pi R^2}{3}\left(\gamma'-\frac{d\gamma'}{d\log R}\right)$$
$$NkT\log\frac{P}{P_\infty}=\frac{2\gamma v}{r}=\left(\frac{2\gamma'}{R}+\frac{d\gamma'}{dR}\right)v, \qquad (2)$$

where W is the work of formation of a drop and P/P_∞ is the ratio of its vapor pressure to that of a plane interface, P_∞. γ' is the surface tension referred to the Gibbs dividing surface, $\Gamma=0$, and is in general different from γ. With the aid of Eqs. (2) and the kinetic assumptions of the Becker-Döring theory, it can be shown that j, the rate of condensation in molecules per cm³ is given by

$$j=\frac{a_0N_1'}{3n}\left(\frac{3W}{\pi kT}\right)^{\frac{1}{2}}\exp^{-W/kT}$$
$$W=(4\pi r^2\gamma)/3 \qquad (3)$$
$$n=4\pi NR^3/3v,$$

where a_0N_1' is twice the rate of collision of vapor molecules per cm³, and n is the number of molecules in the critical droplet which must be expressed in terms of R and not in terms of r, the radius of the surface of tension, when γ depends on curvature. Comparison of Eqs. (2) with experiment involves the usual uncertainty of assigning an arbitrary value to j, not directly observed, which is supposed to lead to rapid production of fog at the critical supersaturation pressure. A value of the order of magnitude of 10 is customarily assigned, although Head[10] has suggested that a much higher value should properly be used.

Therefore, we see that when surface tension is dependent on curvature, a somewhat more elaborate analysis than that made by LaMer and Pound is necessary, even if the macroscopic assumptions of the Becker-Döring theory are accepted. The effective surface tension, having a meaning subject to the ambiguities of the Becker-Döring theory, calculated from the data of Sander and Damköhler confirms the conclusion that surface tension decreases with increasing curvature.

The rapid change in slope of this effective surface tension, considered as a function of temperature, may be attributed to the competing effects of the usual increase of surface tension at lower temperatures and the decrease of surface tension at lower temperatures because of the decrease in size of the critical embryo. It is of interest to remark that Sander and Damköhler suggested the onset of crystallization as a cause of departure of their results from the simple Becker-Döring theory. Whether this is true must be decided by experiment, but in the light of the present analysis it does not seem necessary.

* AEC Postdoctoral fellow, 1949–1950.

[1] V. K. LaMer and G. M. Pound, J. Chem. Phys. **17**, 1337 (1949).
[2] V. K. LaMer and G. M. Pound, J. Chem. Phys. (in press). We are indebted to Professors LaMer and Pound for sending us this manuscript in advance of publication.
[3] R. Becker and W. Döring, Chem. d. Physik **24**, 719 (1935).
[4] M. Volmer and H. Flood, Zeits. f. physik. Chemie (A) **170**, 273 (1934).
[5] R. C. Tolman, J. Chem. Phys. **17**, 333 (1949).
[6] J. G. Kirkwood and F. P. Buff, J. Chem. Phys. **17**, 338 (1949).
[7] A. Sander and G. Damköhler, Naturwiss. **31**, 460 (1943).
[8] W. Band, J. Chem. Phys. **7**, 324 (1939).
[9] J. E. Mayer and M. G. Mayer, *Statistical Mechanics* (John Wiley and Sons, Inc., New York, 1940).
[10] R. M. Head, Thesis, California Institute of Technology, 1949.

Glass Electrode Behavior in Acid Solutions

EDWARD E. SINCLAIR
Department of Chemistry, Amherst College, Amherst, Massachusetts
AND
ARTHUR E. MARTELL
*Department of Chemistry, Clark University, Worcester, Massachusetts**
May 2, 1950

IN connection with Dole's[1] criticism of our paper on glass electrode measurements in acid solutions,[2] it is felt that several factors should be pointed out.

1. Dole used some of the data in Table II of our paper to show a rough agreement of our data with his theory. He also rejected data that did not agree with his theory on the basis that they were not "true, reversible, thermodynamic potentials." As a matter of fact, the authors have pointed out that none of the potentials which were measured in the acid solutions more concentrated than $1N$ were of the steady, reproducible type observed with the same electrodes in the more dilute acid solutions, and this applies to the data used by Dole. The data for $5N$ acid solutions in Table II, for example, were the potentials observed about three hours after immersion of the electrodes in the acid solutions—about the length of time over which observations in each of the dilute solutions were carried out. These data were presented primarily to show the poor agreement in $5N$ solutions of the potentials associated with the individual electrodes as compared to the good agreement of the potentials of the same electrodes in the dilute acid solutions. Actually, the character of these potentials was much the same as those presented in Table IV, i.e., the dilute solution potentials rapidly attained the steady values indicated, whereas the potentials in the $5N$ acid solutions were slowly changing to more negative values. It is therefore believed that the apparent agreement of our data with the theory of Dole is fortuitous.

2. Dole suggested that these slowly changing potentials observed by us indicate chemical attack of the electrode and cited deviations observed by Dole, Roberts and Holley[3] in the presence of molecular hydrogen fluoride as an example of such attack. It is felt that, in view of the specific and well-known reaction between hydrogen fluoride and glass, a comparison of the action of this reagent with that of hydrochloric and sulfuric acids is not justified.

3. It is agreed, however, that the nature of these potentials may very well be taken to indicate that some process (or possibly processes) occurs in the strongly acid solutions which does not occur in the dilute acid solutions. Whatever the nature of the process, it appears to approach a steady state only very slowly.

In this connection, it is pertinent to note that (a) the potentials observed by us always changed in the same direction, i.e., toward greater negative deviations from hydrogen electrode behavior, and (b) electrodes showing these unsteady negative deviations invariably resumed normal hydrogen electrode function when immersed in solutions of higher pH.

4. It has been pointed out that ours is not the only data which shows considerable disagreement with the water electrode theory. Hubbard, Hamilton and Finn[4] have reported that they have repeatedly prepared Corning 015 glass electrodes which, while showing no definite voltage departures in sulfuric acid solutions, showed very large negative deviations in hydrochloric acid solutions. Indeed, virtually all published data concerned with the negative deviations of glass electrodes show a lack of reproducibility that is not observed in the dilute acid solutions. On the basis of this information, it does not seem likely that the glass electrode potentials observed in the strongly acid solutions can be attributed solely to the obviously stable and reproducible electrode reaction which must proceed in the dilute solutions. Hence, if the assumption of Dole is correct, namely that the net reaction at the glass electrode during operation in pure acid solutions is the transfer of the hydrated proton, then it does not seem likely that this is the only reaction which takes place in the concentrated acid solutions. It is considerations such as these which have led the authors to refer to the water electrode theory as "unsatisfactory" and to suggest the possibility of the participation, or better the interference, of anions in the normal glass electrode reaction. The authors intend to discuss these points in greater detail in another paper to be published soon.

* On leave 1949–50, Department of Chemistry, University of California, Berkeley, California.
[1] M. Dole, J. Chem. Phys. **18**, 573 (1950).
[2] E. Sinclair and A. Martell, J. Chem. Phys. **18**, 224 (1950).
[3] Dole, Roberts, and Holley, J. Am. Chem. Soc. **63**, 725 (1941).
[4] Hubbard, Hamilton, and Finn, J. Research Nat. Bur. Stand. **22**, 339 (1939).

The Chain-Breaking Process in Acetaldehyde Photolysis

VICTOR E. LUCAS* AND OSCAR K. RICE
University of North Carolina, Chapel Hill, North Carolina
May 11, 1950

HADEN AND RICE[1] showed by comparison of results in steady and in intermittent light that, in addition to a second-order gas phase recombination, a chain-breaking step of approximately first order, presumably taking place at the wall, can play an appreciable role in acetaldehyde photolysis. A very rapidly rotating sector has the effect of reducing I, the light intensity, to a fixed fraction, in our case one-fourth, and gives, we believe, greater accuracy than comparison of results at different, directly measured, intensities. Thus the ratio $\rho_\infty = 2K_\infty/K_s$ (K_∞ = rate with very fast sector, K_s = rate under steady illumination) is a measure of the effect of decreasing I fourfold. At high concentrations of radicals (high intensity or high K_s) the chain-breaking step in the gas phase predominates, the rate is proportional to $I^{\frac{1}{2}}$, and ρ_∞ should equal 1. As K_s decreases the unimolecular wall reaction comes to predominate in chain-breaking, the rate becomes proportional to I, and ρ_∞ would approach 0.5 according to a theoretically calculated curve (ρ_∞ *vs.* $\log K_s$), if diffusion could be neglected.

We have performed a series of experiments[2] to elucidate the effects connected with diffusion of the radicals to the wall. Acetaldehyde was illuminated with ultraviolet light (3130A) in a cylindrical quartz vessel, length 5 cm, diameter 2.5 cm, at 200°C (unless otherwise noted), and at 10 cm pressure of acetaldehyde (unless otherwise noted). In some of the experiments the face of the vessel was covered with a diaphragm having an opening 1 cm in diameter; in other cases the diaphragm was omitted and the cell completely flooded with light.

Case 1. Diaphragm present.—ρ_∞ became as great as 1.1 at high K_s. As K_s decreased ρ_∞ decreased more rapidly than theoretically expected. These deviations probably result from the diffusion. (a) At very high radical concentrations (high I or K_s) the lifetime of the radicals will be so short that little diffusion takes place. (b) At somewhat lower I diffusion occurs but the radicals do not reach the walls; the diffusion will lower the concentration of the radicals and increase their lifetime, hence the amount of reaction. Comparing (b) with (a), we see that this can result in ρ_∞ becoming greater than 1. (c) At still lower intensity the radicals get to the wall and only then are destroyed there. This will eventually cause ρ_∞ to become abnormally low (compare (c) with (b)).

Case 2. No diaphragm.—The effect of diffusion was, as might be expected, largely eliminated, and ρ_∞ followed the theoretical curve reasonably well.

Case 3. 40 cm of CO_2 *added to 10 cm acetaldehyde-diaphragm present.*—In the middle range of K_s (where $\rho_\infty \sim 0.8$) values of ρ_∞ slightly exceeded those of Case 1 for same K_s. The CO_2, by preventing diffusion, prevents the falling-off in rate due to the wall reaction from appearing until lower intensities are reached.

Case 4. 40 cm of acetaldehyde-diaphragm present.—Similar effect as in Case 3, when compared to Case 1 at values of K_s which would indicate equal radical concentrations [i.e., K_s(40 cm) $= 4 \times K_s$(10 cm)].

Differences of Cases 3 and 4 from Case 1 were not quite as large as might have been anticipated, but chain-breaking at the ends of the vessel, where less diffusion is required, might well complicate the picture. However, the effects in the higher range of intensities were harder to understand. In Case 3 values of ρ_∞ greater than 1 were not much in evidence (possibly due to experimental error), while in Case 4 they appeared about as in Case 1.

Case 5. Same as Case 3 but no diaphragm.—ρ_∞ about the same as Case 2 except in lower range of K_s, where ρ_∞ was lower than in Case 2. This difference may not be significant, since there were not many runs.

We may add that treating the walls with KCl solution, which suppresses many wall reactions, apparently had no effect in this case.

We have also performed some experiments at 200° and 300°C, using variable sector speed, and have calculated k_3, the rate constant of the gas-phase chain-breaking reaction, by the method of Haden and Rice. We used high intensity and a cell without diaphragm, conditions calculated to minimize the effects of diffusion, and to make the wall reaction of least importance. On the assumption that the chain-breaking step is $2CH_3 \rightarrow C_2H_6$, we find $k_3 = 6.0 \times 10^{13}$ cc mole^{-1} sec.$^{-1}$ at 200°C, with an activation energy $E_3 = 2.8$ kcal. per mole. This is based on Grahame and Rollefson's[4] absolute rates at 200°C, Leermakers'[5] value, 10.0 kcal. per mole, of the over-all activation energy, and Gorin's[6] value of 0.7 for the efficiency of production of radicals by light absorption. For comparison Haden and Rice's results should be divided by 4. If this is done their value of k_3 is 10.0×10^{13}. The agreement is reasonable, but we consider the new value more accurate. However, it does not agree very well with Dodd,[7] if correction is made for the different assumed efficiency for radical production by light.

Our measurements indicate that 8.5 to 9 kcal. per mole would be a better value of the over-all activation energy. If we use this, instead of Leermakers' value, E_3 is close to zero, which is more reasonable, since the value of k_3 is very close to the estimated collision number of about 10^{14} cc mole^{-1} sec.$^{-1}$. The determination of E_3 cannot be considered to be highly accurate, but the frequency factor in k_3 can certainly not be larger than the collision number. Indeed, it is remarkable that k_3 shows no indication of a steric factor. This is contrary to the conclusions of other investigators of the recombination of methyl radicals;[7] we may be dealing with a different reaction, but this makes our result no less surprising.

Finally, we have calculated the rate constant for the wall reaction at 200°C as approximately 0.8 sec.$^{-1}$, corresponding to an accommodation coefficient of about 10^{-5}. This is smaller than the value obtained by Haden and Rice, but despite this we believe

the activation energy to be near zero in contrast to their value of 7.8 kcal. per mole. This value is very sensitive to the experimental results, and Haden and Rice's estimate rested on comparison of experiments at 200° and 300°C, which were not run under exactly similar circumstances.

* Present address: Firestone Tire and Rubber Company, Akron, Ohio.
[1] W. L. Haden, Jr. and O. K. Rice, J. Chem. Phys. **10**, 445 (1942).
[2] V. E. Lucas, Thesis, University of North Carolina, 1947.
[3] D. C. Grahame and G. K. Rollefson, J. Chem. Phys. **8**, 98 (1950).
[4] J. A. Leermakers, J. Am. Chem. Soc. **56**, 1537 (1934).
[5] E. Gorin, Acta Physicochimica U.R.S.S. **9**, 681 (1938).
[6] R. E. Dodd, J. Chem. Phys. **18**, 234 (1950).
[7] See R. A. Marcus and E. W. R. Steacie, Zeits. f. Naturforch. **4a**, 332 (1949).

The Gas Phase Exchange Reaction between HBr and Br_2*

HOMER JACOBSON**
Chemistry Department, Brookhaven National Laboratory, Upton, New York
May 12, 1950

THE exchange reaction between gaseous HBr and Br_2 is known from previous investigations[1-3] to be rapid, being reported as almost complete within two min. at room temperature with approximately equivalent amounts of reactants at a total pressure of about 100 mm.[2,3] We have studied the reaction with a dynamic mixing and separation procedure in which the contact time was of the order of 0.5 sec. and the total pressure about one mm, with approximately equivalent amounts of the reactants. The reaction is found to be complete within a few seconds, and estimates of its half-time have been obtained.

Using Br_2 tagged with Br^{82}, the extent of reaction was determined by measuring the specific activities of the Br_2 and HBr subsequent to mixing and separation. The reactants were passed through individual flowmeters and throttling valves into a mixing tube, where the exchange took place. The mixture then passed into two traps in tandem, the first held at −120°C (with a slush of partially frozen *n*-butyl chloride) trapping out the Br_2, and the second at −193°C congealing the HBr. Separation of Br_2 from HBr was shown to be quantitative by chemical analysis of the trapped materials. After a sufficient amount of the gases had been collected, the traps were removed from the line, and the gases dissolved in ammonia water, from which the bromine was precipitated as AgBr. Reproducible counting of precipitates up to 60 mg/cm² in thickness was obtained, provided the precipitation was performed in one M NH_3, and the solution was filtered immediately. The Br_2 used was tagged with Br^{82} by repeated gas phase exchange with anhydrous $AlBr_3$, in which pile irradiated KBr had been dissolved. Chlorofluorocarbon oils and greases were used in the apparatus throughout to minimize reaction with bromine.

The data obtained in 22 runs can be summarized as follows. In a preliminary run it was shown that no exchange took place between HBr (*g*) and Br_2 (*s*) in the −120° trap. With 12-sec. contact time at 23 mm 98 percent exchange took place. In 18 runs at room temperature (18–24°C), pressures 0.5–2.0 mm, and contact times of 0.4–0.9 sec., half-times of exchange of 0.14–0.75 sec. were observed. In 2 runs at 21° and 18°, 1.1 mm pressure, and 0.5 sec. contact time, with the mixing chamber loosely packed with SiO_2 wool, half-times of 0.06 and 0.08 sec. were observed. The increased rate suggests a heterogeneous reaction, which is consistent with a certain amount of irreproducibility found in the other data. This irreproducibility obscured any systematic trend of half-time with temperature or pressure. Runs at activity levels of 10^{-3} to 3×10^{-6} microcurie/cc showed that the exchange is not caused primarily by radiation activation. Several of the runs were done in total darkness, with no indication of a photochemical effect in the others. The reaction is believed not to have been diffusion controlled. Calculation indicated that the gases had mixed completely within the first 5 percent of their stay in the mixing chamber, in which time the mean diffusion path length of the gases was about twice the mixing chamber diameter.

We believe it likely that the reaction proceeds in a heterogeneous fashion on the walls of the vessel, as in the case of the Br_2-C_2H_4 reaction,[6,7] a conclusion differing from that of Libby and Dodgen.[5]

Grateful acknowledgment is made to Dr. R. W. Dodson for advice and constructive criticisms.

* Research carried out under the auspices of the AEC.
** Now at Brooklyn College, New York.
[1] Brejneva, Roginsky, and Schilinsky, Acta Physiochemica (U.R.S.S.) **5**, 549 (1936).
[2] L. Liberatore and J. Wiig, J. Chem. Phys. **8**, 168 (1940).
[3] W. F. Libby, J. Chem. Phys. **8**, 348 (1940).
[4] L. Liberatore and J. Wiig, J. Chem. Phys. **8**, 349 (1940).
[5] H. W. Dodgen and W. F. Libby, J. Chem. Phys. **17**, 951 (1949).
[6] T. D. Stewart and K. R. Edlund, J. Am. Chem. Soc. **45**, 1014 (1923).
[7] R. G. W. Norrish, J. Chem. Soc. **55** (1926).

Errata: The Structure of Uranium Hexafluoride as Determined by the Diffraction of Electrons on the Vapor

[J. Chem. Phys. **18**, 27 (1950)]
S. H. BAUER
Department of Chemistry, Cornell University, Ithaca, New York

SEVERAL errors crept into the manuscript with the above title. The conclusions deduced therein are in no way altered when the appropriate corrections are made.

(1) Footnote 17, p. 35: Dr. V. Schomaker called my attention to the unreasonably large value quoted for the bond compression energy, upon solidification of hexamethylenetetramine. An estimate close to 4 kcal. makes sense.

If to permit a more favorable packing arrangement in solid UF_6, configuration H_1 is favored over A_4, a net bond extension energy just under 12 kcal. would have to be introduced (assuming the stretching force constant for U−F to be around 4×10^5 dynes/cm). This is still sufficiently small to permit the change $A_4 \rightarrow H_1$ to take place upon crystallization from the vapor.

(2) P. 41: Drs. Fumi and Castellan pointed out that the symmetry number for model C_4 is not 8. We have made the computation for C_3 for which $\sigma=8$, as was our intention. Insofar as the electron diffraction data are concerned C_3 is as acceptable as C_4; this can be readily ascertained from Fig. 4b and Fig. 5.

(3) P. 41: Drs. Bigeleisen and Hastings indicated that when the directly measured heat of vaporization is used to obtain the experimental entropy (Masi, J. Chem. Phys. **17**, 756 (1949)), the agreement at 273°K between $S°_{exp}$ (87.56) and $S°_{BMST}$ (87.65) is much better than with $S°_{Bauer}$ (88.65). Clearly the alternate frequency assignment is not entirely suitable. I wish to stress, however, that it was proposed not as a final one, but only to show that the argument in favor of $\sigma=24$ is not as compelling as it may appear on the surface. Actually, the matter will be settled shortly when the infra-red spectrum of UF_6 is re-run at Harvard University, down through the KRS range.

To those who called these errors to my attention I am sincerely grateful.

Microwave Spectra and Molecular Constants of Tertiary Butyl Chloride, Bromide, and Iodide*

JOEL Q. WILLIAMS† AND WALTER GORDY
Department of Physics, Duke University, Durham, North Carolina
May 3, 1950

THE present study was undertaken primarily to determine whether microwave spectroscopy could be used to obtain knowledge of the structure of molecules of the tertiary butyl type. The large number of these and similar trimethyl compounds make such studies attractive.

Although these molecules have a high degree of symmetry, several factors combine to make their microwave spectra com-

TABLE I. Observed absorption frequencies and molecular constants for tertiary butyl halides.

	Transition $J \rightarrow J+1$	Frequency (Mc/sec.)[a]	B(Mc/sec.)	I_B(g cm²)
$(CH_3)_3CCl^{35}$	4→5	30150	3016	278.2×10^{-40}
	5→6	36210		
	6→7	42200		
$(CH_3)_3CCl^{37}$	4→5	29530	2954	284.1×10^{-40}
	5→6	35460		
	6→7	41330		
$(CH_3)_3CBr^{79}$	6→7	28610	2044	410.5×10^{-40}
	7→8	32690		
	8→9	36790		
	9→10	40885		
$(CH_3)_3CBr^{81}$	6→7	28610	2028	413.7×10^{-40}
	7→8	32690		
	8→9	36790		
	9→10	40885		
$(CH_3)_3CI^{127}$	8→9	28085	1562	537.7×10^{-40}
	9→10	31185		
	10→11	34310		
	11→12	37490		
	12→13	40570		

[a] ±30 Mc/sec.

TABLE II. Carbon halogen distances.

Link	Tertiary butyl halides[a] with ∠CCC = 111° 30′	Tertiary butyl halides[a] with ∠CCC = 109° 28′	Methyl halides[b]	Added covalent radii[c]
CCl	1.82A	1.78A	1.779	1.78
CBr	1.98	1.94	1.936	1.93
CI	2.19	2.14	2.139	2.12

[a] Here $d_{CC} = 1.54$A, $d_{CH} = 1.093$ and ∠HCH = 109° 28′ are assumed.
[b] From Gordy, Simmons, and Smith, Phys. Rev. **74**, 243 (1948).
[c] The revised value 0.99A for the C radius proposed by Gordy (J. Chem. Phys. **15**, 81 (1947)) is used with the halogen radii from Pauling, *Nature of the Chemical Bond* (Cornell University Press, Ithaca, New York, 1940), p. 164.

plex. These are principally the nuclear coupling of the halogen, the separation of the lines of different K by centrifugal stretching, and the torsional oscillation or restricted internal rotation of the CH_3 groups. There is also the question whether the molecules behave exactly like symmetric-top rotators. Without a complete analysis of the structure of the spectra, it was found possible to prove the symmetric-top configuration and to obtain the moments of inertia, I_B, to better than one percent accuracy.

Because of their large moments of inertia it was convenient to observe the lines of rather high J. A similar series of lines was observed for each transition. One line was prominent in each series. From qualitative considerations it is possible to conclude that this strong line is not likely more than two to four megacycles from the position of the unperturbed rotational transition of the ground vibrational state. Also, it appears that the displacement of this line for neighboring transitions is very nearly the same, probably within a megacycle of the same amount. This may be seen by substituting reasonable values for the centrifugal stretching and nuclear coupling constants in the appropriate equations. It is evident that for high J the lines of low K have the smallest perturbations from both nuclear coupling and centrifugal effects. For high J the nuclear coupling alone would produce an approximately symmetric group of lines with the stronger ones near the center of symmetry. We assume that the strongest line is for the ground vibrational state.

Table I lists the frequencies of the observed transitions, the B values and the moments of inertia, I_B. Table II gives the carbon-halogen distances obtained from these, with assumed values for other parameters. The chloride and bromide have been measured with electron diffraction.[1] For each the value $d_{CC} = 1.54 \pm 0.02$A and ∠CCC = 111.5° ± 2° were obtained with $d_{CCl} = 1.78 \pm 0.03$ and $d_{CBr} = 1.92 \pm 0.03$. This value for angle CCC appears incompatible with reasonable values for the bond lengths (see Table II). The present work indicates that this angle is tetrahedral or very nearly tetrahedral, and that the carbon halogen distances are essentially the same as those of the methyl halides.

* The research reported in this document has been made possible through support and sponsorship extended by the Geophysical Research Directorate of the Air Force Cambridge Research Laboratories under Contract No. W(19-122)ac-35. It is published for technical information only and does not represent recommendations or conclusions of the sponsoring agency.
† Texas Company Fellow.
[1] J. W. Beach and D. P. Stevenson, J. Am. Chem. Soc. **60**, 475 (1938).

Carrier-Free Radioisotopes from Cyclotron Targets. IX. Preparation and Isolation of Re 183, 184 from Tantalum*

JEANNE D. GILE, WARREN M. GARRISON, AND JOSEPH G. HAMILTON
Crocker Laboratory, Radiation Laboratory, and Divisions of Medical Physics, Experimental Medicine, and Radiology; University of California, Berkeley and San Francisco, California
May 8, 1950

THE long-lived radioisotopes[1] of rhenium, $Re^{183, 184}$, were produced by bombardment of tantalum with 40-Mev alpha-particles in the 60-inch cyclotron at Crocker Laboratory. At this energy, radioactive rhenium is produced[2] by the nuclear reactions; $Ta^{181}(\alpha, n)Re^{184}$, $Ta^{181}(\alpha, 2n)Re^{183}$, $Ta^{181}(\alpha, 3n)Re^{182}$. 46-day Hf^{181} is produced concurrently by (n, p) reaction. The short-lived[2] activities (Re^{182} and isomer of Re^{184}) were allowed to decay out prior to the chemical separation reported here.

A C.P. tantalum metal target ($\frac{1}{4}$ in. Ta strip, silver-soldered to a water-cooled copper plate) was bombarded for a total of 80 μa-hr. at a maximum beam intensity of 10 μa. The bombarded surface (approximately 0.5 g) was removed by milling and dissolved in a minimum volume of 16 N HNO_3 containing 10 percent HF by volume. The HF was removed by evaporation and the bulk of the tantalic acid was separated by centrifugation with repeated reduction in volume of the HNO_3 solution. The carrier-free $Re^{183, 184}$ as perrhenate, was quantitatively retained in supernatant. The HNO_3 solution was evaporated almost to dryness and transferred to an all-glass[3] distilling flask with 15 ml of 36 N H_2SO_4. 9 N HBr was added dropwise while a stream of CO_2 was bubbled through the H_2SO_4 solution at 240°C. The distillate, containing the carrier-free radio-rhenium, HBr, Br_2, and a small amount of H_2SO_4, was collected in a trap of 16 N HNO_3 cooled with ice. This solution was evaporated on a steam bath to the 1 ml volume of H_2SO_4 carried over in the distillation. The H_2SO_4 was diluted to 3 N and the $Re^{183, 184}$ was co-precipitated with 2 mg of Cu^{++} by the addition of H_2S. The CuS was dissolved in a minimum volume of dilute HNO_3. This solution was evaporated to dryness, diluted with water to 25 ml, heated to 60°C and neutralized with a stoichiometric amount of NaOH. Under these conditions CuO is precipitated without scavenging the carrier-free radio-rhenium. The supernatant was evaporated to dryness on 20 mg of added NaCl and re-dissolved quantitatively with the addition of 2 ml of water to give an isotonic saline solution of carrier-free Re^{183} for subsequent biological investigation.

The activity was identified by chemical separation with carrier, by absorption measurements and by half-life determinations. A tracer amount of activity added to a solution containing carrier amounts of Ta, Hf, and Re was quantitatively recovered in the Re fraction following chemical separation.[4] The radiation characteristics were obtained by aluminum and lead absorption measurements and showed the 0.2- and 0.8-Mev beta-particles and 1.0-Mev gamma-ray previously reported[2] for Re^{184}. 14 days after bombardment the activity showed an approximately 60-day half-life which began to lengthen perceptibly after 6 weeks. The difference between this value and the 52-day period previously found[2] for Re^{184} is presumably due to the 240-day Re^{183} which is produced concurrently.

We wish to thank Professor G. T. Seaborg for helpful sugges-

tions, Mr. T. Putnam, Mr. B. Rossi, and the 60-inch cyclotron crew at Crocker Laboratory for bombardments, and Mrs. Alberta Mozley for technical assistance in counting.

* This document is based on work performed under Contract No. W-7405-eng-48-A for the AEC.

[1] G. T. Seaborg and I. Perlman, Rev. Mod. Phys. **20**, 585 (1948).
[2] G. Wilkinson and H. G. Hicks, Phys. Rev. **77**, 314 (1950).
[3] J. A. Scherrer, J. Research Nat. Bur. Stand. **21**, 95 (1938).
[4] F. P. Treadwell and W. T. Hall, *Analytical Chemistry* (John Wiley and Sons, Inc., New York, 1942), Vol. II.

Polymorphism of Cesium and Thallium Halides*

L. G. SCHULZ
Institute for the Study of Metals, University of Chicago, Chicago, Illinois
May 12, 1950

SALTS having the CsCl type crystal structure were deposited by evaporation in a vacuum onto cleavage surfaces of mica, LiF, NaCl, KBr, KI, and $CaCO_3$. The deposits were examined with electron diffraction using the methods previously employed.[1] It was found that those crystals in a deposit which touched the substrate very often had the NaCl type structure. There was considerable variation among the individual salts. CsCl and CsBr, for example, had a NaCl structure on all the substrate materials named above, whereas TlI had this structure only on LiF. In general the nature of the atomic matching at the interface was not the dominant factor in determining the structure of the deposit.

The lattice parameters, a_0, of the new structure could be measured to about 0.3 percent and are listed in the second column of Table I. Also included in this table are (1) the interatomic

TABLE I.

Salt	a_0, in A NaCl-type	Interatomic distances in A NaCl-type	Interatomic distances in A CsCl-type	Differences in interatomic distances in A
CsCl	6.94	3.47	3.56	0.09
CsBr	7.23	3.62	3.72	0.10
CsI	7.66	3.83	3.95	0.12
TlCl	6.30	3.15	3.32	0.17
TlBr	6.58	3.29	3.44	0.15
TlI	6.94	3.47	3.64	0.17

distances in the NaCl type structure; (2) the interatomic distances in the CsCl type structure;[2] and (3) the differences of these two interatomic distances.

A more complete discussion of the experimental details and the significance of the results will be given later.

* This research was supported in part by Army Air Force Contract No. AF33(038)-6534.

[1] L. G. Schulz, Phys. Rev. **78**, 316 (1950).
[2] R. W. G. Wyckoff *Crystal Structures* (Interscience Publishers, Inc., New York, 1948).

The Exchange Reaction of Hydroxylamine and Gaseous Nitrogen

B. A. PETHICA, E. R. ROBERTS, AND E. R. S. WINTER
Department of Chemistry, Imperial College, London, England
May 10, 1950

DURING an isotope study of the role of hydroxylamine in biological nitrogen fixation, it became of interest to investigate the possibility of isotope exchange between hydroxylamine and gaseous nitrogen. Previous communications in this journal concerning such exchange have been conflicting. Nishina,[1] using radioactive N^{13}, claimed to have demonstrated exchange with a variety of compounds, including sodium nitrite and hydroxylamine hydrochloride in aqueous solutions. Norris,[2] also using radioactive nitrogen, found very slight exchange with sodium nitrite. Joris[3] used a non-equilibrium mixture of the nitrogen isotopes N^{14} and N^{15} as the gas phase, and observed no change in the ratio $N_2^{29}:N_2^{30}$ when the mixture was enclosed over nitrite and hydroxylamine hydrochloride solution, and therefore concluded that exchange was absent. In view of the above disagreement it was considered advisable to reinvestigate this problem and also to examine exchange of nitrogen in a solution containing free hydroxylamine. The method used by Joris is open to the objection that hydroxylamine solutions are unstable, producing some gaseous products[4,5] including N_2 and N_2O. N_2O could give rise to NO of mass 30 in the mass spectrometer. The experiments reported were carried out by exposing two solutions of hydroxylamine hydrochloride to a nitrogen atmosphere containing 10 percent N^{15}. One solution comprised $0.1M$ $NH_2\cdot OH\cdot HCl$ in distilled water, the other $0.1M$ $NH_2OH\cdot HCl$ in a nitrogen free bacteriological culture medium buffered to *p*H 7.3. This latter solution contained largely free hydroxylamine. The exposure was for 24 hours at room temperature. The hydroxylamine was then reduced to ammonia, the solutions used being saturated with hydrogen to prevent any re-exchange with the atmosphere. The ammonia was quantitatively converted to gaseous nitrogen by means of sodium hypobromite and analyzed for N^{15}. No exchange could be demonstrated in either solution, the mass spectrometer analyses showing no enrichment of N^{15}. The absence of exchange between N_2 and NH_2OH at a physiological *p*H is an additional argument against the suggestion by Virtanen[6] that nitrogen fixation in legumes can occur by reversal of the reaction between NH_2OH and hemoglobin.

[1] Y. Nishina *et al.*, J. Chem. Phys. **9**, 571 (1941).
[2] T. H. Norris, J. Chem. Phys. **9**, 726 (1941).
[3] G. G. Joris, J. Chem. Phys. **9**, 775 (1941).
[4] W. Segal and P. W. Wilson, J. Bact. **57**, 55 (1949).
[5] A. Kurtenacker and F. Werner, Zeits. f. anorg. allgem. Chemie **160**, 387 (1929).
[6] A. I. Virtanen and T. Laine, Suomen. Kemistilehti **188**, 38 (1945).

The Number of Unilateral Solute Impacts on Unit Surface in a Dilute Solution

HOWARD REISS
Department of Chemistry, Boston University, Boston, Massachusetts
May 4, 1950

IN a recent paper[1] the author discussed the rate of nucleation for a liquid phase transition. To compute this rate on an *a priori* basis it was necessary to know how many times each second any square centimeter of planar surface in a dilute solution was struck, on one side, by a solute molecule. The present letter provides this result, β_a, to a degree of accuracy sufficient for the above purpose.

If the solution is dilute, and Fick's law holds,[2] it can be shown by means of a stochastic procedure[3] that the coefficient of diffusion, D, is given by

$$D=\tfrac{1}{6}n\langle l^2\rangle, \tag{1}$$

where n is the jumping frequency and $\langle l^2\rangle$ is the mean square jump length. If the average modulus of the jump length, $|\bar{l}|$, is approximated by

$$|\bar{l}|\simeq(\langle l^2\rangle)^{\frac{1}{2}}, \tag{2}$$

the average speed of progression of a solute molecule between impacts can be written in the form

$$\bar{v}=n|\bar{l}|\simeq\frac{6D}{(\langle l^2\rangle)^{\frac{1}{2}}}. \tag{3}$$

We thus obtain $\bar{v}$ in terms of the macroscopic parameter, D, and the modulus of the mean jump length, which can be nicely approximated by the distance between equilibrium positions in the liquid lattice. The latter cannot vary greatly from solution to solution and can be estimated when the molar volume of the solvent is known. The necessity for computing the difficult quantity, n, has been obviated. The issue of liquid partition functions and diffusional activation energies is therefore avoided.

Now, any molecule within a distance v of a surface element dS, and traveling towards it, will strike dS during one second.

Originate a spherical coordinate system at dS. The volume element

$$d\tau = r^2 \sin\vartheta d\vartheta d\varphi dr \tag{4}$$

will contain $C_a d\tau$ molecules (where C_a is the uniform concentration of solute) of which the fraction

$$(dS\cos\vartheta)/(4\pi r^2) \tag{5}$$

will strike dS during one second provided that

$$r \leqslant v. \tag{6}$$

Expression (5) is a statement of the isotropic distribution of velocity vectors. According to this formulation

$$\beta_a dS = \frac{C_a dS}{4\pi}\int_0^v \int_0^{\pi/2} \int_0^{2\pi} \sin\vartheta \cos\vartheta d\varphi d\vartheta dr$$

$$= \frac{3}{2}\frac{D}{(\langle l^2\rangle)^{\frac{1}{2}}} C_a dS, \tag{7}$$

or

$$\beta_a = \frac{3}{2}\frac{D}{|l|}C_a.$$

This value is accurate enough for use in the above-mentioned nucleation theory, especially since the rate of nucleation is dependent mostly upon an exponential factor, already evaluated, which does not contain β_a.

[1] H. Reiss, J. Chem. Phys. **18**, 840 (1950).
[2] Longsworth, Ann. N. Y. Acad. Sci. **46**, 212 (1945).
[3] Chandrasekhar, Rev. Mod. Phys. **15**, 2 (1943).

Reinvestigation of the Reaction Involving Nitrogen Pentoxide and Nitric Oxide

HAROLD S. JOHNSTON AND ROBERT L. MILLS
Department of Chemistry, Stanford University, Stanford, California
May 12, 1950

IT was suggested recently[1] that the reaction between NO and N_2O_5 be restudied[2] to elucidate the mechanism of the decomposition of nitrogen pentoxide. During the past two years we have completed this reinvestigation over a 100,000-fold range of total pressure at 27°C. Limited work has been done at 0° and 40°. Special techniques[3] for the study of fast reactions were required at high total pressures. Foreign gases such as CO_2 and N_2 were almost as effective as the reactants themselves in maintaining the high first-order rates.

At total pressures of 7000 mm (mostly N_2) the observed first-order rate constant was 0.25 sec.$^{-1}$ and the extrapolated value at limiting high pressure was 0.29 sec.$^{-1}$. The energy of activation at 7000 mm was 21±1 kcal./mole. At total pressures of 0.07 mm the first-order rate constant divided by the total concentration of gases was 1.93×10^5 cc/mole-sec., and its value extrapolated to zero pressure is 2.34×10^5 cc/mole-sec. The energy of activation at limiting low pressure is 14.5±0.5 kcal./mole. This study is thus the first for which at one temperature both the high pressure limit and the low pressure limit of a unimolecular reaction have been essentially attained.

The mechanism proposed by Smith and Daniels[2] for the reaction of NO and N_2O_5 and the mechanism proposed by Ogg[4] for the decomposition of N_2O_5 alone have been confirmed and extended. Analysis of the mechanism shows that the rate of the initial reaction of N_2O_5 and NO is that of the elementary unimolecular decomposition

$$N_2O_5 = NO_2 + NO_3.$$

The rate constants can be expressed in terms of reasonable values of "effective number of oscillators" and molecular cross sections. Some of the anomalies associated with the decomposition of N_2O_5 appear to be removed by these mechanisms and this experimental confirmation of them.

A complete summary of these data, a review of the decomposition of N_2O_5, and an examination of theories of unimolecular reactions will be submitted to the appropriate journals in the near future.

[1] R. A. Ogg, Jr., J. Chem. Phys. **18**, 572 (1950); Ogg, Richardson, and Wilson, J. Chem. Phys. **18**, 573 (1950).
[2] J. H. Smith and F. Daniels, J. Am. Chem. Soc. **69**, 1735 (1947).
[3] H. S. Johnston and D. M. Yost, J. Chem. Phys. **17**, 386 (1949).
[4] R. A. Ogg, Jr., J. Chem. Phys. **15**, 613 (1947).

Theoretical Explanation of the Chemical Effects of Ultrasonics

VIRGINIA GRIFFING
Department of Chemistry, Catholic University of America, Washington, D. C.
May 19, 1950

RECENT investigations in this laboratory of chemical reactions induced by high intensity sound waves have led to the following qualitative explanation of these phenomena. In order to be specific, consider the experimental facts, already reported in the literature,[1] that under certain conditions water saturated with carbon tetrachloride will release free chlorine upon irradiation with high intensity ultrasonic waves. This reaction will not take place unless there is a gas dissolved in the solution. Furthermore, at a given intensity it will take place with certain gases in the solution such as He, N_2, and O_2 but will not occur when CO_2 is dissolved in the solution. These results have been verified for the experimental conditions in this laboratory and in addition it has been shown that Ne, A, and Xe also give the effect whereas no reaction occurs when the solution is saturated with N_2O, SF_6, or CCl_2F_2.

In order to explain these data, it is assumed that a gas dissolved in the solution forms also minute bubbles in the sound field. The liquid serves as an efficient transducer which carries the energy of the high intensity sound wave from the source to the interfaces between the small bubbles and the liquid. In the adiabatic compression of a sound wave, the production of a high temperature is dependent upon the existence of a large difference between the adiabatic and isothermal compressibility. As the sound wave travels through the liquid, the temperature difference due to the adiabatic compression is of the order of a degree centigrade while at these intensities a small bubble of gas may be compressed to half its volume producing a temperature variation of several hundred degrees. A temperature gradient in the gas bubble is then set up, which produces appreciable periodic temperature variation in the liquid adjoining the gas bubble.[2] If the intensity is sufficiently high, the temperature variation in the liquid adjoining the bubble is sufficiently great to cause the chemical reaction to take place. The same thermal processes are responsible for the loss of acoustic energy.

According to this idea, two thermal properties of the gas content of the bubbles are important. Firstly, $(\gamma-1)$ will determine the temperature reached in the compressed bubble. As the γ of the gas approaches that of the liquid, the temperature reached becomes much lower. This explains why vapors such as ether inhibit these reactions even if the solution is saturated with air. Secondly, the thermal conductivity of the gas will determine how much the high gas temperature affects the liquid. In a case in which the reaction occurs in the gas phase, the thermal conductivity of the gas should be much less important or have the opposite effect.

Experimental and theoretical work is in progress in this laboratory to test the validity of this theory. About twenty gases are being tested having thermal properties which would place them either in a class with N_2 as gases which can bring about reactions or with N_2O which does not cause chemical reactions to take place. The rare gases make it possible to study the effect of thermal conductivity relatively independent of the specific heat. On the basis of this theory one would predict that Xe lies between N_2 and N_2O; one actually finds that less free chlorine is produced when the water is saturated with Xe than with N_2. Up to the present time all the known experimental facts fit these ideas

qualitatively and preliminary work indicates that quantitative agreement may also be found.

Thus, if this explanation is correct it should be possible to arrange chemically inert gases in the order of the amount of free chlorine that is produced in the reaction discussed here or some other convenient product. The dividing line between those that cause reactions and those that do not could then be shifted arbitrarily by varying the acoustic intensity. Furthermore a study of a series of reactions that go with measurable speed at different temperatures should give further evidence for understanding the phenomena. There is an intensity threshold below which these reactions will not take place no matter what gas is present but little can be said about its value until the absolute value of the sound intensity is measured. It is hoped to publish a full report of this work in the near future.

[1] Weissler, Cooper, and Snyder, J. Am. Chem. Soc. **72**, 1769 (1950).
[2] These ideas were stimulated by a talk given in the Catholic University Physics Department by Richard R. Carhart, of the California Institute of Technology. His talk was taken from his Ph.D. thesis "Theory of viscous and thermal attenuation of sound by small spheres."

The Rate Constant of the Methyl Radical Recombination Reaction

ROBERT GOMER*
Gibbs Chemical Laboratory, Harvard University, Cambridge, Massachusetts
May 18, 1950

IT has proved possible to estimate the lifetime of methyl radicals in a static system and to compute the rate constant of the homogeneous second-order recombination reaction:

$$CH_3+CH_3\rightarrow C_2H_6\cdots, \quad (1)$$

as follows: Mercury dimethyl was irradiated with a medium pressure mercury arc and provision was made for chopping the light beam with a rotating sector having a light to dark ratio of one.

The theory of the rotating sector has been worked out by Dickinson[1] for the case:

$$X+h\nu\rightarrow nR\cdot\cdots, \quad (2)$$
$$R\cdot+R\cdot\rightarrow R_2\cdots. \quad (3)$$

The equations cannot be solved readily for the case where the radicals $R\cdot$, formed in the primary process, disappear by both first- and second-order reactions, nor will the speed of light interruption have any effect on the rate of reaction (3) when it predominates, since it then is proportional to I_a. It is therefore necessary to have some means of determining the steady state concentration of $R\cdot$, which is proportional to $I_a^{\frac{1}{2}}$. In the present case the formation of methane was used as a "pilot" reaction for this purpose.

It is possible to adjust the light intensity in such a way that the rate of ethane formation is arbitrarily large compared to the rate of methane formation.[2] Working in the range where $R_{C_2H_6}/R_{CH_4}\approx 25$, the bulk of CH_3 radicals disappears by ethane formation. The formation of methane can be measured quite accurately, however, and is proportional to the CH_3 steady state concentration.[2]

It was found that the experimentally obtained curve of $R_{CH_4}/\bar{R}_{CH_4}$ *versus* $\log\Delta t_1$ at 175° (where R_{CH_4} refers to methane formation under interrupted and $\bar{R}_{CH_4}$ to that quantity under steady illumination and Δt_1 to the time of one light flash) follows the theoretical curve very well, leading to superposition when the mean lifetime is given the value 10 milliseconds at a (bimolecular rate of ethane formation of 3.6×10^{-11} mole/cc sec. This leads to a value of the rate constant of reaction (1) of 7×10^{13} (moles/cc)$^{-1}$ sec.$^{-1}$, at 175°.

The measurements are being extended to other substances yielding CH_3 radicals, and to higher temperature ranges in order to obtain the activation energy of reaction (1). Details of the work and the significance of the large value of k_1 and its apparent independence of pressure in the range of 5 to 100 mm[3] will be discussed in full at a later time.

The author wishes to express his gratitude for many valuable suggestions and advice to Professor G. B. Kistiakowsky, and to the AEC which is supporting this work.

* AEC Postdoctoral Fellow 1949–50.
[1] W. A. Noyes, Jr. and P. A. Leighton, *The Photochemistry of Gases* (Reinhold Publishing Corporation, New York City, 1941), pp. 202–209.
[2] R. Gomer and W. A. Noyes, Jr., "The photochemistry of mercury dimethyl," J. Am. Chem. Soc. **71**, 3390 (1949).
[3] R. Gomer and W. A. Noyes, Jr., "Photochemical studies. Ethylene oxide," J. Am. Chem. Soc. **72**, 106 (1950).

A Reply to H. S. Gutowsky and E. M. Peterson Regarding the Ozone Spectrum

RICHARD M. BADGER AND M. KENT WILSON*
Gates and Crellin Laboratories of Chemistry, California Institute of Technology, Pasadena, California
May 12, 1950

TO avoid unnecessary confusion regarding the ozone spectrum it appears desirable to point out that the analysis of the infra-red spectrum based on an acute angled molecular model proposed by Gutowsky and Peterson[1] appears to be completely excluded on at least two different grounds. (Incidentally the heading of columns 2 and 3 of their Table I appear to be interchanged.)

The spectrum of ozone was carefully examined in this laboratory at both room and dry ice temperatures. Some moderate changes were observed in the relative intensities of the band maxima, due to unequal narrowing of the bands at the low temperature, but the possibility is completely excluded that any of the seven bands under discussion is a difference band involving a lower excited level of 750 cm^{-1} or greater.

The acute angled model consequently fails to account for the band at 1110 cm^{-1}. In any case the large difference between the observed and predicted frequencies completely rules out the possibility that 1110 cm^{-1} is $\nu_1-\nu_2$ of an acute angled molecule, and makes the alternative interpretation, $3\nu_3-\nu_2$, most improbable.

* Present address: Mallinckrodt Chemical Laboratory, Harvard University.
[1] H. S. Gutowsky and E. M. Peterson, J. Chem. Phys. **18**, 564 (1950).

Notice

THE Journal of Chemical Physics is a research journal intended to provide a medium for the publication of research results in the field of chemical physics. The Journal is published by the American Institute of Physics. The only income of the Journal is from subscriptions, from the page charge levied on institutions supporting the research which is published in the Journal, provided they wish to honor the charge, and minor income from the sale of back numbers, etc. The amount of material which can be accepted in the Journal is, in the long run, limited by the subscription income.

Recent increases in the cost of printing and a very considerable increase in the number of manuscripts submitted to the editor's office have resulted in this limitation becoming very real. Individuals who are interested in the health and growth of the Journal will aid this by subscribing to the Journal or by bringing the opportunity to subscribe to the attention of others who may be interested in the Journal.